Investigating the Mechanism and Role of Linker Histone Dynamics during Plant Reproduction

---

Dissertation

zur

Erlangung der naturwissenschaftlichen Doktorwürde
(Dr. sc. nat.)

vorgelegt der

Mathematisch-naturwissenschaftlichen Fakultät

der

Universität Zürich

von
Jasmin Anita Schubert

von/aus

Deutschland

Promotionskommission

Prof. Dr. Ueli Grossniklaus (Vorsitz)

PD Dr. Célia Baroux (Leiterin der Dissertation)

Prof. Dr. Christoph Ringli

Dr. Fredy Barneche

Prof. Dr. Andrzej Jerzmanowski

Zürich, 2018

Table of Content

I. Zusammenfassung

Im Gegensatz zu Tieren, bei denen die Keimzellen bereits früh in der Embryonalentwicklung entstehen, entwickeln sich die Keimzellen in Pflanzen erst spät im Lebenszyklus, nämlich während der Blütenentwicklung. Der Lebenszyklus der Blütenpflanzen besteht aus zwei heteromorphen Generationen: Die diploide sporophytische und die haploide gametophytische Generation. Während der Entwicklung der pflanzlichen Keimzellbahn durchläuft eine einzelne somatische Zelle die Meiose und differenziert sich zum multizellulären Gametophyten welcher die Gameten enthält. In der Modelpflanze *Arabidopsis thaliana* differenzieren sich die Keimzellen aus einer einzelnen somatischen Zelle in die sogenannte Archospore. Die Archospore formiert dann direkt die Pollensporenmutterzelle (PMC) in den Antheren oder die Megasporenmutterzelle (MMC) in dem weiblichen Ovulengewebe. Die Differenzierung der Sporenmutterzellen (SMC) markiert den Übergang zwischen somatischer zu reproduktiver Zellidentität. Es wurde bereits gezeigt, dass Pflanzen- und Tierchromatin bei der Differenzierung der weiblichen und männlichen Keimzellen eine Reprogrammierung erfahren. Der erste Schritt dieses Prozesses ist der transiente Verlust der Linker Histone (H1) in den Vorläuferzellen der SMC. Allerdings sind der Mechanismus und die Rolle des Verlustes der Linker Histone für die Differenzierung der Keimbahnzellen noch ungeklärt. Unsere Hypothese ist, dass der Verlust der Linker Histone während der Keimzellenentwicklung eine zelluläre Reprogrammierung ermöglicht. Diese Reprogrammierung versetzt die Zellen in einen pluripotenten Grundzustand zurück, der eine spätere Differenzierung in die Keimzelle erlaubt.

Das Ziel dieser Doktorarbeit ist zu untersuchen, welchem Mechanismus der Verlust der Linker Histone während der SMC Bildung zugrunde liegt und was für eine Rolle der Verlust für den Wechsel der Zellidentität bedeutet. Um diese Untersuchung durchzuführen, haben wir zunächst ein genetisch induzierbares System adaptiert und optimiert. Dieses System erlaubt uns, gezielt Linker Histone mit veränderten Aminosäuren zu exprimieren, die putative Ziele von post-transkriptionellen Modifikationen (PTMs) sind. Dieses Vorgehen ermöglicht es uns *in vivo* zu testen, ob die Linker Histon-Dynamik wichtig für die Regulation der Keimzellen-Vorläuferzellen ist. Unsere Resultate weisen darauf hin, dass PTMs in der globulären Domäne und dem N-terminalen Ende des Linker Histones wichtig für den Verlust und die Chromatinverdichtung sind.

II. Abstract

In contrast to animals, where the germline is set aside early in embryogenesis, the plant germline is determined late in development during floral organ formation. The life cycle of flowering plants consists of two heteromorphic generations. One is a diploid sporophytic generation and the other is a haploid gametophytic generation. During the development of the plant germline, a single somatic cell in the flower undergoes meiosis and finally gives rise to a multicellular gametophyte that harbors the gametes. The formation of the reproductive lineage in *Arabidopsis thaliana* begins with a single somatic cell that acquires a reproductive fate and differentiates to form an archesporial cell. This archesporial cell develops to form either the Microspore Mother Cell (also called Pollen Mother Cell, PMC) in the anthers or the Megaspore Mother Cell (MMC) within the female ovule tissue. This Spore Mother Cell (SMC) specification marks the somatic-to-reproductive cell fate transition. Previously it was shown that similar to animals, plant chromatin undergoes large-scale remodeling during male and female germline differentiation during the somatic-to-reproductive cell fate transition. The hallmark of this process is a transient eviction of linker histones (H1) from the germline precursor cells. However, the mechanism of H1 eviction and its role in germline differentiation remains unclear. We hypothesize that eviction of H1 in the germline precursor cells allow cellular reprogramming, by resetting the cell into a pluripotent ground state prior to meiosis. During this study, we aimed to uncover what the mechanism of linker histone eviction is during the SMC differentiation process and what the role of linker histone eviction is during the somatic-to-reproductive cell fate transition in plants.

To do this test, we first adapted and optimized an inducible, molecular genetics system that allows to conditionally express H1 constructs with post-transcriptional modified sites. This allowed testing for their importance in the regulation of H1 dynamics in the germline precursor cells *in vivo*. Our results suggest that post-transcriptional modifications in the globular domain and the N-tail of H1 are important for eviction and chromatin compaction.

III. Introduction

1. Structure of the Chromatin

Chromatin is a complex of proteins, RNA and DNA that constitutes the physiological state of the genome in eukaryotes. In prokaryotes, chromatin is not present but it coincident with the development of the nucleus and the chromosomes in eukaryotes. Chromatin's role is to pack the complex, linear DNA into the nucleus. This packaging folds, in the case of a human cell, the 2 m long DNA into the nucleus which has a diameter of around 5 to 10 µm. This DNA organization is done in the form of chromatin, which is in its basic structure the same in nearly all eukaryotes from single-celled yeasts to complex multicellular organism (Gross et al. 2015). DNA organization and folding into chromatin happens with the help of proteins, called histones. The major histones, also called core histones, are small, basic proteins that facilitate binding of the negative charged DNA. The core histones can be divided into four types called H2A, H2B, H3 and H4, which are very similar among different eukaryotes (Cooper GM. 2000). They are arranged in a histone octamer made of two H2A/H2B dimers and one H3/H4 tetramer (See Figure 1 and Figure 2 A).

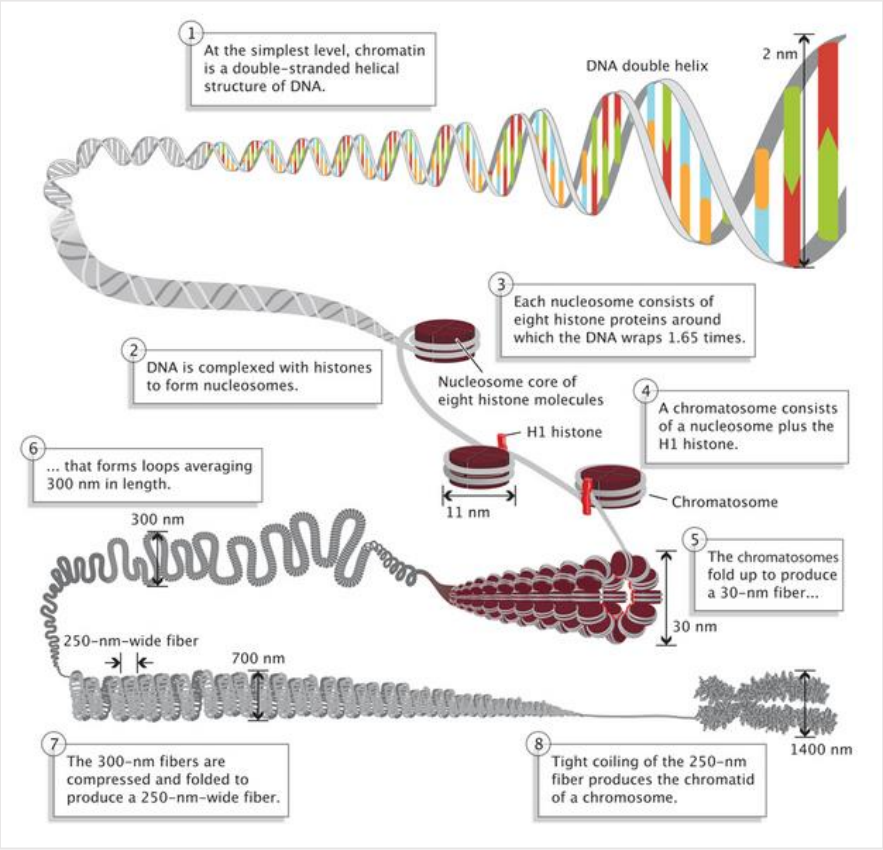

Figure 1: Traditional chromatin model. Chromatin has a highly complex structure with several levels of organization (picture adapted from Pray et al. 2008). Note: The fifth point is currently under debate since the 30 nm fiber might be an artefact resulting from chromatin preparation for *in vitro* studies. Other more recent models suggest that the DNA rather folds dynamical into different more "disordered" structures of nucleosome patches (Bian and Belmont 2012). It seems that chromosome compaction of nucleosome fibers can occur without a regular 30 nm chromatin fiber (Joti et al. 2012).

This octamer was found by nuclease digestion and electron microscopic studies to pack the DNA in a 145-147 base-pair unit and it is repeated every 200 base-pairs. This organization structure is called nucleosome (Luger et al. 1997). The nucleosome core particles are separated from each other by 10-80 base-pair of linker DNA, which can vary in size between organisms, cell types and

DNA regions within the same cell. This linker DNA and the DNA wrapped around the nucleosome interacts with linker (H1) histones. The in vivo existence of 30 nm fiber is under debate (see point 5, Figure 1), because several studies found that a large part of DNA in the nucleus is associated into 10-nm rather than 30-nm fibers (Reviewed in Razin and Gavrilov 2014). Further, the distribution of linker histones was identified not to be homogeneous along nucleosomes as it was long thought (Ricci et al. 2015). Super-resolution nanoscopy provided the evidence that nucleosomes are rather organized in heterogeneous groups of varying size along the DNA fiber, which for dense clusters of nucleosomes correlates with a high number of linker histones presence at those clutches (Ricci et al. 2015). It was further revealed that the distribution of nucleosomes along the DNA was cells-type-specific based on the cells potency stage (Ricci et al. 2015).

Further it should be mentioned that recent studies which applied Hi-C methods to learn about interaction within chromatin, discovered that chromosomes folds in a hierarchy of structures with increasing complexity, from nucleosomes and chromatin fibers to chromatin loops, chromosome domains, chromosome compartments and, finally, chromosome territories (Bonev and Cavalli 2016).

1.1. Chromatin, epigenetic marks and their functions

The degree of chromatin or nucleosome packaging is further also influenced or regulated by i) biochemical modifications on histone tails ii) biochemical modifications on the DNA and iii) the composition of the core histones in the nucleosome.

These biochemical modifications on DNA and core histones are also called epigenetic marks. Since they have a big impact on the chromatin packaging they also have an influence on chromatin functions. Besides packaging the DNA into the nucleus the chromatin dynamically regulates a lot of processes related to DNA, including transcription, replication, recombination and repair (Tom Misteli 2005).

1.1.1. Gene expression

During development and differentiation cells change their transcriptional profiles. These differentiation processes correlate with changes in the distribution of epigenetic marks (Meister, Mango, and Gasser 2011). The different distribution of epigenetic marks can change the packing stage of the chromatin under certain conditions in a quite dynamic manner (Fransz and De Jong 2002). Originally, two forms of chromatin had been identified based on cytological criteria, the densely packed heterochromatin, which usually entails repressive transcription state, and the less dense packed euchromatin, which usually allows for a permissive transcription state (Franklin and Cande 1999; Fransz and De Jong 2002). They are characterized by a different distribution of epigenetic marks and thus different accessibility to the transcription (see Figure 2 B). In most organisms, two forms of heterochromatin can be distinguished, the facultative heterochromatin and the constitutive heterochromatin. The facultative heterochromatin is restrained to specific cell types and can become decondensed and transcriptionally permissive under certain developmental or environmental signals. Whereas the constitutive heterochromatin can mostly be

found around centromeres and telomeres, which represent regions which are rich in repetitive elements and are invariably transcriptionally inert.

1.1.2. Modifications on core histones

Core histones and their structure are highly conserved between eukaryotes. They consist of a globular domain and an unstructured N- and C-tail. Core histones can be posttranslationally modified, mainly but not exclusively on their N-terminal tails (see Figure 2 A). Modifications include: lysine acetylation, serine and threonine phosphorylation, arginine and lysine methylation, crotonylation, formylation, proline isomerization, ubiquitination and ADP-ribosylation, arginine citrullination, SUMOylation and many other modifications on other amino acids (Kouzarides 2007). These modifications can play a role in organizing the chromatin compaction states and thereby influencing transcription and gene expression. Another regulation level is the core histone itself, which can be exchanged with other histone variants depending on cell type, stage of development or organism (see Figure 2). This regulation of chromatin properties by modifications or exchange of and on core histones is counted to the epigenetic modifications. Other modifications which have a direct or indirect influence on the nucleosome include noncoding-RNAs and ATP-dependent nucleosome-sliding or remodeling by the recruitment of non-histone chromatin binding proteins to the nucleosome (Arnaudo and Garcia 2013; Desvoyes et al. 2014; Grimanelli and Roudier 2013; Jenuwein 2001).

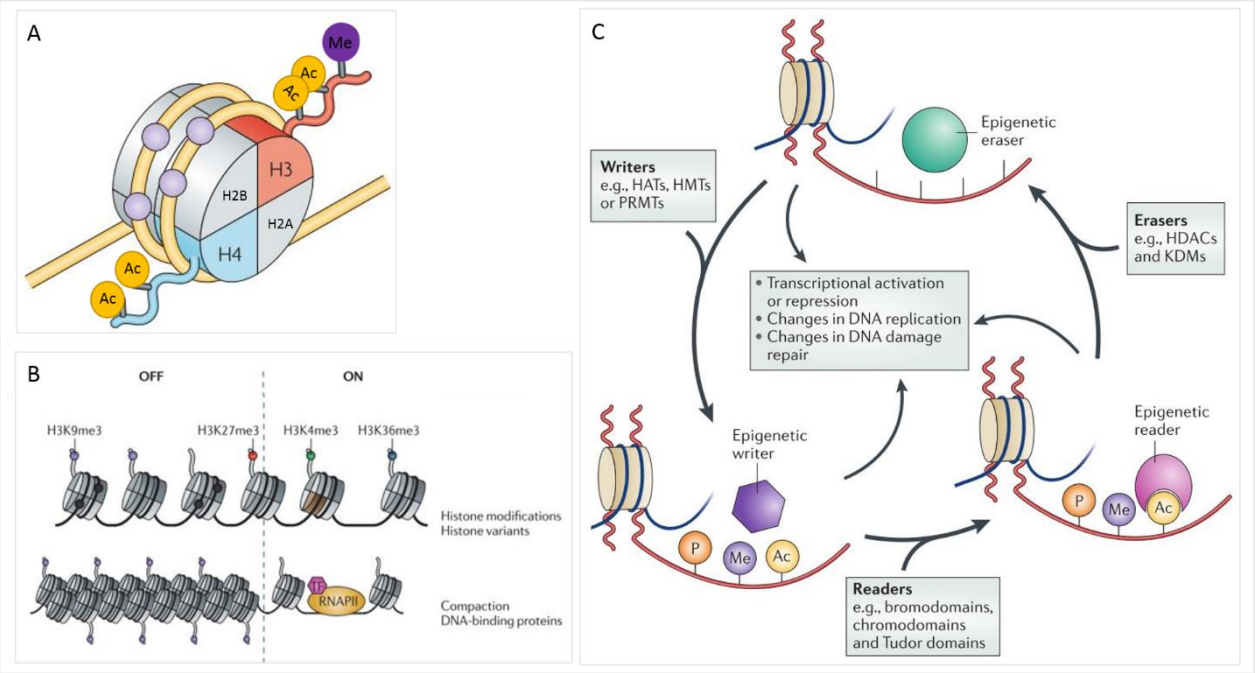

Figure 2: Chromatin modifications on histone tails and their influence on gene expression. (A) Major chromatin modifications occur directly on the DNA (light purple circles). Histone tails of H3 and H4 protrude from the nucleosome and are targets of PTMs (Post-translational modifications) like for example acetylation (Ac, yellow) and methylation (Me, purple). (B) The

combination of different epigenetic modifications on core histones and the DNA have an influence on the chromatin accessibility to the transcriptional machinery (RNA Pol II). (C) A set of epigenetic writers and erasers regulate the establishment, maintenance and resetting of the epigenetic marks, while the readers interpret the information of the epigenetic marks. Writer and erasers are proteins which catalyze specific biochemical modifications on the DNA or histone tails, like establishing new modifications or remove some, whereas the readers bind to specific modifications and recruit transcriptional modulators, like repressors or activators of the transcriptional machinery. (Pictures adapted and modified from A: Cedar and Bergman 2009, B: Zhou, Goren, and Bernstein 2011, C: Falkenberg and Johnstone 2014).

Epigenetic modifications on core histones like methylation of lysine 4 and 9 in histone H3, also called H3K4me and H3K9me, are conserved histone marks, which can be found from yeast to mammals and plants. Some of them mostly correlate with transcriptionally active regions, like H3K4me2/me3 and H3K36me3, whereas other PTMs like H3K9me2 correlates with silenced heterochromatin and H3K27me3 is occurring with silenced euchromatin (Roudier et al. 2011; Schubert et al. 2006). Other histone marks are more specific to certain organisms, like H3K79ac and H3K56me3 in humans or H3K14me2 and H3K64ac in yeasts (Garcia et al. 2007). Compared to other organisms, plants entail both conserved and unique histone modifications (Klose and Zhang 2007; Fuchs et al. 2006; Johnson et al. 2004). In plants methylation on histones, mainly occurs on lysine and arginine residues of histone H3 and H4. Histone H3 can be mono-, di- or trimethylated at lysine 4, 9, 27, 36 and 79. Whereas arginine methylation on histone H3 is restricted to mono- or dimethylation at position 2, 17 and 26. Histone H4 can be mono-, di- or trimethylated at lysine 4, 9, 20, 27, 36 and 79. Whereas arginine methylation on histone H4 is restricted to mono- or dimethylation at position 2, 3, 17 and 26. On both histones, H3 and H4 the methylation of arginine and lysine are apart from a few exceptions catalyzed by HMTs (Histone methyltransferases) (Nelissen et al. 2007).

In Arabidopsis and other plants, H3K9me2 is important for silencing transposons and other DNA repeats (Pikaard and Scheid 2014). Another evolutionary conserved H3 modification that is engaged in gene silencing in many developmental processes is methylation of H3K27 catalyzed by the Polycomb complex 2 (PRC2) (Cedar and Bergman 2009). In Arabidopsis, this mark is restricted to transcribed regions of single genes (~ 4,400 in total) and is not preferentially associated with low-nucleosome density regions (Zhang et al. 2007). The maintenance of H3K27me3 is generally independent of other epigenetic pathways, such as DNA methylation or RNA interference (Zhang et al., 2007). Other roles of histone methylation in plants were determined by analyzing mutants. For example loss of function mutants of ARABIDOPSIS TRITHORAX RELATED3 (ATXR3/SDG2), which is one major H3K4 trimethyltransferase in Arabidopsis, exhibit pleiotropic defects in sporophytic and gametophytic development (Berr et al. 2010; Guo et al. 2010). In contrast, the methyltransferase ARABIDOPSIS TRITHORAX1 (ATX1/SDG27) regulates flowering time and flower organ identity by deposition of H3K4me and thereby facilitates active transcription of the FLOWERING LOCUS C (FLC) and other flower homeotic genes (Alvarez-Venegas et al. 2003; Pien et al. 2008). In the moss *Physcomitrella patens* and to some extent in *A.thaliana* the perturbation of H3K27 methylation leads to the acquisition of gametophytic traits in the sporophyte (Okano et al. 2009). ASHH2/SDG8 is the major H3K36 di/trimethyltransferase in Arabidopsis, which is required for controlling flowering time by activation of FLC (Zhao et al. 2005). The H3K36me2/me3 of FLC regulates shoot branching and carotenoid composition (Cazzonelli et al. 2009). Depletion of ASHH2/SDG8 leads to multiple

defects such as early flowering, reduced organ size, as well as abnormal carotenoid composition (Cazzonelli et al. 2009; Xu et al. 2008; Zhao et al. 2005).

Histone methylation is a dynamic process, which can be reversed by histone demethylase. Two types of demethylases, lysine-specific demethylase1 (LSD1) and Jumonji C (JmjC) domain-containing proteins (JMJs), operate to remove methyl groups from different methylated substrates which are dependent on distinct mechanisms and cofactors (Klose and Zhang 2007; Shi et al. 2004; Tsukada et al. 2006). In Arabidopsis, it was shown that LSD1 mediates H3K4me/me2 and is required for flowering time control (Jiang et al. 2007). Further, five JMJs-domain proteins were found in Arabidopsis which show demethylase activity. From those JMJ15 & JMJ14 are required for H3K4me1/2/3 and a lock of JMJ14 leads to early flowering, reduction of non-CG methylation and defects in RNA silencing (Deleris et al. 2010; Searle et al. 2010).

1.1.3. Methylation of the DNA

Another epigenetic modification is methylation of the DNA. In most eukaryotes methylation occurs on cytosine (5mC), which typically is a silencing mark of transposon elements (TEs) and endogenous genes. In plants, cytosine methylation occurs on CG, CHG and CHH sequence context, which is different from animals, where it just occurs on CG dinucleotides (Chan, Henderson, and Jacobsen 2005). In plants, DNA methylation is mostly enriched on transposons, retrotransposons, rDNA arrays and centromeric repeats**.** These methylations are established by *de novo* methyltransferases and are maintained by maintenance methyltransferases. In Arabidopsis *de novo* methyltransferases like DOMAINS REARRANGED METHYLTRANSFERASE 1 and 2 (DRM1/2) methylate in all three sequence contexts via RNA-directed DNA methylation (RdDM) (Cao and Jacobsen 2002). CG methylation is maintained by METHYLTRANSFERASE1 (MET1) (Kankel et al. 2003; Zhang et al. 2010) and also regulated by the chromatin remodeling ATPases DECREASE IN DNA METHYLATION 1 (DDM1), VARIANT IN METHYLATION 1, 2, 3 (VIM1, 2, 3) and the chromatin remodeling protein DRD1 (Jeddeloh, Stokes, and Richards 1999; Kanno et al. 2005; Woo, Dittmer, and Richards 2008). Methylation in the i) CHG and ii) CHH context are maintained by i) CHROMOMETHYLASE3 (CMT3) with a combinatory role of the histone methyltransferase KRYPTONITE (KYP) mediated H3K9 methylation (Bartee, Malagnac, and Bender 2001; Jackson et al. 2002; Lindroth et al. 2001) and by ii) DRM1 and DRM2 via RdDM pathway which is partially contributed by CMT3 (Cao and Jacobsen 2002; Furner and Matzke 2011; Lindroth et al. 2001). DNA methylation is a fragile epigenetic mark, which can be erased by active and passive demethylation pathways (Jullien et al. 2012). One example for active DNA demethylation is the DNA glycosylase DEMETER (DME). A consequence of DME loss, can be seen in *dme* mutant in Arabidopsis development. Lack of DME and eventually DNA demethylation activity in the central cell impaired endosperm development. Specifically, it happens as a consequence of the lack of expression of two key maternally expressed imprinted genes *FERTILIZATION-INDEPENDENT SEEDS* (*FIS2*) and *MEDEA* (*MEA*) (Choi et al. 2002). Imprinted genes means here that they are differentially expressed depending on the parent from which they are inherited (Reviewed in Raissig, Baroux, and Grossniklaus 2011). Here, *FIS2* and *MEA* encode essential subunits of Polycomb repressive

complex2 (PRC2) which regulates expression of a wide range of genes that are important for endosperm development (Jullien et al. 2006). Passive DNA demethylation is mediated by MET1 suppression via RETINOBLASTOMA REATED1 (RBR1) bound with MULTICOPY SUPPRESSOR OF IRA1 (MSI1) during female gametogenesis (Jullien et al. 2008) leading to expression of maternally imprinted genes like *FIS2* and *FWA* (*FLOWERING OF WAGENINGEN*) (Jullien et al. 2008).

2. Introduction to linker histones

The role of core histones and their modifications in modulating chromatin structure and regulating genes has been largely investigated and is relatively well known. In contrast, the function of linker histones, also called H1s, which are ubiquitous components of the chromatin is not so well understood yet. Even though more and more research is done on linker histones and their functions. Like the core histones, the linker histones are found in all eukaryotes, where they play a critical role in the proper folding of the DNA in a higher compaction state and thereby influencing gene regulation (see also Figure 1 and section 1.1.). Even though they are evolutionary conserved, their sequence differences make them to the most divergent group of all histones.

In animals and plants, numerous H1 isoforms exist, which are partly present in the same but also in different tissues and developmental stages. They are supposed to have redundant but also specific functions in nucleosome/DNA binding. For example, humans and mice have eleven linker histone variants, from which five, H1.1 to H1.5 are replication-dependent and called also somatic linker histones, and six others are tissue or developmental stage-specific (Godde and Ura 2009).

In flowering plants (angiosperms) we can separate linker histones into somatic- and stress-induced linker histones (Bray et al. 1999). The model plant *Arabidopsis thaliana* contains three linker histones *H1.1*, *H1.2* and *H1.3*, which have the same evolutionary origin (Kotliński et al. 2017). Two of them, *H1.1* and *H1.2* are ubiquitously expressed and belong to the somatic linker histones, whereas *H1.3* is mostly stress induced and shows a different expression pattern and a higher binding affinity to chromatin compared to the two somatic variants (Ascenzi and Gantt 1999; Rutowicz et al. 2015). The difference between H1.1, H1.2 and H1.3 is also recalled in their structure (see below section 1.2.1).

2.1. Structure and chromatin binding mode of linker histones in animals and plants

What the linker histones have in common between all higher eukaryotes is their three-domain structure with a well-structured alpha-helical globular domain, a flexible short N-tail and a long intrinsically disordered basic C-tail (see figure 3). The intrinsic discorded tail can adapt various secondary structures upon interacting with a target molecule. The tail structure mainly determines the subtype specificity and influences binding properties of the linker histone (Bradbury et al. 1975; Hansen et al. 2006). Interestingly, the stress-induced linker histones in angiosperm have much shorter C-tail compared to the somatic variants (Ascenzi and Gantt 1999).

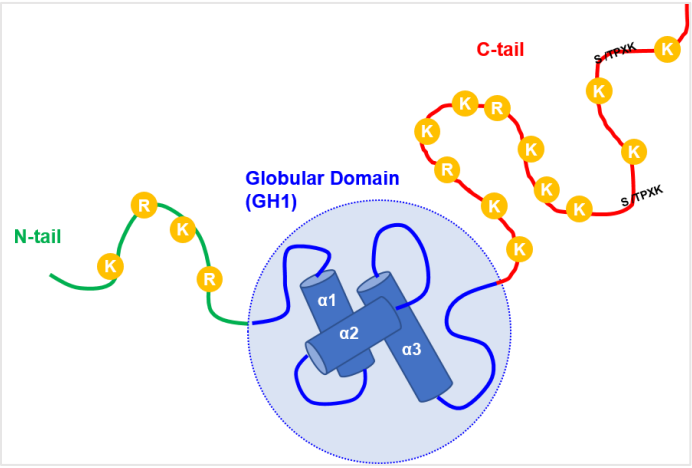

Figure 3: Schematic representation of linker histone structure of *Arabidopsis thaliana*. Linker histones consist of a three-domain structure including a short flexible N-tail (green), a structured globular domain (GH1, blue) and a long basic intrinsically disorder C-tail (red). The three alpha helices of the globular domain and the high amount of arginines (R) and lysines (K) in the N- and C-tail, which makes them highly positive charged are highlighted. In addition, the S/TPxK motif in the C-tail is shown. It is also a target of phosphorylation by Cyclin-dependent kinases (CDKs) during the cell-cycle in animals. (Scheme adapted and modified from Baroux, unpublished)

Although a lot is known about the structure of linker histones in animals and plants, there is still a controversy about how they bind to the linker DNA, how they interact with the nucleosome and how the binding influences the 3D organization of the chromatin. Three main different models of linker histones interaction/binding to the nucleosome and the linker DNA have been considered so far. The differences between the models are the exact position of the GH1 domain in the chromatin fiber and the exact interaction of the linker histone tails with the nucleosome and the linker DNA. The model from Syed et al. 2010 is a symmetrical one, which is similar to the historical ones, which were based on micrococcal nuclease (MNase) and DNase I footprinting experiments. In those models GH1 is located at the center of the nucleosome, interacts with the DNA minor groove and with both, entering and exiting linker DNAs (see Figure 4 A) (Staynov and Crane-Robinson 1988; Syed et al. 2010). The models from (Song et al. 2014; Zhou et al. 2013) are both asymmetric ones where GH1 bridges the nucleosome core and one entering or exiting linker DNA asymmetrically (off-dyad binding). The difference between these two asymmetrically models is the orientation of the GH1 α3 helix to the major groove of the nucleosome DNA near the dyad axis (see Figure 4 B, C).

The recent crystallization of the globular domain of chicken linker histone H5 in complex with the nucleosome by Zhou and colleagues (Zhou et al. 2015) suggested that other linker histones, different to H5 might bind to the nucleosome via distinct structural modes by either off- or on dyad binding. The authors hypothesized, that the different binding modes could lead to distinct higher-order structure of chromatin (more or less condensed) and thereby may have an influence on gene transcription.

The recent first crystal structure of the whole H1 molecule bound to nucleosome (Bednar et al. 2017) showed the interaction for the GH1 domain with both linker DNAs and with the nucleosome dyad (similar to the one mentioned above, described by Zhou et al. 2015). However, the possibility that other modes of binding exist for other linker histone isoforms or different chromatin environments cannot be ruled out.

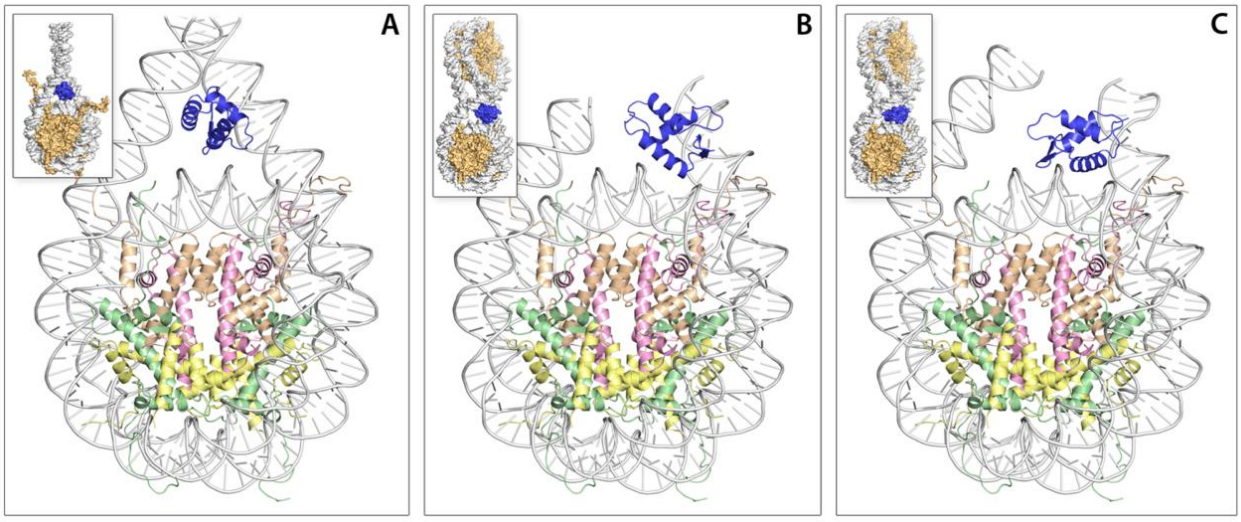

Figure 4: 3D models of the GH1 domain of Arabidopsis H1.2 in complex with a nucleosome. (A) Symmetric model of the GH1-nucleosome complex from Syed et al. 2010, (B) asymmetric model from Zhou et al. 2013, (C) asymmetric model from Song et al. 2014. The presented structures correspond to the respective H1-nucleosome models obtained from the authors, with the original GH1 replaced by the 3D model of the Arabidopsis H1.2 GH1 (blue), which was constructed by using a crystal structure of linker histone H5 (PDB|1hst) (Ramakrishnan et al. 1993) as a template. Schematic representations of GH1-mononucleosome and GH1-dinucleosome complexes are shown in the upper left corners. (Picture adapted and modified from Kotliński et al. 2016).

Another important role in the binding affinity of the linker histone to the DNA is mediated by the intrinsically discorded C-tail. Studies showed, that the deletion or mutations of the C-tail lead to shorter fluorescence recovery after photobleaching (FRAP), which suggest that the C-tail is important for the stability of the linker histone at the DNA, whereas the deletion of the N-tail also reduced H1's binding affinity (Contreras et al. 2003) but is non-essential for the formation of higher-order chromatin structures (Allan et al. 1986; öberg and Belikov 2012). In addition, it has been shown that phosphorylation at the C-tail is affecting its secondary structure (Hendzel et al. 2004) and its binding affinity with the DNA. This might be explained by the fact, that the C-tail is highly positively charged, which enables electrostatic interactions with the negatively charged DNA (Raghuram et al. 2009).

2.2. PTMs in linker histones in animals and plants

Similar to core histones are linker histones targets of common post-translational modifications (PTMs) like methylation, phosphorylation and acetylation (Wisniewski et al. 2007). In comparison to core histones is the knowledge about the function of PTMs of linker histones still widely unknown. The best characterized role of a PTM in linker histones is phosphorylation during the cell-cycle. In mouse fibroblasts, Talasz and colleagues showed (Talasz et al. 1996), that the linker histones become progressively phosphorylated during cell cycle progression, starting from late G1-phase and are maximal phosphorylated at late G2- and M- phase. After those phases they become rapidly dephosphorylated. Phosphorylation of linker histones by CDKs during the cell

cycle was also found in plants, like in rice, tobacco, corn, and algae (Zhang, Letham, and John 1996; Sauter, Mekhedov, and Kende 1995; Slaninová et al. 2003; Zhao and Grafi 2000). Based on this correlation it was hypothesized that phosphorylation of linker histones during the cell cycle contributes to chromatin structure and dynamics, which means decondensation during interphase and chromosome condensation during mitosis (Liao and Mizzen 2016). It is still unknown, if the linker histones get dephosphorylated or if new linker histones which are not phosphorylated get incorporated before G1-phase.

It was demonstrated that phosphorylation in the C-tail of H1s, increases its mobility *in vivo* (Lever et al. 2000; Misteli et al. 2000) and weakens its binding to chromatin (Contreras et al. 2003; Roque et al. 2008). Part of the phosphorylation during the cell cycle is done by CDKs, which phosphorylate the C-tail at the S/TPxK motif. At a certain point, more phosphorylation increases again the affinity to the chromatin, which might be explained by the fact that the C-tail is an intrinsically disordered protein, which can change its conformation based on interaction with a target molecule or just simply change its conformation based on PTMs.

Recent studies using mass spectrometry showed that linker histones are targets of a much bigger variety of PTMs, which in contrast to core histones, can also target in a high proportion the globular domain and the C-tail. In linker histones from human, mouse and Drosophila, multiple sites are targets of phosphorylation, mono-, di- and trimethylation, acetylation, formylation, citrullination and ubiquitinylation (Christophorou et al. 2014; Johnson et al. 2004; Villar-Garea and Imhof 2008; Wisniewski et al. 2007). In *Arabidopsis thaliana* linker histones H1.1 and H1.2 are also targets of many different PTMs like phosphorylation, acetylation, mono- and dimethylation, formylation, crotonylation and propionylation (Kotliński et al. 2016). However, also here the function of most PTMs is known, neither in mammals nor in plants.

2.3. Dynamic and interaction partners of linker histones in animals and plants

FRAP experiments in animals and plants showed that core histones are relatively stable associated with chromatin, whereas linker histones are rapidly exchanged (Launholt et al. 2006; Misteli et al. 2000; Phair and Misteli 2000). Experiments showed that H1.1-GFP signals were fully recovered in less than ten minutes while H2B-GFP signals were still not fully recovered after 30 minutes (Lever et al. 2000). But the residence time of H1s varies between cell types, due to the presence of different H1 sub-types, their different structures, their different PTMs and due to competition for chromatin binding with other molecules (Raghuram et al. 2009; Talasz et al. 1996). Interestingly, there is a higher ratio of H1 per nucleosomes in differentiated cells compared to embryonic stem cells (Fan et al. 2003; Ricci et al. 2015). The role of this difference in linker histone distribution between different cell types will be discussed in the next parts (1.2.4 and 1.2.5). Since linker histones are very dynamic proteins with a high affinity to chromatin, they might be removed by chromatin remodelers to facilitate access to DNA for processes like transcription and replication (Antosch, Mortensen, and Grasser 2012; Pedersen et al. 2011). However, in the absence of competitors the linker histones would rapidly bind again to the DNA. One group of proteins found in animals and plants have been suggested to compete with the linker histone of binding with the DNA, the High Mobility Group (HMG) proteins (Jerzmanowski, Przewloka, and Grasser 2000).

HMGs are like core and linker histones chromosomal components, which can facilitate chromatin structural changes at certain cellular processes (Bustin 1999). They got their name based on their first isolation in the 1970s as proteins which migrated with a high mobility in polyacrylamide gels (Reeves 2011). In the narrowest traditional sense, the HMG protein family consists of six proteins and is subdivided into three subfamilies: the HMG-1,-2 subfamily, the HMG-I,Y subfamily and the HMG-14,-17 subfamily. These subfamilies are similar in several physical characteristics (reviewed in Bustin 1999); however, each of the subfamilies has a unique protein signature and a characteristic sequence motif. These sequence motifs are the main site of interaction between the HMG proteins and the DNA or chromatin targets. The subgroup HMG1 proteins can bind to linker DNA like the linker histones and contain a winged-helix GH1–type domain, which is also similar to the one of linker histones (Jerzmanowski, Przewloka, and Grasser 2000). It is suggested that some HMG proteins compete with the linker histones under certain conditions for transiently binding to the DNA and the nucleosome (Frédéric Catez et al. 2002). The HMG proteins are less abundant compared to linker histones at the chromatin but have a higher mobility, which gives them the ability to effectively compete with the linker histones. The HMGs in animal and plants are very similar but plant-specific HMGs also exist (Andrzej Jerzmanowski and Kotlinski 2011; Klosterman and Hadwiger 2002; Pedersen and Grasser 2010). Scientists from the plant and the animal field hypothesize that HMG proteins do not fold the chromatin into a higher order state but rather keep the DNA in an open stage if they are bound (Bustin, Catez, and Lim 2005; Frederic Catez 2006; Robert D. Phair et al. 2004).

For core histones it was demonstrated that many chaperones play a role in core histone transit and assembly with the chromatin. In contrast, for linker histones it is not clear whether their association with chromatin is also mediated by chaperones (Ransom, Dennehey, and Tyler 2010). *In vitro* studies identified human protein NUCLEAR AUTOANTIGENIC SPERM PROTEIN (NASP) as a potential histone H1 chaperone, which can associate with both core histones and linker histones (Richardson et al. 2000). NASP can load H1 molecules onto the DNA *in vitro*, but evidence *in vivo* is still missing. Another potential histone H1 chaperone is the NUCLEOSOME ASSEMBLY PROTEIN (NAP) family. *In vitro* studies by Kepert and colleagues (Kepert et al. 2005) showed that NAP1 can load and unload linker histones on the DNA. For plants so far, no specific linker histone chaperones have been identified. Even though NAP1 functions as a core histone chaperone for H2B and H2A in rice and tobacco (Zhu et al. 2006). Further other protein chaperones like NAP-Related Protein (NRP) and Homolog of Histone Chaperone (HIRA) were identified to be specific for some core histones (Nie et al. 2014; Zhu et al. 2006).

The interaction partners of linker histones are just started to be revealed. Recently ~100 interaction partners for H1.0 were identified by mass spectrometry (Kalashnikova et al. 2013). Some identified interaction partners for mammals are: FACILITATES CHROMATIN TRANSCRIPTION COMPLEX (FACT), proteins involved in rRNA-biogenesis, TATA-BOX BINDING PROTEIN ASSOCIATED 1 (TAF1) and HETEROCHROMATIN PROTEIN 1 (HP1). The roles of those interactions with the linker histones will be discussed in the next parts 1.2.4 and 1.2.5. Interestingly, about two-third of the identified interaction partners mediate their contact via the N-tail-GH1 fragment, while the rest one-third mediates its contacts via the C-tail.

2.4. Role of linker histones in animals

At the beginning of linker histone research it was thought that the role of H1s is only the structural one. More recent studies provided evidence that H1 is also involved in more specific regulation of gene expression (Shen and Gorovsky 1996). Experiments by Yang et al. 2013, Lu et al. 2009 and 2013, also showed that linker histones can have gene repressive functions on certain genes. They found that linker histones of Drosophila and mouse embryonic stem cells contribute to the repression of specific genes by either recruiting the histone methylase Su(var)3–9, which catalyzes H3K9me2 or by recruiting the DNA methyltransferases DNMT1 and DNMT3B, which physically excluding SET7/9 histone methyltransferases, which catalyze H3K4 methylation, a mark of active genes. Another example for a repressive function of linker histones is the H1.4 methylation at K26 (H1.4K26me). This PTM is bound by HP1 which promotes heterochromatin formation (Daujat et al. 2005). However, the opposite function can also be mediated by linker histones. H1.4K34ac is bound by TAF1, a subunit of the transcription factor TFIID (Kamieniarz and Izzo 2012), which upon bounding recruits chromatin remodelers to move histones, including H1 and thus facilitates gene transcription.

A surprising discovery was that H1s were not essential in lower eukaryotes, like in *Saccharomyces cerevisiae* and *Tetrahymena thermophile* (Xuetong Shen et al. 1995; Ushinsky et al. 1997). Also in mammals, the knock-out of individual H1 subtypes did not lead to visible phenotypes, which implied that certain H1 variants can replace each other's functions (Fan et al. 2003). This hypothesis was encouraged by data from Fan and colleagues (Fan et al. 2003), which showed that in mice the knock-out of three H1 subtypes led to a reduction of 50% of the total H1 pool. This reduction surprisingly was enough to cause embryo lethality at development stage E11.5. This result showed that the ratio of linker histones to nucleosome seems to be a critical factor for normal development. This results opened up new scientific questions, which are a) if the ratio of linker histones to nucleosomes determines or is involved in a cell's identity and b) if this ratio is involved in a cells differentiation processes. Since embryonic stem cells contain approximately one linker histone per two nucleosomes whereas differentiated cells contain four linker histones to five nucleosomes (Fan et al. 2005; Woodcock, Skoultchi, and Fan 2006). But not only the ratio between linker histones and nucleosomes changes during differentiation but also the overall amount of linker histones (see also section 1.2.5.). This correlation between reduced linker histone nucleosome ratios and the pluripotent state of a cell leads to the hypothesis that in pluripotent stem cells a larger portion of the genome is maintained in an accessible state (Ricci et al. 2015). Other experiments from Hajkova and colleagues (Hajkova et al. 2008) also suggest a role of linker histones during differentiation processes. They found that shortly after the migration of mouse primordial germ cells (PGCs) into the gonads (E11.5) they are rapidly losing their linker histones, before their whole chromatin landscape changes. But already at stage E12.5 linker histones reappear at the chromatin (Figure 5) (Hajkova et al. 2008). A similar phenomenon was observed in plants by She and colleagues (She et al. 2013), which will be discussed in more detail in the next part (section 1.2.5.). One hypothesis, which tries to explain the linker histone eviction and reloading during differentiation processes is, that the lack of linker histones gives the chromatin more flexibility. Thus, this flexibility gives the possibility to rearrange the chromatin and maybe also to rearrange the transcriptional status of the differentiating cell. This hypothesis is encouraged by data showing that locus-specific binding of linker histones H1.0 and H1.X in regulatory regions

of pluripotency factors like NANOG, OCT4, FOXA2 and SOX17, which are upregulated in stem cells but downregulated in differentiated cells, coincides with their repression after the onset of differentiation (Shahhoseini et al. 2010; Terme et al. 2011). In addition, Christophorou and colleagues (Christophorou et al. 2014) found a correlation between linker histone presence, gene transcription and differentiation process in mouse embryonic stem (ES) cells. They showed by proteomic analysis of ES cells that the linker histones H1.2, H1.3 and H1.4 are targets of the enzyme PEPTIDYLARGININE DEIMINASE (PAD4), which converts the amino acid arginine into the non-coding amino acid citrulline. This conversion correlates with the H1 displacement from DNA, chromatin decondensation and expression of pluripotency markers in embryonic stem cells. If a similar mechanism based on citrullination exists in plants has not been investigated so far.

In conclusion, there is a correlation between linker histone presence, correct development and differentiation processes in mammals. Further does the eviction of linker histones correlate with changes in chromatin structure and changes in gene expression. Chromatin structure in turn, is partly controlled by linker histones, their subtypes, their abundance and their localization.

2.5. Role of linker histones in plants

A correlation between linker histone presence and chromatin organization was observed in tobacco cell culture. In parenchymal cells from whole plants overexpressing H1 resulted in considerable increase in heterochromatin density but only in selected areas of the nuclei (Calikowski et al. 2000). Further, the under-condensation of nuclear chromatin was found in cell cultures lacking tobacco somatic linker histones. This observation encouraged data from other studies, which showed that chromatin from plants with decreased level of major somatic variants of H1 was less condensed than chromatin from control-transformed plants (Prymakowska-Bosak et al. 1999). Calikowski and colleagues (Calikowski et al. 2000) also found in some tobacco cell lines, which overexpressed histone H1, no increase in heterochromatin content, even though in 30% of them the nuclear structure was markedly changed as compared to the nuclei from control cells (Calikowski et al. 2000). Further, it should be mentioned that other specific linker histone variants knockdown in tobacco caused floral developmental phenotypes, including male sterility (Prymakowska-bosak et al. 1999; Przewloka et al. 2002). A similar phenotype, which means defects in flower development but also in chromatin organization was detected in triple mutants in *Arabidopsis thaliana* lacking all three linker histones (Wierzbicki and Jerzmanowski 2005). The linker histones were downregulated by an RNAi approach and showed various heritable developmental defects, which severity correlated with the total reduction of H1s. In some plants, *H1* expression was reduced by 90% leading to developmental defects in the vegetative- and generative phase. These plants further exhibit stochastic changes in DNA methylation, like hypo- and hypermethylation, in different gene contexts. The developmental abnormalities observed in T0 plants with downregulation of *H1* genes increase in subsequent generations and did not strictly co-segregate with the H1-dsRNA transgene. This suggests that the downregulation of the *H1* genes was not the direct cause of the observed developmental abnormalities but rather permits some secondary changes to occur, due to altered chromatin organization. What and where in the genome the secondary changes occur are still mostly unknown.

Other scientists continued the work on linker histone and chromatin organization by genome-wide analysis of DNA methylation profiles. They found that the hypermethylation on heterochromatic regions and transposable elements of *ddm1* mutants (DEFICIENT IN DNA METHYLATION 1), could be partially rescued on certain loci by an H1 knockdown. This suggests that for certain loci DDM1 is no longer required for DNA methylation if H1 is absent (Brzeski and Jerzmanowski 2003; Zemach et al. 2013). Later studies showed specific examples of correlations between methylation and linker histones. A study by Rea and colleagues (Rea et al. 2012), showed that DME, a DNA glycosidase which acts like a DNA demethylase, interacts with maternal H1.2. This interaction leads to an activation of the maternal allele of the Polycomb gene *MEDEA* (*MEA*) in the Arabidopsis endosperm. In addition, maternal linker histones are required for the activation of several other imprinted loci by DME (Rea et al. 2012).

Other studies suggested a role of linker histones mediated methylation in stress response in *Arabidopsis thaliana* (Rutowicz et al. 2015). They showed on a global level that *h1.3* mutant plants lack a substantial part of stress-related DNA methylation. They suggest that the stress induced linker histones in plants are important to mediate adaptive response to complex environmental stress via global alteration of chromatin properties which may favor reprogramming of the epigenetic landscape and gene expression (Rutowicz et al. 2015).

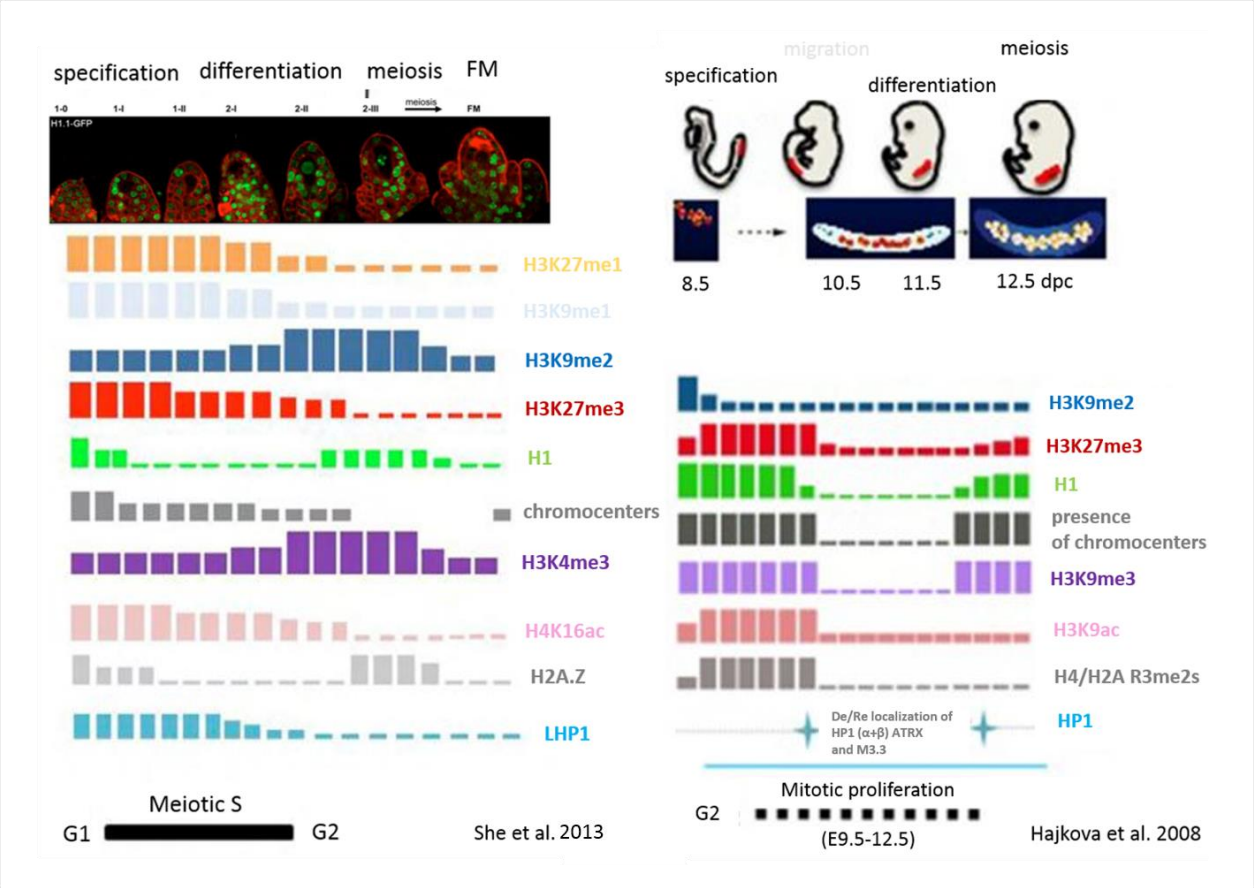

Figure 5: Chromatin dynamics in plant Spore Mother Cells (SMCs) shows similarities to that in animal PGCs. Left: Chromatin dynamics in the Arabidopsis SMC and in the functional

megaspore (FM). The small panel on top shows *pH1.1::H1.1-GFP* expression during the SMC development with a transient eviction of H1.1.-GFP at stage 1-I/1-II and a reappearance of the signal at stage 2-II (red = FM4-64 cell membrane staining). Right: chromatin dynamics in mouse PGCs. Similarly, to animal PGCs, plant SMCs undergo drastic changes in chromatin modification patterns. However, events are asynchronous in plant SMCs and are characterized by both gain and depletion of marks, while animal PGCs at stage 10.5 show a marked depletion of all marks analyzed. The schemes summarize studies from She et al. 2013 and from Hajkova et al. 2008. (Image modified from She and Baroux 2014).

Experiments done by She and colleagues in *Arabidopsis thaliana* showed that chromatin undergoes a huge rearrangement at the somatic to reproductive cell fate transition during sexual reproduction in plants (She et al. 2013). This cell fate transition occurs during male and female sporogenesis, thus during the development of the Megaspore Mother Cell (MMC) (female) and the Pollen Mother Cell (PMC) (male). The hallmark of the chromatin rearrangement is the transient loss of linker histones (see Figure 5). This process is reminiscent to the linker histone loss in PGC cells of animals (see 1.2.4.) (Hajkova et al. 2008). But the correlation between linker histone presence and differentiation and dedifferentiation processes is not well understood until now. Even so in the maize root and in callus cultured maize cells treated with auxin, alterations in linker histone variants' ratios also correlates with plant cell differentiation and dedifferentiation processes (Alatzas, Srebreva, and Foundouli 2008).

Another possible role of linker histones in plants was quite surprising for the scientific community, several studies with cultured tobacco cells determined a role of linker histone in microtubule organization (Calikowski et al. 2000). The results suggested that linker histones are responsible for nucleating microtubules (Hotta, Haraguchi, and Mizuno 2007; Nakayama et al. 2008), which are important for a lot of cellular processes like forming correct cell shape and growth.

Taken together, there is evidence that in plants linker histones play roles in chromatin organization and in both DNA methylation and demethylation processes during plant development and reproduction but also in stress response. Further, it seems that they are involved in microtubule organization. However, the most interesting role of linker histones in plants might be their function in differentiation processes like the ones during sexual reproduction in flowering plants.

3. Female sporogenesis in flowering plants

In contrast to most animals, where the germline is set aside early in embryogenesis, the plant germline is determined late in development, during floral organ formation. The life cycle of flowering plants consists of two heteromorphic generations. One is a diploid sporophytic generation and the other is a haploid gametophytic generation. During the development of the plant germline, also called reproductive lineage, normally single somatic cells in the flower undergo meiosis and give finally rise to gametophytes that harbor the gametes. In the formation of the female reproductive lineage of *Arabidopsis thaliana*, a single somatic cell per ovule acquires reproductive fate and differentiates to form an archesporial cell, which directly forms the

megaspore mother cell (MMC). It can be distinguished from the surrounding cells by its sub-epidermal localization and its enlarged size. The MMC is characterized by its commitment to meiosis and gives rise to a megaspore. This megaspore develops into four megaspores from which three undergo apoptosis and one, which is called functional megaspore (FM), survives (Figure 3). The FM undergoes three rounds of mitosis and finally forms the female gametophyte (embryo sac). For simplicity, the cell arising from the MMC after meiosis will be called FM. Further, we defined the spore mother cell (SMC) or in the female case the MMC, as the first cell of the plant germline as discussed in (Ueli Grossniklaus 2011).

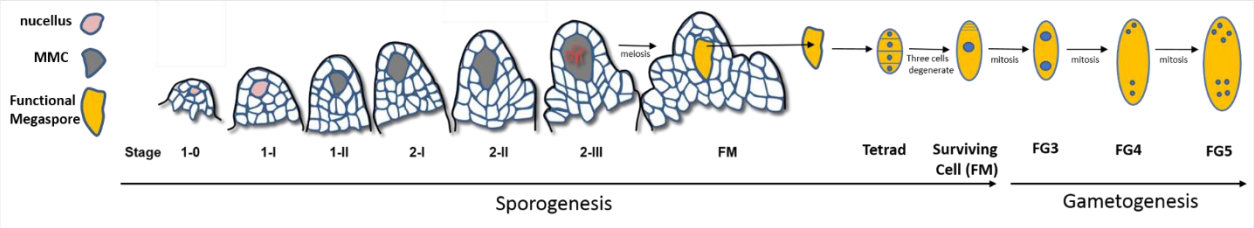

Figure 3: Female sporogenesis and part of female gametogenesis in *Arabidopsis thaliana*. The sub-epidermal nucellar cell of the sporophytic tissue (somatic cell) enlarges to differentiate into megaspore mother cell (MMC). The MMC undergoes meiosis to give rise to the megaspore. For simplification throughout this thesis we call this cell Functional Megaspore (FM). This cell divides into 4 cells, from which three will undergo apoptosis and one will survive. This surviving cell, also called FM will finally give rise to the female gametophyte (FG). The FG undergoes three rounds of mitosis to consist at stage FG5 of an eight nucleate, seven-celled female gametophyte (embryo sac). (Figure adapted and modified from Baroux, unpublished).

3.1. Regulation of female sporogenesis in flowering plants

Plant sexual germline formation has attracted the attention of scientists because the transition from sporophytic to reproductive fate by reprogramming a somatic cell is a key step in the plant life cycle. Recent studies showed the importance of transcriptional and translational regulations and highlighted the role of epigenetic regulatory pathways and hormonal activity for the development of the spores and the gametes (Schmidt, Schmid, and Grossniklaus 2015). It is hypothesized that the formation of one MMC represses the formation of additional MMCs by communication between the other cell types during sporogenesis and thus restricts germline formation to only one cell per ovule (Grossniklaus and Schneitz 1998). However, it still remains unclear whether the restriction to the formation of one MMC is achieved by one cell overcoming the mechanism that usually represses the development into a MMC or if a signaling pathway induces a fate change in one somatic cell, or whether a combination of both is involved. Since the MMC and FM are located in a defined site in the ovule, it speaks for the position to be an important factor in cell fate acquisition. A role of signaling from sporophytic ovule tissue during the selection of the FM has been reviewed in (Schmidt, Schmid, and Grossniklaus 2015). Further, the role of callose accumulation before the initiation of meiosis around the megaspore mother cell was reviewed by Koltunow (Koltunow 1993). One hypothesis is that this callose accumulation might

work as a physical signaling barrier to hormones or other signaling compounds to other cells, which otherwise may disrupt proper meiosis. A recent study found that a balance between WUSCHEL (WUS) activation is important for ovule primordia formation including the development of the integuments (Zhao et al. 2017). They further showed that WUS has a role in specifying the MMC itself and that WUS needs to be inactivated by RETINOBLASTOMA HOMOLOG RBR1 (RBR1) soon after MMC formation to allow entry into meiosis. But still not all players and all signaling pathways are known in this regulatory network, since *WUS* misexpression in designated MMC alone cannot induce mitosis instead of meiosis (Zhao et al. 2017). Other researchers found a role of hormones in germline specification in plants. The plant hormones auxins and cytokinins influence ovule patterning and megasporogenesis by affecting the expression of *PIN-FORMED* (*PIN1*) an auxin efflux carrier (Bencivenga et al. 2012). The hormone levels themselves are regulated by the transcription factors SPOROCYTLESS/NOZZLE (SPL/NZZ) and BELL1 (BEL1) (Bencivenga et al. 2012). In addition to hormonal and positioning effects on the germline development researches found evidence for the involvement of epigenetic pathways in germline definition. In particular those pathways involving DNA methylation and small RNA-based gene regulation (Garcia-Aguilar et al. 2010; Olmedo-monfil et al. 2010; Singh et al. 2011). Arabidopsis plants heterozygous for a RNA helicase called MNEME (MEM) developed multiple sub-epidermal enlarged cells in ~ 21% of ovules (Schmidt et al. 2011). A similar phenotype was observed in *ago9* mutants where depending on the allele 37 - 48% of ovules developed multiple sub-epidermal enlarged cells (Olmedo-monfil et al. 2010). These sub-epidermal cells of *ago9* and *mem* mutants, directly give rise to a female gametophyte in the absence of meiosis (Olmedo-monfil et al. 2010; Schmidt, Schmid, and Grossniklaus 2015) . But at the moment, no evidence has been described that could demonstrates the formation of viable offspring from the unreduced, super-numerous gametophytes seen in the Arabidopsis *ago9* and *mem* mutants. Interestingly, AGO9 has been detected only in the L1 layer of developing ovules and not in the MMC, whereas *MEM* transcripts are highly enriched in the MMC but can also be found in the sporohytic tissue around the MMC, although at a much lower level (Schmidt, Schmid, and Grossniklaus 2015). This expression pattern suggests that MEM and AGO9 likely repress the acquisition of reproductive fate in the surrounding, sporophytic tissue in a non-cell-autonomous manner (Olmedo-monfil et al. 2010; Schmidt et al. 2011). Similar phenotypes have been found in mutants of *rdr6* (RNA-DEPENDENT RNA POLYMERASE6) and *sgs3* (SUPPRESSOR OF GENE SILENCING3), which are known to be required for the biogenesis of trans-acting siRNAs (Olmedo-monfil et al. 2010). Another hypothesis is that abiotic and biotic stress induces conditions of germline specifications. Heat stress as the abundance of reactive oxygen species (ROS) were reported to influence the meiotic fate decision of SMCs and was reviewed in (Schmidt, Schmid, and Grossniklaus 2015). However, at the moment it is unknown whether the influence of stress on germline specification acts via changes in the activity of epigenetic pathways or through independent mechanisms. Therefore further investigations need to be done. Besides the involvement of DNA methylation and small RNA pathways, epigenetic pathways have an influence on chromatin organization and histone modifications as already described in this introduction. Lately She and colleagues found that large-scale chromatin reprogramming establishes an epigenetic and transcriptional state in the Arabidopsis MMC that is distinct from that in the surrounding somatic tissue (She et al. 2013) (Figure 5). These changes likely contribute to the acquisition of reproductive fate, rather than being only a precondition for meiosis (She et al. 2013). This is backed up by the finding that the additional sub-epidermal enlarged cells in *ago9*, *sgs3* and *rdr6* mutants have similar histone modifications

and histone variant dynamics (She et al. 2013). Further data from the same publication found as a hallmark of this large-scale chromatin rearrangement linker histones eviction in the early stages of MMC development, before they got again detectable just prior to meiosis in the MMC (She et al. 2013) (Figure 5). In addition they showed preliminary data which suggest a correlation between linker histone eviction and the proteasome pathway (She et al. 2013). The application of syringolin A, a proteasome inhibitor (Groll et al. 2008), seemed to be sufficient to keep the linker histone proteins present in the MMC, at stages where they were evicted before. Even so this experiment gives the evidence that the proteasome pathway is involved in regulating linker histone presence and absence during SMC development in plants the exact mechanism of linker histone regulation during that developmental stage is not clear. The open questions are, if linker histones get removed from the DNA by electrostatic repulsion or by conformational changes based on PTMs on the linker histones or are they actively removed by linker histone chaperones? Further it is not known, how exactly the eviction of linker histones influence the acquisition of the MMC to undergo meiosis and to finally develop into the female gametophyte.

IV. PhD objectives

Plant sexual reproduction is marked by several cell fate transitions: during sporogenesis, gametogenesis, and embryogenesis. Data from She and colleagues (She et al. 2013) and Hajkova and colleagues (Hajkova et al. 2008) (mentioned in Introduction) found chromatin rearrangement at differentiation processes during mammals' gonad and plant SMC development. The hallmark of this rearrangement is a transient loss of linker histones. The aim of my thesis is to answer:

1) What is the mechanism of linker histone eviction during the SMC differentiation process?

2) What is the role of linker histone eviction during the somatic-to-reproductive cell fate transition in plants?

In chapter 1 I started, in the framework of a collaborative project, to characterize the phenotype of stable knockout- and induced knockdown -lines of all three linker histone variants in *Arabidopsis thaliana*. I studied the relation between linker histones and their phenotypic consequences in developmental decisions involving cell-fate transitions.

In chapter 2 I adapted and optimized the dexamethasone-inducible system, which allowed me to conditionally express inducible knockdowns of putative linker histone regulators and inducible variants of H1 *in vivo*. I further characterized the effects of that induction-system on the plants' fertility.

In chapter 3 I describe the establishment of plant lines and a cloning strategy for functional testing the role of different linker histone modulators and linker histone PTMs in the regulation of H1 dynamics in the germline precursor cells *in vivo.*

In chapter 4 I address the question if linker histone chaperones (NAPs, NRPs and HIRA) play a role in linker histone dynamics during MMC development.

In chapter 5 I ask the question if the proteasome pathway plays a role in linker histone dynamics during SMC development. Specifically, I started to analyze the role of plant E3-ligases, the CULLIN proteins. In addition, I also initiated an investigation of the role of PTMs in the N- tail, the C-tail and the globular domain of H1 and their influence on linker histone presence during female sporogenesis.

In chapter 6 I address the question if the protein AGMATINE DEIMINASE (AIH) has an effect on linker histone dynamics during sporogenesis and if it has an effect on germline differentiation. In the same chapter I also preliminary characterized the role of one mutation in the N-tail domain of H1 in its dynamics during differentiation and development.

References

Alatzas, Anastasios, Ljuba Srebreva, and Athina Foundouli. 2008. “Distribution of Linker Histone Variants during Plant Cell Differentiation in the Developmental Zones of the Maize Root, Dedifferentiation in Callus Culture after Auxin Treatment.” *Biological Research* 41(2): 205–15.

Allan, James et al. 1986. “Roles of H1 Domains in Determining Higher Order Chromatin Structure and H1 Location.” *Journal of Molecular Biology* 187(4): 591–601.

Alvarez-Venegas, Raul et al. 2003. “ATX-1 , an Arabidopsis Homolog of Trithorax, Activates Flower Homeotic Genes.” *Current Biology* 13: 627–37.

Antosch, M., S. A. Mortensen, and K. D. Grasser. 2012. “Plant Proteins Containing High Mobility Group Box DNA-Binding Domains Modulate Different Nuclear Processes.” *Plant Physiology* 159(3): 875–83.

Arnaudo, Anna M, and Benjamin A Garcia. 2013. “Proteomic Characterization of Novel Histone Post-Translational Modifications.” *Epigenetics & Chromatin* 6(1): 24.

Ascenzi, R., and J. S. Gantt. 1999. “Molecular Genetic Analysis of the Drought-Inducible Linker Histone Variant in Arabidopsis Thaliana.” *Plant Molecular BiologyPlant molecular biology* 41(2): 159–69.

Bartee, L., F. Malagnac, and J. Bender. 2001. “Arabidopsis Cmt3 Chromomethylase Mutations Block Non-CG Methylation and Silencing of an Endogenous Gene.” *Genes and Development* 15(14): 1753–58.

Bednar, Jan et al. 2017. “Structure and Dynamics of a 197 Bp Nucleosome in Complex with Linker Histone H1.” *Molecular Cell* 66(3): 384–397.e8.

Bencivenga, S., S. Simonini, E. Benkova, and L. Colombo. 2012. “The Transcription Factors

BEL1 and SPL Are Required for Cytokinin and Auxin Signaling During Ovule Development in Arabidopsis." *The Plant Cell* 24(7): 2886–97.

Berr, Alexandre et al. 2010. "*Arabidopsis SET DOMAIN GROUP2* Is Required for H3K4 Trimethylation and Is Crucial for Both Sporophyte and Gametophyte Development." *The Plant Cell* 22(10): 3232–48.

Bian, Qian, and Andrew S. Belmont. 2012. "Revistiting Higher-Order and Large-Scale Chromatin Organization." *Current Opion Cell Biology* 24(3): 359–66.

Bonev, Boyan, and Giacomo Cavalli. 2016. "Organization and Function of the 3D Genome." *Nature Reviews Genetics* 17(11): 661–78.

Bradbury, Morton, Shirley Danby, Henry Rattle, and Vincenzo Giancotti. 1975. "Studies on the Role and Mode of Operation." *Eur.J.Biochem.* 105(57): 97–105.

Bray, Elizabeth A. et al. 1999. "Water-deficit Induction of a Tomato H1 Histone Requires Abscisic Acid." *Plant Growth Regulation* 29: 35–46.

Brzeski, Jan, and Andrzej Jerzmanowski. 2003. "Deficient in DNA Methylation 1 (DDM1) Defines a Novel Family of Chromatin-Remodeling Factors." *Journal of Biological Chemistry* 278(2): 823–28.

Bustin, Michael. 1999. "Regulation of DNA-Dependent Activities by the Functional Motifs of the High-Mobility-Group Chromosomal Proteins." *Molecular and Cellular Biology* 19(8): 5237–46.

Bustin, Michael, Frédéric Catez, and Jae Hwan Lim. 2005. "The Dynamics of Histone H1 Function in Chromatin." *Molecular Cell* 17(5): 617–20.

Calikowski, Tomasz, Piotr Koźbial, Mieczyslaw X. Kuraś, and Andrzej Jerzmanowski. 2000. "Perturbation in Linker Histone Content Has No Effect on the Cell Cycle but Affects the Cell Size of Suspension Grown Tobacco BY-2 Cells." *Plant Science* 157(1): 51–63.

Cao, Xiaofeng, and Steven E. Jacobsen. 2002. "Role of the Arabidopsis DRM Methyltransferases in de Novo DNA Methylation and Gene Silencing." *Current Biology* 12(13): 1138–44.

Catez, Frederic. 2006. "Determinants of Histone H1 Mobility and Chromatin Binding in Living Cells." *Nat Struct Mol Biol.* 13(4): 305–10.

Catez, Frédéric, David T. Brown, Tom Misteli, and Michael Bustin. 2002. "Competition between Histone H1 and HMGN Proteins for Chromatin Binding Sites." *EMBO Reports* 3(8): 760–66.

Cazzonelli, C. I. et al. 2009. "Regulation of Carotenoid Composition and Shoot Branching in Arabidopsis by a Chromatin Modifying Histone Methyltransferase, SDG8." *the Plant Cell Online* 21(1): 39–53.

Cedar, Howard, and Yehudit Bergman. 2009. "Linking DNA Methylation and Histone Modification: Patterns and Paradigms." *Nature Reviews Genetics* 10(5): 295–304.

Chan, Simon W.L., Ian R. Henderson, and Steven E. Jacobsen. 2005. "Gardening the Genome: DNA Methylation in Arabidopsis Thaliana." *Nature Reviews Genetics* 6(5): 351–60.

Choi, Yeonhee et al. 2002. "DEMETER, a DNA Glycosylase Domain Protein, Is Required for Endosperm Gene Imprinting and Seed Viability in Arabidopsis." *Cell* 110(1): 33–42.

Christophorou, Maria A. et al. 2014. "Citrullination Regulates Pluripotency and Histone H1

Binding to Chromatin." *Nature* 507(7490): 104–8.

Contreras, Alejandro et al. 2003. "The Dynamic Mobility of Histone H1 Is Regulated by Cyclin/CDK Phosphorylation." *Molecular and cellular biology* 23(23): 8626–36.

Daujat, Sylvain et al. 2005. "HP1 Binds Specifically to Lys26-Methylated Histone H1.4, Whereas Simultaneous Ser27 Phosphorylation Blocks HP1 Binding." *Journal of Biological Chemistry* 280(45): 38090–95.

Deleris, Angelique et al. 2010. "Involvement of a Jumonji-C Domain-Containing Histone Demethylase in DRM2-Mediated Maintenance of DNA Methylation." *EMBO Reports* 11(12): 950–55.

Desvoyes, Bénédicte et al. 2014. "Looking at Plant Cell Cycle from the Chromatin Window." *Frontiers in Plant Science* 5(July): 1–12.

Falkenberg, Katrina J., and Ricky W. Johnstone. 2014. "Histone Deacetylases and Their Inhibitors in Cancer, Neurological Diseases and Immune Disorders." *Nature Reviews Drug Discovery* 13(9): 673–91.

Fan, Yuhong et al. 2003. "H1 Linker Histones Are Essential for Mouse Development and Affect Nucleosome Spacing in Vivo." *Molecular and cellular biology* 23(13): 4559–72. h

Fan, Yuhong et al. 2005. "Histone H1 Depletion in Mammals Alters Global Chromatin Structure but Causes Specific Changes in Gene Regulation." *Cell* 123(7): 1199–1212.

Franklin, A. E., and W. Z. Cande. 1999. "Nuclear Organization and Chromosome Segregation." *The Plant Cell* 11(4): 523–34.

Fransz, Paul F., and J. Hans De Jong. 2002. "Chromatin Dynamics in Plants." *Current Opinion in Plant Biology* 5(6): 560–67.

Fuchs, Jörg, Dmitri Demidov, Andreas Houben, and Ingo Schubert. 2006. "Chromosomal Histone Modification Patterns - from Conservation to Diversity." *Trends in Plant Science* 11(4): 199–208.

Furner, Ian J., and Marjori Matzke. 2011. "Methylation and Demethylation of the Arabidopsis Genome."

Garcia-Aguilar, Marcelina, Caroline Michaud, Olivier Leblanc, and Daniel Grimanelli. 2010. "Inactivation of a DNA Methylation Pathway in Maize Reproductive Organs Results in Apomixis-like Phenotypes." *The Plant Cell* 22(10): 3249–67.

Garcia, Benjamin A. et al. 2007. "Organismal Differences in Post-Translational Modifications in Histones H3 and H4." *Journal of Biological Chemistry* 282(10): 7641–55.

Godde, James S., and Kiyoe Ura. 2009. "Dynamic Alterations of Linker Histone Variants during Development." *International Journal of Developmental Biology* 53(2–3): 215–29.

Grimanelli, Daniel, and François Roudier. 2013. 104 Current Topics in Developmental Biology *Epigenetics and Development in Plants. Green Light to Convergent Innovations.*

Groll, Michael et al. 2008. "A Plant Pathogen Virulence Factor Inhibits the Eukaryotic Proteasome by a Novel Mechanism." *Nature* 452(7188): 755–58.

Gross, David S., Surabhi Chowdhary, Jayamani Anandhakumar, and Amoldeep S. Kainth. 2015. "Chromatin." *Current Biology* 25(24): R1158–63.

Grossniklaus, U, and K Schneitz. 1998. “The Molecular and Genetic Basis of Ovule and Megagametophyte Development.” *Seminars in cell & developmental biology* 9: 227–38.

Grossniklaus, Ueli. 2011. “Plant Germline Development: A Tale of Cross-Talk, Signaling, and Cellular Interactions.” *Sexual Plant Reproduction* 24(2): 91–95.

Guo, L., Y. Yu, J. A. Law, and X. Zhang. 2010. “SET DOMAIN GROUP2 Is the Major Histone H3 Lysine 4 Trimethyltransferase in Arabidopsis.” *Proceedings of the National Academy of Sciences* 107(43): 18557–62.

Hajkova, Petra et al. 2008. “Chromatin Dynamics during Epigenetic Reprogramming in the Mouse Germ Line.” *Nature* 452(7189): 877–81.

Hansen, Jeffrey C., Xu Lu, Eric D. Ross, and Robert W. Woody. 2006. “Intrinsic Protein Disorder, Amino Acid Composition, and Histone Terminal Domains.” *Journal of Biological Chemistry* 281(4): 1853–56.

Hendzel, Michael J., Melody A. Lever, Ellen Crawford, and John P H Th’Ng. 2004. “The C-Terminal Domain Is the Primary Determinant of Histone H1 Binding to Chromatin in Vivo.” *Journal of Biological Chemistry* 279(19): 20028–34.

Hotta, Takashi, Tokuko Haraguchi, and Koichi Mizuno. 2007. “A Novel Function of Plant Histone H1: Microtubule Nucleation and Continuous plus End Association.” *Cell structure and function* 32(2): 79–87.

Jackson, James P., Anders M. Lindroth, Xiaofeng Cao, and Steven E. Jacobsen. 2002. “Control of CpNpG DNA Methylation by the KRYPTONITE Histone H3 Methyltransferase.” *Nature* 416(6880): 556–60.

Jeddeloh, Jeffrey A., Trevor L. Stokes, and Eric J. Richards. 1999. “Maintenance of Genomic Methylation Requires a SWI2/SNF2-like Protein.” *Nature Genetics* 22(1): 94–97.

Jenuwein, T. 2001. “Translating the Histone Code.” *Science* 293(5532): 1074–80. h

Jerzmanowski, A., M. Przewloka, and K. D. Grasser. 2000. “Linker Histones and HMG1 Proteins of Higher Plants.” *Plant Biology* 2(6): 586–97.

Jerzmanowski, Andrzej, and Maciej Kotlinski. 2011. “Conserved Chromatin Structural Proteins - a Source of Variation Enabling Plant-Specific Adaptations?” *New Phytologist* 192(3): 563–66.

Jiang, Danhua, Wannian Yang, Yuehui He, and Richard M. Amasino. 2007. “*Arabidopsis* Relatives of the Human Lysine-Specific Demethylase1 Repress the Expression of *FWA* and *FLOWERING LOCUS C* and Thus Promote the Floral Transition.” *The Plant Cell* 19(10): 2975–87.

Johnson, Lianna et al. 2004. “Mass Spectrometry Analysis of Arabidopsis Histone H3 Reveals Distinct Combinations of Post-Translational Modifications.” *Nucleic Acids Research* 32(22): 6511–18.

Joti, Yasumasa et al. 2012. “Chromosomes without a 30-Nm Chromatin Fiber.” *Nucleus* 3(5): 404–10.

Jullien, Pauline E., Tetsu Kinoshita, Nir Ohad, and Frédéric Berger. 2006. “Maintenance of DNA Methylation during the Arabidopsis Life Cycle Is Essential for Parental Imprinting.” *the Plant Cell Online* 18(6): 1360–72.

Jullien, Pauline E. et al. 2008. “Retinoblastoma and Its Binding Partner MSI1 Control Imprinting in Arabidopsis.” *PLoS Biology* 6(8): 1693–1705.

Jullien, Pauline E. et al. 2012. “DNA Methylation Dynamics during Sexual Reproduction in Arabidopsis Thaliana.” *Current Biology* 22(19): 1825–30.

Kalashnikova, Anna A. et al. 2013. “Linker Histone H1.0 Interacts with an Extensive Network of Proteins Found in the Nucleolus.” *Nucleic Acids Research* 41(7): 4026–35.

Kamieniarz, Kinga, and Annalisa Izzo. 2012. “A Dual Role of Linker Histone H1. 4 Lys 34 Acetylation in Transcriptional Activation.” *Genes & Development* (26): 797–802.

Kankel, Mark W. et al. 2003. “Arabidopsis MET1 Cytosine Methyltransferase Mutants.” *Genetics* 163(3): 1109–22.

Kanno, Tatsuo et al. 2005. “A SNF2-like Protein Facilitates Dynamic Control of DNA Methylation.” *EMBO Reports* 6(7): 649–54.

Kepert, J Felix et al. 2005. “NAP1 Modulates Binding of Linker Histone H1 to Chromatin and Induces an Extended Chromatin Fiber Conformation.” *The Journal of biological chemistry* 280(40): 34063–72.

Klose, Robert J., and Yi Zhang. 2007. “Regulation of Histone Methylation by Demethylimination and Demethylation.” *Nature Reviews Molecular Cell Biology* 8(4): 307–18.

Klosterman, Steven J., and Lee A. Hadwiger. 2002. “Plant HMG Proteins Bearing the AT-Hook Motif.” *Plant Science* 162(6): 855–66.

Koltunow, A. M., and Anna M. Koltunow. 1993. “Apomixis: Embryo Sacs and Embryos Formed without Meiosis or Fertilization in Ovules.” *the Plant Cell Online* 5(10): 1425–37.

Kotliński, Maciej et al. 2016. “Histone H1 Variants in Arabidopsis Are Subject to Numerous Post-Translational Modifications, Both Conserved and Previously Unknown in Histones, Suggesting Complex Functions of H1 in Plants.” *PLoS ONE* 11(1): 1–19.

Kotliński Maciej et al. 2017. “Phylogeny-Based Systematization of Arabidopsis Proteins with Histone H1 Globular Domain.” *Plant Physiology* 174(May): pp.00214.2017.

Kouzarides, Tony. 2007. “Chromatin Modifications and Their Function.” *Cell* 128(4): 693–705.

Launholt, Dorte et al. 2006. “Arabidopsis Chromatin-Associated HMGA and HMGB Use Different Nuclear Targeting Signals and Display Highly Dynamic Localization within the Nucleus.” *The Plant cell* 18(November): 2904–18.

Lever, Melody A., John P.H. Th’ng, Xuejun Sun, and Michael J. Hendzel. 2000. “Rapid Exchange of Histone H1.1 on Chromatin in Living Human Cells.” *Nature* 408(6814): 873–76.

Liao, Ruiqi, and Craig A. Mizzen. 2016. “Interphase H1 Phosphorylation: Regulation and Functions in Chromatin.” *Biochimica et Biophysica Acta - Gene Regulatory Mechanisms* 1859(3): 476–85.

Lindroth, A. M. et al. 2001. “Requirement of Chromomethylase 3 for Maintenance of Cpxpg Methylation.” *Science* 292(5524): 2077–80.

Lu, Xingwu et al. 2009. “Linker Histone H1 Is Essential for Drosophila Development, the Establishment of Pericentric Heterochromatin, and a Normal Polytene Chromosome Structure.” *Genes and Development* 23(4): 452–65.

Lu, Xingwu et al. 2013. “Drosophila H1 Regulates the Genetic Activity of Heterochromatin by Recruitment of Suv(Var)3-9.” *Science* 340(6128): 78–81.

Luger, K et al. 1997. “Crystal Structure of the Nucleosome Core Particle at 2.8 A Resolution.” *Nature* 389(6648): 251–60.

Meister, Peter, Susan E. Mango, and Susan M. Gasser. 2011. “Locking the Genome: Nuclear Organization and Cell Fate.” *Current Opinion in Genetics and Development* 21(2): 167–74.

Misteli, T et al. 2000. “Dynamic Binding of Histone H1 to Chromatin in Living Cells.” *Nature* 408: 877–81.

Misteli, Tom. 2005. “Concepts in Nuclear Architecture.” *BioEssays* 27(5): 477–87.

Nakayama, Takateru, Takeharu Ishii, Takashi Hotta, and Koichi Mizuno. 2008. “Radial Microtubule Organization by Histone H1 on Nuclei of Cultured Tobacco BY-2 Cells.” *Journal of Biological Chemistry* 283(24): 16632–40.

Nelissen, Hilde, Tommaso Matteo Boccardi, Kristiina Himanen, and Mieke Van Lijsebettens. 2007. “Impact of Core Histone Modifications on Transcriptional Regulation and Plant Growth.” *Critical Reviews in Plant Sciences* 26(5–6): 243–63.

Nie, Xin et al. 2014. “The HIRA Complex That Deposits the Histone H3.3 Is Conserved in Arabidopsis and Facilitates Transcriptional Dynamics.” *Biology open* 3: 794–802.

Öberg, Christine, and Sergey Belikov. 2012. “The N-Terminal Domain Determines the Affinity and Specificity of H1 Binding to Chromatin.” *Biochemical and Biophysical Research Communications* 420(2): 321–24.

Okano, Yosuke et al. 2009. “A Polycomb Repressive Complex 2 Gene Regulates Apogamy and Gives Evolutionary Insights into Early Land Plant Evolution.” *Proceedings of the National Academy of Sciences of the United States of America* 106(38): 16321–26.

Olmedo-monfil, Vianey et al. 2010. “Control of Female Gamete Formation by a Small RNA Pathway in Arabidopsis.” *Nature* 464(7288): 628–32.

Pedersen, Dorthe S. et al. 2011. “The Plant-Specific Family of DNA-Binding Proteins Containing Three HMG-Box Domains Interacts with Mitotic and Meiotic Chromosomes.” *New Phytologist* 192(3): 577–89.

Pedersen, Dorthe S., and Klaus D. Grasser. 2010. “The Role of Chromosomal HMGB Proteins in Plants.” *Biochimica et Biophysica Acta - Gene Regulatory Mechanisms* 1799(1–2): 171–74.

Phair, R. D., and Tom Misteli. 2000. “High Mobility of Proteins in the Mammalian Cell Nucleus.” *Nature* 404(6778): 604–9.

Phair, Robert D. et al. 2004. “Global Nature of Dynamic Protein-Chromatin Interactions In Vivo: Three-Dimensional Genome Scanning and Dynamic Interaction Networks of Chromatin Proteins.” *Molecular and Cellular Biology* 24(14): 6393–6402.

Pien, S. et al. 2008. “ARABIDOPSIS TRITHORAX1 Dynamically Regulates FLOWERING LOCUS C Activation via Histone 3 Lysine 4 Trimethylation.” *the Plant Cell Online* 20(3): 580–88.

Pikaard, Craig S, and Ortrun Mittelsten Scheid. 2014. “Epigenetic Regulation in Plants.” *Cold Spring Harbor Perspective in Biology* (6:a019315): 1–31.

Prymakowska-Bosak et al. 1999. “Linker Histones Play a Role in Male Meiosis and the Development of Pollen Grains in Tobacco” *The Plant Cell* 11(December): 2317–29.

Przewloka, Marcin R. et al. 2002. “The ‘Drought-Inducible’ Histone H1s of Tobacco Play No Role in Male Sterility Linked to Alterations in H1 Variants.” *Planta* 215(3): 371–79.

Raghuram, Nikhil, Gustavo Carrero, John Th’ng, and Michael J. Hendzel. 2009. “Molecular Dynamics of Histone H1.” *Biochemistry and Cell Biology* 87(1): 189–206.

Raissig, Michael T., Célia Baroux, and Ueli Grossniklaus. 2011. “Regulation and Flexibility of Genomic Imprinting during Seed Development.” *The Plant Cell* 23(1): 16–26.

Ramakrishnan, V. et al. 1993. “Crystal Structure of Globular Domain of Histone H5 and Its Implications for Nucleosome Binding.” *Nature* 362(6417): 219–23.

Ransom, Monica, Briana Dennehey, and Jessica Tyler. 2010. “Chaperoning Histones during DNA Replication and Repair.” *Cell* 140(2): 183–95.

Razin, Sergey V, and Alexey A Gavrilov. 2014. “Chromatin without the 30-Nm Fiber.” *Epigenetics* 9(5): 653–57.

Rea, Matthew et al. 2012. “Histone H1 Affects Gene Imprinting and DNA Methylation in Arabidopsis.” *The Plant Journal : for cell and molecular biology* 71(5): 776–86.

Reeves, Raymond. 2011. “HMG Nuclear Proteins: Linking Chromatin Structure to Cellular Phenotype.” *Sciences-New York* 1799(509): 1–25.

Ricci, Maria Aurelia et al. 2015. “Chromatin Fibers Are Formed by Heterogeneous Groups of Nucleosomes In Vivo.” *Cell* 160(6): 1145–58.

Richardson, Richard T. et al. 2000. “Characterization of the Histone H1-Binding Protein, NASP, as a Cell Cycle-Regulated Somatic Protein.” *Journal of Biological Chemistry* 275(39): 30378–86.

Roque, Alicia, Inma Ponte, José Luis R Arrondo, and Pedro Suau. 2008. “Phosphorylation of the Carboxy-Terminal Domain of Histone H1: Effects on Secondary Structure and DNA Condensation.” *Nucleic acids research* 36(14): 4719–26.

Roudier, Fraṇois et al. 2011. “Integrative Epigenomic Mapping Defines Four Main Chromatin States in Arabidopsis.” *EMBO Journal* 30(10): 1928–38.

Rutowicz, Kinga et al. 2015. “A Specialized Histone H1 Variant Is Required for Adaptive Responses to Complex Abiotic Stress and Related DNA Methylation in Arabidopsis.” *Plant Physiology* 169(November): 2080–2101.

Sauter, Margret, Sergei L. Mekhedov, and Hans Kende. 1995. “Gibberellin Promotes Histone H1 Kinase Activity and the Expression of Cdc2 and Cyclin Genes during the Induction of Rapid Growth in Deepwater Rice Internodes.” *The Plant Journal* 7(October 1994): 623–32.

Schmidt, Anja, Wuest, Samuel, Vijverberg, Kitty, Baroux. Celia, Kleen, Daniela, and Ueli Grossniklaus. 2011. “Transcriptome Analysis of the Arabidopsis Megaspore Mother Cell Uncovers the Importance of RNA Helicases for Plant Germline Development.” *PLoS biology* 9(9).

Schmidt, A., M. W. Schmid, and U. Grossniklaus. 2015. “Plant Germline Formation: Common Concepts and Developmental Flexibility in Sexual and Asexual Reproduction.” *Development* 142(2): 229–41.

Schubert, Daniel et al. 2006. “Silencing by Plant Polycomb-Group Genes Requires Dispersed Trimethylation of Histone H3 at Lysine 27.” *EMBO Journal* 25(19): 4638–49.

Searle, Iain R et al. 2010. “Downloaded from Genesdev.Cshlp.Org on March 8, 2016 - Published by Cold Spring Harbor Laboratory Press RESEARCH COMMUNICATION.” *Genes & development* 24: 986–91.

Shahhoseini, Maryam et al. 2010. “Evidence for a Dynamic Role of the Linker Histone Variant H1x during Retinoic Acid-Induced Differentiation of NT2 Cells.” *FEBS Letters* 584(22): 4661–64.

She, Wenjing et al. 2013. “Chromatin Reprogramming during the Somatic-to-Reproductive Cell Fate Transition in Plants.” *Development (Cambridge, England)* 140(19): 4008–19.

She, Wenjing, and Célia Baroux. 2014. “Chromatin Dynamics during Plant Sexual Reproduction.” , 5(July): 354.

Shen, X., and M. a Gorovsky. 1996. “Linker Histone H1 Regulates Specific Gene Expression but Not Global Transcription in Vivo.” *Cell* 86(3): 475–83.

Shen, Xuetong, Lanlan Yu, Joyce W. Weir, and Martin A. Gorovsky. 1995. “Linker Histories Are Not Essential and Affect Chromatin Condensation in Vivo.” *Cell* 82(1): 47–56.

Shi, Yujiang et al. 2004. “Histone Demethylation Mediated by the Nuclear Amine Oxidase Homolog LSD1.” *Cell* 119(7): 941–53.

Singh, Manjit et al. 2011. “Production of Viable Gametes without Meiosis in Maize Deficient for an ARGONAUTE Protein.” *The Plant Cell* 23(2): 443–58.

Slaninová, Miroslava et al. 2003. “The Alga Chlamydomonas Reinhardtii UVS11 Gene Is Responsible for Cell Division Delay and Temporal Decrease in Histone H1 Kinase Activity Caused by UV Irradiation.” *DNA Repair* 2: 737–50.

Song, F. et al. 2014. “Cryo-EM Study of the Chromatin Fiber Reveals a Double Helix Twisted by Tetranucleosomal Units.” *Science* 344(6182): 376–80.

Staynov, D Z, and C Crane-Robinson. 1988. “Footprinting of Linker Histones H5 and H 1 on the Nucleosome.” *The EMBO Journal* 7(12): 3685–91.

Syed, Sajad Hussain et al. 2010. “Interactions and 3D Organization of the Nucleosome.” *PNAS* 107(21): 9620–25.

Talasz, Heribert, Wilfried Helliger, Bernd Puschendorf, and Herbert Lindner. 1996. “In Vivo Phosphorylation of Histone H1 Variants during the Cell Cycle.” *Biochemistry* 35(6): 1761–67.

Terme, Jean Michel et al. 2011. “Histone H1 Variants Are Differentially Expressed and Incorporated into Chromatin during Differentiation and Reprogramming to Pluripotency.” *Journal of Biological Chemistry* 286(41): 35347–57.

Tsukada, Yu Ichi et al. 2006. “Histone Demethylation by a Family of JmjC Domain-Containing Proteins.” *Nature* 439(7078): 811–16.

Ushinsky, S. C. et al. 1997. “Histone H1 in Saccharomyces Cerevisiae.” *Yeast (Chichester, England)* 13(2): 151–61. h

Villar-Garea, Ana, and Axel Imhof. 2008. “Fine Mapping of Posttranslational Modifications of the Linker Histone H1 from Drosophila Melanogaster.” *PLoS ONE* 3(2).

Wierzbicki, Andrzej T, and Andrzej Jerzmanowski. 2005. “Suppression of Histone H1 Genes in Arabidopsis Results in Heritable Developmental Defects and Stochastic Changes in DNA Methylation.” *Genetics* 169(2): 997–1008.

Wisniewski, Jacek R, Alexandre Zougman, Sonja Krüger, and Matthias Mann. 2007. “Mass Spectrometric Mapping of Linker Histone H1 Variants Reveals Multiple Acetylations, Methylations, and Phosphorylation as Well as Differences between Cell Culture and Tissue.” *Molecular & cellular proteomics : MCP* 6(1): 72–87.

Woo, Hye Ryun, Travis A. Dittmer, and Eric J. Richards. 2008. “Three SRA-Domain Methylcytosine-Binding Proteins Cooperate to Maintain Global CpG Methylation and Epigenetic Silencing in Arabidopsis.” *PLoS Genetics* 4(8).

Woodcock, Christopher L., Arthur I. Skoultchi, and Yuhong Fan. 2006. “Role of Linker Histone in Chromatin Structure and Function: H1 Stoichiometry and Nucleosome Repeat Length.” *Chromosome Research* 14(1): 17–25.

Xu, L. et al. 2008. “Di- and Tri- but Not Monomethylation on Histone H3 Lysine 36 Marks Active Transcription of Genes Involved in Flowering Time Regulation and Other Processes in Arabidopsis Thaliana.” *Molecular and Cellular Biology* 28(4): 1348–60.

Yang, Seung-Min, Byung Ju Kim, Laura Norwood Toro, and Arthur I Skoultchi. 2013. “H1 Linker Histone Promotes Epigenetic Silencing by Regulating Both DNA Methylation and Histone H3 Methylation.” *Proceedings of the National Academy of Sciences of the United States of America* 110(5): 1708–13.

Zemach, Assaf et al. 2013. “The Arabidopsis Nucleosome Remodeler DDM1 Allows DNA Methyltransferases to Access H1-Containing Heterochromatin.” *Cell* 153(1): 193–205.

Zhang, K., D. S. Letham, and P. C. John. 1996. “Cytokinin Controls the Cell Cycle at Mitosis by Stimulating the Tyrosine Dephosphorylation and Activation of P34cdc2-like H1 Histone Kinase.” *Planta* 200(1): 2–12.

Zhang, Meishan, Josphert N. Kimatu, Kezhang Xu, and Bao Liu. 2010. “DNA Cytosine Methylation in Plant Development.” *Journal of Genetics and Genomics* 37(1): 1–12.

Zhang, Xiaoyu et al. 2007. “Whole-Genome Analysis of Histone H3 Lysine 27 Trimethylation in Arabidopsis.” *PLoS Biology* 5(5): 1026–35.

Zhao, Jing, and Gideon Grafi. 2000. “The High Mobility Group I / Y Protein Is Hypophosphorylated in Endoreduplicating Maize Endosperm Cells and Is Involved in Alleviating Histone H1-Mediated Transcriptional Repression *.” *The Journal of biological chemistry* 275(35): 27494–99.

Zhao, Xin’Ai et al. 2017. “RETINOBLASTOMA RELATED1 Mediates Germline Entry in *Arabidopsis*.” *Science* 356(6336): eaaf6532.

Zhao, Zhong et al. 2005. “Prevention of Early Flowering by Expression of FLOWERING LOCUS C Requires Methylation of Histone H3 K36.” *Nature Cell Biology* 7(12): 1156–60.

Zhou, B.-R. et al. 2013. “Structural Insights into the Histone H1-Nucleosome Complex.” *Proceedings of the National Academy of Sciences* 110(48): 19390–95.

Zhou, Bing-Rui et al. 2015. “Structural Mechanisms of Nucleosome Recognition by Linker Histones.” *Molecular cell* 59(4): 628–38.

Zhou, Vicky W., Alon Goren, and Bradley E. Bernstein. 2011. “Charting Histone Modifications

and the Functional Organization of Mammalian Genomes." *Nature Reviews Genetics* 12(1): 7–18.

Zhu, Yan et al. 2006. "Arabidopsis NRP1 and NRP2 Encode Histone Chaperones and Are Required for Maintaining Postembryonic Root Growth." *The Plant Cell* 18(11): 2879–92.

V. Chapter 1

Initial characterization of the role of linker histones in robust developmental decisions in *Arabidopsis thaliana*

Part of the work presented in this chapter was conducted in the framework of a collaborative project between A. Jerzmanowski's, C. Ringli's, F. Barneche's - and our lab. The aim was to better understand the role of all three linker histone variants of *A. thaliana* on the plant's phenotype. Therefore we studied the relation between linker histones and genome organization/packaging and their phenotypic consequences.

Here I will present the parts I conducted for this collaborative work, which will be published together with the data from the other labs as: Rutowicz, K., Lirski, M., Mermaz, B., Schubert, J., Teano, G., Mestiri, I., Kroteń, M.A., Fabrice, T.N., Fritz, S., Grob, S., Ringli, C., Cherkezeyan, L., Barneche, F., Jerzmanowski, A., and Baroux, C.*: "Linker histones regulate fine-scale chromatin organization and modulate developmental decisions in Arabidopsis".*

As mentioned above the aim of this collaboration was to better understand the relation of linker histones on chromatin organization and their phenotypic consequences, especially at developmental transitions, where chromatin undergoes large-scale rearrangement.

Therefore I conducted the following experiments:

i) Measuring and monitoring flowering time in *3h1* mutants, complemented lines, wild types and other H1 mutants.
ii) Measuring root length, and number of lateral roots in several experiments and determining the best, stable conditions to conduct the experiment.
iii) Preparing plant material for the root hair experiment.
iv) Designed and cloned dexamethasone-inducible knockout lines of H1.1 and H1.2 and select transformed plant lines which show functional knockdown of H1s.

I further contributed to this study with experimental design and interpretation of results.

Abbreviation	
3h1	*h1.1-1/h1.1-1;h1.2-2/h1.2-2; h1.3-2/h1.3-2*
amiRNA[H1.1;H1.2], BG	*pRPS5a::LhGR2-GUS::pOP6::amiRNA[H1.1;H1.2]; h1.1-1/h1.1-1;h1.2-2/h1.2-2; h1.3-2/h1.3-2; pH1.1::H1.1-GFP/pH1.1::H1.1-GFP;pH1.2::H1.2-ECFP/pH1.2::H1.2-ECFP*
BG	*h1.1-1/h1.1-1;h1.2-2/h1.2-2; h1.3-2/h1.3-2*; *pH1.1::H1.1GFP/pH1.1::H1.1-GFP; pH1.2::H1.2-ECFP/pH1.2::H1.2-ECFP*
Dex	Dexamethasone
DNA	Deoxyribonucleic acid
dpi	days post induction
ECFP	Enhanced cyan fluorescent protein
EtOH	Ethanol
FM	Functional Megaspore

GFP	Green fluorescent protein
hpi	hours post induction
MMC	Megaspore Mother Cell
RNA	Ribonucleic Acid
SMC	Spore Mother Cell
wt	Wild-type

Introduction

Linker (H1) histones are major elements, which are important for plant and animal chromatin organization. Even though they are evolutionary conserved, their sequence differences make them to the most divergent group of all histones in eukaryotes. Numerous H1 variants co-exist in one cell and have redundant but also specific functions. They differ in their DNA/nucleosome binding affinity and have been shown to be involved in control of genetic programs at development and differentiation processes (Hergeth and Schneider 2015; Pan and Fan 2016). The H1 variants are typically structured in three parts: a globular domain (GH1), a highly basic N-tail and a long basic C-tail. The recent first crystallization of the whole H1 molecule bound to nucleosome suggests that the GH1 domain interacts with the nucleosome dyad as well as with both linker DNAs (Bednar et al. 2017). Further, it is thought that the C-tail, which varies among variants and species harbors the chromatin compaction potential. It interacts with linker DNA and ties them together while reducing their flexibility (Bednar et al. 2017; Zhou et al. 2013). But the differences in the linker histone variants in their structure also confers their different binding capacity.

The high number of H1 variants co-existing in one cell, with partially redundant functions, may also explain, why researchers found that H1 is not crucial in lower eukaryotes (Shen et al. 1995; Ushinsky et al. 1997). But a H1 knockout experiment in mice, which reduced the total H1 pool by 50%, led to embryo lethality and showed that linker histones are essential for correct development in animals (Fan et al. 2003). Even though, H1 depletion has a moderate impact on global gene expression in mammalian cell culture (Fan et al. 2005; Sancho et al. 2008) it can affect genes expression by not repressing the pluripotency genes, what finally impairs the embryonic stem cell differentiation and embryogenesis (Zhang et al. 2012).

H1 contributes to the control of epigenetic marks, by establishing and maintaining DNA methylation patterns in fungi (Seymour et al. 2016), plants (Rea et al. 2012; Wierzbicki and Jerzmanowski 2005; Zemach et al. 2013) and animals (Fan et al. 2005; Yang et al. 2013). In animals, it also contributes in modulating H3 methylation (Lu et al. 2013; Yang et al. 2013). H1s influence on chromatin structure and organization influences gene regulation and other genome activities like DNA replication, chromosome segregation and DNA repair (Hergeth and Schneider 2015; Maresca, Freedman, and Heald 2005; Thiriet and Hayes 2009).

Nevertheless, the importance of H1 for the development of multicellular eukaryotes is still poorly understood. One of the reasons for this is that a lot studies of chromatin and H1s is done in the very complex animal model, which contains a high number of linker histone variants. However, it is possible to do chromatin and linker histone studies also in plants, in which mutants, which lack all H1 variants are still viable.

The model plant Arabidopsis contains three linker histone variants: *H1.1*; *H1.2* and *H1.3* (Kotliński et al. 2017; Wierzbicki and Jerzmanowski 2005). They are enriched at TEs, gene bodies and 3'-

UTRs, and are negatively correlated with H3K4me3 levels, an epigenetic mark associated with active chromatin (Rutowicz et al. 2015). An RNAi based approach, which led to a >90% expression reduction of all three H1 variants in Arabidopsis, produced several developmental aberrations and sterility in those plants (Wierzbicki and Jerzmanowski 2005). These phenotypes are consistent with the role of H1 in stabilizing a functional ordered chromatin conformation, for correct targeting of DNA and core histone modifications (Hergeth and Schneider 2015; Wierzbicki and Jerzmanowski 2005).

The lack of H1s and their deleterious consequences can be overcome by a progressive introgression of lesions at all three linker histone variants (*h1.1-1, h1.2-2, h1.3-2).* In this way created triple homozygous mutant, will be called thereafter *3h1*. This mutant showed no detectable levels of H1 protein in immunostaining and Western Blot (She et al. 2013). Further it does not show obvious developmental abnormality (Rutowicz et al. 2015), even though its DNA methylation is altered at both, TEs and gene bodies (Zemach et al. 2013). But, our lab found that it shows severe alterations in chromatin organization which coincides with mild, specific developmental phenotypes (Rutowicz and Lirski, unpublished). Therefore the Arabidopsis *3h1* mutant provided the unique opportunity to investigate H1s roles in a multicellular eukaryote, which is normally masked by the catastrophic impact of H1 depletion. Therefore my part was to characterize some phenotypes of *3h1* plants at developmental decisions, while my colleagues and our collaborators characterized other phenotypes at developmental transitions and the compaction state of chromatin in *3h1*s.

Results

***3h1* loss impairs the robustness of developmental decisions involving cell fate transitions**

Since different experiments in animals and plants showed that the loss of linker histones has a wide range of severity for the organisms. Reaching from embryo lethality (Fan et al. 2005) to nearly no detectable change (Harshman et al. 2013). Therefore we wanted to know if there are certain time points in an organism's life-cycle where they are more important. Our hypothesis is that linker histones are more essential, in a plant life cycle, when the chromatin undergoes large-scale rearrangement, like at developmental transitions. Therefore we analyzed *3h1* mutants for impaired phenotypes at developmental transitions like flowering, lateral root- and root hair formation. We observed that *3h1* mutant plants flowered earlier (Figure 1A), produced more lateral roots (Figure 1B) and to a low, yet reproducible frequency, produced multicellular root hairs (Figure 1C). Interestingly not all three H1 variants are equivalently important in those developmental transition processes. Our results indicate that H1.1 and H1.2 are largely contributing to flowering and lateral root development. This is in agreement with the literature, which describes general roles for the different H1 variants but also their specific functions. Interestingly some of the phenotypes resemble mild phenotypes of PRC2 mutants (Gu, Xu, and He 2014). PRC2 was shown to regulate enrichment of H3K27me3 at regulatory loci at these developmental transitions (Bouyer et al. 2011; Gu, Xu, and He 2014; Zhu, Rosa, and Dean 2015). Thus it might be that the moderate failures in developmental transitions in the *3h1* mutant could be consequences of altered H3K27me3 levels. This would indicate that H1 provides a spatial chromatin organization, which is competent to integrate environmental and developmental cues to ensure robust developmental transitions.

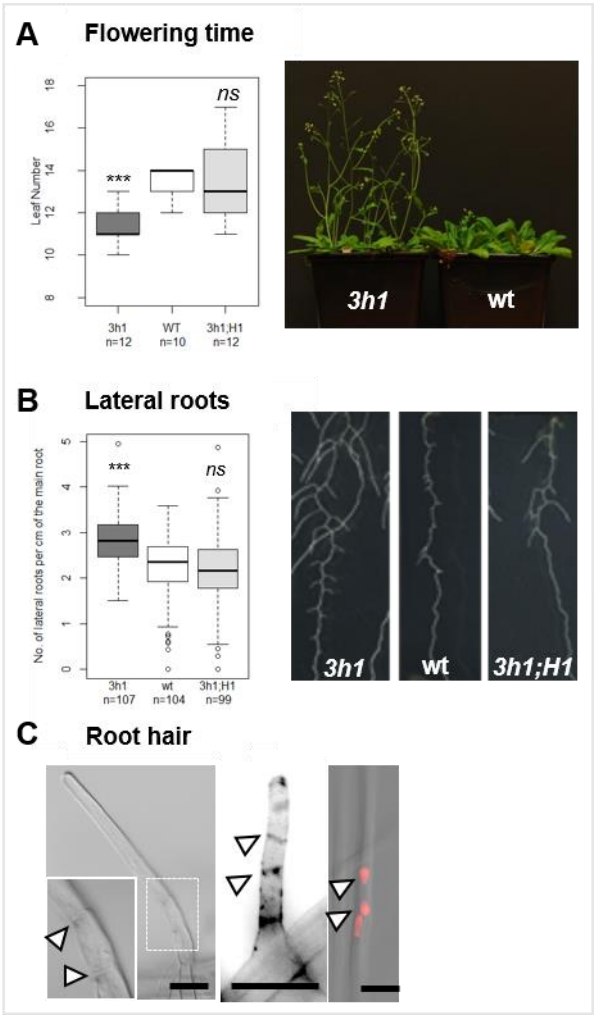

Figure 1. H1 depletion correlates with altered developmental decisions (A to C) H1 depletion affects the robustness of developmental transitions, specifically inducing (A) early flowering (measured as the number of rosette leaves at bolting), (B) increased number of lateral roots (8 DAG seedlings) and (C) occasional multicellular root hairs. Wild-type segregants (wt) were compared with triple mutant tissues/seedlings (*3h1*) and, whenever indicated, with complemented lines expressing H1.1 and H1.2 variants only (*3h1;* H1*).* Scale bar = 10 µm. Statistical tests (A, B Welch t-test) were performed against wt replicates, *** p <0.001, ns, not significant. See also Supplemental Figure 1 to 3.

Inducible knockdown of *H1.1* and *H1.2*

To overcome the likely adaptation of the plant to the lack of linker histones, while in parallel maintain stable lines without linker histones, we aimed to create inducible knockdown lines. Even so, the aim was to create inducible knockdown lines against all three linker histone variants of *A.thaliana*, we also wanted to create inducible knockdown lines against just certain combinations of linker histones. The reason is, to better distinguish and compare the individual contributions of the different linker histone variants to phenotypic consequences. We cloned a Dex-inducible amiRNA, which simultaneously targets *H1.1* and *H1.2* into our BG line (pH1.1::H.1-GFP; pH1.2::H1.2.ECFP; *3h1*) to functionally screen and identify plant lines, in which the amiRNA successfully downregulates *H1.1* and *H1.2* (Figure 2 A and B). Finally, we identified two independent insertion lines (JS146_3; JS145_1.8), in which we successfully downregulate *H1.1* and *H1.2* in a conditional manner after Dex-induction. Before induction we detected fluorescent signals of H1.1-GFP and H1.2-ECFP labeled linker histones (Figure 2 C). 5 days after induction the fluorescent signal was not present anymore (See Figure 2 D), which indicates that the amiRNA is functional and downregulates the linker histones. The next steps would be to use this plants lines to study the phenotypic differences before and after induction in developmental transitions and compare the results to the stable *3h1* mutant line. Since the experiments indicate that the amiRNA is functional in targeting *H1.1* and *H1.2* the same construct can be used to transform it into plant lines, which contain labeled *H1.1*, *H1.2* and *H1.3.* In this situation, we would be able to distinguish the contribution of the different linker histones to the phenotypic consequences during developmental transitions, since in this situation just *H1.1* and *H1.2* would be knockdown but *H1.3* would still be expressed.

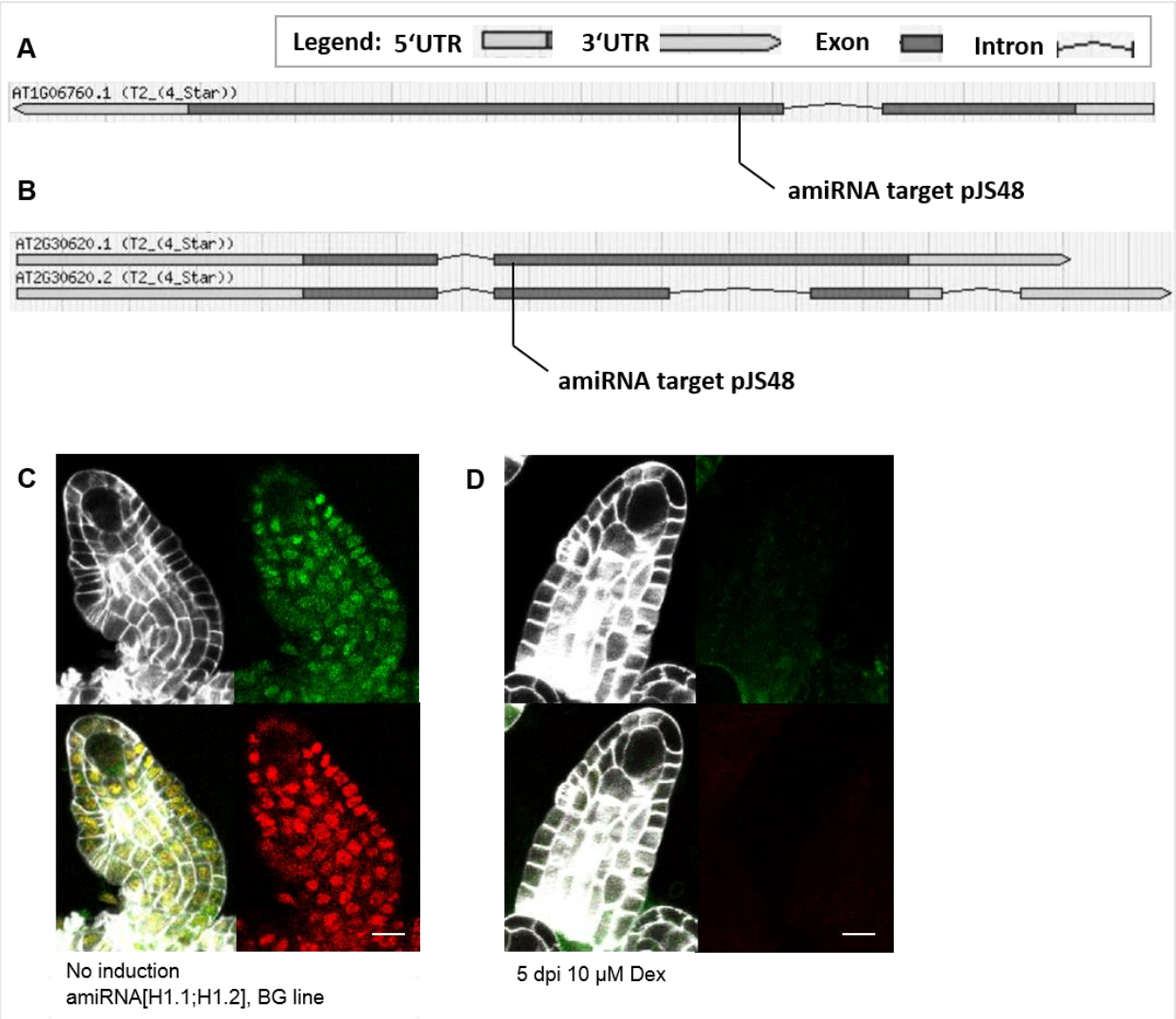

Figure 2: Inducible knockdown of H1s. The target sequences and mismatches for the different amiRNAs can be found in the Supplemental Table 1. Gene models for (A) *AT1G06760.1* (*H1.1*) (B) *AT2G30620.1*; *AT2G30620.2* (*H1.2*). In (A and B) is the target of amiRNA construct pJS48 highlighted. (C and D) We identified two independent insertion lines (JS146_3; JS145_1.8), in which we successfully knockdown *H1.1* and *H1.2* after Dex-induction with 10 µM Dex 5 days post induction (dpi). Green = pH1.1::H1.1-GFP; red = pH1.2::H1.2-ECFP; grey = Renaissance counter stain; scale bar = 10 µm.

Discussion

The role of linker histones in plants was already subject of some scientific examinations (Rea et al. 2012; Wierzbicki and Jerzmanowski 2005; Zemach et al. 2013). One of them showed that RNAi knockdown lines and stable *3h1* mutant plants are still able to build a whole body plan, which suggests that linker histones are not essential for cell lineage development and organogenesis (Wierzbicki and Jerzmanowski 2005). This is consistent with the finding that *3h1* mutant plants show just moderate changes in gene expression profiles (Wierzbicki and Jerzmanowski 2005), which further indicates that H1s are not critical factors for the basic functions of the plants genome.

Interestingly both RNAi and *3h1* mutant plant lines showed different levels of impaired development in the floral organs. The RNAi lines showed nearly full sterility, whereas the stable *3h1* mutants developed normal, fertile floral organs (Rutowicz et al. 2015; Wierzbicki and Jerzmanowski 2005). This might be explained by an adaptation over generations of the plant to the loss of the linker histones. This is also the reason, why we cloned inducible amiRNAs against the linker histone variants to circumvent those adaptation processes. But those different levels of severity at certain developmental processes, also illustrates that linker histones might be critical factors at those developmental transition phases. Our hypothesis is that H1s are especially important during developmental transitions, where the chromatin undergoes large-scale rearrangement. Some of those developmental transitions did we analyzed in this chapter, like flowering, lateral root- and root hair development. Indeed we found that *3h1* mutants had earlier flowering (Figure 1 A), more lateral roots (Figure 1 B) and occasionally but reproducibly multicellular root hairs (Figure 1 C). Therefore our findings suggest that H1s are important at developmental transition phases, where the chromatin undergoes a large-scale reorganization. H1s role might be to control/regulate that certain genes get transcribed and that they are accessible to other modifying molecules, like for example DNA- and histone de- and methyltransferases. This hypothesis is encouraged by findings from the animal field, which showed that depletion of H1 in mouse embryonic stem cells leads to a four-fold change in H4K12ac and a two-fold decrease in H3K27me3 (Fan et al. 2005). Similar correlations have also been found in the plant field. She and colleagues (She et al. 2013) showed that at the somatic-to-reproductive cell transition in Arabidopsis linker histone eviction correlates with a reduction in H3K27me3. Further, some of the phenotypes reported in this chapter remind of a mild *prc2* mutant phenotype (Gu, Xu, and He 2014). PRC2 is responsible for the enrichment of H3K27me3 at regulatory loci during certain developmental transitions (Bouyer et al. 2011; Gu, Xu, and He 2014; Zhu, Rosa, and Dean 2015). Therefore the impaired developmental transitions in the *3h1* mutant might be caused by altered H3K27me3 levels. This would further indicate a role of H1s in providing a chromatin framework, which is functional in integrating different cues to ensure robust development.

All in all the results of this chapter indicate a role of linker histones for robust developmental transitions. The detailed molecular mechanism will be described and discussed by including the results from our collaboration partners. The final discussion including all data will be published under the title mentioned in the beginning of this chapter.

Material and Methods

Plant material and growth conditions

The *Arabidopsis thaliana* plants used in all experiments were in Col-0 ecotype unless it is specified otherwise. The *h1.1h1.2h1.3 (3h1)* mutant was described before (She et al. 2013) and it showed no detectable levels of H1 in Western Blot and immunostaining experiments (She et al. 2013), (www.agrisera.com/en/artiklar/h1-histone-h1.html). Mutant complementation lines were generated by transforming *3h1* via floral dip method (Clough and Bent 1998) with H1 tagged variants (pH1.1::H1.1-RFP, pH1.2::H1.1-(G/C)FP, pH1.3::H1.3-GFP) described before (Rutowicz et al. 2015; She et al. 2013). The *3h1* was complemented with either two (H1.1, H1.2) or all three

H1 variants to generate the following lines: *3h1-comp^{1,2}= h1.1h1.2h1.3;H1.1-RFP-T;H1.2-GFP* (line #KR276), *3h1-comp^{1,2,3} = h1.1h1.2h1.3;:H1.1-RFP-T;H1.2-CFP*;H1.3-GFP (lines #KR264 and #KR265).

Seeds were surface sterilized and rinsed with sterile water before transfer onto germination medium (½ MS medium, 0.8% agar). They were placed over the plate using a toothpick to ensure uniform distribution, stratified 2-4 days at 4°C and transferred into a plant growth incubator (Percival, Germany) with long-day photoperiod (16 h, 22 °C day/8 h, 18 °C night) and light flux around 120 µM*s^{-1}*m^{-2} for routine experiments. Scoring of lateral root production was testing under continuous light (light flux around 100 µM*s^{-1}*m^{-2}, Aralab FitoClima 1200). When the flowering stage was necessary the 10 days-old seedlings were transferred into the soil and grown at 19-21°C with a 16/8hrs photoperiod.

Analysis of developmental transitions

Flowering time

Plants for flowering experiments were grown in the growth chamber under the long daylight regime. To avoid positional effect, different genotypes were always randomly arranged over the growth area. The number of rosette leaves was counted when the inflorescence was about 0.5 cm long.

Root length and lateral root scoring

Seedlings were grown vertically on square Petri dishes under a continuous light regime. The plates were scanned 8 days after germination to score for the number of lateral roots. Root (main and lateral) lengths were scored using manual vector tracing in Fiji, reported at scale (Schindelin et al. 2012).

Lateral root primordia

For microscopic observations of lateral root primordia, five days old seedlings grown under continuous light were fixed in 70% ethanol, rinsed once in sterile water and mounted in water on microscope slides (5 roots aligned/slide covered with 40x22mm coverglass). Primordia were scored according to published developmental scale (Malamy and Benfey 1997).

Cloning and image analysis of Dex-inducible knockdowns of H1s

The amiRNA against *H1.1 and H1.2* (construct: pJS48) was designed using the wmd3 databased (Schwab et al. 2006) and synthesized by Genescript including att1 and att2 sites. Following the amiRNA against H1.1 and H1.2 (vector pJS48) was cloned via Gateway into the pRPS5a::LhGR2-GUS::pOP6 vector (Ian Moore, Oxford). The construct was then transformed via *Agrobacterium tumefaciens* (GV3101) to homozygous *pH1.1::H1.1-GFP, pH1.2::H1.2-ECFP, 3h1 lines* (BG lines, [JS65 and JS67]) as described in chapter 3. Positive T1s were identified as described in chapter

3, based on BASTA selection and GUS reporter assay after 10 µM Dex-treatment. amiRNA construct pJS48: sequence rev. complement: TTCTGAATCGCGTACTGGCTA.

Dex-induction and imaging

We analyzed 18 independent lines of Dex-inducible amiRNA[*H1.1;H1.2*] and found two which were functional (JS146_3 (BG background JS67); JS145_1.8 (BG background JS65)). Single inflorescences induced with 10 µM Dex-solution (0.01% EtOH in water) or Mock (0.01% EtOH in water) were dissected after 3 to 4 days post induction (dpi). Single carpels were freshly dissected and mounted in ddH_2O and directly imaged. Serial images of fluorescent signals in whole-mount ovule primordia were recorded by confocal laser-scanning microscopy with a Leica SP5-R (Leica Microsystems) using a 63× GLY lens (glycerol immersion, NA 1.4). Signals of GFP and ECFP were acquired sequentially. Images were overlaid with DIC channel.

β-*Glucuronidase (GUS) reporter assay*

Single inflorescences induced with 10 µM Dex-solution (0.01% EtOH) or Mock (0.01% EtOH) were dissected after 2 days post induction (dpi). Single carpels were slightly cut open and emerged in 4 mM x-Glu solution, vacuum infiltrated for 5 min followed by a 2 hour incubation at 37°C, washed with phosphate buffer and mounted in 80% glycerol. Imaged at the DMR (Leica) microscope with 20x or 40x dry objective. Final concentration of GUS-solution Triton X-100 10%, EDTA 10 mM, Ferrocyanide 2 mM, Ferricyanide 2 mM, Na2HP04 100 mM, NaH2P04 100 mM, x-Glu 4 mM.

References

Bednar, Jan et al. 2017. “Structure and Dynamics of a 197 Bp Nucleosome in Complex with Linker Histone H1.” *Molecular Cell* 66(3): 384–397.e8.

Bouyer, Daniel et al. 2011. “Polycomb Repressive Complex 2 Controls the Embryo-to-Seedling Phase Transition.” *PLoS Genetics* 7(3).

Clough, Steven J. and Andrew F. Bent. 1998. “Floral Dip: A Simplified Method for Agrobacterium-Mediated Transformation of *Arabidopsis Thaliana*.” *Plant Journal* 16(6): 735–43.

Fan, Yuhong et al. 2003. “H1 Linker Histones Are Essential for Mouse Development and Affect Nucleosome Spacing in Vivo.” *Molecular and cellular biology* 23(13): 4559–72.

Fan et al. 2005. “Histone H1 Depletion in Mammals Alters Global Chromatin Structure but Causes Specific Changes in Gene Regulation.” *Cell* 123(7): 1199–1212.

Fyodorov, Dmitry V., Bing-Rui Zhou, Arthur I. Skoultchi and Yawen Bai. 2017. “Emerging Roles of Linker Histones in Regulating Chromatin Structure and Function.” *Nature Reviews Molecular Cell Biology*.

Gu, Xiaofeng, Tongda Xu and Yuehui He. 2014. “A Histone H3 Lysine-27 Methyltransferase Complex Represses Lateral Root Formation in Arabidopsis Thaliana.” *Molecular Plant* 7(6): 977–88.

Harshman, Sean W, Nicolas L Young, Mark R. Parthun and Michael a Freitas. 2013. “H1 Histones: Current Perspectives and Challenges.” *Nucleic acids research* 41(21): 9593–9609.

Hergeth, S. P. and R. Schneider. 2015. “The H1 Linker Histones: Multifunctional Proteins beyond the Nucleosomal Core Particle.” *EMBO reports* 16(11): 1439–53.

Kotliński, Maciej et al. 2017. “Phylogeny-Based Systematization of Arabidopsis Proteins with Histone H1 Globular Domain.” *Plant Physiology* 174(May): pp.00214.2017.

Lu, Xingwu et al. 2013. “Drosophila H1 Regulates the Genetic Activity of Heterochromatin by Recruitment of Suv(var)3-9.” *Science* 340(6128): 78–81.

Malamy, J. E., and P. N. Benfey. 1997. “Organization and Cell Differentiation in Lateral Roots of Arabidopsis Thaliana.” *Development (Cambridge, England)* 124(1): 33–44.

Maresca, Thomas J., Benjamin S. Freedman and Rebecca Heald. 2005. “Histone H1 Is Essential for Mitotic Chromosome Architecture and Segregation in Xenopus Laevis Egg Extracts.” *Journal of Cell Biology* 169(6): 859–69.

Pan, Chenyi and Yuhong Fan. 2016. “Role of H1 Linker Histones in Mammalian Development and Stem Cell Differentiation.” *Biochimica et Biophysica Acta - Gene Regulatory Mechanisms* 1859(3): 496–509.

Rea, Matthew et al. 2012. “Histone H1 Affects Gene Imprinting and DNA Methylation in Arabidopsis.” *The Plant journal : for cell and molecular biology* 71(5): 776–86.

Rutowicz, Kinga et al. 2015. “A Specialized Histone H1 Variant Is Required for Adaptive Responses to Complex Abiotic Stress and Related DNA Methylation in Arabidopsis.” *Plant physiology* 169(November): 2080–2101.

Sancho, Mónica, Erika Diani, Miguel Beato and Albert Jordan. 2008. “Depletion of Human Histone H1 Variants Uncovers Specific Roles in Gene Expression and Cell Growth.” *PLoS Genetics* 4(10).

Schindelin, Johannes et al. 2012. “Fiji: An Open Source Platform for Biological Image Analysis.” *Nature Methods* 9(7): 676–82.

Schwab, Rebecca et al. 2006. “Highly Specific Gene Silencing by Artificial MicroRNAs in Arabidopsis.” *The Plant cell* 18(May): 1121–33.

Seymour, Michael et al. 2016. “Histone H1 Limits DNA Methylation in Neurospora Crassa.” *G3* 6(7): 1879–89.

She, Wenjing et al. 2013. “Chromatin Reprogramming during the Somatic-to-Reproductive Cell Fate Transition in Plants.” *Development (Cambridge, England)* 140(19): 4008–19.

Shen, Xuetong, Lanlan Yu, Joyce W. Weir and Martin A. Gorovsky. 1995. “Linker Histories Are Not Essential and Affect Chromatin Condensation in Vivo.” *Cell* 82(1):

47–56.

Thiriet, Christophe and Jeffrey J. Hayes. 2009. “Linker Histone Phosphorylation Regulates Global Timing of Replication Origin Firing.” *Journal of Biological Chemistry* 284(5): 2823–29.

Ushinsky, S. C. et al. 1997. “Histone H1 in Saccharomyces Cerevisiae.” *Yeast (Chichester, England)* 13(2): 151–61.

Wierzbicki, Andrzej T. and Andrzej Jerzmanowski. 2005. “Suppression of Histone H1 Genes in Arabidopsis Results in Heritable Developmental Defects and Stochastic Changes in DNA Methylation.” *Genetics* 169(2): 997–1008.

Yang, Seung-Min, Byung Ju Kim, Laura Norwood Toro and Arthur I. Skoultchi. 2013. “H1 Linker Histone Promotes Epigenetic Silencing by Regulating Both DNA Methylation and Histone H3 Methylation.” *Proceedings of the National Academy of Sciences of the United States of America* 110(5): 1708–13.

Zemach, Assaf et al. 2013. “The Arabidopsis Nucleosome Remodeler DDM1 Allows DNA Methyltransferases to Access H1-Containing Heterochromatin.” *Cell* 153(1): 193–205.

Zhang, Yunzhe et al. 2012. “Histone h1 Depletion Impairs Embryonic Stem Cell Differentiation.” *PLoS genetics* 8(5): e1002691.

Zhou, B.-R. et al. 2013. “Structural Insights into the Histone H1-Nucleosome Complex.” *Proceedings of the National Academy of Sciences* 110(48): 19390–95.

Zhu, Danling, Stefanie Rosa and Caroline Dean. 2015. “Nuclear Organization Changes and the Epigenetic Silencing of FLC during Vernalization.” *Journal of Molecular Biology* 427(3): 659–69.

Supplement Chapter 1

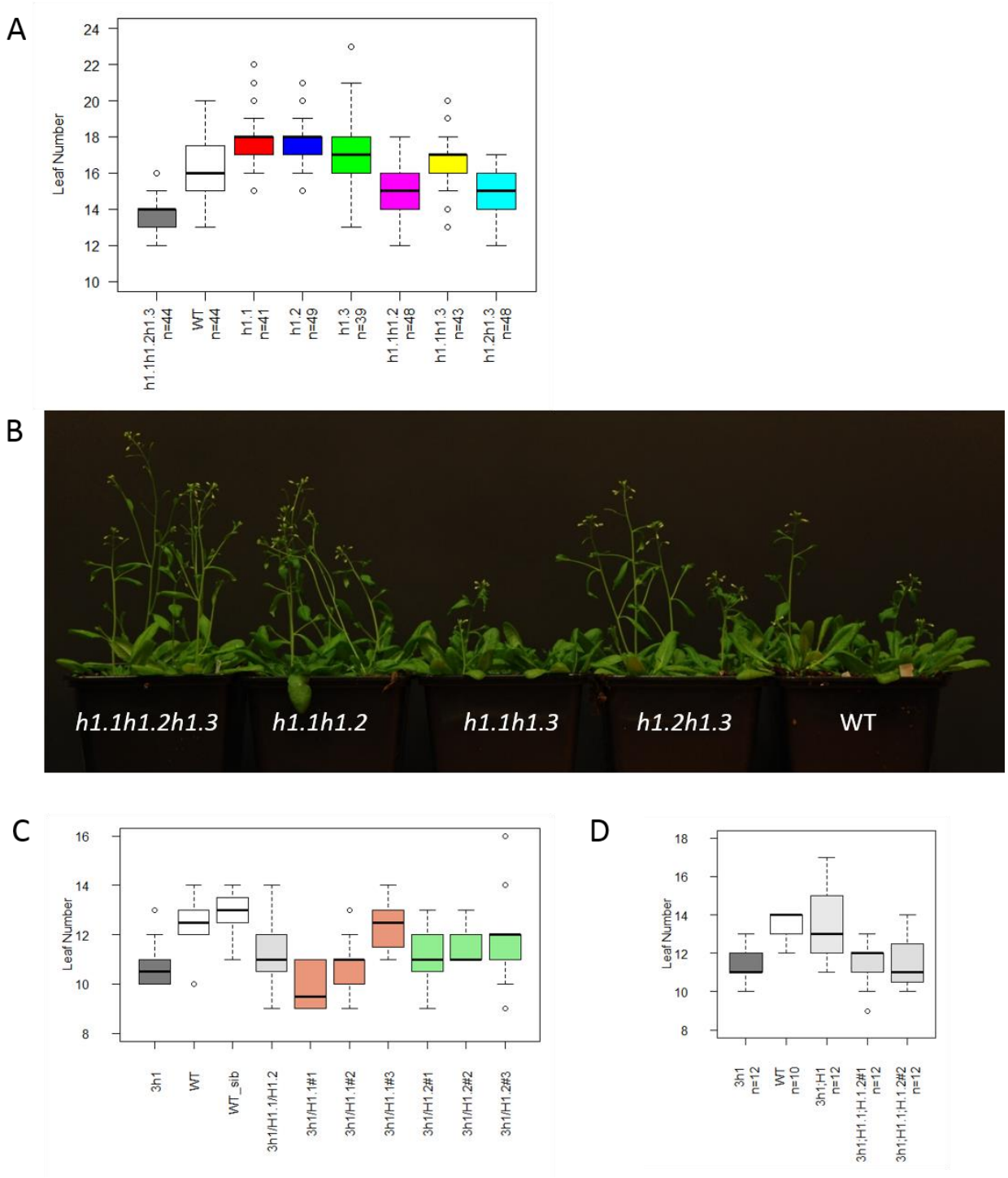

Supplement Figure 1.: Flowering time for different h1 mutants. Flowering time for different h1 mutants (Flowering time under long day conditions (16h day/8 h night); Number of leaves at bolting (~0.5 cm stem). (A) Flowering time for single and double complementation lines. (B) Picture of H1 triple mutant, double mutant and wt plants at flowering stage. (C) Flowering time for H1 triple and double complementation lines (extension of the graph from main figure). (D) Flowering time for H1 triple and single and double complementation lines.

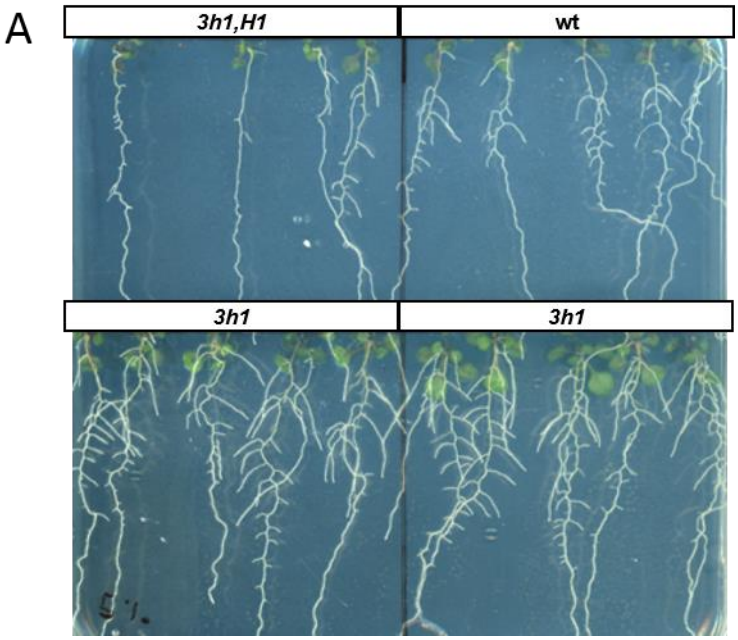

Supplement Figure 2.: Number of lateral roots for different H1 mutants. (A) Scan of plate represents the difference between number of lateral root in different *h1* mutants (8 DAG).

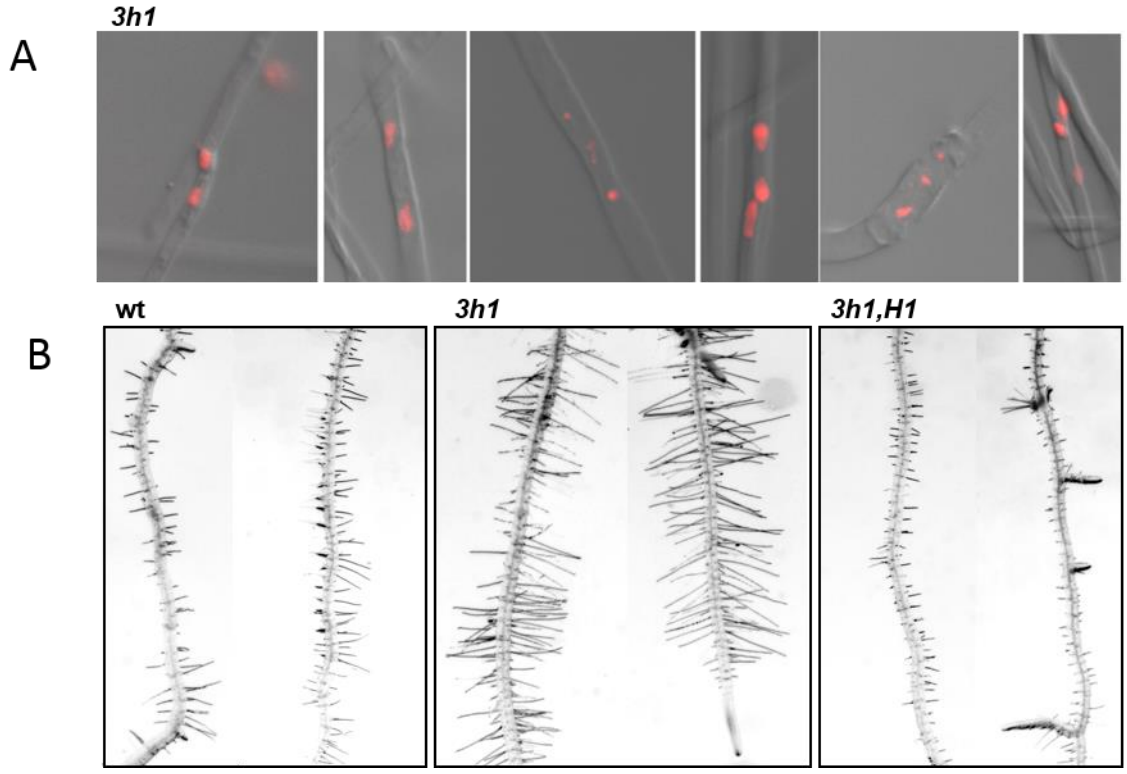

Supplement Figure 3.: Multicellular root hairs in *3h1* mutant. (A) Multicellular root hairs in *3h1* mutant, shown by H2B-RFP. (B) Phenotypes of root hairs in wild-type segregants (wt), triple mutant (*3h1*) and complemented lines expressing H1.1 variant only (*3h1;* H1).

amiRNA	**amiRNA target sequence 5'>3'**
pJS48 (amiRNA) against H1.1	TAGCCA**A**TACGCGATTCAGAA
pJS48 (amiRNA) against H1.2	TAG**C**CA**A**TACGCGATTCAGAA

Supplement table 1.: amiRNA target sequences and mismatches Underlined and in bold are the mismatches of the amiRNA within the target sequence highlighted.

VI. Chapter 2

An induction method for developmental studies in ovules of *A.thaliana*

Jasmin Schubert[1], Marta Mendes[2], Lucia Colombo[2], Hugh Dickinson[3], Ian Moore[3] Célia Baroux[1*]

[1] Institute of Plant and Microbial Biology and Zürich-Basel Plant Science Center, University of Zürich, Zollikerstrasse 107, 8008 Zürich, Switzerland.

[2] Dipartimento di Biologia, Universitá degli Studi di Milano, 20133 Milan, Italy.

[3] Department of Plant Sciences, University of Oxford, Oxford OX1 3RB, United Kingdom.

[*] Author for correspondence (cbaroux@botinst.uzh.ch).

Abbreviations	
3h1	*h1.1-1/h1.1-1;h1.2-2/h1.2-2; h1.3-2/h1.3-2*
Dex	Dexamethasone
dpi	days post induction
EtOH	Ethanol
H1.1^{wt}	*pRPS5a::LhGR2-pOP6::H1.1-RFP*
hpi	hours post induction
hrs	hours
o/N	over Night
PMC	Pollen Mother Cell
pRPS5a>>>>ΔCC-YFP	*pRPS5a::LhGR2-pOP6:: ΔCC-YFP*
RFP	Red fluorescent protein
YFP	Yellow fluorescent protein

Abstract

Background: The study of reproductive process in plants require molecular genetic approaches. Stable mutations, however, can be detrimental effects to plant development inducing sterility or abnormal development of reproductive structures impairing on the analyses. Inducible gene expression systems are thus necessary to induce genetic perturbations in a conditional manner but their use for complex structures such as the ovule deeply embedded in the flower need to be validated and a protocol need to be streamlined for reproducible and reliable induction.

Results: Here we report an application protocol enabling to control gene expression in developing ovules, *in planta*, using a dexamethasone induction system. We demonstrate its efficiency using fluorescent markers like RFP and GUS reporter genes. It allows to induce transgenes in an efficient and precise spatial and temporal manner without compromising plant fertility and temporal development.

Conclusion: Specific in vivo expression of transgenes in developing ovules allow to determine their role in gametogenesis and embryo development, which was not possible before due to systematic lethality effects.

Keywords: Arabidopsis thaliana, ovule, dexamethasone, single inflorescence, fertility

Introduction

To elucidate the genetic and molecular mechanisms of a developmental process, a classical approach consists in analyzing genetic mutants. However, stable mutations can be deleterious and compromise plant viability or fertility thus impairing the study. This is particularly true for reproductive development and for instance the analysis of early ovule development and gametogenesis. To circumvent this problem, several gene induction systems have been engineered that allow for conditional expression of a gene-of-interest in a controlled temporal and spatial manner. Those are based on chemicals such as ethanol (Roslan et al. 2001) or animal hormones such as estradiol (Zuo, Niu, and Chua 2000) or dexamethasone (Craft et al. 2005).
In the absence of Dex, the synthetic transcription factor LhGR is inactivated by the chaperone HSP90. Upon exposure to Dex, the complex dissociates, LhGR translocate to the nucleus and binds to its target, pOP promoter to promote gene transcription (Craft et al. 2005). The dexamethasone (Dex)-inducible system is appreciated for its tight and reliable gene expression control and has been widely used to study for example regulation of leaf orientation morphology (Caggiano et al. 2017), epidermal lipid production (Kannangara et al. 2007) and microtubule nucleation in *Arabidopsis thaliana* (Binarova et al. 2006). Dex induction is most of the time a straightforward process when applied by watering whole plants or incubating seedlings or tissue fragments *in vitro*. Local induction in tissues that are embedded such as the reproductive organs remain, however, challenging due to their relative inaccessibility. Here we report an optimized application method for inducing transgene expression in developing ovules of *Arabidopsis thaliana* using the Dex-inducible pOP/LhGR system (Craft et al. 2005). Using a paint brush, a single local application on floral buds with a 10 µM Dex solution dissolved in 0.1% EtOH or DMSO and 0.01% Silwet L-77 is sufficient to detect reporter gene expression after 16 h in developing ovules and anthers. The application formula does not significantly compromise fertility and temporal progression although the background solvent exert a slight negative effect. This application method is suitable to monitor effect of the transgenes over several days in the ovule and the Megaspore Mother Cell.

Results

Dexamethasone application on single inflorescences

Ovule primordia are small, digit-shape structures of 10 - 50 µM length emerging from the placenta encapsulated in the carpel, itself enclosed in the flower bud. Due to their relative inaccessibility, induction in these structures is thus not trivial. A homogenous induction was achieved by local application. First, petals and sepals of individual flower buds are gently pulled apart, without damaging the tissues, with a dissecting needle, under a stereomicroscope (Figure 1 A). Then, a drop of freshly prepared Dex solution is applied at the center of the bud with a paint brush. At that stage the drop should not dry, this is critical for the induction. To ensure that the treated plants should be well watered and placed in a closed environment overnight (Figure 1 B) before tissue harvest and sample preparation (Figure 1 C). Already after ~ 16 h of incubation efficient induction was observed (Figure 1 D and 2). Importantly, the induction solution should be prepared freshly and stored at 4°C and maximal kept for three days. The stock solution of 10 mM Dex in either

DMSO or EtOH should be stored at – 20°C and can be kept for up to one year. A second treatment can enhance the efficiency of induction but might negatively influence the health status of the treated tissue. The plant material can be either directly dissected and mounted in staining solution for image analysis (Figure 1 C1, D) or processed for GUS reporter assay (Figure 1 C2, D).

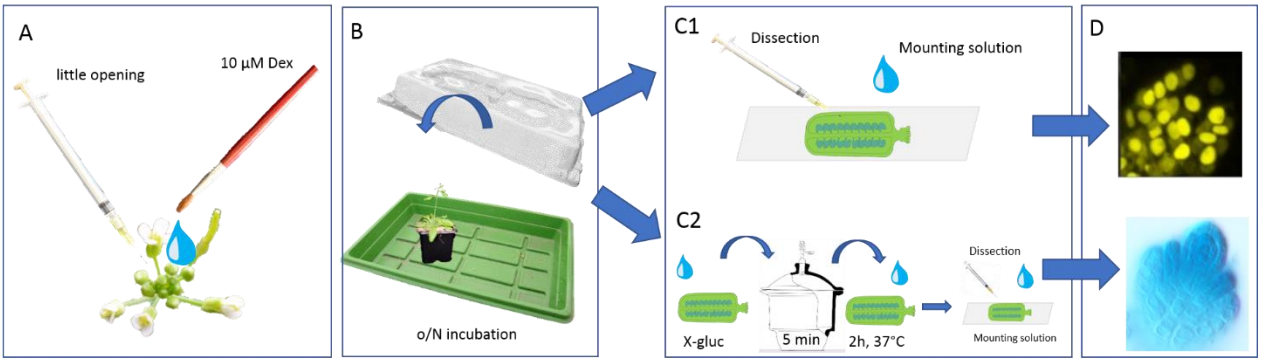

Figure. 1: Schematic representation of steps involved to induce ovules of *Arabidopsis thaliana* with Dex. (A) Single floral buds are gently opened with a dissecting needle under the stereomicroscope allow for a good exposure of the carpel and anthers to the induction solution, applied with a paint brush with soft hairs (B) Plants are kept overnight in a close environment enabling to maintain humidity. (C1) After 16 hrs or several days, carpels are dissected and mounted in 0.5x MS or counterstaining solution for microscopy observation. Alternatively, for GUS reporter detection (C2) the carpels are dissected, opened slightly, vacuum infiltrated 5 min in the staining solution and incubated for 2 h at 37°C. (D) Representative example of nuclear YFP induction (top) and GUS enzymatic reaction (bottom).

Efficient induction in carpel and anthers

For a meaningful use in gene expression control, it is important that the chemical inducer efficiently reaches a large number of organs and cells also in depth. We thus verified the efficiency of the application protocol described in Figure 1. We confirmed that reporter gene expression was induced in all ovules from within one carpel (Figure 2 A, B), throughout the depth of the entire ovule (Figure 2 C) and for different stages (Figure 2 D to G). The protocol is efficient in ovules as in anthers (Figure 3).

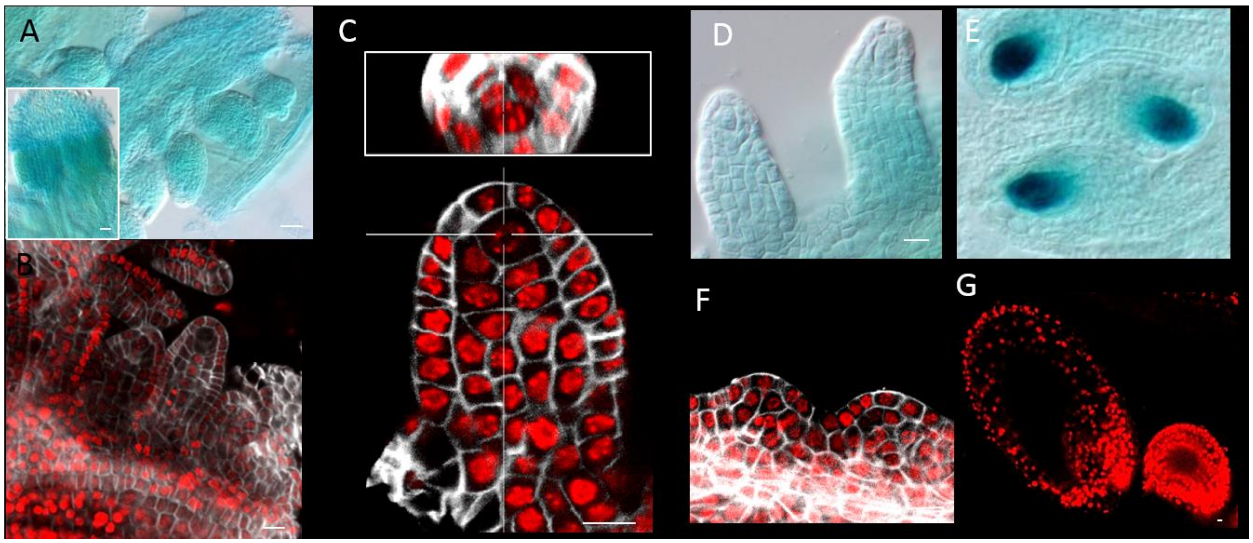

Figure 2: Induction efficiency in ovules. (A to G) Overview of GUS and fluorescent induced constructs. All constructs are driven by RPS5a promoter under Dex-inducible system. (A & B) The whole tissue is induced. (C) The cross-sections shows that the induction works through the whole tissue (depth). (D to G) Different stages of ovule development can be induced (D) stage 1-II and 2-1. (E) Functional Megaspore, (F) ovule primordia pre stage 1-0. (G) Gametophyte and fertilized female gametophyte. (A, D, E) GUS marker line, 2 mM x-Glu. (B, C, F and G) $H1.1^{wt}$-RFPand mutants fused to RFP. Scale bar = 10 µm.

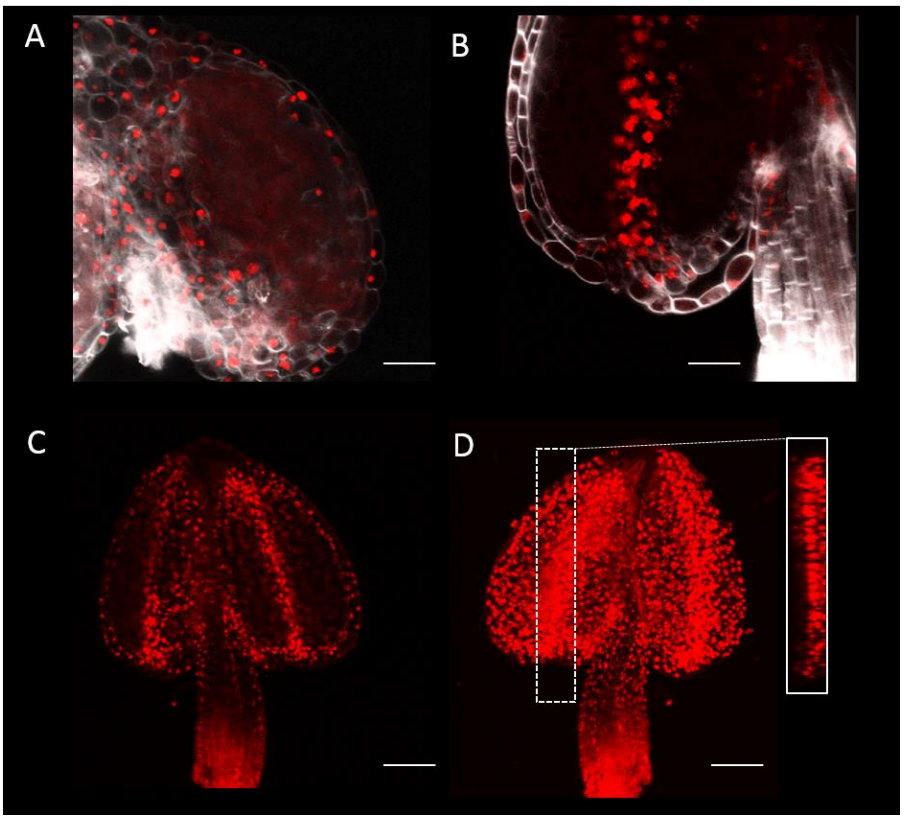

Figure 3: Induction efficiency in anthers. Anthers 5 dpi (days post induction) with 10 µM Dex express inducible chromatin marker. (A) Induced H1.1 mutant fused to RFP expression in anthers but not in PMC (Pollen Mother cells) at floral stage 5. (B) Induced H1.1 mutant fused to RFP expression in anthers but not in tetrads floral stage 10. (C and D) Floral stage 9 (H1.1 mutant fused to RFP). Scale bar = 20 µm. (D) XZ projection. (A, B and C) single plain. (D) Max. projection.

Robust induction of a variety of reporter construct with distinct subcellular localization in ovule development

With the protocol described in Figure 1. we were able to induce different constructs in ovules (Figure 4.). Ranging from membrane to nuclear and from yellow to red fluorescent markers. The signals were present earliest 17 hpi (hours post induction) until at least 7 dpi (days post induction) for the RFP lines. The same protocol was used to induce GUS enzymatic reactions in ovules. Furthermore we could not detect any leakiness of the Dex system, which means no signal in Mock-treated inflorescences with our protocol (Supplemental Figure 1).

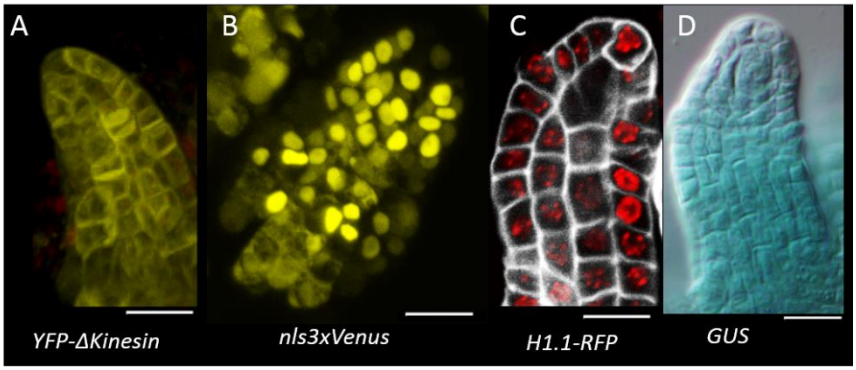

Figure 4: Robust induction of a variety of reporter construct with distinct subcellular localization in ovule development (A to C) Different constructs fused to fluorescent markers. All constructs are driven by RPS5a promoter under Dex-inducible system. (A) Intercellular trafficking compartment (*YFP-Δkinesin*), 24 hpi (h post induction). (B) Nuclear plasma marker (*nls3xmVenus*), 5 dpi. (days post induction). (C) Chromatin marker (*H1.1-RFP*), 5 dpi. (D) GUS marker, 24 hpi, 2mM x-Glu, 2 h incubation. Scale bar = 10 µm.

Impact of chemical induction on plant fertility and developmental progression

We tested the effect of different solvents of the Dex-compound, at different concentrations on the fertility of the treated inflorescences (Figure 5). We found that both EtOH and DMSO affected slightly fertility with an average seed set of 80 % (Mock versus water, Figure 5) with the lowest possible concentration of solvent (0.25% DMSO or 0.4% EtOH). In addition, the presence of Dex at 10 µM in either solvent reduced further fertility by about 15% corresponding to the corresponding Mock. (The fisher exact statistic p values for Dex vs. Mock-treatment for all three cases tested were $p < 0.00001$. Further was the Dex-treatment with 1% EtOH vs. Dex 0.4% EtOH $p < 0.00001$ and also Dex 0.4% EtOH vs. Dex DMSO $p < 0.00001$).

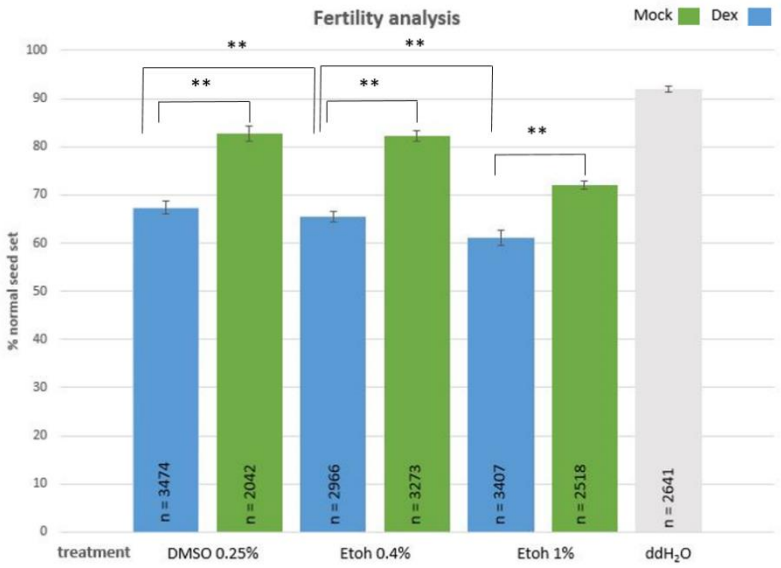

Figure. 5: Fertility analysis of Dex-treated inflorescences. Fertility was scored as the percentage of fully developed seeds in mature siliques produced by inflorescences treated with 10 µM Dex, Mock or water. Dex was either solved in DMSO or EtOH with concentrations as indicated, in a solution including 0.01% Silwet L-77. The solution was applied twice in a time window of 24 h on individual flowers as described in the text on the control plant line *YFP-Δkinesin.* Error bars = standard error to mean between replicate plants. Number of plants: n (DMSO Dex) = 11, n (DMSO Mock) = 5, n (0.4% EtOH Dex) = 8, (0.4% EtOH Mock) = 7, n (1% EtOH Dex) = 10, n (1% EtOH Mock) = 8, n (ddH_20) = 11. For each plant around 10 siliques were analyzed. The total number of seeds scored is indicated in each bar. Abnormal seeds included infertile ovules and aborted seeds. Fisher exact statistic ** = $p < 0.01$.

To determine if the Dex-treatment alters the temporal progression of ovules we treated Col-0 inflorescences with 10 µM Dex. We removed all floral buds, besides two successive floral buds and used one to determine the stage of development via microscopy after fixation and clearing. The remaining floral bud was treated with Dex and after different incubation times (72 h, 124 h) analyzed for developmental progression (Figure 6). We found no differences in ovule progression under Dex-treatment in Col-0 plants compared to the temporal developmental of ovules described in the literature (Grossniklaus and Schneitz 1998; Schneitz, Hülskamp and Pruitt 1995).

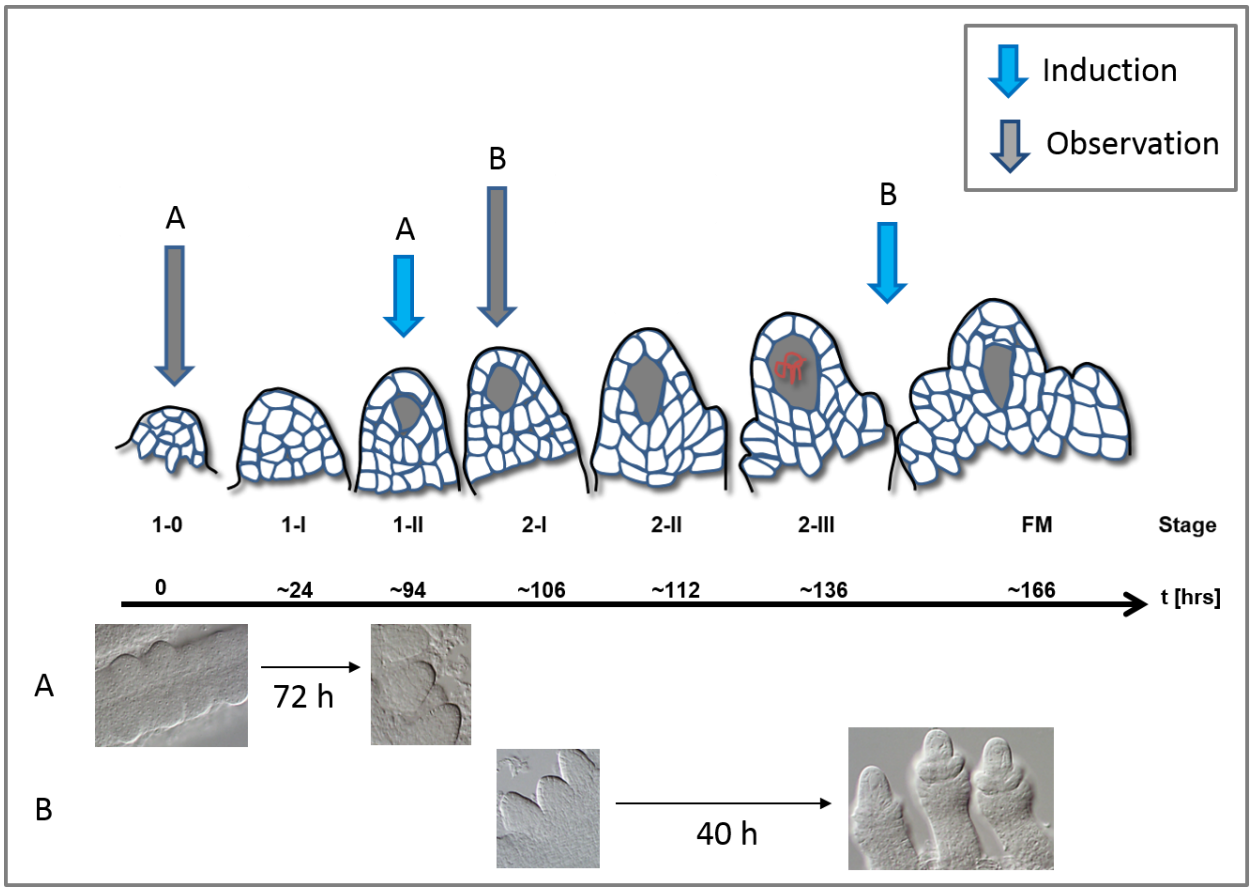

Figure 6: Temporal progression of ovule primordia under Dex-treatment. The scheme represents the temporal progression on ovules under 10 µM Dex-treatment. Further does the scheme illustrates the time of induction and the time of observation. (A & B) Col-0 floral buds were treated with 10 µM Dex (0.1% EtOH) and were analyzed after an induction time of 72 hand 40 h (A) Floral buds were treated at ovule developmental stage 1-0. (B) Floral buds were treated at ovule developmental stage 2-1.

Discussion

Chemically inducible systems offer the benefit to temporally control transgene expression (Moore, Samalova, and Kurup 2006). In combination with tissue-specific promoters driving the activator construct, such systems ultimately allow for fine tuning gene activation also spatially. However, application of the inducer remains cumbersome when the cells of interests are deeply embedded in complex tissues, such as the meiocytes and gametes. Induction by watering is not always an option if transgene activation is expected to be deleterious to plant development ahead of the stage of study. This is the case for example of genes sharing a function in both the vegetative and reproductive phase where stable misexpression through constant induction by watering may prevent floral development. To circumvent this, local application of the inducer is thus preferable. Here, we designed and tested a protocol enabling robust, rapid and efficient induction throughout the carpels and anthers of an inflorescence. The application formula contains the widely used and below a concentration of 0.05% non-toxic detergent Silwet L-77 (Clough and Bent 1998; Dehestani et al. 2010; Francko et al. 2011) which proved essential for a good penetration of the inducer in

the floral tissue. We found that one application of 10 µM Dex with a paintbrush on whole inflorescences is enough to allow a good penetration of the inducer and induce transgene expression in all ovules of the carpel. Occasionally, however, some carpels were not properly induced and this may be due to evaporation of the drop of induction media. We found out that the drop of induction medium should not dry and stay several hours on the floral bud. Covering the treated plant thus appeared as a critical step, likely by ensuring a moist environment preventing fast drying. Despite the robustness and usefulness of the application protocol, Dex-application using even a low concentration of solvent affects slightly the plant's fertility, especially on ovules, since we detected more infertile ovules than aborted seeds. This observation should be kept in mind for functional analyses. Further had the application of Dex no visible effect on the temporal progression of ovule development compared to the literature (Grossniklaus and Schneitz 1998; Schneitz, Hülskamp and Puritt 1995). Compared to other chemical based induction methods like such as ethanol (Roslan et al. 2001) and such based on animal hormones like estradiol (Zuo, Niu, and Chua 2000) has the pOP/LhGR system several advantages. Firstly it is a tight gene expression tool, since in the absence of Dex, the LhGR transcription factor is inactivated by the chaperone HSP90 and just under Dex-treatment the complex dissociates and LhGR translocate to the nucleus and binds to its target pOP promoter to activate gene transcription (Craft et al. 2005). Because of this controllable gene expression is the pOP/LhGR system highly appreciated in the scientific community and has been used in the past for various studies of gene expression (Moore, Samalova and Kurup 2006). But so far not so many studies used the pOP/LHGR system directly on reproductive organs to study also the development of those. Induction on ovules via the pOP/LHGR system has just being reported for older stages, after stage 2-I and Functional Megaspore stage (Gross-Hardt et al. 2002; Pautot et al. 2001; Zhao et al. 2017). In some of the reports the Dex-treatment was either a systematical one via watering and growth media or was sprayed on the whole plant (Gross-Hardt et al.2002; Pautot et al. 2001). The difference of the protocol we describe here, is that it is applied in a controlled local manner to circumvent systematic side effects and shows an efficient induction even in very young ovule primordia. With this study, we extended the spectrum of application of the pOP/LhGR Dex-inducible system (Craft et al. 2005) by providing a robust protocol to efficiently induce transgene expression in developing ovules.

Conclusions

We successfully adapted the Dex-induction system to define a precise application protocol to induce transgenes efficiently and local specific in gametogenesis. This allows for further investigation of genetic and molecular regulators of ovule development. The application of this method to other plant species may help to identify new modulators which are important in the female reproductive development and may finally help to understand and improve the composition and yield of the endosperm.

Material and Methods

Plant material and growth conditions

Arabidopsis seeds were sterilized in Bleach with 0.05 % Triton X-100, washed in 70% EtOH, and sown out on 1/2 Murashige and Skoog (MS) salts (CAROLINE), 1% (w/v) agar pH 5.6.
Seeds were sterilized and stored for 2 to 4 days at 4°C before transferring them to incubators (Percival) with long day conditions of 16 hours light [120 µE m-2 s-1] at 21°C and 8 hours dark at 16°C. The young plants were then transferred to soil and grown in a growth chamber with long day conditions (16 h light/ 8 h dark) at 22°C light and 18°C dark.

The nls3xmVenus (Joop Vermeer, University of Zurich) was cloned with the gateway LR reaction into the *pRPS5a-pop6-LhGR2* vector (Ian Moore, Oxford). The construct was transformed via *Agrobacterium tumefaciens* (GV3101) to Col-0 plants. Positive T1s were identified based on BASTA selection, GUS reporter assay and nls3xmVenus signal after 10 µM Dex-treatment. The RFP construct was synthetized by GeneART (Invitrogen) and cloned via Gateway into the *pRPS5a-pop6-LhGR* vector (Ian Moore, Oxford). The constructs were transformed via *Agrobacterium tumefaciens* (GV3101) to Col-0 plants. Positive T1s were identified based on BASTA selection, GUS reporter assay and RFP signal after 10 µM Dex-treatment. The YFP plasma membrane marker is a Dex-inducible *pRPS5a::LhGR2-pOP6* constructs driving a kinesin fragment fused to an YFP (Ian Moore, Oxford).

Preparation of Dex- stock and induction solution

The stock solution of 10 mM Dex in either DMSO or EtOH should be stored at – 20°C and can be kept for up to one year. Importantly, the induction solution should be prepared freshly and stored at 4°C and maximal kept for three days.

Dex Induction of ovules

Slightly open single inflorescences and paint them with a 10 µM Dex-solution containing 0.01% EtOH. Plants are kept in a high humidity surrounding o/N.

β-Glucuronidase reporter assay

Carpels are dissected and for 5 min vacuum infiltrated with 2 mM *β*-Glucuronidase (GUS) solution. Afterwards they are incubated for 2 h at 37°C in GUS solution, washed with phosphate buffer and mounted in 80 % glycerol. Imaged at the DMR (Leica).

Fluorescence analysis

For fluorescent analysis carpels are dissected and mounted in water or renaissance staining solution (final concentrations: 4% paraformaldehyde; 1:2000 renaissance; 10% glycerol; 0.05% DMSO in 1x PBS (modified from Musielak et al. 2015) and imaged at the SP5 confocal microscope (Leica).

Fertility analysis

Single inflorescences were induced twice in a time window of 24 h with10 µM Dex or Mock. After two weeks the first 10 siliques of the induced inflorescences were cut open and the seed set was measured. (n (siliques)/plan t= 10).

Determining temporal progression of ovules under Dex-induction
We removed all floral buds, besides two successive stages and used one to determine the stage of development. Therefore we fixed the floral buds in (Acetic Acid:EtOH 3:1and stored o/N at 4°C). Afterwards they were transferred in 70% EtOH and finally mounted in clearing solution (chloral hydrate: water: glycerol 8:2:1 by weight) and imaged at DMR (Leica) microscope with 20x or 40x dry objective (NA 0.75 and 0.5). The remaining floral bud was treated with 10 µM Dex-containing 0.1% EtOH and 0.01% Silwet L-77 and was analyzed as the other floral bud for temporal progression after different time periods. In total we analyzed 10 individual floral buds.

Authors' contributions
The experiments were done by JS and MM. JS wrote the manuscript.

Acknowledgements
We thank Ian Moore (Oxford, UK) for providing Plasmids.

Competing interests
The authors declare that they have no competing interests.

Availability of data and materials
The plant material analyzed during the current study are available from the corresponding author on request.

Ethics approval and consent to participate
Not applicable.

Funding
This research was funded by grants from the Swiss National Foundation to C.B.

References

Binarova, P. et al. 2006. "γ-Tubulin Is Essential for Acentrosomal Microtubule Nucleation and Coordination of Late Mitotic Events in Arabidopsis." *The Plant Cell* 18(5): 1199–1212.

Caggiano, M. P. et al. 2017. "Cell Type Boundaries Organize Plant Development." *eLife* 6: 1–32.

Clough, S. J., and Bent, A. S. 1998. "Floral Dip: A Simplified Method for Agrobacterium-Mediated Transformation of *Arabidopsis Thaliana*." *Plant Journal* 16: 735–43.

Craft, J. et al. 2005. "New pOp/LhG4 Vectors for Stringent Glucocorticoid-Dependent Transgene Expression in Arabidopsis." *The Plant Journal* 41(6): 899–918.

Dehestani, A. et al. 2010. "Transformation Efficiency Enhancement of Arabidopsis Vacuum Infiltration by Surfactant Application and Apical Inflorescence Removal." *Trakia J Sci* 8(1): 19–26.

Francko, D. A., Wilson, K. G., Qingshun, Q. L. and Equiza, M. A.. 2011. "A topical spray to enhance plant resistance to cold injury and mortality ." *Technology and Product Reports* 21(1): 109–18.

Gross-Hardt, R., Lenhard, M. and Laux, T. 2002. "WUSCHEL Signaling Functions in

Interregional Communication During Arabidopsis Ovule Development." *Genes & Development* 16: 1129–38.

Grossniklaus, U. and Schneitz, K. 1998. "The Molecular and Genetic Basis of Ovule and Megagametophyte Development." *Seminars in Cell & Developmental Biology* 9: 227–38.

Kannangara, R. et al. 2007. "The Transcription Factor WIN1/SHN1 Regulates Cutin Biosynthesis in Arabidopsis Thaliana." *The Plant Cell* 19(4): 1278–94.

Schneitz, K., Hülskamp, M. and Pruitt, R. E. 1995. "Wild-Type Ovule Development in Arabidopsis Thaliana a Light Microscope Study of Cleared Whole-Mount Tissue." *The Plant Journal* 7(5): 731–49.

Moore, I., Samalova, M. and Kurup, S. 2006. "Transactivated and Chemically Inducible Gene Expression in Plants." *The Plant Journal* 45(4): 651–83.

Pautot, V. et al. 2001. "*KNAT2*: Evidence for a Link between Knotted-like Genes and Carpel Development." *The Plant Cell* 13: 1719–34.

Roslan, H. et al. 2001. "Characterization of the Ethanol-Inducible Alc Gene-Expression System in Arabidopsis Thaliana." *The Plant Journal* 28(2): 225–35.

Zhao, X. A. et al. 2017. "RETINOBLASTOMA RELATED1 Mediates Germline Entry in Arabidopsis." *Science* 356(eaaf6532).

Zuo, J., Niu, Q. W. and Chua, N. H. 2000. "An Estrogen Receptor-Based Transactivator XVE Mediates Highly Inducible Gene Expression in Transgenic Plants." *Plant Journal* 24(2): 265–73.

Supplementary Chapter 2:

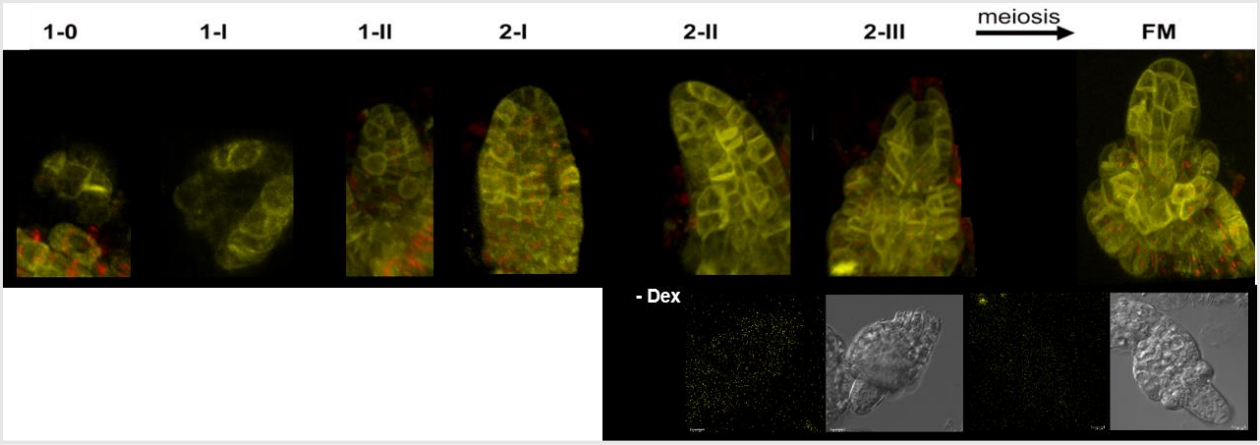

Supplementary figure 1: Figure. S1: Flower buds from the pRPS5a>>ΔCC-YFP reporter line [unpublished, Ian Moore, Oxford] were painted with a solution of 10μM Dex, 0.1% EtOH, 0.01% Silwet L-77, left on the plant for 16 – 18 hr until collection for imaging.

VII. Chapter 3

Establishing plant lines and experimental scheme for robust functional test of H1 candidate modifiers

Abbreviations	
3h1	*h1.1-1/h1.1-1;h1.2-2/h1.2-2; h1.3-2/h1.3-2*
BG	*h1.1-1/h1.1-1;h1.2-2/h1.2-2; h1.3-2/h1.3-2; pH1.1::H1.1-GFP/pH1.1::H1.1-GFP; pH1.2::H1.2-ECFP/pH1.2::H1.2-ECFP* background line
Dex	Dexamethasone
dpi	days post induction
ECFP	Enhanced cyan fluorescent protein
EtOH	Ethanol
FM	Functional Megaspore
GFP	Green fluorescent protein
H1.1^{wt}RFP	*pRPS5a::LhGR2-pOP6::H1.1-RFP*
H1.1*RFP	*pRPS5a::LhGR2-pOP6::H1.1*RFP*
hpi	hours post induction
MMC	Megaspore Mother Cell
o/N	over Night
PCR	Polymerase Chain Reaction
PMC	Pollen Mother Cell
pRPS5a>>amiRNA[X]	*pRPS5a**::**LhGR2-pOP6**::**amiRNA[X]*
pRPS5a>>mVenus	*pRPS5a**::**LhGR2-pOP6**::**nls3xmVenus*
RFP	Red fluorescent protein

1. Generation, screen and validation of a background reporter line

One of the aims of my project is to downregulate candidate factors regulating H1 stability. In order to visually screen for altered H1 dynamics in the engineered mutant lines I generated a background reporter line co-expressing tagged H1.1 and H1.2 variants in the triple h1 mutant and thereafter referred to as **BG line**. The vector *pH1.1::H1.1-GFP* was retransformed into the triple h1 mutant (*3h1*) plants described in (Rutowicz et al. 2015). Positive offspring were selected based on Hygromycin resistance and GFP signal in ovule primordia. We selected single insertion T2 plants based on segregation analysis and a molecular validation using Digital Droplet PCR (Bio-RAD, QX200 system) of Hygromycin. We also checked homozygous *pH1.2::H1.2-ECFP*; *3h1* plant lines (She et al. 2013) via Digital Droplet PCR (Bio-RAD) of Hygromycin for single insertions. The primers 5'-TCTGCGGGCGATTTGTGTA-3'; 5'-TTCGGCTCCAACAATGTCC-3' were used and amplification levels were normalized against FIE. FIE primers: 5'-TAGCAAAGCGGTAAATATCACG-3'; 5'-TGAAGTTCTAAGTGTGGTGAGCCA-3'. The plants which were identified via Digital Droplet PCR to contain a single insertion of either *pH1.1::H1.1-*

GFP or *pH1.2::H1.2-ECFP* (Supplement Table 1) were used for crossing to each other. The offspring of the cross were selected on Hygromycin and Kanamycin and screened for both GFP and ECFP signals. Homozygous lines for both constructs in the *3h1* background were identified by i) screening pollen for two GFP signals, one in each sperm cell (Figure 1) and ii) by screening their offspring for ECFP signals in young seedlings (Figure 1). The lines positive identified for single insertion and homozygosity for all constructs were used in the following experiments as BG lines: JS65, JS67 and JS68 (Supplement Table 2). Those three lines were analyzed for H1.1 and H1.2 presence during Mega Spore Mother Cell (MMC) development via microscopy. We found a similar H1.1 and H1.2 dynamics as described by She and colleagues (She et al. 2013)(Figure 2).

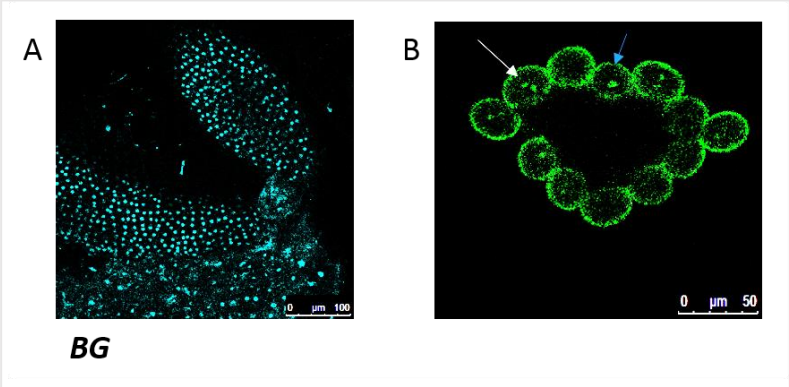

Figure 1: Selection of homozygote plants for BG line. (A) Selection of homozygous plants for *pH1.2::H1.2-ECFP* constructs by microscopy. One week old seedlings were screened for ECFP signal. (A) Scale Bar = 100 µm. (B) Selection of homozygous plants for *H1.1::H1.1-GFP* constructs by microscopy. Pollen were screened for one GFP signal in each sperm cell. The white arrow points to a pollen with two GFP signals, one in each sperm cell and the blue arrow to a pollen where just one sperm cell shows a GFP signal. Scale Bar = 50 µm.

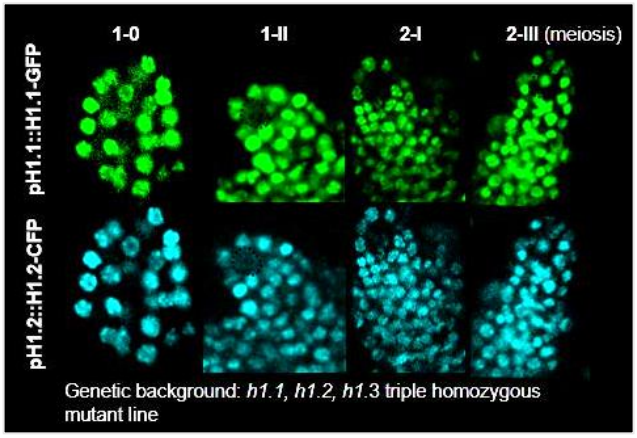

Figure 2: Screen for linker histone dynamics during Megaspore Mother Cell (MMC) development in BG line. The homozygous BG plant lines were screened for linker histone presence during MMC development. The BG line shows a similar linker histone dynamics as that described by She and colleagues (She et al. 2013).

2. The vector-set and cloning scheme of the Dex-inducible system used throughout this thesis

In the following chapters, several H1 mutant variants are described that were generated and expressed in plants; in addition downregulation experiments relied on artificial micro RNAs synthetized by Genescript, GeneART (Invitrogen) or by PCR using primer sets designed on the wmd3 database (Schwab, Ossowski, and Warthmann 2010) or the phantom database (Hauser et al. 2013) and cloned via Gateway system (Hartley, Temple, and Brasch 2000) into the

pRPS5a::LhGR2-pOP6 vector (Ian Moore, Oxford), (Craft et al. 2005) (Figure 3A). This vector comprises a Gateway-compatible cassette to allow for the cloning of a gene-of-interest cloned downstream the synthetic promoter pOP6. Gene expression is conditional thanks to the Dex- LR reaction inducible transcription factor LhGR2 (Craft et al. 2005). Here the promoter of RIBOSOMAL PROTEIN SUBUNIT 5A (RPS5a) (Weijers et al. 2001) ensures LhGR2 expression in a near-ubiquitous manner throughout the plant. The induction control consisting in a H1.1-RFP variant was cloned with the Gateway (Hartley, Temple, and Brasch 2000) into the *pRPS5a::LhGR2-pOP6* vector (Ian Moore, Oxford), (Craft et al. 2005) (Figure 3A). The polycistronic amiRNAs against candidate H1 regulators (See chapter 4 to 6) were either synthesized by GeneART (Invitrogen) with attL sites directly adjacent to clone them via Gateway cloning into the *pRPS5a::LhGR2-pOP6* vector. Alternatively they were designed using the wmd3 database (Schwab, Ossowski, and Warthmann 2010) or the phantom database (Hauser et al. 2013) and cloned into the D-TOPO vector via the CACC sequence. In the last case, we added by PCR an additional EcoRI site on amiRNAJS2 (see chapter 4) and used this site to cut the amiRNA out of the D-TOPO vector and cloned it via ligation reaction into the D-TOPO vector containing the other amiRNA. The D-TOPO vector, which contains containing both amiRNAs was cloned via Gateway cloning into *pRPS5a::LhGR2-pOP6* (Figure 3B).

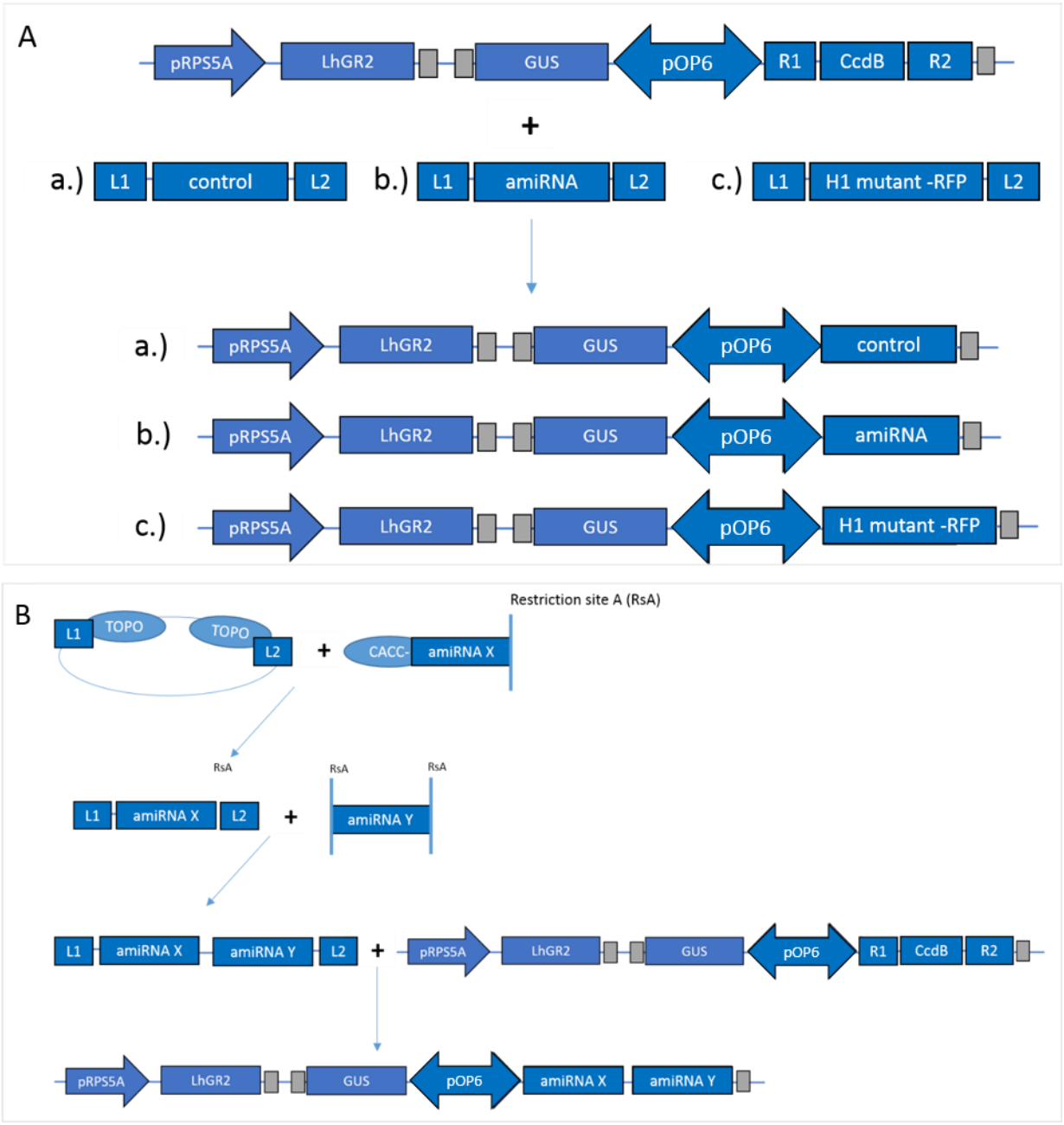

Figure 3: Cloning strategy for Dex-inducible H1 modifiers. (A) Cloning scheme of a.) inducible control b.) single amiRNA and c.) H1 mutant variants. The *pRPS5a::LhGR2-pOP6* vector includes an CcdB site in which we cloned via Gateway cloning either the inducible control, a single amiRNA or an H1 mutant variant. (B) Cloning scheme of Dex-inducible polycistronic amiRNAs. We synthesized two amiRNAs via PCR. On one of the amiRNAs we added the CACC D-TOPO cloning sequence. Via this sequence, we cloned the amiRNA into the D-TOPO vector. By restriction digest (RsA = Restriction site A) we cut one amiRNA out of the D-TOPO vector and cloned it via ligation behind the first amiRNA into the D-TOPO vector. The polycistronic amiRNAs were cloned via Gateway cloning into the *pRPS5a::LhGR2-pOP6* vector. The final cloning product is the *pRPS5a>>amiRNA[X]-amiRNA[Y]*.

The Dex-inducible system works (Craft et al. 2005) on the molecular level via the synthetic transcription factor LhGR, which is driven by a promoter of choice, in our case by the RPS5a promoter (Weijers et al. 2001)(Figure 4). In the absence of Dex, the synthetic transcription factor LhGR is inactivated by the chaperone HSP90. Upon exposure to Dex, the complex dissociates, LhGR translocates to the nucleus and binds to its target, pOP6 promoter to promote gene transcription of the target gene, which is in our case either an H1 mutant variant, an amiRNA(s) or an induction control construct.

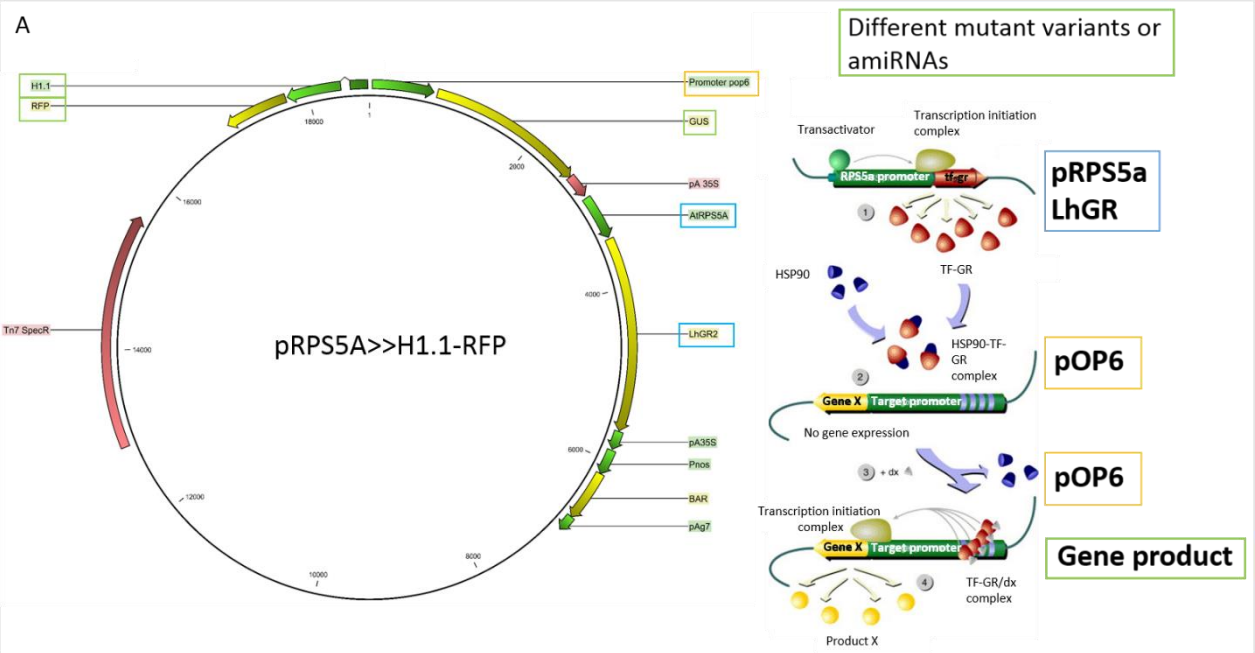

Figure 4: Vector map of Dex-inducible pRPS5a construct with molecular illustration of Dex-system. (A) In the vector map of the Dex-inducible *pRPS5a>>H1.1-RFP* we highlighted the individual cassettes of the Dex-inducible system. It is to highlight that the vector which we used for our experiments also contains a GUS reporter under the control of the *poP6* promoter, which is also activated after Dex-induction. The H1.1-RFP ($H1.1^{wt}$) is in some constructs replaced by other H1 mutants or amiRNAs. On the right site are the molecular steps of the Dex-induction process highlighted. The illustrations show that the synthetic transcription factor LhGR is driven by a promoter of choice, in our case by the *RPS5a* promoter, in the illustration by the *CaMV35S* promoter. In the absence of Dex, the synthetic transcription factor LhGR is inactivated by the chaperone HSP90. Upon exposure to Dex, the complex dissociates, LhGR translocates to the nucleus and binds to its target, the *pOP6* promoter to activate in turn gene transcription of the downstream genes. Due to the palindromic nature of the pOP6 promoter, bidirectional transcription is initiated that allows coordinated expression of the GUS reporter gene and the gene-of-interest cloned in the *att* cassette. Picture adapted and modified from (Gatz and Lenk 1998).

3. Experimental design for functional test using the inducible system

Two distinct strategies were used to generate fluorescently tagged H1 mutant variants and plants expressing amiRNAs against candidate regulators: The inducible H1.1^{wt}RFP control construct, the inducible nls3xmVenus (Koushik et al. 2006) control construct and the H1.1*RFP constructs expressing mutant variants (H1.1*) were transformed and via *Agrobacterium tumefaciens* (GV3101) into *Arabidopsis thaliana* Columbia-0 (Col-0) plants. Positive T1s were identified based on BASTA selection. Afterwards, we pre-selected Dex-responsive lines by a GUS reporter assay, since the *pRPS5a::LhGR2-pOP6* vector also contains a GUS reporter gene under the control of the same pOP6 promoter that drives our gene of interest (H1.1-RFP variants) (Figure 4) and is thus expressed after Dex-induction. Finally, we confirmed the expression of the gene-of-interest by checking RFP or nls3xmVenus signals in carpels following 17 h of 10 µM Dex-treatment as described in chapter 2 of this thesis (Figure 5 A). The same procedure was followed to identify positive T2 plants.

The Dex-inducible single amiRNAs and Dex-inducible polycistronic amiRNAs were transformed by *Agrobacterium tumefaciens* (GV3101) to our BG lines. Positive T1s were identified based on BASTA selection. Afterwards we pre-selected Dex-responsive lines by GUS staining. This step is for the amiRNA lines quite important, since it is the only control of functional induction. Induction of amiRNA cannot be directly verified. Following, positive plants were screened for an absence or change of the H1.1-GFP or H1.2-ECFP signal after Dex-induction that would reveal a possible effect of the candidate amiRNA on H1 turnover (Figure 5 B). The same procedure was followed to identify and verify positive T2 progenies.

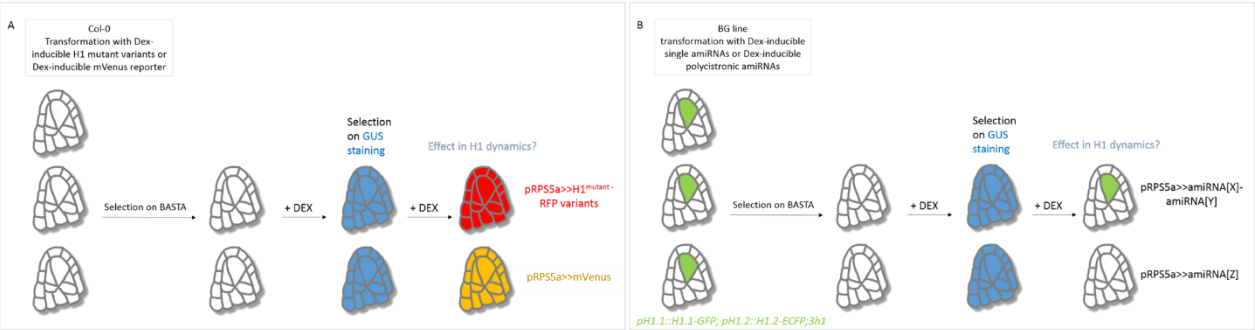

Figure 5: Scheme to identify positively transformed plants and functional screen of altered H1 dynamics. (A) Col-0 plants are transformed with Dex-inducible H1 mutant variants or an induction control reporter construct. The transformed plants are selected on BASTA and on GUS reporter assay after treatment with 10 µM Dex. Plants which show a positive GUS enzymatic reaction, are further screened for RFP signal in plants transformed with the H1 mutant variant construct and for mVenus signal in the plants transformed with the induction control reporter construct. Plants identified as positive transformed are used to screen for effects in H1 dynamics after several hours after Dex-treatment. (B) BG plants are transformed with Dex-inducible single or polycistronic amiRNAs. The transformed plants pre-selected on BASTA and are further screened by a GUS reporter assay after treatment with 10 µM Dex. Plants which showed a positive GUS histochemical reaction are further used to screen for altered GFP (*pH1.1::H1.1-GFP*) and ECFP (*pH1.2::H1.2-ECFP*) signals after 17 to 120 hours post-Dex-induction depending on the experiment.

Precise induction- and analysis timing are important to get information about the influence of the different Dex-inducible constructs on ovule development. In chapter 2 of this thesis, we already described that the treatment of ovule primordia with 10 µM Dex does not alter the temporal progression of ovules in *Arabidopsis thaliana* compared to what was described in the literature (Grossniklaus and Schneitz 1998; Schneitz, Hülskamp and Pruitt 1995). We estimated that a 94 hrs time window post-Dex-induction would allow ovules at stage 1-0 to proceed beyond stage 1-II after which H1 eviction is normally observed. Similarly, we estimated that 120 hrs post induction would allow observing ovules at stage ~2-II (Figure 6). However, it would be good to thoroughly determined whether this estimated developmental progression is also valid under Dex-treatment for time points longer than 120 hpi. Certainly, ovule primordia expressing H1.1^{wt}RFP ranging from 24 hpi up to 120 hpi displayed a homogenous staining throughout all cells (except in the MMC as expected) (Figure 4, chapter 2) which suggest that H1.1^{wt}RFP was induced early during development (hence stage 1-0 or younger) otherwise a mosaic staining would be expected.

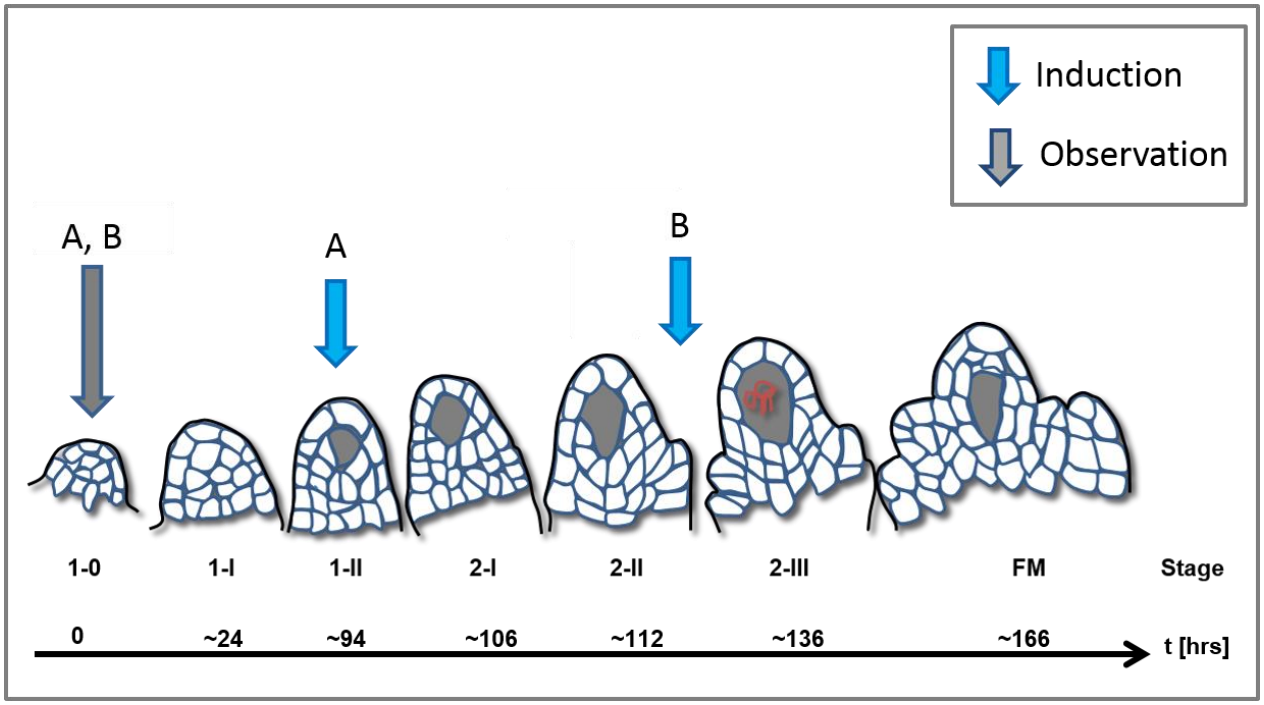

Figure 6: Induction timing and temporal progression of ovule primordia under Dex-treatment. The scheme represents the temporal progression of ovules in *Arabidopsis thaliana* (stages) under 10 µM Dex-treatment. Further, does the scheme illustrate at which stage Dex was applied and after what time or at which developmental stage microscopy observations were done. (A & B) Col-0 floral buds were treated with 10 µM Dex at developmental stage 1-0 or even before that developmental stage. Floral buds were analyzed (A) 94 hpi and (B) 5 dpi (120 hpi).

References

Craft, Judith et al. 2005. "New pOp/LhG4 Vectors for Stringent Glucocorticoid-Dependent Transgene Expression in Arabidopsis." *The Plant journal : for cell and molecular biology* 41(6): 899–918.

Gatz, Christiane, and Ingo Lenk. 1998. “Promoters That Respond to Chemical Inducers.” *Trends in Plant Science* 3(9): 352–58.

Grossniklaus, U, and K Schneitz. 1998. “The Molecular and Genetic Basis of Ovule and Megagametophyte Development.” *Seminars in cell & developmental biology* 9: 227–38.

Hartley, James L., Gary F. Temple, and Michael A. Brasch. 2000. “DNA Cloning Using In Vitro Site-Specific Recombination.” *Genome Research* 10(11): 1788–95.

Hauser, Felix et al. 2013. “A Genomic-Scale Artificial microRNA Library as a Tool to Investigate the Functionally Redundant Gene Space in Arabidopsis.” *The Plant cell* 25(8): 2848–63.

Kay Schneitz, Martin Hülskamp, Robert E. Pruitt. 1995. “Wild-Type Ovule Development in Arabidopsis Thaliana a Light Microscope Study of Cleared Whole-Mount Tissue.pdf.” *The Plant Journal* 7(5): 731–49.

Koushik, Srinagesh V. et al. 2006. “Cerulean, Venus, and venusY67C FRET Reference Standards.” *Biophysical Journal* 91(12): L99–101.

Rutowicz, Kinga et al. 2015. “A Specialized Histone H1 Variant Is Required for Adaptive Responses to Complex Abiotic Stress and Related DNA Methylation in Arabidopsis.” *Plant physiology* 169(November): 2080–2101.

Schwab, Rebecca, Stephan Ossowski, and Norman Warthmann. 2010. “Plant MicroRNAs” eds. Blake C. Meyers and Pamela J. Green. 592: 71–88. http://link.springer.com/10.1007/978-1-60327-005-2 (July 24, 2014).

She, Wenjing et al. 2013. “Chromatin Reprogramming during the Somatic-to-Reproductive Cell Fate Transition in Plants.” *Development (Cambridge, England)* 140(19): 4008–19.

Weijers, D. et al. 2001. “An Arabidopsis Minute-like Phenotype Caused by a Semi-Dominant Mutation in a RIBOSOMAL PROTEIN S5 Gene.” *Development (Cambridge, England)* 128(21): 4289–99.

Supplement Information chapter 3:

Digital Droplet PCR		
Plant	**Insertion**	**Genotype**
JS38#3	single	*h1.1-1/h1.1-1;h1.2-2/h1.2-2; h1.3-2/h1.3-2; pH1.1::H1.1-GFP/pH1.1::H1.1-GFP*
JS38#11	multi	*h1.1-1/h1.1-1;h1.2-2/h1.2-2; h1.3-2/h1.3-2; pH1.1::H1.1-GFP/pH1.1::H1.1-GFP*
JS38#20	single	*h1.1-1/h1.1-1;h1.2-2/h1.2-2; h1.3-2/h1.3-2; pH1.1::H1.1-GFP/pH1.1::H1.1-GFP*
JS38#12	single	*h1.1-1/h1.1-1;h1.2-2/h1.2-2; h1.3-2/h1.3-2; pH1.1::H1.1-GFP/pH1.1::H1.1-GFP*
JS38#14	single	*h1.1-1/h1.1-1;h1.2-2/h1.2-2; h1.3-2/h1.3-2; pH1.1::H1.1-GFP/pH1.1::H1.1-GFP*
JS38#15	double	*h1.1-1/h1.1-1;h1.2-2/h1.2-2; h1.3-2/h1.3-2; pH1.1::H1.1-GFP/pH1.1::H1.1-GFP*
JS44#3	single	*h1.1-1/h1.1-1;h1.2-2/h1.2-2; h1.3-2/h1.3-2; pH1.2::H1.2-ECFP/-*
JS41#5	single or double	*h1.1-1/h1.1-1;h1.2-2/h1.2-2; h1.3-2/h1.3-2; pH1.2::H1.2-ECFP/pH1.2::H1.2-ECFP*
JS41#6	single	*h1.1-1/h1.1-1;h1.2-2/h1.2-2; h1.3-2/h1.3-2; pH1.2::H1.2-ECFP/-*
JS41#7	single	*h1.1-1/h1.1-1;h1.2-2/h1.2-2; h1.3-2/h1.3-2; pH1.2::H1.2-ECFP/-*
JS41#10	single	*h1.1-1/h1.1-1;h1.2-2/h1.2-2; h1.3-2/h1.3-2; pH1.2::H1.2-ECFP/-*
JS42#1	single	*h1.1-1/h1.1-1;h1.2-2/h1.2-2; h1.3-2/h1.3-2; pH1.2::H1.2-ECFP/-*
JS44#5	double	*h1.1-1/h1.1-1;h1.2-2/h1.2-2; h1.3-2/h1.3-2; pH1.2::H1.2-ECFP/pH1.2::H1.2-ECFP*
JS44#8	single or double	*h1.1-1/h1.1-1;h1.2-2/h1.2-2; h1.3-2/h1.3-2; pH1.2::H1.2-ECFP/pH1.2::H1.2-ECFP*
JS44#10	single	*h1.1-1/h1.1-1;h1.2-2/h1.2-2; h1.3-2/h1.3-2; pH1.2::H1.2-ECFP/-*
JS42#5	single	*h1.1-1/h1.1-1;h1.2-2/h1.2-2; h1.3-2/h1.3-2; pH1.2::H1.2-ECFP/-*
JS42#8	single	*h1.1-1/h1.1-1;h1.2-2/h1.2-2; h1.3-2/h1.3-2; pH1.2::H1.2-ECFP/-*
JS42#9	single	*h1.1-1/h1.1-1;h1.2-2/h1.2-2; h1.3-2/h1.3-2; pH1.2::H1.2-ECFP/-*

Supplement Table 1: Digital Droplet PCR identified single insertion lines.

Crossing scheme		
female	**male**	**BG line**
JS38#12 (*h1.1-1/h1.1-1;h1.2-2/h1.2-2; h1.3-2/h1.3-2; pH1.1::H1.1-GFP/pH1.1::H1.1-GFP*)	JS41#5(*h1.1-1/h1.1-1;h1.2-2/h1.2-2; h1.3-2/h1.3-2; pH1.2::H1.2-ECFP/pH1.2::H1.2-ECFP*)	JS65, (JS66)
JS38#3 (*h1.1-1/h1.1-1;h1.2-2/h1.2-2; h1.3-2/h1.3-2; pH1.1::H1.1-GFP/pH1.1::H1.1-GFP*)	JS44#8 (*h1.1-1/h1.1-1;h1.2-2/h1.2-2; h1.3-2/h1.3-2; pH1.2::H1.2-ECFP/pH1.2::H1.2-ECFP*)	JS68
JS44#8 (*h1.1-1/h1.1-1;h1.2-2/h1.2-2; h1.3-2/h1.3-2; pH1.2::H1.2-ECFP/pH1.2::H1.2-ECFP*)	JS38#12 (*h1.1-1/h1.1-1;h1.2-2/h1.2-2; h1.3-2/h1.3-2; pH1.1::H1.1-GFP/pH1.1::H1.1-GFP*)	JS67
JS38#3 (*h1.1-1/h1.1-1;h1.2-2/h1.2-2; h1.3-2/h1.3-2; pH1.1::H1.1-GFP/pH1.1::H1.1-GFP*)	JS44#8 (*h1.1-1/h1.1-1;h1.2-2/h1.2-2; h1.3-2/h1.3-2; pH1.2::H1.2-ECFP/pH1.2::H1.2-ECFP*)	JS64

Supplement Table 2: Parental lines used for the generation of three background (BG) lines.

VIII. Chapter 4

Inducible amiRNAs against *NAPs*, *NRPs*, *HIRA* and their effect on linker histone dynamics during sporogenesis in *Arabidopsis thaliana*

Abbreviations	
3h1	*h1.1-1/h1.1-1;h1.2-2/h1.2-2;h1.3-2/h1.3-2*
amiRNA[HIRA]	*pRPS5a::LhGR2-GUS::pOP6::amiRNA[HIRA]*; BG
amiRNA[NAPs]-amiRNA[NRPs]	*pRPS5a::LhGR2-GUS::pOP6::amiRNA[NAPs]-amiRNA[NRPs]*; BG
BG	*h1.1-1/h1.1-1;h1.2-2/h1.2-2;h1.3-2/h1.3-2 pH1.1::H1.1-GFP/pH1.1::H1.1-GFP; pH1.2::H1.2-ECFP/pH1.2::H1.2-ECFP* background line
Dex	Dexamethasone
DNA	Deoxyribonucleic acid
dpi	days post induction
ECFP	Enhanced cyan fluorescent protein
EtOH	Ethanol
GFP	Green fluorescent protein
$H1.1^{wt}$	*pRPS5a::LhGR2-GUS::pOP6::H1.1-RFP*
hpi	hours post induction
hrs	hours
MMC	Megaspore Mother Cell
o/N	over Night
PCR	Polymerase Chain Reaction
PMC	Pollen Mother Cell
RFP	Red fluorescent protein
WT	Wild-type

Abstract

Linker histones show a dynamic presence during sporogenesis in *Arabidopsis thaliana* (She et al. 2013). In this chapter, we ask whether histone chaperones are involved in this dynamic linker histone presence during sporogenesis. To answer this question we first analyzed publicly available expression data on histone chaperones to identify putative candidates and generated inducible knockdown lines of them to monitor for aberrant linker histone dynamics during sporogenesis. Here we report the test of the NUCLEOSOME ASSEMBLY PROTEIN family (NAPs) and two NAP-RELATED PROTEIN (NRPs) and of HOMOLOG OF HISTONE CHAPERONE (HIRA) as putative candidates to be involved in regulating histone dynamics during sporogenesis in Arabidopsis. We further created and analyzed independent insertion lines, in which we successfully induced a knockdown of the histone chaperone *HIRA* in a conditional manner and used those lines to monitor for developmental changes during plant sporogenesis.

Introduction

Histone chaperones are evolutionarily conserved from yeast over humans and have been shown to play a role in chromatin dis- and reassembly by direct and indirect interacting with histones (Gao et al. 2012; Zhu et al. 2006). In single molecule interaction studies it was shown, that histone chaperones of the NAP (NUCLEOSOME ASSEMBLY PROTEIN) family contribute to the turnover of H1s, by modulating the binding of H1 to the nucleosome *in vitro* and in isolated HeLa cells (Kepert et al. 2005; Yue et al. 2016). In addition, it was found that NAP1 and another histone chaperone HIRA (HOMOLOG OF HISTONE CHAPERONE) are involved in H1 eviction in the formation of the mouse germline (Hajkova et al. 2008).

Studies during plants sporogenesis in *Arabidopsis thaliana* found a dynamic presence of linker histones during Megaspore Mother Cell (MMC) development (She et al. 2013). What is not known, is how this process is regulated and if histone chaperones are involved in linker histone eviction and reloading. This chapter describes the test whether the above-mentioned histone chaperones are involved in linker histone dynamics in MMC development in *A. thaliana*.

The model plant *Arabidopsis thaliana* contains four variants of the histone chaperone *NAP1*: *NAP1;1* to *NAP1;4* and two variants of *NAP1-RELATED PROTEINs*, *NRP1* and *NRP2*. The two last ones have been described as nuclear expressed and binding to H2A/H2B. Interestingly the double mutant *nrp1nrp2* shows a perturbed expression of hundreds of genes in Arabidopsis (Zhu et al. 2006).

Moreover, *A. thaliana* contains one homologue of the animal histone chaperone *HIRA* (Duc et al. 2015), which was already mentioned above to play a role in the formation of the animal germline (Hajkova et al. 2008). In plants, HIRA is responsible for the deposition of H3.3/H3.1 what plays an important role in reprogramming events associated with differentiation and responsiveness to the environment (Nie et al. 2014).

To answer the question whether histone chaperones NAPs, NRPs and HIRA are involved in linker histone dynamics in the MMC during female sporogenesis (She et al. 2013) we designed Arabidopsis knockdown mutants of these histone chaperones.

In plants, the phenotype of loss-of-function mutant *hira* varies from embryo lethality (Phelps-durr et al. 2005) to mild phenotypes in adult plants (Duc et al. 2015; Nie et al. 2014). This variable and partly sever phenotypes precluded to use these mutants for our analyses in the Arabidopsis germline. In contrast the sexadruple mutant of *nap1;1-4,nrp1-2* displays no strong compromise in development under laboratory standards (Zhou et al. 2016). This is partly in contradiction with observations done previously in our lab under our growth conditions (Baroux, unpublished), we found a severely compromised developmental phenotype already in the quadruple mutant of *nap1;1-1,nap1;2-1,nap1;3-1,nap1;4-1*. Therefore to test our hypothesis we used the dexamethasone (Dex)-inducible system (described in chapter 2) to downregulate the histone chaperones via an amiRNA approach.

Our preliminary results indicate that we can successfully downregulate *HIRA* in a conditional manner. However the initial experiments did not indicate a role of NAPs, NRPs or HIRA in linker histone dynamics during female sporogenesis, but this needs to be further confirmed.

Results

Expression of *NAPs*, *NRPs* and *HIRA* during plant reproduction

Data about animal histone chaperone expressions, direct us to find out if their Arabidopsis homologs have a similar expression pattern. We used published RNA-Seq and Microarray data sets to check if the histone chaperones, *NAPs*, *NRPs* and *HIRA* are expressed in reproductive tissues. Figure 1 shows the relative expression level of *NRP1*, *NRP2*, *HIRA*, *NAP1;2* and *NAP1;4* based on RNA-Seq data from Wuest and colleagues (Wuest et al. 2010) and based on Affymetrix ATH1 GeneCHIP data from different publications (Borges et al. 2008; Honys and Twell 2004; Pina and Pinto 2005; Schmidt et al. 2011). The script used for analyzing the RNA-Seq and Microarray data can be found at "https://github.com/VimalRawat1010/Rscripts/blob/master/LabData/.RData".

NRP1 has the highest relative expression in the egg cell compared to the other tested tissues. *NRP2*, *NAP1;2* and *HIRA* show that each of them has a low expression in the synergids, central cells and egg cell compared to their expression in the tromped stage embryo. An opposite expression pattern shows *NAP1;4*. It has the highest z-scores in the male reproductive organs like the PMC (Pollen Mother Cell). The microarray expression data in Figure 1 B confirms the values of *NAP1;4* in the male reproductive tissue. It is present from the earlier developmental stages of unicellular pollen and keeps being expressed in bicellular pollen until their maturity. In the female reproductive tissues, it has a slightly lower z-score in the MMC and in the egg cell compared to some other tissues tested. Looking at the relative expression values of *NAP1;1* and *NAP1;3* in the microarray data it shows that they have a low expression in the ovule, albeit not the lowest compared to their expression in other tissues.

Regarding the Microarray expression data of the *NRPs*, the heat map shows that both *NRP*s are expressed in the ovule. Whereby *NRP2* is also expressed in the MMC, albeit it has a higher expression in the uni- and bicellular pollen. Both *NRPs* have a lower z-score in the egg and central cells compared to their expression in other tested tissues. In the male reproductive lineage both are expressed in early developing stages of the reproductive tissue, like uni- and bicellular pollen. Thus, *NRPs* seem to be more specifically expressed in early developing stages of reproductive tissues on both, male and female sides.

The histone chaperone *HIRA* seems to be less expressed in female reproductive tissues, like the MMC but seems to be highly expressed in male reproductive tissues, like in the PMC, the unicellular-, bicellular- and mature pollen. Thus, *HIRA* seems to be more specifically expressed in the male reproductive tissues than in the female reproductive organs similar to the expression of *NAP1;4*.

It is worth mentioning that, the expression of some of these genes differ between the RNA-Seq and Microarray datasets. For instance, the RNA-Seq data contains no information of *NAP1;1* and *NAP1;3* in some tissues (e.g. floral buds), whereas the Microarray data shows their expressions at floral stages 10 and 12. This might be caused by no detection of those genes in those specific RNA-Seq experiments or they could not be mapped.

All in all the reanalysis of the RNA-Seq and Microarray data shows that all histone chaperone candidates are expressed to a certain level in at least one reproductive tissue during sporogenesis. Thus, they were reasonable candidates to be investigated further for their role in regulating H1 dynamic during sporogenesis.

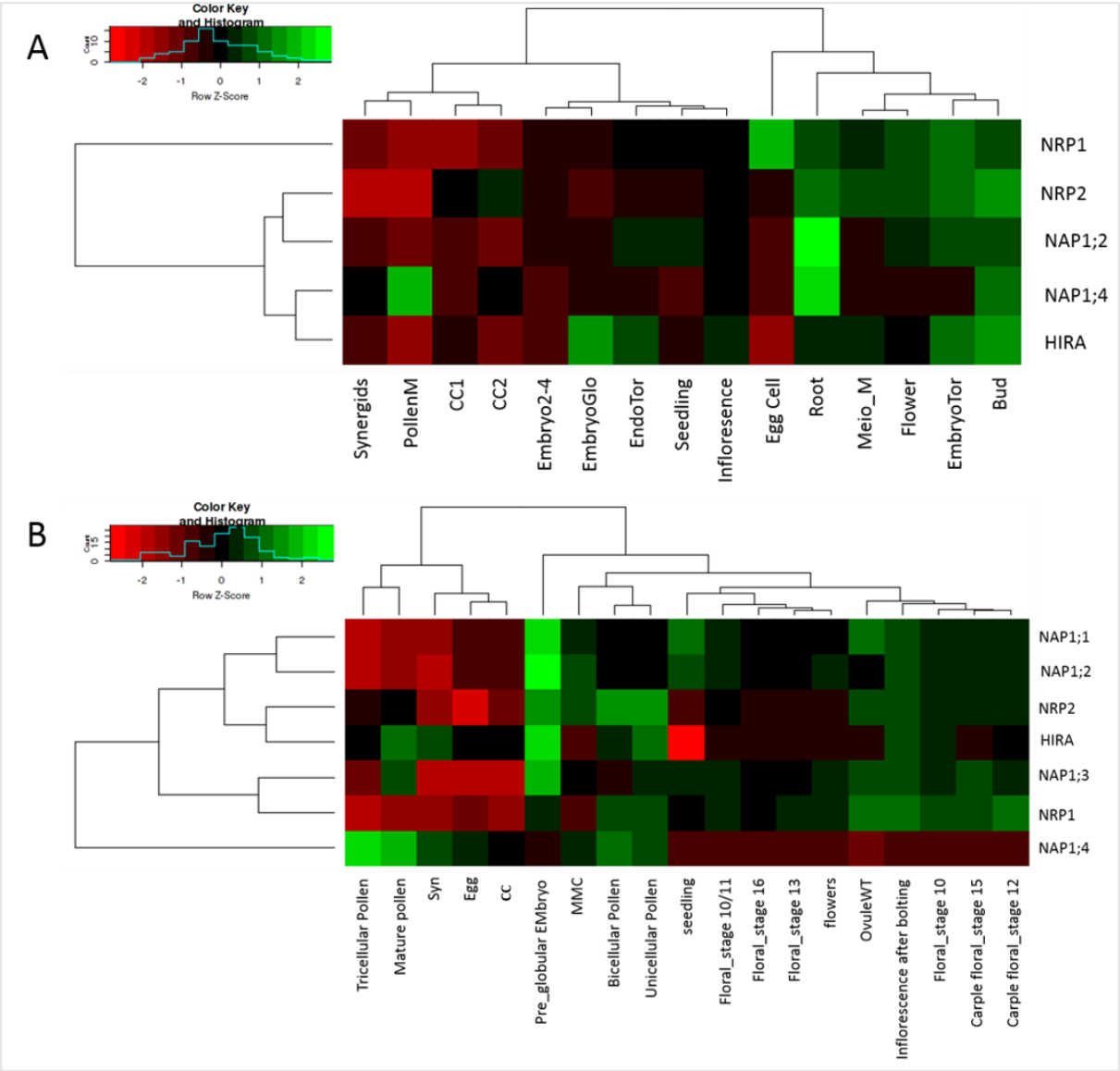

Figure 1.: Heatmap of RNA-Seq and GeneCHIP. Relative expression of *AT1G74560* (*NRP1*); *AT1G18800* (*NRP2*), *AT4G26110* (*NAP1;1*), *AT5G56950* (*NAP1;2*), *AT2G19480* (*NAP1;3*), *AT3G13782* (*NAP1;4*), *AT3G44530* (*HIRA*) in different tissue present in (A) RNA-Seq experiments from Wuest and colleagues (Wuest et al. 2010) and (B) on Affymetrix ATH1 GeneCHIP experiments from different publications (Borges et al. 2008; Honys and Twell 2004; Pina and Pinto 2005; Schmidt et al. 2011). Both heat maps are designed with the R-script published in GitHub (https://github.com/VimalRawat1010/Rscripts/blob/master/LabData/.RData). The tool considers shape and gene expression values to create the dendrograms and colors. The table with normalized expression values can be found in the Supplemental Table 4. Abbreviation: (A) PollenM (pollen Mature), CC1 (central cell), CC2 (central cell), Embryo2-4 (embryo cell stage 2-4), EmbryoGlo (embryo globular stage), EndoTor (endosperm torpedo stage), Meio_M (meiocytes male), EmbryoTor (embryo torpedo stage). (B) Syn (synergids), MMC (megaspore mother cell), Egg (egg cell), CC (central cell).

Dex-inducible amiRNAs against *NAPs* and *NRPs*

To test whether the *NAPs*, *NRPs* and *HIRA* play a role in linker histone eviction during sporogenesis (She et al. 2013) we designed Dex-inducible amiRNAs against the different

candidate genes. A more detailed description of the cloning strategy is described in chapter 3 of this thesis. Inserting four individual amiRNAs to target each *NAP* individually bears a high risk of disrupting essential genes. To overcome these difficulties we rather designed one amiRNA which can target all four *NAPs* and one amiRNA which targets two *NRPs* (Hauser et al. 2013). Since amiRNAs have a high variability in the level they are downregulating their target gene (Schwab et al. 2006), we designed not only one amiRNA, but as a backup, four different amiRNAs. In Figure 2 it is shown that amiRNAs JS3 and JS4 which target all four *NAPs* have their target sites in exon 10 in *NAP1;1*, *NAP1;2*, *NAP1;3* and in exon 9 in *NAP1;4*. The target sequence of JS3 is similar for *NAP1;1 NAP1;2*,*NAP1;3* and *NAP1;4* and differs only by two nucleotides (mismatches). The target sequence of JS4 is similar for *NAP1;1 NAP1;2*,*NAP1;3* and *NAP1;4* and differs by 4 nucleotides (mismatches). The amiRNAs JS1 and JS2 have their target sequences against the *NRPs* in exon 9 for *NRP1* and in exon 2 for *NRP2*. The target sequence of JS1 is the same for *NRP1 and NRP2* except for one nucleotide (mismatch). The target sequence of JS2 is the same for *NRP1 and NRP2* except for two nucleotides (mismatches). The target sequences and the indicated mismatches can be found in Supplemental Table 2.

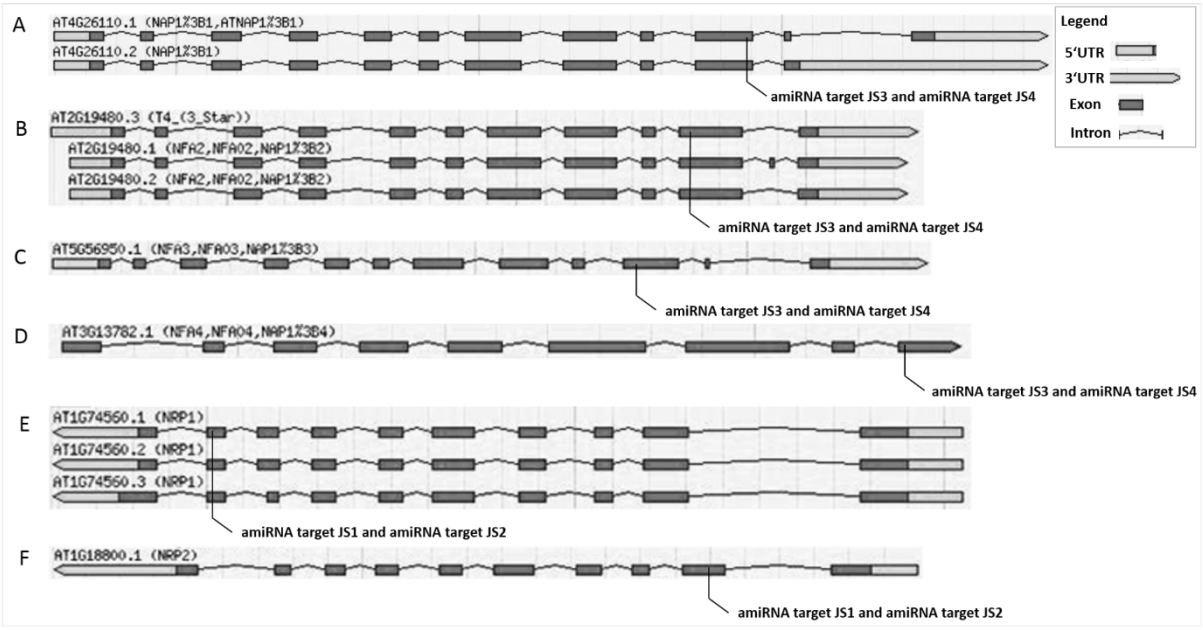

Figure 2.: Gene models of *NAPs* and *NRPs* with the target site of amiRNAs. The target sequence and mismatches for the different amiRNAs can be found in the Supplement. Gene models for (A) *AT4G26110.1 AT4G26110.2* (*NAP1;1*). (B) *AT2G19480.1*; *AT2G19480.2*; *AT2G19480.3* (*NAP1;2*). (C) *AT5G5690.1* (*NAP1;3*). (D) *AT3G13782.1* (*NAP1;4*). (E) *AT1G74560.1*; *AT1G74560.2*; *AT1G74560.3* (*NRP1*). (F) *AT1G18800.1* (*NRP2*). In (A to D) is the target of amiRNAs JS3 and JS4 highlighted and in (E and F) is the target of amiRNAs JS1 and JS2 highlighted.

Dex-inducible polycistronic amiRNAs against all four *NAPs* and both *NRPs* seems to be expressed but not functional

To target in total all six candidate genes (*NAPs* and *NRPs*) we would have to insert at least two independent constructs to our BG line, which already harbors three insertion events. To limit the amount of potential gene disruptive insertion events we designed a polycistronic regulation for two amiRNAs, to reduce the insertion events. Figure 3 A shows a schematic

representation of the important parts of the Dex-inducible polycistronic amiRNAs against *NAPs* and *NRPs*. The RPS5a promoter drives the expression of the transcription factor LhGR2, which can bind under Dex-treatment to pOP6. POP6 drives with the help of two CaMV35S minimal promoters the expression of a GUS cassette and of the polycistronic amiRNAs against NAPs and NRPs. It was shown by Liang and colleagues (Liang et al. 2012) that polycistronic amiRNAs produced from pAMIR319a and pAMIR395a driven by the 35S promoter could be transcribed simultaneously. The scientist identified twelve independent transgenic plants which showed an effective downregulation (measured by RT-PCR) of their individual target genes *FLOWERING LOCUS T (FT*) and *TRIPTYCHON (TRY*). They further obtained the described phenotypes of increased trichome density on leaves and delayed flowering (Koornneef et al. 1994; Liang et al. 2012; Schellmann et al. 2002).

To test if the downregulation of *NAPs* and *NRPs* is sufficient to alter H1 dynamics during female sporogenesis we screened in total 8 individual insertion lines in T1 and T2 (Figure 3 B, see also Supplemental information for more details). We did not find any alterations in the linker histone expression at the stages 1-II and 2-II after the induction time of maximal 82 hours, compared to not induced reporter lines (BG lines: *pH1.1::H1.1-GFP*; *pH1.2::H1.2-ECFP; 3h1*). Our results described in chapter 2 and chapter 3 of this thesis have shown that the induction time might be not enough to reach the developmental stages to monitor for altered linker histone dynamics. Furthermore, we lacked a good counterstain to be sure that we were looking at the MMC. Just in a few cases, we could identify the MMC with DIC (n-total < 20).

To determine if BASTA resistant plants activate the pOP6 cassette under Dex-treatment, we performed GUS histochemical staining. Figure 3 C shows the *GUS* expression signal in a Dex-induced ovule primordium compared to Mock-treated ovules (negative control).

To test whether the amiRNAs successfully downregulate the *NAPs* and *NRPs*, we conducted a functional test. Dex-induced and non-induced plants were treated with UV light, since *nap1;1-4* and *nrp1-2* loss-of-function mutants have been described to be hypersensitive to this genotoxic stress (Zhou et al. 2016). Figure 3 D shows the condition of induced and not induced plants 12 days after the last UV treatment. We could not detect any difference in the phenotype between induced and not induced plants after the UV treatment, which suggests that either the amiRNA is not functional or that the UV treatment did not provoke enough genotoxic stress to the induced *NAP* and *NRP* knockouts.

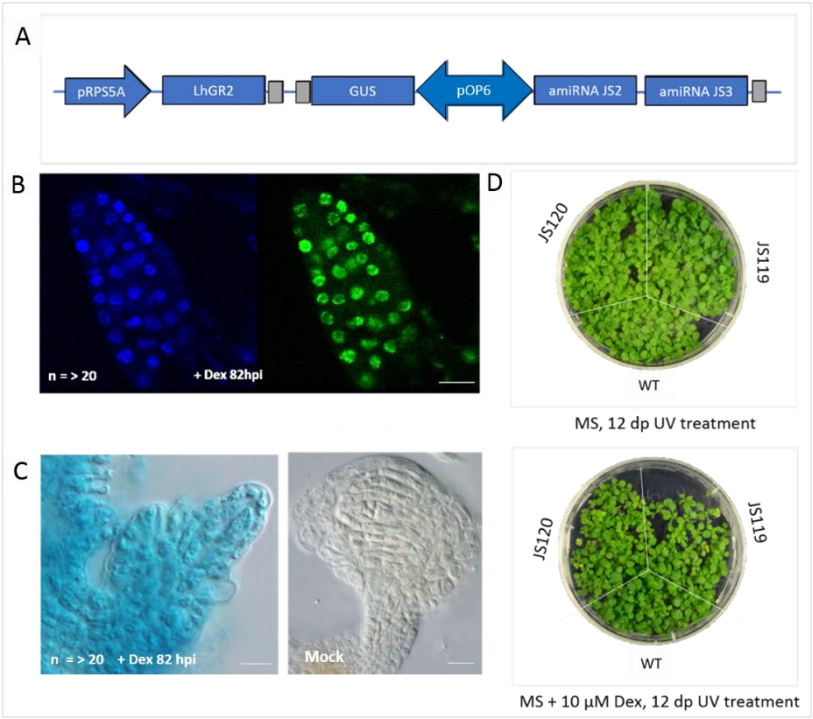

Figure 3.: Dex-inducible polycistronic amiRNA against *NAPs* and *NRPs* expression in plants. (A) Scheme of the construct for polycistronic with Dex-inducible amiRNAs against *NAPs* and *NRPs* under the RPS5a promoter. The RPS5a promoter drives

LhGR2 expression. The LhGR2 transcription factor can bind after Dex-treatment to pOP6. POP6 drives the expression of a) *GUS* and b) polycistronic amiRNAs against *NAPs* and *NRPs*. Small gray boxes are poly A signals. (B) SP5 images of *amiRNA[NRPs; NAPs]*, they show eviction of GFP and ECFP (*pH1.1::H1.1-GFP* and *pH1.2::H1.2-ECFP; 3h1*) in the MMC, 82 hpi with 10 µM Dex. Eight individual lines were analyzed with n-total > 20 ovules (for more details about the lines see Supplemental information). Scale bar = 10 µm. C) control for GUS histochemical staining, 24 hpi with 10 µM Dex (left) and Mock-treated transgenic lines (right). (D) Plates showing plant growth after UV treatment of wild-type (WT), the *NRPs* and *NAPs* knockdown lines JS120 and JS119, respectively. Eight-day-old plants were irradiated with 3700 J/m^2 UV once a day for 3 days and then grown under long-day conditions for 12 days before taking the photograph. The upper plate contains ½ MS medium, while the bottom plate contains ½ MS medium with 10 µM dexamethasone to induce amiRNAs.

Dex-inducible amiRNA against *HIRA* evokes seedlings hypersensitivity to genotoxic stress

We designed one amiRNA (amiRNA JS5), which has its target site in exon 8 and another amiRNA (amiRNA JS6) which has its target site in exon 3, in both gene models of HIRA (Figure 4 A).The two gene models of *HIRA* differ in the size and number of exons (Figure 4 A). The amiRNA target sequence and the indicated mismatches can be found in the Supplement, table 2.

To test if the downregulation of *HIRA* is sufficient to alter H1 dynamics during female sporogenesis (She et al. 2013) we screened in total three individual insertion lines in T1 and T2 of the amiRNA JS6 (Figure 4 B, see Supplemental information for more details about lines). Similar to the results for the amiRNAs against *NAPs*, we did not find any alteration in the linker histone expression at the stages 1-II and 2-II after an induction time of maximal 82 hours, compared to not induced reporter lines (BG line: *pH1.1::H1.1-GFP; pH1.2::H1.2-ECFP, 3h1*). Moreover, for these results it needs to be mentioned that our findings described in chapter 2 and chapter 3 of this thesis have shown that the time after induction might not be enough to reach the developmental stages to monitor for altered linker histone dynamics. Furthermore, we also lack here a good counterstain to be sure that we were looking at the MMC. Just in a few cases, we identify with DIC the MMC (n-total < 25).

To determine if the BASTA resistant plants activate the pOP6 cassette under Dex-treatment, we performed GUS histochemical staining. Figure 4 C shows the *GUS* expression signal in a Dex-induced ovule primordium compared to Mock-treated ovules (negative control).

In humans, it has been shown that *HIRA* serves as a chromatin bookmarking system to facilitate transcription recovery after genotoxic stress (Adam, Polo, and Almouzni 2013). Since we wanted to test if our amiRNA can successfully downregulate *HIRA* after Dex-treatment, we did a UV stress experiment. We stressed Dex-induced and non-induced plants with UV light 3 days in a row with a total intensity of 3750 J/m^2. Figure 4 D shows the state of induced and non-induced plants 12 days after the last UV treatment. We could detect a visible difference in two independent insertion lines between the induced and non-induced plants in their health status after the UV treatment. This observation indicates that the inducible amiRNA can successfully downregulate *HIRA*.

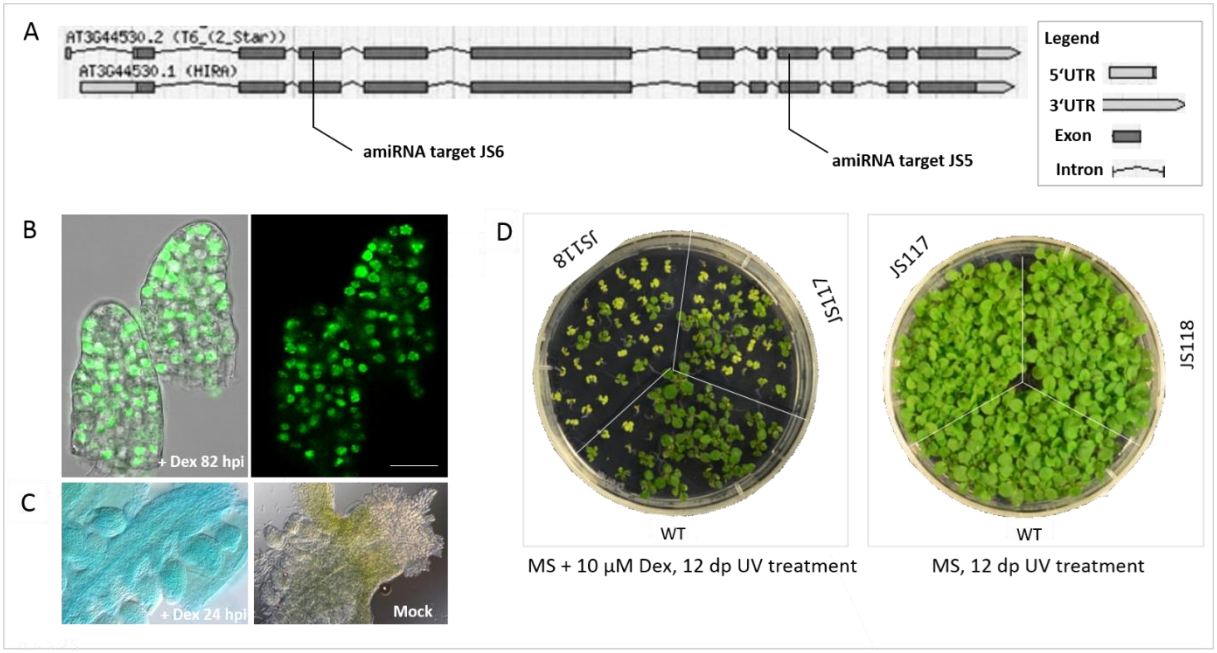

Figure 4.: Dex-inducible amiRNA against HIRA is functional in plants. (A) Gene model *AT3G44530*. The amiRNA target site is highlighted. The amiRNA target sequence and mismatches of amiRNA JS5 and amiRNA JS6 can be found in the Supplement. (B) No expression of *pH1.1::H1.1-GFP* or *pH1.2::H1.2-ECFP*; *3h1* in MMC, 82 hpi 10 µM Dex in *amiRNA[HIRA]* constructs. Three lines were tested with n-total ≥ 25 ovules (See Supplemental information for more details). SP5 images. Scale bar = 10 µm. (C) control with GUS reporter assay, 24 hpi with 10 µM Dex-treated (left) and Mock-treated (right) of *amiRNA*[*HIRA*] plants. (D) Plates showing plant growth after UV treatment of wild-type (WT) and *HIRA* knockdown lines JS118 and JS117. Eight-day-old plants were irradiated with 3700 J/m^2 UV once a day for 3 days and then grown under long-day conditions for 12 days before taking the photographs. The right plate contains ½ MS medium, while the left plate contains ½ MS medium and 10 µM Dex to induce the amiRNAs.

Discussion

Our goal was to create Dex-inducible amiRNA constructs to conditionally and simultaneously downregulate the expression of histone chaperone candidates. This strategy will help to determine if they are involved in linker histone dynamics during female sporogenesis.

We could successfully downregulate *HIRA* in a conditional manner, but not *NAPs* and *NRPs* with the inducible polycistronic approach. We showed via GUS histochemical staining that the pOP6 cassette is induced what suggests that also the amiRNAs against either *HIRA* or the *NAPs*, *NRPs* are expressed as well. However, we did not measure the level of downregulation with a direct approach. UV stress treatment of transformed plants showed sensitivity to genotoxic stress in the induced downregulated *hira* mutants in comparison to the non-induced WT-like plants. Whereas the same test showed no phenotypic difference between the induced and non-induced positive transformed plants of the polycistronic expressed amiRNAs against *NAPs* and *NRPs*. It might be that the polycistronic expression of amiRNAs containing the same MIR backbone are not functional due to self-alignment of the amiRNAs to each other, since polycistronic expressed amiRNAs with different MIR backbones have been shown to successfully downregulate their individual targets in plants (Liang et al. 2012). The UV stress experiment needs to be repeated under the same conditions as before but including a positive

control for the functionality of the UV stress (Zhou et al. 2016). In addition, the knockdown of *NAPs*, *NRPs*, should be proven by RT-PCR on seedlings after Dex-induction, at least for the *NAPs* and *NRPs* which are expressed in seedlings. For those NAPs and NRPs which are not expressed in seedlings it might be possible to screen for other *nap1;1-4,nrp1-2* mutant phenotypes as impaired postembryonic root growth caused by knockout of *nrp1-2* (Zhu et al. 2006) or a reduction in Homologous Recombination (HR) in *nap1;1-4 mutants* under normal growth conditions or under a wide range of genotoxic or abiotic stresses (Gao et al. 2012) after Dex-induction.

Regarding the genotoxic sensitive phenotype in the induced amiRNA *hira* plant lines, it might be, that an off-target of the amiRNA designed against *HIRA* creates this genotoxic phenotype. To conclude about this possibility an amiRNA resistant variant of *HIRA* needs to be cloned and checked for its complementary potential in the induced amiRNA lines under genotoxic stress. But since our results are consistent with findings by Adam and colleagues (Adam, Polo, and Almouzni 2013), which showed that *HIRA* plays an important role in DNA repair after UV damage in humans and with findings by Nie and colleagues (Nie et al 2014), who found that Arabidopsis *HIRA* function is required for transcription of genes responsive to abiotic stress, is the most plausible scenario that the genotoxic sensitive phenotype is caused by a downregulation of *HIRA*.

Our analysis of published expression results suggests that all histone chaperone candidates besides *HIRA* and *NAP1;4* seemed to be expressed in a spatial and temporal manner which would allow them to play a role during female sporogenesis. This is in agreement with other studies which showed nuclear expression of the *NRPs*, *HIRA* and *NAP1;4*, and to a lower extend also nuclear expression of *NAP1;1*,*NAP1;2* and *NAP1;3*, which were described to be also cytoplasmic expressed (Dong et al. 2005). Recently it was shown that the subcellular localization of plant NAPs and NRPs changes based on environmental growth conditions, developmental stages and cell-type specific regulation (Liu et al. 2009; Phelps-durr et al. 2005; Zhu et al. 2006). The histone chaperones NAPs, NRPs and HIRA have been described to play a role in core histone and linker histone loading and unloading on the DNA in eukaryotes (Kepert et al. 2005; Zhou et al. 2015). Our analysis of published expression data shows that *NAP1;4* is more specifically expressed in male reproduction tissue during sporogenesis. This expression pattern fits findings of Liu and Zhou (Liu et al. 2009; Zhou et al. 2015). Both found that *NAP1;4* is expressed in different tissues compared to the other *NAPs.* They found it mostly expressed in pollen grains compared to other plant tissue. Further, they showed that also the protein structure of NAP1;4 is different from the other three NAPs. *NAP1;4* encodes a much shorter protein lacking canonical sequences. Our analysis of published expression results of *HIRA* showed that it is more specifically expressed in male reproductive tissues during sporogenesis. This specific expression of *HIRA* in male reproductive tissues is consistent with results from Ingouff and colleagues (Ingouff et al. 2010). They found that just a specific subset of H3 variants are expressed in plant male gametes, which makes it different from chromatin of the non-gametic male lineage. Certain H3 variants have been described to co-localize with HIRA in plants and associate with HIRA in animals (Corpet and Almouzni 2009; Nie et al. 2014).

We observed no difference in linker histone expression during female sporogenesis in neither the induced amiRNA lines against *HIRA* nor the polycistronic amiRNAs against *NAPs* and *NRPs*, after 82 hours post induction, even though we could show positive transcription of the inserted vector with our GUS histochemical staining in the female ovule primordia. However, we found (compare chapter 2 and 3) that the induction time of 82 hours might not be long

enough for induced ovule primordia of stage 1-I to reach a developmental stage of 2-I or 2-II to conclude about altered linker histone expression during female sporogenesis. Thus, it would be necessary to repeat this experiments with at least three more independent transformed lines and samples, collected after longer induction time of 5 days and with a counterstain to easily identify the MMC.

All in all, we assume based on our data that we could successfully downregulate *HIRA* in an inducible manner and that *HIRA* might be involved in either DNA repair like in animals or in H3 deposition after UV stress in plants. Further, our results suggest that *HIRA* might play a role during male sporogenesis rather than during female sporogenesis.

In summary, our work paved the way to further studies on *NAPs*, *NRPs* and *HIRA* by providing a detailed expression profile during plant sporogenesis based on re-analysis of existing data. Further we provided plant lines with an inducible downregulation of *HIRA* and possibly also plant lines with an inducible downregulation of *NAPs* and *NRPs.* However, more lines need to be screened and lines with amiRNAs targeting the *NAPs* and *NRPs* independently might be created.

Material and Methods

Plant material and growth conditions

Arabidopsis seeds were sterilized in 3% Bleach with 0.01% Triton X-100, washed in 70% EtOH, and sown out on 1/2 Murashige and Skoog (MS) salts (CAROLINE), 1% Sucrose, 1% (w/v) agar pH 5.6.

Seeds were sterilized and stored for 2 to 4 days at 4°C before transferring them to incubators (Percival) with long day conditions of 16 hours light [120 µE m-2 s-1] at 21°C and 8 hours dark at 16°C. The young plants were then transferred to soil and grown in a growth chamber with long day conditions (16h light/ 8h dark) at 22°C light and 18°C dark.

The creation of the BG line is described in chapter 3 of this thesis.

The amiRNA constructs against all four NAPs (amiRNA JS3 and JS4) and both NRPs (amiRNA JS5 and JS6) were designed with the Phantom database (Hauser et al. 2013). amiRNA JS1 sequence rev. complement: GAGCGGAAATATAACGTGATA. amiRNA JS2 sequence rev. complement: GCGAGAAATATAACGTGATA. amiRNA JS3 sequence rev. complement: ATGCTGTATCATGGTTTACTA. amiRNA JS4 sequence rev. complement: GTGCTGTCTCATGGTTTACTA.

The amiRNAs mentioned above were cloned as described in chapter 3 first separately into D-TOPO system. At the amiRNA JS2 was via PCR an additional EcoRI site synthesized. The primer sequence for the PCR are 5'->3' JS64: GTAAAACGACGGCCAGTCTTAAGCTCGG and 5'->3' JS65: CTAGAATTCGGATCCCCCCATGGCG. EcoRI- site underlined.

Afterwards, the amiRNA JS2 was cut out with EcoRI and cloned via ligation reaction into the D-TOPO vector containing the amiRNA JS3. This vector including both amiRNAs was then cloned via Gateway into the pRPS5a::LhGR2-GUS::pOP6 vector (Ian Moore, Oxford). The constructs were transformed via *Agrobacterium tumefaciens* (GV3101) to homozygous *pH1.1::H1.1-GFP, pH1.2::H1.2-ECFP, 3h1 lines* (BG lines). Positive T1s were identified based

on BASTA selection and GUS reporter assay after 10 µM Dex -treatment as described in chapter 3.

The Dex-inducible amiRNAs against *HIRA* (amiRNA JS5 and JS6) were designed and cloned by using the wmd3 database and protocol (Schwab et al. 2006). The amiRNA JS6 was transformed via *Agrobacterium tumefaciens* (GV3101) to homozygous *pH1.1::H1.1-GFP, pH1.2::H1.2-ECFP, 3h1 lines* (BG lines) as described in chapter 3. Positive T1s were identified as described in chapter 3, based on BASTA selection and GUS reporter assay after 10 µM Dex-treatment. amiRNA JS5 sequence rev. complement: ACGTCACGCATTCCTTTTGA and amiRNA JS6 sequence rev. complement: TTGCACAACACAGTGCATATA.

Primer Sequences for amiRNA amplification:

See Supplement Table 1.

Dex-induction and imaging

We analyzed 3 independent lines of Dex-inducible *amiRNA*[*HIRA*], 8 independent lines of Dex-inducible *amiRNA*[*NRPs*]-[*NAPs*].

Single inflorescences induced with 10 µM Dex-solution (0.01% EtOH in water) or Mock (0.01% EtOH in water) were dissected after 3 to 4 days post induction (dpi). Single carpels were freshly dissected and mounted in ddH_2O and directly imaged.

Serial images of fluorescent signals in whole-mount ovule primordia were recorded by confocal laser-scanning microscopy with a Leica SP5-R (Leica Microsystems) using a 63× GLY lens (glycerol immersion, NA 1.4). Signals of GFP and ECFP were acquired sequentially. Images were overlaid with DIC channel.

***β*-Glucuronidase (GUS) reporter assay**

Single inflorescences induced with 10 µM Dex-solution (0.01% EtOH) or Mock (0.01% EtOH) were dissected after 2 days post induction (dpi). Single carpels were slightly cut open and emerged in 4 mM x-Glu solution, vacuum infiltrated for 5 min followed by a 2 hour incubation at 37°C, washed with phosphate buffer and mounted in 80% glycerol. Imaged at the DMR (Leica) microscope with 20x or 40x dry objective. Final concentration of GUS-solution Triton X-100 10%, EDTA 10 mM, Ferrocyanide 2 mM, Ferricyanide 2 mM, Na2HP04 100 mM, NaH2P04 100 mM, x-Glu 4 mM.

UV treatment

Plants of *amiRNA[HIRA] amiRNA[NRPs]-amiRNA[NAPs]* and Col-0 were grown on 10 µM Dex- or Mock-plates for 8 days at long day conditions in a growth incubator (Percival) before the first UV treatment. We run a total radiation treatment of 3750 J/m^2 per day (GS GeneLinker™ UV chamber (Bio-RAD)). The treatment was paused three times to rotate the plate, to get a more uniform irradiation for the seedlings. The lid of the petri dish was closed when irradiated. We repeated the treatment three days in a row. In between the treatments the

plates were placed immediately back into the growth incubator. Pictures of the plates were taken 12 days post the last UV treatment (UV-C light).

Reanalysis of published expression data

For the reanalysis of published RNA-Seq and Microarray expression data we used a tool, for which the R-script can be found at https://github.com/VimalRawat1010/Rscripts/blob/master/LabData/.RData. The analysis includes data from (Borges et al. 2008; Honys and Twell 2004; Pina and Pinto 2005; Schmidt, Anja, Wuest, Samuel, Vijverberg, Kitty, Baroux. Celia, Kleen and Grossniklaus 2011; Wuest et al. 2010). The tool considers for the dendrograms and the coloring the shape and gene expression values.

References

Adam, Salomé, SE Polo, and Geneviève Almouzni. 2013. “Transcription Recovery after DNA Damage Requires Chromatin Priming by the H3. 3 Histone Chaperone HIRA.” *Cell* 155(1): 94–106.

Borges, F. et al. 2008. “Comparative Transcriptomics of Arabidopsis Sperm Cells.” *Plant Physiology* 148(2): 1168–81.

Corpet, Armelle, and Geneviève Almouzni. 2009. “Making Copies of Chromatin: The Challenge of Nucleosomal Organization and Epigenetic Information.” *Trends in Cell Biology*.

Dong, Aiwu et al. 2005. “Interacting Proteins and Differences in Nuclear Transport Reveal Specific Functions for the NAP1 Family Proteins in Plants.” *Plant Physiology* 138(July): 1446–56.

Duc, Céline et al. 2015. “The Histone Chaperone Complex HIR Maintains Controls Nucleosome Occupancy and Counterbalances Impaired Histone Deposition in CAF-1 Mutants.” *The Plant Journal : for cell and molecular biology*: 707–22.

Gao, Juan et al. 2012. “NAP1 Family Histone Chaperones Are Required for Somatic Homologous Recombination in Arabidopsis.” *The Plant cell* 24(4): 1437–47.

Hajkova, Petra et al. 2008. “Chromatin Dynamics during Epigenetic Reprogramming in the Mouse Germ Line.” *Nature* 452(7189): 877–81.

Hauser, Felix et al. 2013. “A Genomic-Scale Artificial microRNA Library as a Tool to Investigate the Functionally Redundant Gene Space in Arabidopsis.” *The Plant cell* 25(8): 2848–63.

Honys, David, and David Twell. 2004. “Transcriptome Analysis of Haploid Male Gametophyte Development in Arabidopsis.” *Gene Biology* 5(11): R85.1-R85.13.

Ingouff, Mathieu et al. 2010. “Zygotic Resetting of the HISTONE 3 Variant Repertoire Participates in Epigenetic Reprogramming in Arabidopsis.” *Current Biology* 20(23): 2137–43.

Kepert, J. Felix et al. 2005. “NAP1 Modulates Binding of Linker Histone H1 to Chromatin and Induces an Extended Chromatin Fiber Conformation.” *The Journal of biological chemistry* 280(40): 34063–72.

Koornneef, M. et al. 1994. “The Phenotype of Some Late-Flowering Mutants Is Enhance by a

Locus on Chromosome 5 That Is Not Effetive in the Landsberg Erecta Wild-Type." *Plant Journal* 6: 911–19.

Liang, Gang, Hua He, Yang Li, and Diqiu Yu. 2012. "A New Strategy for Construction of Artificial miRNA Vectors in Arabidopsis." *Planta* 235(6): 1421–29.

Liu, Ziqiang et al. 2009. "Molecular and Reverse Genetic Characterization of NUCLEOSOME ASSEMBLY PROTEIN1 (NAP1) Genes Unravels Their Function in Transcription and Nucleotide Excision Repair in Arabidopsis Thaliana." *Plant Journal* 59(1): 27–38.

Nie, Xin et al. 2014. "The HIRA Complex That Deposits the Histone H3.3 Is Conserved in Arabidopsis and Facilitates Transcriptional Dynamics." *Biology open* 3: 794–802.

Phelps-durr, Tara L., Julie Thomas, Phil Vahab, and Marja C. P. Timmermans. 2005. "Maize Rough sheath2 and Its Arabidopsis Orthologue ASYMMETRIC LEAVES1 Interact with HIRA , a Predicted Histone Chaperone , to Maintain Knox Gene Silencing and Determinacy during Organogenesis." *The Plant Cell*: 1–13.

Pina, Cristina, and Francisco Pinto. 2005. "Gene Family Analysis of the Arabidopsis Pollen Transcriptome Reveals Biological Implications for Cell Growth , Division Control , and." *Plant Physiology* 138(June): 744–56.

Schellmann, S. et al. 2002. "TRIPTYCHON and CAPRICE Mediate Lateral Inhibition during Trichome and Root Hair Patterning in Arabidopsis." *EMBO Journal* 21(19): 5036–46.

Schmidt, Anja, Wuest, Samuel, Vijverberg, Kitty, Baroux. Celia, Kleen, Daniela, and Ueli Grossniklaus. 2011. "Transcriptome Analysis of the Arabidopsis Megaspore Mother Cell Uncovers the Importance of RNA Helicases for Plant Germline Development." *PLoS biology* 9(9).

Schwab, Rebecca et al. 2006. "Highly Specific Gene Silencing by Artificial MicroRNAs in Arabidopsis." *The Plant cell* 18(May): 1121–33.

She, Wenjing et al. 2013. "Chromatin Reprogramming during the Somatic-to-Reproductive Cell Fate Transition in Plants." *Development (Cambridge, England)* 140(19): 4008–19.

Wuest, Samuel E. et al. 2010. "Arabidopsis Female Gametophyte Gene Expression Map Reveals Similarities between Plant and Animal Gametes." *Current Biology* 20(6): 506–12.

Yue, Hongjun et al. 2016. "Single-Molecule Studies of the Linker Histone H1 Binding to DNA and the Nucleosome." *Biochemistry* 55(14): 2069–77.

Zhou, Wangbin et al. 2016. "Distinct Roles of the Histone Chaperones NAP1 and NRP and the Chromatin-Remodeling Factor INO80 in Somatic Homologous Recombination in Arabidopsis Thaliana." *Plant Journal* 88(3): 397–410.

Zhou, Wangbin, Yan Zhu, Aiwu Dong, and Wen Hui Shen. 2015. "Histone H2A/H2B Chaperones: From Molecules to Chromatin-Based Functions in Plant Growth and Development." *Plant Journal* 83(1): 78–95.

Zhu, Yan et al. 2006. "Arabidopsis NRP1 and NRP2 Encode Histone Chaperones and Are Required for Maintaining Postembryonic Root Growth." *The Plant Cell* 18(11): 2879–92.

Supplements Chapter 4:

Name	amiRNA	Sequence from 5' to 3'	information	Database used
JS1	amiRNA JS1	gaTATCACGTTATATTTCCGCTCtctctctttgtattcc	I miR-s	Phantom
JS2	amiRNA JS1	gaGAGCGGAAATATAACGTGATAtcaaagagaatcaatga	II miR-a	Phantom
JS3	amiRNA JS1	gaGAACGGAAATATATCGTGATTtcacaggtcgtgatatg	III miR*s	Phantom
JS4	amiRNA JS1	gaAATCACGATATATTTCCGTTCtctacatatatattcct	IV miR*a	Phantom
JS5	JS1_A_gate	CACCGAATTCCTGCAGCCCcaaacacacg	JS1_A_gate	Phantom
JS6	JS1_B_gate	GGATCCCCCcatggcgatgcctta	JS1_B_gate	Phantom
JS7	amiRNA JS2	gaTATCACGTTATATTTCTGCGCtctctctttgtattcc	I miR-s	Phantom
JS8	amiRNA JS2	gaGCGCAGAAATATAACGTGATAtcaaagagaatcaatga	II miR-a	Phantom
JS9	amiRNA JS2	gaGCACAGAAATATATCGTGATTtcacaggtcgtgatatg	III miR*s	Phantom
JS10	amiRNA JS2	gaAATCACGATATATTTCTGTGCtctacatatatattcct	IV miR*a	Phantom
JS11	amiRNA JS3	gaTAGTAAACCATGATACAGCATtctctctttgtattcc	I miR-s	Phantom
JS12	amiRNA JS3	gaATGCTGTATCATGGTTTACTAtcaaagagaatcaatga	II miR-a	Phantom
JS13	amiRNA JS3	gaATACTGTATCATGCTTTACTTtcacaggtcgtgatatg	III miR*s	Phantom
JS14	amiRNA JS3	gaAAGTAAAGCATGATACAGTATtctacatatatattcct	IV miR*a	Phantom
JS15	JS4_mir1	gaTAGTAAACCATGAGACAGCACtctctctttgtattcc	I miR-s	Phantom
JS16	JS4_mir2	gaGTGCTGTCTCATGGTTTACTAtcaaagagaatcaatga	II miR-a	Phantom
JS17	JS4_mir3	gaGTACTGTCTCATGCTTTACTTtcacaggtcgtgatatg	III miR*s	Phantom
JS18	JS4_mir4	gaAAGTAAAGCATGAGACAGTACtctacatatatattcct	IV miR*a	Phantom
JS19	JS5_mir1	gaTCAAAAAGGAATGCGTGACGTtctctctttgtattcc	I mir-s	WMD3
JS20	JS5_mir2	gaACGTCACGCATTCCTTTTTGAtcaaagagaatcaatga	II mir-a	WMD3
JS21	JS5_mir3	gaACATCACGCATTCGTTTTTGTtcacaggtcgtgatatg	III mir*s	WMD3
JS22	JS5_mir4	gaACAAAAACGAATGCGTGATGTtctacatatatattcct	IV mir*a	WMD3
JS23	JS5_A	CTGCAAGGCGATTAAGTTGGGTAAC	suitable for pRS300	WMD3
JS24	JS5_B	GCGGATAACAATTTCACACAGGAAACAG	suitable for pRS300	WMD3
JS25	JS6_mir1	gaTATATGCACTGTGTTGTGCAAtctctctttgtattcc	I mir-s	WMD3
JS26	JS6_mir2	gaTTGCACAACACAGTGCATATAtcaaagagaatcaatga	II mir-a	WMD3
JS27	JS6_mir3	gaTTACACAACACAGAGCATATTtcacaggtcgtgatatg	III mir*s	WMD3
JS28	JS6_mir4	gaAATATGCTCTGTGTTGTGTAAtctacatatatattcct	IV mir*a	WMD3
JS29	JS5_A (TOPO)	CACCCTGCAAGGCGATTAAGTTGGGTAAC	suitable for TOPO cloning	WMD3

Supplement Table 1.: Primer sequences for amiRNA amplification. For the amiRNAs JS1, JS2, JS3 were in addition to their specific primers (e.g. JS1 to JS4 for amiRNA JS1) the general primers JS5 and JS6 used.

amiRNA	amiRNA target sequence 5'>3'
JS1 against *NRP1*	GAGC**A**GAAATATAACGTGATA
JS1 against *NRP2*	GAGC**A**GAAATATAA**T**GTGATA
JS2 against *NRP1*	G**T**GCTGTCTCATGGTTTACTG
JS2 against *NRP2*	G**T**GCTGTCTCATGG**T**TTACTG
JS3 against *NAP1;1*	**G**TGCTGT**C**TCATGGTTTACT**G**
JS3 against *NAP1;2*	GTGCTGT**C**TCATGGTT**T**ACT**G**
JS3 against *NAP1;3*	GTGCTGT**C**TCATGGTTTACT**G**
JS3 against *NAP1;4*	GTGC**T**GT**C**TCATGGTTTAC**TG**
JS4 against *NAP1;1*	**A**TGCAGTTTCATGGTTTACG**G**
JS4 against *NAP1;2*	**A**TGCAGT**T**TCATGGTT**T**ACG**G**
JS4 agianst *NAP1;3*	**A**TGCAGTTTCATGGTTTACG**G**
JS4 against *NAP1;4*	**A**TGC**A**GT**T**TCATGGTTTAC**GG**
JS5 against *HIRA*	ACGTCA**T**GCATTCCTTTTGA
JS6 against *HIRA*	TTG**G**ACAACACAGTGCATATA

Supplement Table 2.: amiRNA target sequences and mismatches. Underlined and in bold are the mismatches of the amiRNA within the target sequence highlighted.

Lines analyzed for H1 dynamics		
line #	**constrcuts**	# ovules analyzed
JS88#24	*pRPS5a::LhGR2-GUS::pOP6::amiRNA[HIRA]; h1.1-1/h1.1-1;h1.2-2/h1.2-2; h1.3-2/h1.3-2 pH1.1::H1.1-GFP/pH1.1::H1.1-GFP; pH1.2::H1.2-ECFP/pH1.2::H1.2-ECFP*	n < 15
JS88#25	*pRPS5a::LhGR2-GUS::pOP6::amiRNA[HIRA]; h1.1-1/h1.1-1;h1.2-2/h1.2-2; h1.3-2/h1.3-2 pH1.1::H1.1-GFP/pH1.1::H1.1-GFP; pH1.2::H1.2-ECFP/pH1.2::H1.2-ECFP*	n < 15
JS88#26	*pRPS5a::LhGR2-GUS::pOP6::amiRNA[HIRA]; h1.1-1/h1.1-1;h1.2-2/h1.2-2; h1.3-2/h1.3-2 pH1.1::H1.1-GFP/pH1.1::H1.1-GFP; pH1.2::H1.2-ECFP/pH1.2::H1.2-ECFP*	n < 15
JS89#1	pRPS5a::LhGR2-GUS::pOP6::amiRNA[NAPs]amiRNA[NRPs]; h1.1-1/h1.1-1;h1.2-2/h1.2-2; h1.3-2/h1.3-2 pH1.1::H1.1-GFP/pH1.1::H1.1-GFP; pH1.2::H1.2-ECFP/pH1.2::H1.2-ECFP	n < 5
JS89#2	pRPS5a::LhGR2-GUS::pOP6::amiRNA[NAPs]amiRNA[NRPs]; h1.1-1/h1.1-1;h1.2-2/h1.2-2; h1.3-2/h1.3-2 pH1.1::H1.1-GFP/pH1.1::H1.1-GFP; pH1.2::H1.2-ECFP/pH1.2::H1.2-ECFP	n < 5
JS89#4	pRPS5a::LhGR2-GUS::pOP6::amiRNA[NAPs]amiRNA[NRPs]; h1.1-1/h1.1-1;h1.2-2/h1.2-2; h1.3-2/h1.3-2 pH1.1::H1.1-GFP/pH1.1::H1.1-GFP; pH1.2::H1.2-ECFP/pH1.2::H1.2-ECFP	n < 5
JS89#5	pRPS5a::LhGR2-GUS::pOP6::amiRNA[NAPs]amiRNA[NRPs]; h1.1-1/h1.1-1;h1.2-2/h1.2-2; h1.3-2/h1.3-2 pH1.1::H1.1-GFP/pH1.1::H1.1-GFP; pH1.2::H1.2-ECFP/pH1.2::H1.2-ECFP	n < 5
JS89#6	pRPS5a::LhGR2-GUS::pOP6::amiRNA[NAPs]amiRNA[NRPs]; h1.1-1/h1.1-1;h1.2-2/h1.2-2; h1.3-2/h1.3-2 pH1.1::H1.1-GFP/pH1.1::H1.1-GFP; pH1.2::H1.2-ECFP/pH1.2::H1.2-ECFP	n < 5
JS89#7	pRPS5a::LhGR2-GUS::pOP6::amiRNA[NAPs]amiRNA[NRPs]; h1.1-1/h1.1-1;h1.2-2/h1.2-2; h1.3-2/h1.3-2 pH1.1::H1.1-GFP/pH1.1::H1.1-GFP; pH1.2::H1.2-ECFP/pH1.2::H1.2-ECFP	n < 5
JS89#8	pRPS5a::LhGR2-GUS::pOP6::amiRNA[NAPs]amiRNA[NRPs]; h1.1-1/h1.1-1;h1.2-2/h1.2-2; h1.3-2/h1.3-2 pH1.1::H1.1-GFP/pH1.1::H1.1-GFP; pH1.2::H1.2-ECFP/pH1.2::H1.2-ECFP	n < 5
JS89#9	pRPS5a::LhGR2-GUS::pOP6::amiRNA[NAPs]amiRNA[NRPs]; h1.1-1/h1.1-1;h1.2-2/h1.2-2; h1.3-2/h1.3-2 pH1.1::H1.1-GFP/pH1.1::H1.1-GFP; pH1.2::H1.2-ECFP/pH1.2::H1.2-ECFP	n < 5

Supplement Table 3.: Plant lines (T1s) analyzed for GUS histochemical staining for linker histone presence during sporogenesis after Dex-treatment. JS117 selfed offspring of JS88#24; JS118 selfed offspring of JS88#25; JS119 selfed offspring of JS89#6; JS120 selfed offspring of JS89#7.

Microarray																					
Gene Name	**Gene**	**OvuleWt**	**Egg**	**Cen**	**Syn**	**MMC**	**flowers**	**seedling_pina**	**pollen_unicellular_honys_uc**	**pollen_bicellular_honys_bc**	**pollen_tricellular_honys_tc**	**pollen_mature_borges**	**globularEmbryo**	**preglobularEmbryo**	**heartEmbryo**	**inflorescence_inflorescenceAfterBolting_Col_0**	**flowers_floralStage10_Col_0**	**flowers_floralStage1011_Col_0**	**flowers_floralStage13_Col_0**	**carpels_floralStage12_Col_0**	**flowers_floralStage16_Col_0**	**carpels_floralStage15_Col_0**
NRP1	*AT1G74560*	10.29	6.81	6.18	6.3	7.25	8.89	8.34	9.52	9.24	5.54	4.48	8.93	9	8.57	9.9	9.46	8.98	9.14	9.76	8.62	9.67
NRP2	*AT1G18800*	7.71	5.19	6.17	5.92	7.69	6.87	6.46	8.34	8.29	6.78	6.51	8.72	8.57	9.27	7.7	7.43	7.08	6.88	7.5	6.76	7.41
NAP1;1	*AT4G26110*	8.74	6.21	6.27	5.29	7.71	7.65	8.74	7.66	7.21	4.99	5.66	10.33	10.46	10.04	8.5	8.19	7.8	7.41	8.21	7.26	8.04
NAP1;2	*AT5G56950*	6.78	5.53	5.48	4.17	7.37	6.86	7.45	6.59	6.47	4.13	4.81	10.11	10.07	9.81	7.77	7.31	7.13	6.78	7.07	6.62	7.16
NAP1;3	*AT2G19480*	9.7	6.95	7.07	7.03	8.98	9.21	9.46	9.32	8.76	7.62	10.35	10.92	11.03	10.62	9.59	9.48	9.27	9.1	9.43	8.96	9.66
NAP1;4	*AT3G13782*	3.91	5.89	5.71	6.66	6.15	4.31	4.23	6.8	6.88	8.95	8.41	4.94	4.96	5.59	4.48	4.07	4.17	4.48	4.28	4.4	4.1
HIRA	*AT3G44530*	6.21	6.4	6.37	6.71	6.05	6.18	5.3	6.8	6.45	6.32	6.36	7.17	7.21	7.08	6.71	6.5	6.24	6.18	6.33	6.23	6.26

RNASeq																
Gene Name	**Gene**	**EmbryoGob**	**Embryo2_4**	**Meio_M**	**CC1**	**CC2**	**EmbrTor**	**EndoTor**	**Seedling**	**Root**	**Flower**	**PollenM**	**Inorescence**	**EggCell**	**Synergids**	**Bud**
NRP1	*AT1G74560*	262.55	256.42	435.3	0.25	38.19	550.05	273.56	306.06	482.04	442.62	0.25	325.72	754.11	16.88	476.32
NRP2	*AT1G18800*	55.31	69.2	149.19	90.19	124.75	157.94	71.57	78.26	161	143.32	2.28	96.14	78.1	1.74	185.96
NAP1;2	*AT5G56950*	58.76	49.34	67.19	28.38	0.16	161.74	123.13	107.53	336.17	103.66	0.16	98.06	12.74	4.37	151.65
NAP1;4	*AT3G13782*	25.39	7.45	12.15	0.58	36.25	11.16	10.18	3.12	146.15	11.94	133.33	30.07	4.45	34.05	86.33
HIRA	*AT3G44530*	62.43	12.3	37.76	19.91	6.31	56.47	47.71	20.26	42.42	33.17	0.37	42.95	1.53	12.43	64.39

Supplement Table 4.: Normalized expression values of *NAPs* and *NRPs* from RNA-Seq and Microarray data. The table shows normalized expression values of *NAPs* and *NRPs* of RNA-Seq data from Wuest and colleagues (Wuest et al. 2010) and (B) Microarray data from Schmidt, Borges, Pina and

Honys (Borges et al. 2008; Honys and Twell 2004; Pina and Pinto 2005; Schmidt et al. 2011). The script used for analyzing the RNA-Seq and Microarray data can be found at "https://github.com/VimalRawat1010/Rscripts/blob/master/LabData/.RDat.

References of Supplement

Adam, Salomé, Sophie E. Polo, and Geneviève Almouzni. 2013. "Transcription Recovery after DNA Damage Requires Chromatin Priming by the H3. 3 Histone Chaperone HIRA." *Cell* 155(1): 94–106.

Borges, F. et al. 2008. "Comparative Transcriptomics of Arabidopsis Sperm Cells." *Plant Physiology* 148(2): 1168–81.

Corpet, Armelle, and Geneviève Almouzni. 2009. "Making Copies of Chromatin: The Challenge of Nucleosomal Organization and Epigenetic Information." *Trends in Cell Biology*.

Dong, Aiwu et al. 2005. "Interacting Proteins and Differences in Nuclear Transport Reveal Specific Functions for the NAP1 Family Proteins in Plants." *Plant Physiology* 138(July): 1446–56.

Duc, Céline et al. 2015. "The Histone Chaperone Complex HIR Maintains Controls Nucleosome Occupancy and Counterbalances Impaired Histone Deposition in CAF-1 Mutants." *The Plant Journal : for cell and molecular biology*: 707–22.

Gao, Juan et al. 2012. "NAP1 Family Histone Chaperones Are Required for Somatic Homologous Recombination in Arabidopsis." *The Plant cell* 24(4): 1437–47.

Hajkova, Petra et al. 2008. "Chromatin Dynamics during Epigenetic Reprogramming in the Mouse Germ Line." *Nature* 452(7189): 877–81.

Hauser, Felix et al. 2013. "A Genomic-Scale Artificial microRNA Library as a Tool to Investigate the Functionally Redundant Gene Space in Arabidopsis." *The Plant cell* 25(8): 2848–63.

Honys, David, and David Twell. 2004. "Transcriptome Analysis of Haploid Male Gametophyte Development in Arabidopsis." *Gene Biology* 5(11): R85.1-R85.13.

Ingouff, Mathieu et al. 2010. "Zygotic Resetting of the HISTONE 3 Variant Repertoire Participates in Epigenetic Reprogramming in Arabidopsis." *Current Biology* 20(23): 2137–43.

Kepert, J. Felix et al. 2005. "NAP1 Modulates Binding of Linker Histone H1 to Chromatin and Induces an Extended Chromatin Fiber Conformation." *The Journal of biological chemistry* 280(40): 34063–72.

Koornneef, M. et al. 1994. "The Phenotype of Some Late-Flowering Mutants Is Enhance by a Locus on Chromosome 5 That Is Not Effetive in the Landsberg Erecta Wild-Type." *Plant Journal* 6: 911–19.

Liang, Gang, Hua He, Yang Li, and Diqiu Yu. 2012. "A New Strategy for Construction of Artificial miRNA Vectors in Arabidopsis." *Planta* 235(6): 1421–29.

Liu, Ziqiang et al. 2009. "Molecular and Reverse Genetic Characterization of NUCLEOSOME ASSEMBLY PROTEIN1 (NAP1) Genes Unravels Their Function in Transcription and Nucleotide Excision Repair in Arabidopsis Thaliana." *Plant Journal* 59(1): 27–38.

Nie, Xin et al. 2014. "The HIRA Complex That Deposits the Histone H3.3 Is Conserved in Arabidopsis and Facilitates Transcriptional Dynamics." *Biology open* 3: 794–802.

Phelps-durr, Tara L., Julie Thomas, Phil Vahab, and Marja C. P. Timmermans. 2005. “Maize Rough sheath2 and Its Arabidopsis Orthologue ASYMMETRIC LEAVES1 Interact with HIRA , a Predicted Histone Chaperone , to Maintain Knox Gene Silencing and Determinacy during Organogenesis.” *The Plant Cell*: 1–13.

Pina, Cristina, and Francisco Pinto. 2005. “Gene Family Analysis of the Arabidopsis Pollen Transcriptome Reveals Biological Implications for Cell Growth , Division Control , and.” *Plant Physiology* 138(June): 744–56.

Schellmann, S. et al. 2002. “TRIPTYCHON and CAPRICE Mediate Lateral Inhibition during Trichome and Root Hair Patterning in Arabidopsis.” *EMBO Journal* 21(19): 5036–46.

Schmidt, Anja, Wuest, Samuel, Vijverberg, Kitty, Baroux. Celia, Kleen, Daniela, and Ueli Grossniklaus. 2011. “Transcriptome Analysis of the Arabidopsis Megaspore Mother Cell Uncovers the Importance of RNA Helicases for Plant Germline Development.” *PLoS biology* 9(9).

Schwab, Rebecca et al. 2006. “Highly Specific Gene Silencing by Artificial MicroRNAs in Arabidopsis.” *The Plant Cell* 18(May): 1121–33.

She, Wenjing et al. 2013. “Chromatin Reprogramming during the Somatic-to-Reproductive Cell Fate Transition in Plants.” *Development (Cambridge, England)* 140(19): 4008–19.

Wuest, Samuel E. et al. 2010. “Arabidopsis Female Gametophyte Gene Expression Map Reveals Similarities between Plant and Animal Gametes.” *Current Biology* 20(6): 506–12.

Yue, Hongjun et al. 2016. “Single-Molecule Studies of the Linker Histone H1 Binding to DNA and the Nucleosome.” *Biochemistry* 55(14): 2069–77.

Zhou, Wangbin et al. 2016. “Distinct Roles of the Histone Chaperones NAP1 and NRP and the Chromatin-Remodeling Factor INO80 in Somatic Homologous Recombination in Arabidopsis Thaliana.” *Plant Journal* 88(3): 397–410.

Zhou, Wangbin, Yan Zhu, Aiwu Dong, and Wen Hui Shen. 2015. “Histone H2A/H2B Chaperones: From Molecules to Chromatin-Based Functions in Plant Growth and Development.” *Plant Journal* 83(1): 78–95.

Zhu, Yan et al. 2006. “Arabidopsis NRP1 and NRP2 Encode Histone Chaperones and Are Required for Maintaining Postembryonic Root Growth.” *The Plant Cell* 18(11): 2879–92.

IX. Chapter 5

Role of Cullin E3-ligases on H1 dynamics in sporogenesis and influence of mutation in H1 on its stability.

Abbreviations	
3h1	*h1.1-1/h1.1-1;h1.2-2/h1.2-2; h1.3-2/h1.3-2*
aa	Amino acid
amiRNA[CUL1;CUL2]; BG	*pRPS5a::LhGR2-pOP6::amiRNA[CUL1;CUL2];h1.1-1/h1.1-1;h1.2-2/h1.2-2; h1.3-2/h1.3-2 pH1.1::H1.1-GFP/pH1.1::H1.1-GFP; pH1.2::H1.2-ECFP/pH1.2::H1.2-ECFP*
amiRNA[CUL3;CUL3b]; BG	*pRPS5a::LhGR2-pOP6::amiRNA[CUL3a;CUL3b];h1.1-1/h1.1-1;h1.2-2/h1.2-2; h1.3-2/h1.3-2 pH1.1::H1.1-GFP/pH1.1::H1.1-GFP; pH1.2::H1.2-ECFP/pH1.2::H1.2-ECFP*
amiRNA[CUL4]; BG	*pRPS5a::LhGR2-pOP6::amiRNA[CUL4];h1.1-1/h1.1-1;h1.2-2/h1.2-2;h1.3-2/h1.3-2 pH1.1::H1.1-GFP/pH1.1::H1.1-GFP; pH1.2::H1.2-ECFP/pH1.2::H1.2-ECFP*
BG	*h1.1-1/h1.1-1;h1.2-2/h1.2-2; h1.3-2/h1.3-2 pH1.1::H1.1-GFP/ pH1.1::H1.1-GFP; pH1.2::H1.2-ECFP/pH1.2::H1.2-ECFP* background line
Dex	Dexamethasone
DNA	Deoxyribonucleic acid
dpi	days post induction
ECFP	Enhanced cyan fluorescent protein
EtOH	Ethanol
FM	Functional Megaspore
GFP	Green fluorescent protein
H1.1^{11xG}RFP	*pRPS5a::LhGR2-GUS::pOP6::H1.1^{11xG}RFP* (11 amino acid mutations in Globular domain of H1)
H1.1^{11xN}RFP	*pRPS5a::LhGR2-GUS::pOP6::H1.1^{11xN}RFP* (11 amino acid mutation in N-tail of H1)
H1.1^{1xN}RFP	*pRPS5a::LhGR2-GUS::pOP6::H1.1^{1xN}RFP* (1 amino acid mutation in N-tail of H1)
H1.1^{26xC}RFP	*pRPS5a::LhGR2-GUS::pOP6::H1.1^{26xC}RFP* (26 amino acid mutation in C-tail of H1)
H1.1^{3xC}RFP	*pRPS5a::LhGR2-GUS::pOP6::H1.1^{3xC}RFP* (3 amino acid mutation in C-tail of H1)
H1.1^{3xG}RFP	*pRPS5a::LhGR2-GUS::pOP6::H1.1^{3xG}RFP* (3 amino acid mutations in Globular domain of H1)
H1.1^{6xGC}RFP	*pRPS5a::LhGR2-GUS::pOP6::H1.1^{6xGC}RFP* (6 amino acid mutation distributed in C-tail and Globular domain of H1)
H1.1^{wt}RFP	*pRPS5a::LhGR2-GUS::pOP6::H1.1-RFP*
hpi	hours post induction
hrs	hours
MIR395[CUL1;CUL2] MIR319a[CUL4]MIR172a [CUL3a;CUL3b]	*pRPS5a::LhGR2-pOP6::MIR395[CUL1;CUL2]MIR319a[CUL4]MIR172a[CUL3a;CUL3b]*
MMC	Megaspore Mother Cell
o/N	over Night
PCR	Polymerase Chain Reaction

PMC	Pollen Mother Cell
RFP	Red fluorescent protein
RNA	Ribonucleic Acid
SMC	Spore Mother Cell
WT	Wild-type

Abstract

H1 linker histones have been described to be targets of several PTM (Post-translational modifications) like phosphorylation, acetylation, and methylation in plants and animals (Kotliński et al. 2016; Villar-Garea and Imhof 2008). It has been previously shown that H1 eviction at the somatic-to-reproductive-transition phase is susceptible to proteasome inhibition suggesting a putative role for ubiquitination (She et al. 2013). Ubiquitination is facilitated by Cullin-based E3 ligases, we thus asked whether those enzymes influence H1 dynamics during plants sporogenesis. We found that amino acid mutations targeted against lysine residues, putative targets of ubiquitination, in the globular domain of H1.1 alters H1.1s stability and plants with those mutant variants also showed an aberrant MMC (Megaspore Mother Cell) development. Similar effects were observed in inducible knockdowns of *CULLIN4*. These results indicate that at least three amino acids in the globular domain of H1.1 and a functional CULLIN4 are important for H1s stability and MMC formation during the somatic-to-reproductive cell fate change.

Introduction

Plant and animal chromatin undergo large-scale remodeling during male and female germline differentiation (Hajkova et al. 2008; She et al. 2013). The hallmark of this process is a transient eviction of linker histones (H1's) from the germline precursor cells. The application of a proteasome inhibitor is sufficient to interfere with the eviction of linker histones during the somatic-to-reproductive transition in *Arabidopsis thaliana* (She et al. 2013). This suggests that H1 ubiquitination might be involved in H1 degradation, analogously to what has been proposed in animal cells (Izzo and Schneider 2015; Wisniewski et al. 2007). In plants, ubiquitination is facilitated by Cullin-based E3 ligase complexes (Biedermann and Hellmann 2011). Until now four classes of Cullin-based E3 ligases have been identified in *Arabidopsis thaliana*: CUL1, CUL2, CUL3a/3b, and CUL4 (Lee and Kim 2011). The four *CULLINs* belong to different E3 ligase complexes, which are for CUL3A and CUL3B the BCR, for CUL4 the DCX and for CUL1/CUL2 the SCF complex (Biedermann and Hellmann 2011). E3-ligase-mediated protein degradation are especially important during development (Rape, Michael 2018). For example, the loss-of-function *cul3* mutation in mouse leads to embryo lethality by increased accumulation of the protein cyclin E, which causes cell-type-specific effects on S-phase regulation and thereby causing ectopic patterning in embryonic and extra-embryonic tissue (Singer et al. 1999).

Similarly, in plants depletion of *CULLIN3A* and *CULLIN3B* is embryo lethal (Thomann et al. 2005). Likewise, the *cullin1* mutant is also embryo lethal (Shen et al. 2002), but at an earlier stage then the *cul3a/cul3b* mutant. *cul4* homozygous hypomorphic mutants show various developmental abnormalities in, for example, stomata- and root formation (Bernhardt et al. 2006), whereas amorphic *cul4* mutants are embryo lethal (Dumbliauskas et al. 2011). So far, the phenotype of *cul2* mutants has not been described in plants.

Interestingly in human cells, it was shown that CUL4A directly interacts with H1.2 (Kim et al. 2013), which allows the hypothesis that plant linker histones may also interact with CULLIN proteins during development and might possibly be targeted to degradation via ubiquitination. To test this hypothesis we analyzed the effect of *CULLINs* downregulation on H1 stability in the MMC. To this aim, we constructed inducible knockdowns of the four different CULLIN proteins and analyzed linker histone stability and MMC development.

Cullin-based E3 ligases are thought to ligate ubiquitin residues in their target protein on lysine (Stewart et al. 2016), therefore we tested whether the mutations of selected residues in H1 would make them degradation-resident.

In addition to ubiquitination phosphorylation might possibly play a role in the stability of H1 protein (Lever et al. 2000; Misteli et al. 2000), therefore we mutated amino acid (aa) residues from predicted phosphorylation sites like the S/TPxK motif (Kotliński et al. 2016).

The results give insights into the role of CULLIN proteins and certain aa on H1 stability during female sporogenesis in *Arabidopsis thaliana.*

Results

Expression of *CUL1, CUL2, CUL3A, CUL3B, CUL4* during plant reproduction

CULLIN proteins are part of the proteasome pathway in *Arabidopsis thaliana* (Biedermann and Hellmann 2011). The proteasome inhibitor test done by She and colleagues (She et al. 2013) indicated a role of the proteasome pathway in the eviction of linker histones during the female sporogenesis in *A. thaliana*. We first wanted to know if the different *CULLINs* are expressed at the right spatial and temporal manner to be involved in this process. We used published RNA-Seq and Microarray data to plot their relative expression in different reproductive and embryonic tissue (Figure 1). The plot shows the relative expression level of *CUL1*, *CUL2*, *CUL3A*, *CUL3B* and *CUL4* based on (A) RNA-Seq data from Wuest and colleagues (Wuest et al. 2010) and (B) Microarray data from Schmidt, Borges, Pina and Honys (Borges et al. 2008; Honys and Twell 2004; Pina and Pinto 2005; Schmidt et al. 2011). The script used for analyzing the RNA-Seq and Microarray data can be found at "https://github.com/VimalRawat1010/Rscripts/blob/master/LabData/.RData". It is worth mentioning that the data of the RNA-Seq and Microarray experiments can just be superficially compared since they have different bias and other limitations. But the script we used, treats both data sets exactly the same.

The reanalysis of the published expression data shows that *CUL3A* and *CUL3B* are much less expressed in the MMC or the ovule, compared to their expression in other tested tissues. The RNA-Seq plot shows that *CUL3A* is expressed in the male meiocytes. The Microarray profiling data shows that *CUL3A* is expressed in the egg cell and in the embryo starting from the pre/globular stage. Whereas the RNA-Seq data indicates less expression of *CUL3A* in the egg cell or the globular embryo, but shows an expression of it in the torpedo staged embryo. We found also different results between the Microarray- and RNA-Seq data for *CUL3B*. Here the RNA-Seq data shows a very low expression of *CUL3B* in mature pollen or the globular embryo and also weak expression in the torpedo staged embryo. Whereas the Microarray expression data suggest a little higher expression of *CUL3B* in mature pollen and in the pre/globular and heart staged embryo.

For *CUL1* the RNA-Seq results show a weaker expression in male meiocytes compared to its expression in mature pollen and the embryo at torpedo stage. This agrees with the Microarray data, which also shows weak expression of *CUL1* in uni-, bi-, tricellular and mature pollen. Furthermore, does the reanalysis of the published data suggest that C*UL1* is just very weakly expressed in the ovule or the MMC compared to its expression in other tissues plotted.

Both data sets show a high expression of *CUL2* in male meiocytes/ unicellular pollen and a decrease of its expression during its progression to mature pollen. Like *CUL3A*, *CUL3B* and *CUL1* also *CUL2* seems to be very low expressed in female sporogenesis tissues, like ovules and MMCs compared to their expression levels in other tissues. Furthermore, showed our reanalysis of the public expression data different results for the expression of *CUL2* in egg- and central cell, the synergids and the globular embryo stage. The RNA-Seq data indicates higher expression in the central cell compared to the other tissues mentioned above, whereas the Microarray data suggest weak expression of it in those tissues.

In contrast to the other *CULLINs*, suggest the reanalysis of the expression data that *CUL4* has a very high expression in the female MMC and the egg cell. Furthermore, do both data sets indicate that *CUL4* is expressed less in the pre-/globular- and torpedo staged embryo compared to its expression level in the MMC in the Microarray data and the egg cell in the RNA-Seq data. In the male tissue, the RNA-Seq and Microarray data show different expression levels. The RNA-Seq data shows very low expression of *CUL4* in either male meiocytes or mature pollen, whereas the Microarray data suggest rather a medium expression of *CUL4* in uni- and bicellular pollen, compared to its expression in other tissues in each data set.

The reanalysis of the expression data of both data sets suggests that from the *CULLIN* genes tested, *CUL4* is one with a high expression in the MMC. Unfortunately, we don't have expression data specific to MMC development before the MMC stage. Thus we do not know if *CUL4* is expressed also in the sub-epidermal nucellar cell of the sporophytic tissue (somatic cell), which gives rise to the MMC. This could give us a hint if *CUL4* is a potential candidate to mediate linker histone eviction prior to MMC stage.

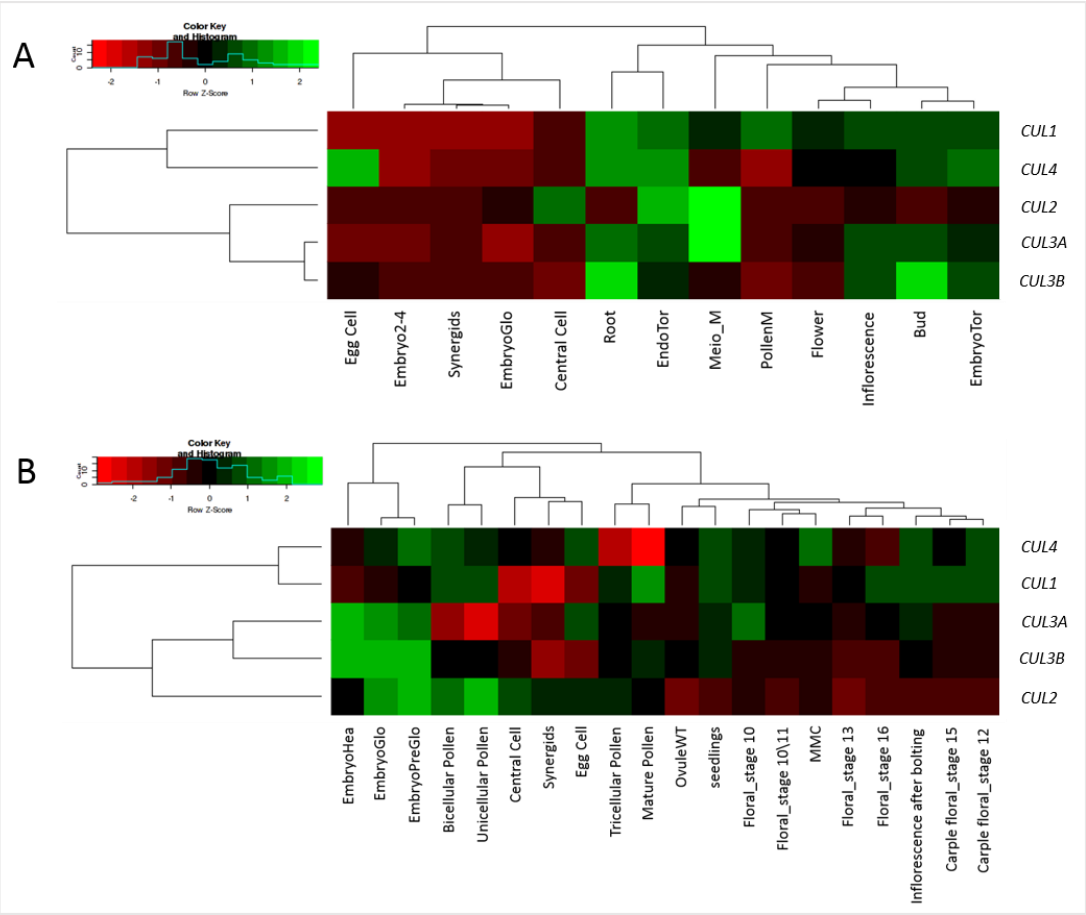

Figure 1.: Heatmap of RNA-Seq and GeneCHIP. Relative Expression of *CUL1* (*AT4G02570*), *CUL2* (*AT1G02980*), *CUL3A* (*AT1G26830*), *CUL3B* (*AT1G69670*), *CUL4* (*AT5G46210*) in different tissue present in (A) RNA-Seq experiments from Wuest and colleagues (Wuest et al. 2010) and (B) on Affymetrix ATH1 GeneCHIP experiments from different publications (Borges et al. 2008; Honys and Twell 2004; Pina and Pinto 2005; Schmidt et al. 2011). Both heat maps are designed with the R-script published in GitHub (https://github.com/VimalRawat1010/Rscripts/blob/master/LabData/.RData). The tool considers shape and gene expression values to create the dendrograms and colors. The table with normalized expression values can be found in the Supplement. Abbreviation: (A) PollenM (pollen mature), Embryo2-4 (embryo cell stage 2-4), EmbryoGlo (embryo globular stage), EndoTor (endosperm torpedo stage), Meio_M (meiocytes male), EmbryoTor (embryo torpedo stage). (B) MMC (megaspore mother cell), EmbryoHea (embryo heart stage), EmbryoPreGlo (embryo pre-globular stage).

Aberrant MMC development and altered linker histone stability in inducible *cul4* knockdowns

Since considerable evidence (She et al. 2013) suggest a role of the proteasome pathway in linker histone eviction during MMC formation and our reanalysis of public expression data revealed the presence of CUL4 in the MMC, we decided to test if CUL4 is involved in the degradation of linker histones during female sporogenesis. First, we designed a Dex-inducible amiRNA against *CUL4* and checked if it successfully downregulates *CUL4*. We identified three independent insertion lines which showed (Figure 2 B) known *cul4*, *fusca* or hyperphotomorphogenic phenotype upon induction with Dex. This experiment suggests that the amiRNA against *CUL4* is functional and therefore we analyzed linker histone expression

and MMC formation 5 dpi (days post induction) of the amiRNA[*CUL4*]; BG lines (Figure 2 A, C to E). Three plant lines showed a persistence of linker histone H1.1 signal in 45%, 39% and 12% of ovules upon induction with Dex in comparison to only 4.5% in the control BG line treated the same way. We also observed aberrant development of MMCs in the same lines from 38%, 18% and 38%, which was never observed for the control, Dex-treated BG line (JS64) (Figure 2 C and Supplement Figure 2 B). As criteria for a normal or WT development of a MMC we considered its shape, size, position and H1.1-GFP signal. Thus, ovules with no apparent MMC, based on morphological- and H1-levels criteria or ovules with two enlarged cells with persistent H1 levels were defined in our analysis as aberrant MMCs. We observed in the induced plants phenotypes of two enlarged MMC-like cells and no MMC development (Figure 2 E and Supplement Figure 1 B). In Figure 2 D we plotted the observed phenotypes of no MMC identification, aberrant H1.-GFP stability and two enlarged like MMC cells after Dex-induction compared to induced BG line (JS64). Interestingly one line, which showed no *fusca* phenotype in T2, still had significantly different MMC formation, meaning we could not identify an clear MMC after induction in T1 (see Supplement table 1). This observation can be explained either by errors in observation and identifying the MMC or by a varying degree of *CUL4* knockdown in the independent insertion lines, similar to what was seen by Chen and colleagues (Chen et al. 2006). But all in all, the results suggest that *CUL4* is important for regulating H1.1 stability which in turn influence the development of the MMC.

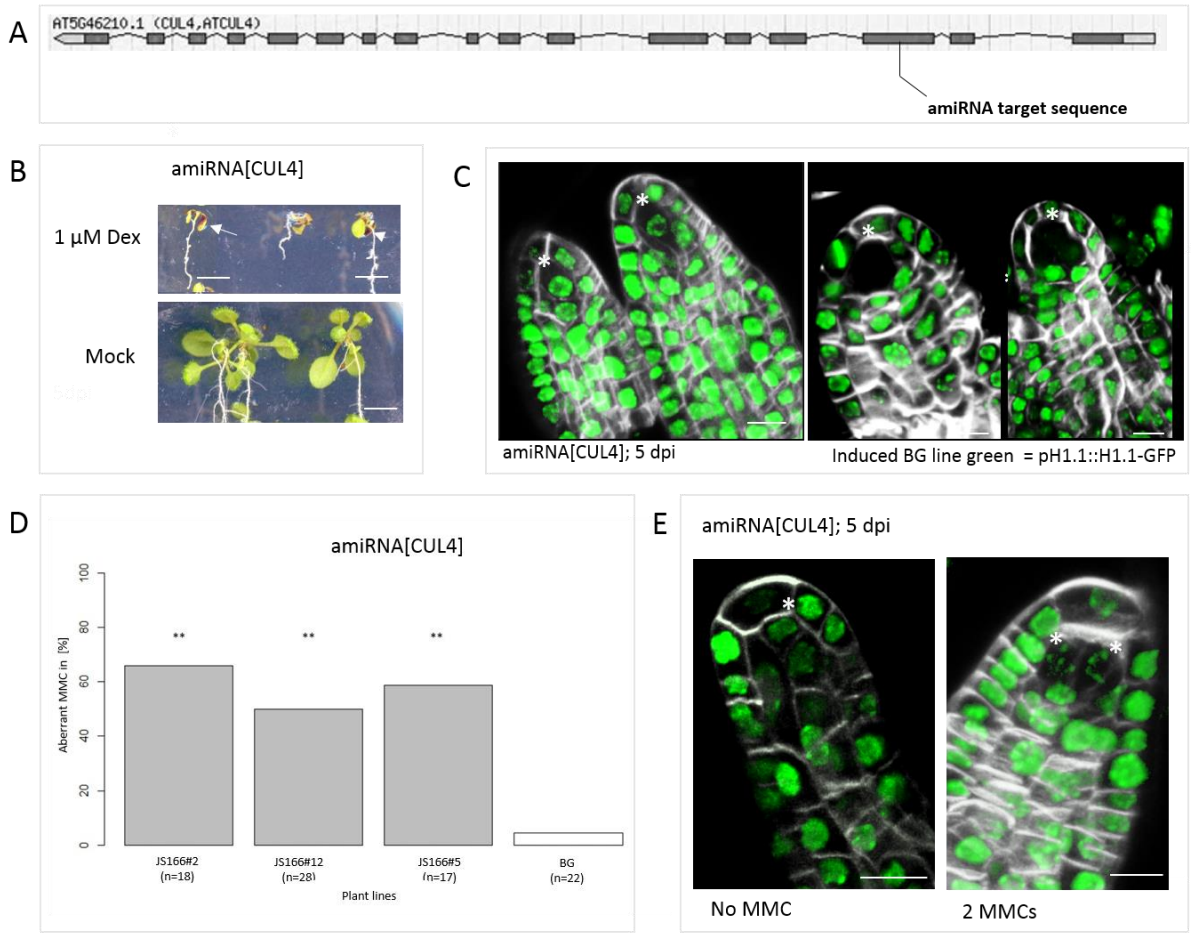

Figure 2: Dex-inducible amiRNA against CULLIN4 causes aberrant expression of H1.1 and abnormal development of the MMC during female sporogenesis in *Arabidopsis thaliana*. (A) Gene model of *AT5G46210.1* (*CUL4*) with the amiRNA target site shown. The

target sequence and mismatches for the different amiRNAs can be found in the Supplement (B) *cul4* knockdown mediates a *fusca* phenotype (Chen et al. 2006) in the light. The upper and bottom panels show 11-d-old light-grown inducible amiRNA[*CUL4*] seedlings, induced in the upper panel and Mock-treated in the lower panel. The induced *cul4* mutants show impaired growth of true leaves, anthocyanin accumulation (arrow) in the cotyledons, typical for a hyperphotomorphogenic response, originally described in the *fusca* mutant (Castle and Meinke 1994) and mimicked by *cul4* mutants (Chen et al. 2006). Scale bar = 5 mm. (C) Expression of *H1.1-GFP* in amiRNA[*CUL4*], BG and BG line, both lines were induced 4 to 5 dpi 10 µM Dex. Gray = Renaissance counterstaining signal. (D) Three independent insertion lines of amiRNA[*CUL4*], as well as one BG line, have been tested for aberrant MMC development, which included expression of p*H1.1::H1.1-GFP* at stages 1-II until 2-II; no MMC or more than one enlarged MMC like cell. 66% (total-n = 18), 50% (total-n = 28), 58.8% (total-n = 17). One background line was tested also after 4 to 5 dpi with 10 µM Dex-treatment: no eviction of H1 4.5% (n-total = 22) and no observation of aberrant MMC development. n corresponds to the number of the analyzed ovules. ** indicates statistically significant difference from the control tested by the Fisher exact test ($p < 0.01$). JS166#2 $p = 0.000035$; JS166#12 $p = 0.000496$, JS166#5 $p = 0.000263$. (E) Aberrant development of ovule primordia after induction. Phenotypes: no MMC, two enlarged MMC-like cells with GFP signal.

Aberrant MMC development in inducible *cul3a* and *cul3b* knockdowns

To determine if CUL3A and CUL3B play a role in MMC development and linker histone expression during sporogenesis in *Arabidopsis thaliana*, we designed one inducible amiRNA which targets both *CUL3A* and *CUL3B* (Figure 3 A). In one out of four positive T1 plants, 27% of the ovules did not show typical MMC features (size, shape, position and/or H1.1 signal) upon induction (n = 42) compared to only 3.6% ovules in induced BG line (n = 28) (Figure 3B and C). The rest of the amiRNA[*CUL3A, CUL3B*] ovules showed a WT like MMC development and also normal H1.1 signals.

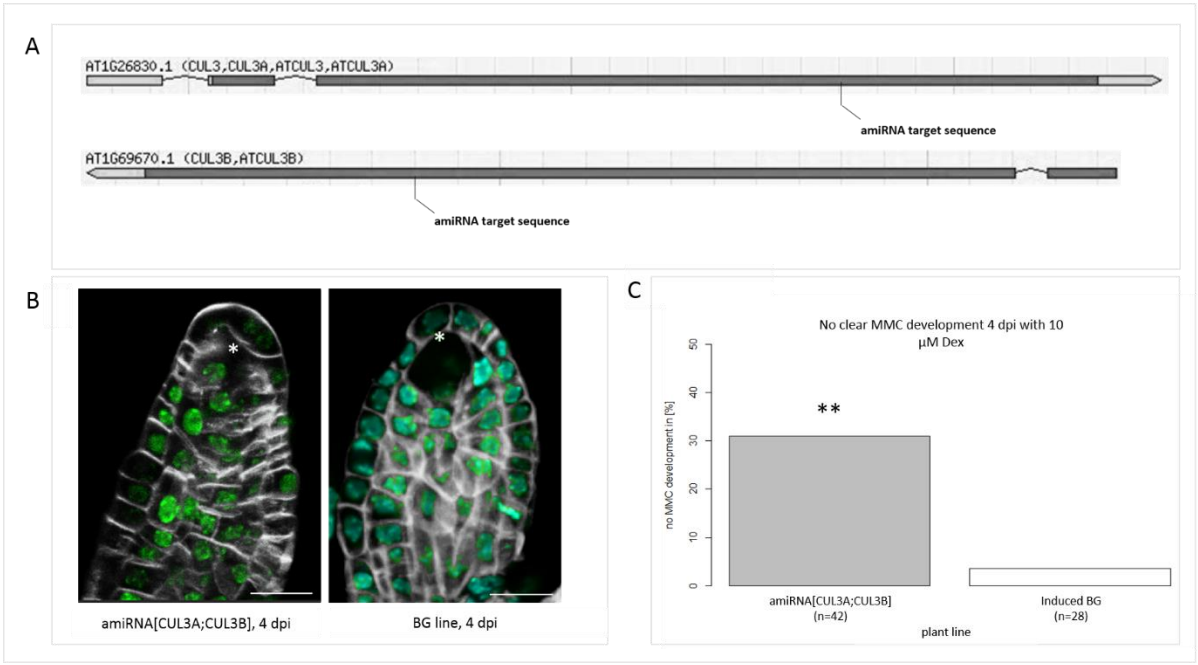

Figure 3: Dex-inducible amiRNA[*CUL3A,CUL3B*] shows aberrant MMC development. (A) Gene model of *AT1G26830.1* (*CUL3A*) with the amiRNA target highlighted. Gene model of *AT1G69670.1* (*CUL3B*) with the amiRNA target highlighted. The target sequence and

mismatches for the different amiRNAs can be found in the Supplement. (B) Expression of *H1.1-GFP* in amiRNA[*CUL3A;CUL3B*] and BG line 4 dpi with 10 µM Dex. (left) no MMC is detectable (right) normal MMC detectable. Green = *pH1.1::H1.1-GFP*. Gray = Renaissance counterstain. Scale bar = 10 µm. (C) One plant line showed a significant (p = 0.00539) development of aberrant MMCs compared to BG line after 4 dpi with 10 µM Dex. amiRNA[*CUL3A,CULB*],BG (n-total = 42) 30% developed no detectable MMC. BG plant 4 dpi with 10 µM Dex, (total n = 28) 3.6% showed no detectable MMC. ** $p < 0.01$ (Fisher exact test) compared to induced BG control.

Dex-inducible knockdown of *cul1* and *cul2*

To test whether *CUL1* and *CUL2* play a role in linker histone degradation during female sporogenesis and correct MMC formation we designed an inducible amiRNA against both *CUL1* and *CUL2* (Figure 4 A and B). We identified 15 independent positive insertion lines of Dex-inducible amiRNA[*CUL1;CUL2*] based on BASTA selection. Out of 15 independent insertion lines, we identified two lines which showed a *cul1;cul2* mutant phenotype, described by Gilkerson and colleagues (Gilkerson et al. 2009)(see Figure 4 C). Those two lines can be used in the future to screen for altered linker histone dynamics in MMC development after Dex-induction.

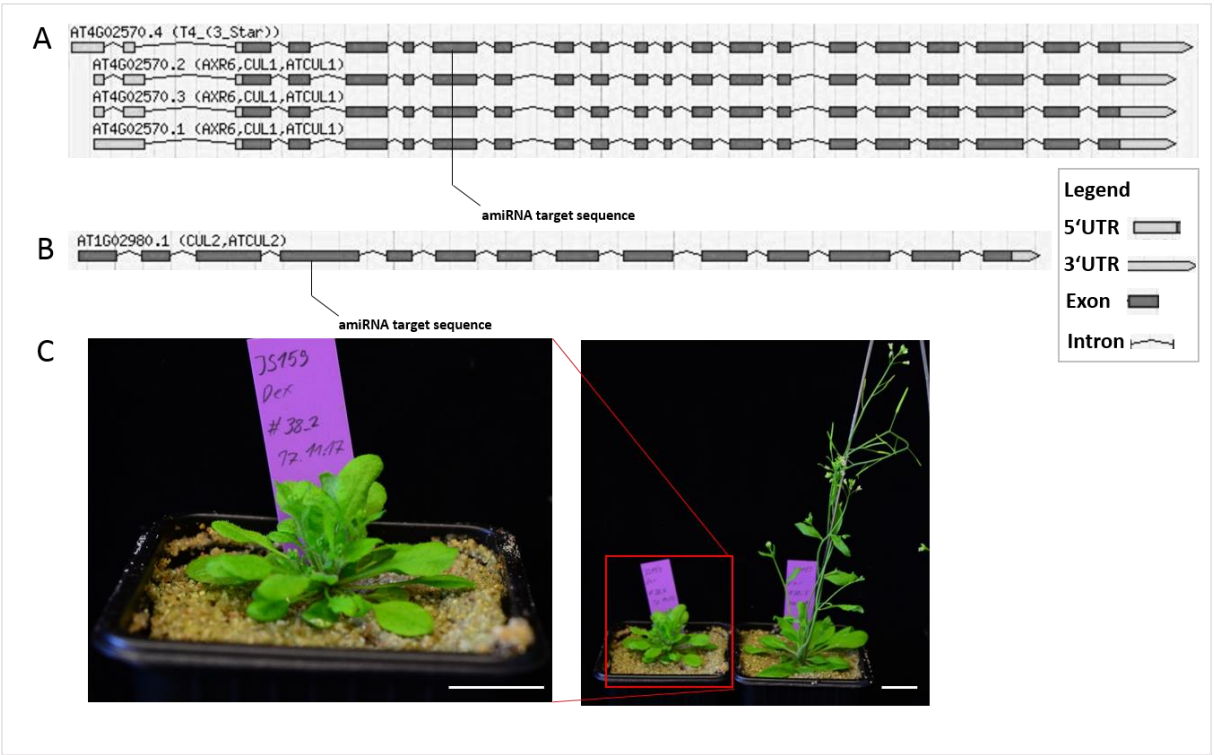

Figure 4: amiRNA knockdown of CULLIN1 and CULLIN2. (A) Gene model of *AT4G02570.1*; *AT4G02570.2*; *AT4G02570.3* and *AT4G02570 .4* (*CUL1*) with the amiRNA target site highlighted. (B) Gene model of *AT1G02980.1* (*CUL2*) with the amiRNA target highlighted. The target sequence and mismatches for the different amiRNAs can be found in the Supplement. We identified positive T1s plants, based on BASTA selection. But we have not yet tested them for an effect in sporogenesis and gametogenesis. The target sequence and mismatches for the different amiRNAs can be found in the Supplement (C) Morphological phenotype of

amiRNA[*CUL1, CUL2*] in comparison to segregating wt/heterozygote plant after three weeks of watering with 10 µM Dex. Scale bar = 1.6 cm.

Design of the inducible H1 synthetic variants for testing the role of PTMs on H1 stability

To characterize the role of putative ubiquitination and phosphorylation in H1 on its stability, we designed several H1 mutant variants with altered amino acids (aa) predicted to be phosphorylated and ubiquitinated (Figure 5 A). We selected these aa based on (i) a physical map of PTMs on H1.1 and H1.2 of *A. thaliana* produced from LC-MS experiments (Kotliński et al. 2016), (ii) sequence alignments of H1s between *A. thaliana*, mouse and humans, in which the PTMs were annotated (Wisniewski et al. 2007), and (iii) available prediction algorithms for ubiquitination target sites (Chen et al. 2011; Radivojac et al. 2011; Walton et al. 2016). We designed eight variants where (I) three lysine were mutated to arginine in the globular domain (3xG), (II) or eleven lysine to arginine in the globular domain (11xG), (III) one serine to alanine in the N-tail (1xN), (IV) eleven lysine to arginine in the N-tail (11xN), (V) two serine to alanine and one threonine to valine in the C-tail (3xC), (VI) sixteen lysine to arginine in the C-tail (16xC), (VII) twenty-six lysine to arginine in the C-tail (26xC) and (VIII) one lysine in the globular domain and five lysine in the C-tail to arginine (6xGC). We generated constructs where these H1 mutant variants are expressed under the Dex-inducible system and are fused to a red fluorescent protein (RFP) (Shaner et al. 2008). This way, the expression of the mutant variants can be induced at specific time points, and protein dynamics can be monitored during germline differentiation. We assessed the PTM sites in different H1 domains (N-tail, globular domain and C-tail) separately not to perturb the tertiary structure of H1.1 too much (Figure 5 A). We decided to start the series of mutations in H1.1 and not H1.2 or H1.3, due to the fact that *H1.3* was never detected during MMC development (She et al. 2013) and due to time reasons. After the identification of positively transformed plants, expressing the mutant H1.1 variant, we crossed those plants to plants harboring pH1.1::H1.1-GFP to directly compare the linker histone dynamics of both variants in one plant.

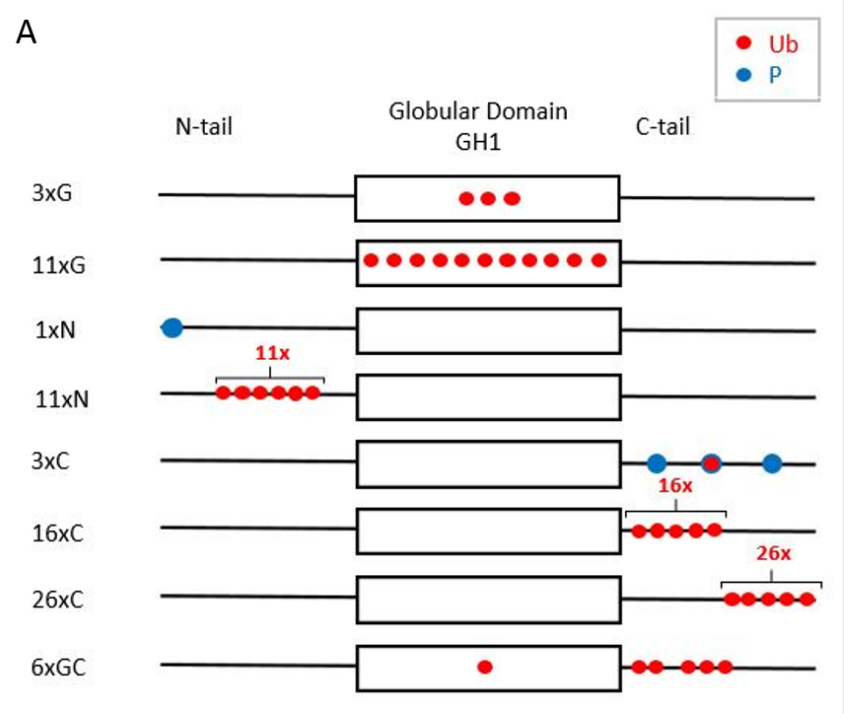

Figure 5: Schematic presentation of cloned H1.1 mutant variants. (A) The model shows the three structural parts of linker histones in *A. thaliana* (N-terminal, globular [box] and C-terminal) as well as modified amino acids that are predicted targets of ubiquitination (red) (Chen et al. 2011; Radivojac et al. 2011; Walton et al. 2016), targets of phosphorylation (blue) (Kotliński et al. 2016). Left: Name of each mutant construct based on the number of aa changes (6x, 11x) and the domain. Each variant was fused, at the end of their C-terminal domain to the

fluorescent reporter protein RFP (Shaner et al. 2008) and designed to be expressed under the Dex-inducible system (Samalova, Brzobohaty, and Moore 2005).

H1.1^{3xG}RFP expressing plants show abnormal H1.1 stability and higher chromatin compaction

As we already described in the introduction, during SMC development She and colleagues (She et al. 2013) detected transient H1 eviction. Here we tested whether the H1.1^{3xG}RFP variant would have different H1 dynamics than the wild-type version of the protein. We identified that an H1.1^{3xG}RFP mutant variant shows an absence of H1 eviction during 1-II and 2-II stage in < 10% (n-total = 100) of the SMCs (Spore Mother Cell) analyzed (Figure 6 A). This variant has three lysine-to-arginine conversions in the globular domain of H1.1. We hypothesize that the mutated lysines might be targets of ubiquitination in the wild-type protein, which in turn would lead to proteasomal degradation. As arginine cannot be ubiquitinated, the mutated version H1.1^{3xG}RFP cannot be degraded by the proteasome pathway and therefore cannot be evicted. This result is consistent with the proteasome inhibitor test described earlier by She and colleagues (She et al. 2013). With the same variant, we found, in several independent lines, a change in the H1 signal levels in MMC at prophase where the protein should be present (She et al. 2013) 3 dpi with Dex (Figure 6 B and Supplement Figure 2 A) which we did not detect in the induced H1.1-RFP control construct 5 dpi with Dex (Figure 6 C). We first interpreted this result as a defect in H1 reloading. However, the possibility remains that the ovule stage relative to the time of treatment differs for this variant compared to the H1.1^{wt}RFP control. Even though we showed in chapter 3 of this thesis that the Dex-treatment alone has no influence on the temporal progression of the MMC. But also our results in chapter 2 and 3 of this thesis suggest that the induction time might not be long enough to reach the developmental stages to monitor for altered linker histone dynamics. Therefore it would be recommended to repeat the induction experiments and analyze H1's stability after 5 dpi.

To analyze whether the mutant variants have altered properties in terms of stability/turnover onto the chromatin, we performed fluorescence recovery after photobleaching (FRAP) experiments (Figure 6 D). We found no significant difference in fluorescence recovery during the first 30 sec between the H1.1^{3xG}RFP mutant and the wild-type H1.1-GFP signal. We observed that the mutant has more and larger chromocenters. This increase in chromocenters might be caused by the defective eviction or defective reloading of mutated H1.1 (Figure 6 D).

In addition, we wanted to know if the H1.1^{3xG}RFP mutant variant has an effect during plant development. We expected that the mutant H1.1 variant would be dominant over the WT-variant, because our hypothesis is that the H1.1^{3xG}-RFP variant, cannot be marked by PTM in the mutated globular domain and therefore persists on the chromatin, whereas the WT-variant would be evicted. Therefore, we tested seedling development ability and lateral root development in H1.1^{3xG}RFP transgenic lines in Col-0 background (Supplemental Figure 3 and 4). In two independent lines out of three tested, we identified a significant difference between the development of seedling on Dex- and Mock-medium. On Dex-medium we found ~64% (n = 132) of all seedlings of the line JS121 to be paler and smaller in comparison to the Mock control. On Mock-plates the line JS121 just showed in 0.41% (n = 1) this small and white phenotype. For the line JS93, the difference was not so drastic but still significant. For the development of the number of lateral roots and root length, we did not find any difference between the H1.1^{3xG}RFP mutant plants, WT and *3h1* plants.

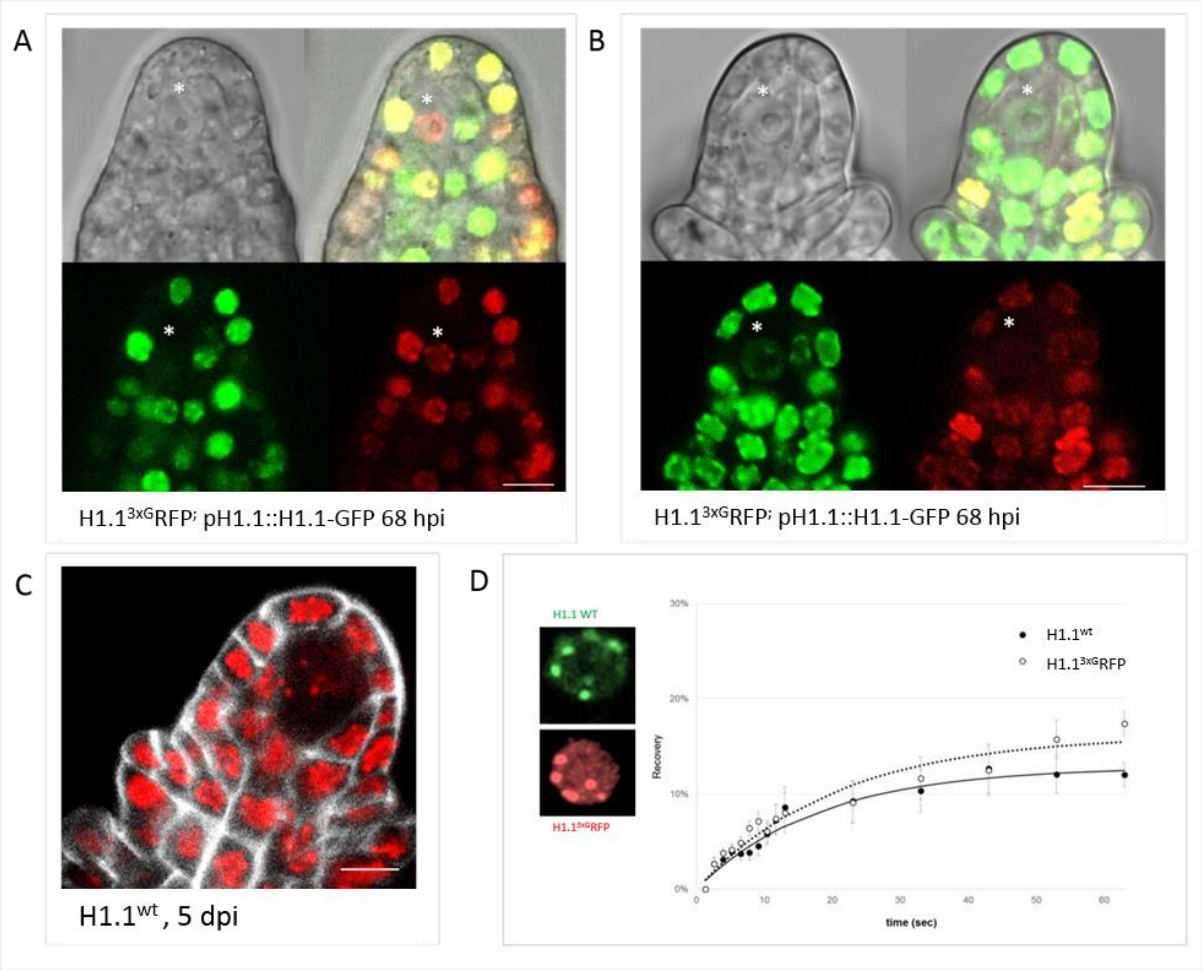

Figure 6: H1.1^{3xG}RFP mutant shows altered H1 expression compared to WT. (A) Some cases (n < 5) showed at developmental stage 2-I eviction of H1.1-GFP, but no eviction of H1.1^{3xG}RFP in MMCs 68 hpi (hours post induction) with 10 µM Dex. (B) Reloading of pH1.1::H1.1-GFP but not of H1.1^{3xG}RFP 68 hpi with 10 µM Dex compared to (C) vector control line, which shows reloading of H1.1^{wt} at the same stage 2-III, 5dpi with 10 µM Dex. (D) Observation of nuclear organization in lines expressing the mutant variant H1.1^{3xG}RFP showed a higher compaction of heterochromatin in roots. FRAP (Fluorescence Recovery After Photobleaching) curves show similar speed in the immediate recovery phase (no significant difference on fits), but long-term recovery of the H1.1^{3xG}RFP variant is slower. (A to C) Scale bar = 10 µm.

Inducible H1.1^{3xC}RFP and H1.1^{1xN}RFP synthetic variants show normal expression pattern of H1.1 in ovule primordia

To determine if phosphorylation of certain amino acids of H1 has an influence on its stability we exchanged in one variant in the N-tail the amino acid serine at position 2 to alanine to prevent its putative phosphorylation. In another variant we exchanged in the C-tail the serine at position 229 and 263 to alanine and threonine at position 250 to valine, to also prevent their putative phosphorylation. The three amino acids in the C-tail are all part of the S/TPxK motif, which is a target of phosphorylation by the Cyclin-Dependent Kinases (CDKs) (Contreras et al. 2003) (reviewed also earlier in Introduction of this thesis). The mutant variants H1.1^{3xC}RFP

and H1.1^{1xN}RFP showed normal linker histone signals after 3 dpi (Figure 7 A and B). The results suggest that the mutated amino acids are either no targets of PTMs or that the modifications on this particular amino acids have no influence on H1.1 eviction and reloading during female sporogenesis. Furthermore, do we need to keep in mind that our results describe in chapter 2 and 3 of this thesis have shown that the induction time might be not enough to reach the developmental stages to monitor for altered linker histone dynamics during this developmental process. Therefore it would be recommended to repeat the induction experiments and analyze H1's stability after 5 dpi with 10 µM Dex.

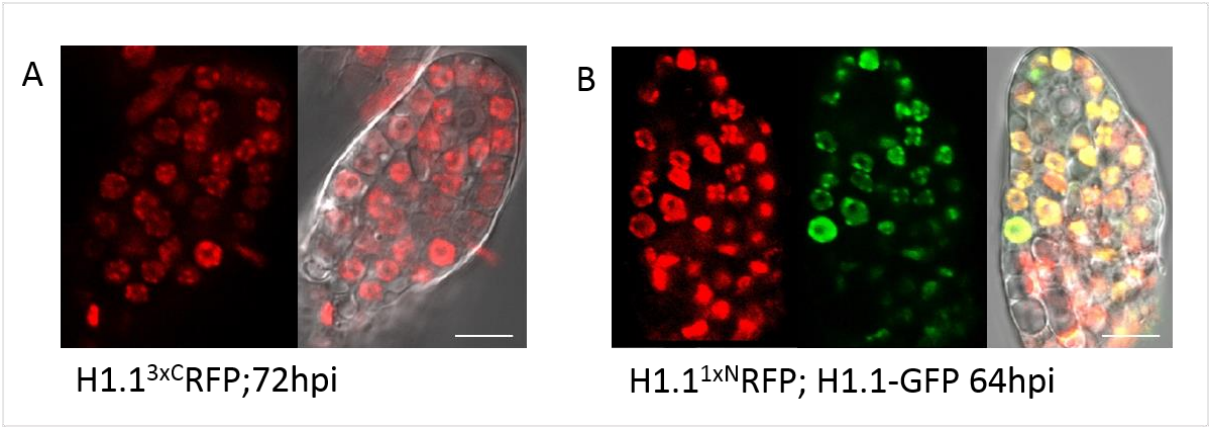

Figure 7: H1.1^{3xC}RFP and H1.1^{1xN}RFP variants shown WT eviction pattern of H1 in MMC development. (A) Expression of *H1.1^{3xC}RFP* variant 72 hpi with 10 µM Dex. Eviction of *H1.1^{3xC}RFP* variant at stage 1-II. Two independent insertion lines were analyzed (n-total = 9 at stages 1-I to 2-III). Red = RFP. Scale bar = 10 µm. (B) Expression of *H1.1^{1xN}RFP* variant 64 hpi with 10 µM Dex. Eviction of *H1.1^{1xN}RFP* variant and H1.1-GFP signals at stage 2-I. One insertion line was analyzed (n-total = 15 at stages 1-II to FM). Red = RFP, green = GFP. Scale bar = 10 µm.

The other five designed mutant H1 variants are still in the cloning phase. The RFP constructs *attL1-H1.1^{11xG}RFP-attL2*, *attL1-H1.1^{16xC}RFP-attL2*, *attL1-H1.1^{26xC}RFP-attL2*, *attL1-H1.1^{11xN}RFP-attL2* and *attL1-H1.1^{6xGC}RFP-attL2* are recombined into entry vectors and transformed to E.coli DH5alpha and need to be cloned via Gateway cloning into the *pRPS5a::LhGR2-GUS::pOP6::* vector (Ian Moore, Oxford) to transform them to Col-0 plants and screen them 5 dpi with 10 µM Dex for altered H1 stability.

Discussion

Our results have started to unravel how linker histone dynamics regulate the somatic-to-reproductive cell-fate transition in *A. thaliana*. We identified PTMs sites which are putative regulators of linker histone dynamics. Our data suggest that amino acid modifications, which prevent potential ubiquitination in the GH1 domain of H1.1 can alter its stability in the developing SMC. Our findings further indicate that *CUL4* is involved in H1 linker histone eviction during the somatic-to-reproductive transition in *Arabidopsis thaliana* and that a knockdown of *CUL4* leads to altered MMC formation.

We identified by functional screens for the amiRNA constructs against *CUL4* and *CUL1;CUL2* plant lines which showed the expected phenotypes for downregulations of the target gene(s). For downregulation of *CUL4* we identified plants with a hyperphotomorphic/*fusca* phenotype.

This phenotype was previously described by Chen and colleagues (Chen et al. 2006) to be caused by loss-of-function of *cul4*.

For the downregulation of *CUL1*;*CUL2* we identified two independent insertion lines, which showed after Dex-treatment a phenotype of *cul1-7* mutants (described by Gilkerson et al. 2009). Since we found in both amiRNA constructs against i) *CUL4* and ii) *CUL1;CUL2* several independent insertion lines, which showed the same phenotype in i) *fusca* phenotype and in ii) smaller plants, it indicates that those phenotypes are probably not caused by an insertion site effect, but rather by the knockdown of i) *CUL4* or ii) by *CUL1* and/or *CUL2*. We still need to confirm that the phenotypes are not caused by off-target genes downregulation. This needs to be tested by rescuing the phenotypes with amiRNA resistant variants of i) *CUL4* and ii) *CUL1* and *CUL2*. Furthermore, downregulation of the target genes needs to be confirmed by qPCR experiments. In addition, it should be checked that the phenotypes are not caused by a general accumulation of proteins, which normally would be marked for degradation by the CULLIN E3-ligase proteins. Interestingly we found varying degrees of the *fusca* phenotype after induction in the plant lines harboring the *amiRNA[CUL4]* construct. This might be a result of variable degrees of *cul4* downregulation and can be tested by correlating the *fusca* phenotype with qPCR based *CUL4* expression measurements.

It still needs to be tested whether the *amiRNA[CUL1;CUL2]* plant lines, which showed the *cul1-7* plant phenotype also show altered H1 stability. Whereas the analysis of the four independent insertion lines of *amiRNA[CUL4]* revealed that three of them showed the *fusca* phenotype and also a significant degree of aberrant MMC development and H1 stability.

For the amiRNA designed against *CUL3A* and *CUL3B* we did not do a function screen for an *CUL3A/cul3a cul3b/cul3b* phenotype (Figueroa et al. 2005). Nevertheless, we identified one inducible insertion line, in which we could not identify the MMC in 30% of ovules analyzed. At the moment we cannot conclude if this phenotype is caused by downregulation of *CUL3A* and *CUL3B* or by an insertion site– or off-target effect. Further experiments need to be done to clarify these questions. QPCR of induced seedlings could show if *CUL3A* and *CUL3B* are downregulated. Further complementation experiments with an amiRNA resistant *CUL3* variant, should clarify if the phenotype is caused by a downregulation of *CUL3A* and/or *CUL3B* or by off-target effects. However, so far, we cannot conclude about any role of *CUL3A* and *CUL3B* in H1 stability during plant sporogenesis.

To summarize the findings of a putative role of CULLIN proteins in H1 stability, we can conclude that we designed three inducible amiRNA constructs against i) *CUL4* ii) *CUL1;CUL2* and *CUL3A, CUL3B.* For the designed amiRNA constructs against *CUL4* and *CUL1;CUL2* we identified several independent insertion lines with a putative downregulation of the target genes. Those lines can be used to further study the role of those genes in H1 stability. In addition, the lines can be used to study the role of those genes in other processes, where a conditional downregulation of the genes are favorable or necessary.

The results mentioned above indicate a role of *CUL4* in linker histone stability during the female sporogenesis in *Arabidopsis thaliana*. Our hypothesis is that *CUL4* dependent ubiquitin ligase complex mediates linker histone eviction by ubiquitination of certain aa in H1 and further proteasomal degradation, similar to what has been proposed in animal cells (Izzo and Schneider 2015; Wisniewski et al. 2007). Our results suggest that three amino acids in the globular domain of H1 might be targets of ubiquitination by *CUL4*. We found that the mutation of lysine(89), lysine(104) and lysine(111) to arginine was enough to alter H1s eviction from the chromatin but also it's reloading to the DNA during SMC development. To our surprise, we

could not confirm the change in H1 dynamics in this mutant variant by FRAP experiments. But we found that the H1.1^{3xG}RFP mutant had a slower recovery compared to the WT, which fits with the impaired reloading phenotype. Based on our observations we cannot conclude if the change in H1s stability in the H1.1^{3xG}RFP mutant is caused by i) the deficiency of the mutated H1 to bind to the DNA or by II) the deficiency of the mutated H1 to get marked with ubiquitin and degraded. Binding assays of the mutated variant and the DNA could answer this question as well as western-blots to prove ubiquitination.

Interestingly the H1.1^{3xG}RFP mutant variant showed more and larger chromocenters, which might be caused by the defective eviction or defective reloading of the mutated H1.1. In addition, we detected in two cases (n-total = 100) the development of two enlarged MMC-like cells, which indicates a miss-regulation of SMC formation in the H1.1^{3xG}RFP mutant (Supplement Figure 2 B). This might be caused by the increase of chromocenters, which may alter transcription and thereby influences the robustness of developmental decisions (see chapter 1 of this thesis). To this hypothesis does also fit our observation that the H1.1^{3xG}RFP mutant showed abnormalities during seedling development (Supplement Figure 3).

In the two H1 mutant variants, where we mutated aa, which are putative phosphorylation targets, we detect no obvious changes in H1 stability. This finding surprised us, since phosphorylation is a well-known post-translational regulator of histone dynamics (Izzo and Schneider 2015), especially during cell-fate transition. But our results suggest that the mutated amino acids are either not targets for phosphorylation or that those amino acids are not involved in regulation of H1s stability. But our experiments were limited, because of i) number of independent insertion lines tested and ii) time of examination after induction with Dex. Since our results presented in chapter 2 and 3 of this thesis, have shown that the induction time might not be enough to reach the developmental stages to monitor for altered linker histone dynamics. Therefore, we cannot exclude that phosphorylation of certain amino acids in and outsides of the S/TPxK motif in H1.1 play a role in linker histone stability during sporogenesis in *A. thaliana*. Induction experiments with more independent insertion lines and longer induction time need to be performed to obtain a conclusive answer.

Based on our *cul4* knockdown and 3xG mutant results, which are consistent with the proteasome inhibitor test described by She and colleagues (She et al. 2013), we propose a hypothesis that H1 eviction during the SMC development is mediated by ubiquitination of amino acids in the globular domain of H1 by CULLIN4 dependent E3-ligases and further degradation by proteasomal. In turn, this may allow the chromatin to decondens and probably influence DNA methylation and epigenetic reprogramming via activation of specific transcription processes which are important for correct MMC development. But the hypothesis and the detailed mechanism need to be further investigated and proven.

Material and Methods

Plant material and growth conditions

Arabidopsis seeds were sterilized in 3% Bleach with 0.01% Triton X-100, washed in 70% EtOH, and sown out on 1/2 Murashige and Skoog (MS) salts (CAROLINE), 1% sucrose, 1% (w/v) agar pH 5,6.

For FRAP and germination experiments the sterilized seeds were sown on 1/2 Murashige and Skoog (MS) salts (CAROLINE), 1% sucrose, 1% (w/v) agar pH 5,6 containing either 1 µM, 10 µM Dex- or Mock- (0.01% EtOH) plates.

Sterilized seeds on plates were stored for 2 to 4 days at 4°C before transferring them to incubators (Percival) with long day conditions of 16 hours light [120 µE m-2 s-1] at 21°C and 8 hours dark at 16°C. The young plants were then transferred to soil and grown in a growth chamber with long day conditions (16h light/ 8h dark) at 22°C light and 18°C dark.

For FRAP experiments plants were grown on plates as mentioned above, under long day conditions in an incubator (Percival) for 7 days.

Hyperphotomorphogenic phenotype experiments: Plants were grown on 1 µM Dex- or Mock- plates for 5 days in incubators (Percival) with continuous light conditions [120 µE m-2 s-1] at 21°C. Afterwards, they were stored for two days at 4°C in the dark before transferred again for another 6 days to continuous light, before they were imaged.

T2 plants transformed with Dex-inducible amiRNA against *CUL1* and *CUL2* were watered three weeks with 10 µM Dex before monitoring for morphological phenotypes.

Cloning

The creation of the BG line is described in chapter 3 of this thesis.

The Dex-inducible amiRNAs are designed with the Phantom database (Hauser et al. 2013) besides the amiRNA against *CUL4*, which was designed with the wmd3 database (Schwab, Ossowski, and Warthmann 2010). The attL1-amiRNA-attL2 constructs were synthesized by Genescript and cloned via Gateway into the *pRPS5a::LhGR2-GUS::pOP6::* vector (Ian Moore, Oxford). The constructs were transformed via *Agrobacterium tumefaciens* (GV3101) to homozygous *pH1.1::H1.1-GFP, pH1.2::H1.2-ECFP, 3h1 lines* (BG lines). Positive T1s were identified based on BASTA selection and GUS reporter assay after 10 µM Dex-treatment as described in chapter 3.

One Dex-inducible amiRNA was designed to polycistronic express amiRNAs against different genes. In particular it was *MIR395[CUL1;CUL2]MIR319a[CUL4]MIR172a[CUL3a;CUL3b].* This construct was synthesized by Genescript and cloned via Gateway into the *pRPS5a::LhGR2-GUS::pOP6::* vector (Ian Moore, Oxford). The construct was transformed to *Agrobacterium tumefaciens* (GV3101) and stored as a glycerol stock.

The RFP constructs $H1.1^{3xG}$, $H1.1^{3xC}$, $H1.1^{1xN}$ were synthesized by Genescript and cloned via Gateway into the *pRPS5a::LhGR2-GUS::pOP6::* vector (Ian Moore, Oxford). The constructs were transformed via *Agrobacterium tumefaciens* (GV3101) to Col-0 plants. Positive T1s were identified based on BASTA selection and GUS reporter assay after 10 µM Dex -treatment as described in chapter 3.

The RFP constructs *attL1-*$H1.1^{11xG}$*RFP-attL2*, *attL1-*$H1.1^{16xC}$*RFP-attL2*, *attL1-*$H1.1^{26xC}$*RFP-attL2*, *attL1-*$H1.1^{11xN}$*RFP-attL2* and *attL1-*$H1.1^{6xGC}$*RFP-attL2* were synthesized by Genescript and the plasmid was re-sequenced by us and transformed to E.coli DH5alpha to produce our own glycerol stock.

Positive T1 plants of the genotypes *H1.1^{3xG}RFP*, *H1.1^{3xC}RFP* and *H1.1^{1xN}RFP* were crossed to *pH1.1::H1.1-GFP*/ *pH1.1::H1.1-GFP;3h1* plants. Positive plants of the crosses were identified by detecting GFP signals and RFP signals after 10 µM Dex-induction.

Dex-induction by brushing and imaging

We analyzed in detail 4 independent lines of Dex-inducible *amiRNA[CUL4];* 4 independent lines of Dex-inducible *amiRNA[CUL3a; CUL3b]*; 7 independent lines of Dex-inducible *H1.1^{3xG}RFP*; 2 lines of Dex-inducible *H1.1^{3xC}RFP* (of 6 independent insertion lines) and 1 lines of Dex-inducible *H1.1^{1xN}RFP* (of 5 independent insertion lines).

Single inflorescences induced with 10 µM Dex-solution (0.01% EtOH) or Mock (0.01% EtOH) were dissected after 4 to 5 days post induction (dpi). Single carpels were freshly dissected in either fresh Renaissance staining solution (final concentrations: 4% paraformaldehyde;1:2000 Renaissance;10% glycerol; 0.05% DMSO in 1x PBS (modified from Musielak et al. 2015) or in ddH_20 and directly imaged.

Serial images of fluorescent signals in whole-mount ovule primordia were recorded by confocal laser-scanning microscopy with a Leica SP5-R (Leica Microsystems) using a 63× GLY lens (glycerol immersion, NA 1.4). Signals of Renaissance and GFP, ECFP were acquired sequentially. Images were partly overlaid with DIC channel.

***β*-Glucuronidase (GUS) reporter assay**

Single inflorescences induced with 10 µM Dex-solution (0.01% EtOH) or Mock (0.01% EtOH) were dissected after 2 days post induction (dpi). Single carpels were slightly cut open and submerged in x-Glu solution (Triton X-100 10%, EDTA 10 mM, Ferrocyanide 2 mM, Ferricyanide 2 mM, Na2HP04 100 mM, NaH2P04 100 mM, x-Glu 4 mM.), vacuum infiltrated for 5 min followed by a 2 hour incubation at 37°C, washed with phosphate buffer and mounted in 80% glycerol. Imaged at the DMR (Leica) microscope with 20x or 40x dry objective.

FRAP

Measurements were done on root tips of two weeks old seedlings grown as described above. One sample was prepared at a time: the root was excised and delicately mounted (without squashing) in liquid ½ MS between slide and coverslip (precleaned with EtOH), sealed with transparent nail polish and let 10min equilibrate upside down on the microscope platform before measurements. The imaging chamber was set at a constant temperature of 20°C (higher/fluctuating temperatures induce nuclei juggling). Bleaching and imaging were done using an APO PL 40x oil immersion objective, NA 1.3, over a single plane. Bleaching was performed in euchromatin within ROI of 1 µm diameter using 3-5 pulses until near total bleach was obtained (488nm 80% laser, 100% transmission) and post-bleach images were recorded 10 times with 1 sec interval then 10 times with 60 sec interval with a 7% transmission. For analyzing fluorescence recovery, images were first corrected for nuclear drifts occurring during acquisition, using a rigid registration approach in Fiji (Schindelin et al. 2012). When a single image captured several nuclei, registration did not always perform well for all, hence single nuclei were cropped for registration and analysis. Fluorescence measurements were done on the bleach ROI, a control ROI near and outside the nucleus, and over the whole nucleus. Calculation of fluorescence recovery was done as described by Rosa and colleagues (Rosa et al. 2014) whereby the initial intensity was normalized at 1 for each image before average

calculation. Curve fitting was done in Matlab using the set of normalized data using a two-component fit.

Protein sequence alignment and prediction of ubiquitination sites in *Arabidopsis thaliana* H1

We aligned the sequence of *H1.1* and *H1.2* from *Arabidopsis thaliana* to the sequences of *H1.1 Mus musculus* and *H1.1 Homo sapiens* and compared the ubiquitination sites of mouse and human as published by Wisniewski and colleagues (Wisniewski et al. 2007) to *Arabidopsis thaliana*. In addition we used prediction tools of ubiquitination to predict further ubiquitination sites in *Arabidopsis thaliana*. In detail, we used the tools described by Chen, Radivojac and Walton (Chen et al. 2011; Radivojac et al. 2011; Walton et al. 2016).

Reanalysis of published expression data

For the reanalysis of published RNA-Seq and Microarray expression data, we used a tool, for which the R-script can be found at https://github.com/VimalRawat1010/Rscripts/blob/master/LabData/.RData. The analysis includes data from (Borges et al. 2008; Honys and Twell 2004; Pina and Pinto 2005; Schmidt et al. 2011; Wuest et al. 2010). The tool considers for the dendrograms and the coloring the shape and gene expression values.

Germination assay
See Supplemental Figure 3

Lateral root measurement
See Supplemental Figure 4

References

Bernhardt, Anne et al. 2006. “CUL4 Associates with DDB1 and DET1 and Its Downregulation Affects Diverse Aspects of Development in Arabidopsis Thaliana.” *Plant Journal* 47(4): 591–603.

Biedermann, Sascha, and Hanjo Hellmann. 2011. “WD40 and CUL4-Based E3 Ligases: Lubricating All Aspects of Life.” *Trends in Plant Science* 16(1): 38–46.

Borges, F. et al. 2008. “Comparative Transcriptomics of Arabidopsis Sperm Cells.” *Plant Physiology* 148(2): 1168–81.

Castle, L. A., and D. W. Meinke. 1994. “A FUSCA Gene of Arabidopsis Encodes a Novel Protein Essential for Plant Development.” *Plant Cell* 6(1): 25–41.

Chen, H. et al. 2006. “Arabidopsis CULLIN4 Forms an E3 Ubiquitin Ligase with RBX1 and the CDD Complex in Mediating Light Control of Development.” *the Plant Cell Online* 18(8): 1991–2004.

Chen, Zhen et al. 2011. “Prediction of Ubiquitination Sites by Using the Composition of K-Spaced Amino Acid Pairs.” *PloS one* 6(7): e22930.

Contreras, Alejandro et al. 2003. “The Dynamic Mobility of Histone H1 Is Regulated by cyclin/CDK Phosphorylation.” *Molecular and cellular biology* 23(23): 8626–36.

Dumbliauskas, Eva et al. 2011. “The Arabidopsis CUL4-DDB1 Complex Interacts with MSI1

and Is Required to Maintain MEDEA Parental Imprinting." *The EMBO Journal* 30(4): 731–43.

Figueroa, Pablo et al. 2005. "Arabidopsis Has Two Redundant Cullin3 Proteins That Are Essential for Embryo Development and That Interact with RBX1 and BTB Proteins to Form Multisubunit E3 Ubiquitin Ligase Complexes in Vivo." *The Plant Cell* 17(4): 1180–95.

Gilkerson, Jonathan et al. 2009. "Isolation and Characterization of cul1-7, a Recessive Allele of CULLIN1 That Disrupts SCF Function at the C Terminus of CUL1 in Arabidopsis Thaliana." *Genetics* 181(3): 945–63.

Hajkova, Petra et al. 2008. "Chromatin Dynamics during Epigenetic Reprogramming in the Mouse Germ Line." *Nature* 452(7189): 877–81.

Hauser, Felix et al. 2013. "A Genomic-Scale Artificial microRNA Library as a Tool to Investigate the Functionally Redundant Gene Space in Arabidopsis." *The Plant cell* 25(8): 2848–63.

Honys, David, and David Twell. 2004. "Transcriptome Analysis of Haploid Male Gametophyte Development in Arabidopsis." *Gene Biology* 5(11): R85.1-R85.13.

Izzo, Annalisa, and Robert Schneider. 2015. "The Role of Linker Histone H1 Modifications in the Regulation of Gene Expression and Chromatin Dynamics." *Biochimica et Biophysica Acta (BBA) - Gene Regulatory Mechanisms*: 1–10.

Kim, Kyunghwan et al. 2013. "Linker Histone H1.2 Cooperates with Cul4A and PAF1 to Drive H4K31 Ubiquitylation-Mediated Transactivation." *Cell Reports* 5(6): 1690–1703.

Kotliński, Maciej et al. 2016. "Histone H1 Variants in Arabidopsis Are Subject to Numerous Post-Translational Modifications, Both Conserved and Previously Unknown in Histones, Suggesting Complex Functions of H1 in Plants." *PLoS ONE* 11(1): 1–19.

Lee, Jae Hoon, and Woo Taek Kim. 2011. "Regulation of Abiotic Stress Signal Transduction by E3 Ubiquitin Ligases in Arabidopsis." *Molecules and Cells* 31(3): 201–8.

Lever, Melody A., John P.H. Th'ng, Xuejun Sun, and Michael J. Hendzel. 2000. "Rapid Exchange of Histone H1.1 on Chromatin in Living Human Cells." *Nature* 408(6814): 873–76.

Misteli, T. et al. 2000. "Dynamic Binding of Histone H1 to Chromatin in Living Cells." *Nature* 408: 877–81.

Pina, Cristina, and Francisco Pinto. 2005. "Gene Family Analysis of the Arabidopsis Pollen Transcriptome Reveals Biological Implications for Cell Growth , Division Control , and." *Plant Physiology* 138(June): 744–56.

Radivojac, Predrag et al. 2011. "Identification, Analysis and Prediction of Protein Ubiquitination Sites." *Proteins* 78(2): 365–80.

Rape, Michael. 2018. "Post-Translational Modifications: Ubiquitylation at the Crossroads of Development and Disease." *Nature Reviews Molecular Cell Biology* 19(1): 59–70.

Rosa, Stefanie et al. 2014. "Cell Differentiation and Development in *Arabidopsis* Are Associated with Changes in Histone Dynamics at the Single-Cell Level." *The Plant Cell Online* 26(12): 4821–33.

Samalova, Marketa, Bretislav Brzobohaty, and Ian Moore. 2005. "pOp6/LhGR: A Stringently Regulated and Highly Responsive Dexamethasone-Inducible Gene Expression System for Tobacco." *The Plant Journal : for cell and molecular biology* 41(6): 919–35.

Schindelin, Johannes et al. 2012. "Fiji: An Open Source Platform for Biological Image

Analysis." *Nature Methods* 9(7): 676–82.

Schmidt, Anja, Wuest, Samuel, Vijverberg, Kitty, Baroux. Celia, Kleen, Daniela, and Ueli Grossniklaus. 2011. "Transcriptome Analysis of the Arabidopsis Megaspore Mother Cell Uncovers the Importance of RNA Helicases for Plant Germline Development." *PLoS biology* 9(9).

Schwab, Rebecca, Stephan Ossowski, and Norman Warthmann. 2010. "Plant MicroRNAs" eds. Blake C. Meyers and Pamela J. Green. 592: 71–88.

Shaner, Nathan et al. 2008. "Improvng the Photostability of Bright Monomeric Orange and Red Fluorescent Proteins." *Nature Methods* 5(6): 545–51.

She, Wenjing et al. 2013. "Chromatin Reprogramming during the Somatic-to-Reproductive Cell Fate Transition in Plants." *Development (Cambridge, England)* 140(19): 4008–19.

Shen, Wen-Hui et al. 2002. "Null Mutation of AtCUL1 Causes Arrest in Early Embryogenesis in Arabidopsis." *Molecular Biology of the Cell* 13(June): 1916–28.

Singer, Jeffrey D., Mark Gurian-West, Bruce Clurman, and James M. Roberts. 1999. "Cullin-3 Targets Cyclin E for Ubiquitination and Controls S Phase in Mammalian Cells." *Genes and Development* 13(18): 2375–87.

Stewart, Mikaela D., Tobias Ritterhoff, Rachel E. Klevit, and Peter S. Brzovic. 2016. "E2 Enzymes: More than Just Middle Men." *Cell Research* 26(4): 423–40.

Thomann, Alexis et al. 2005. "Arabidopsis CUL3A and CUL3B Genes Are Essential for Normal Embryogenesis." *Plant Journal* 43(3): 437–48.

Villar-Garea, Ana, and Axel Imhof. 2008. "Fine Mapping of Posttranslational Modifications of the Linker Histone H1 from Drosophila Melanogaster." *PLoS ONE* 3(2).

Walton, Alan et al. 2016. "It's Time for Some 'Site'-Seeing: Novel Tools to Monitor the Ubiquitin Landscape in Arabidopsis Thaliana." *The Plant Cell* 28(1): 6–16.

Wisniewski, Jacek R., Alexandre Zougman, Sonja Krüger, and Matthias Mann. 2007. "Mass Spectrometric Mapping of Linker Histone H1 Variants Reveals Multiple Acetylations, Methylations, and Phosphorylation as Well as Differences between Cell Culture and Tissue." *Molecular & cellular proteomics : MCP* 6(1): 72–87.

Wuest, Samuel E. et al. 2010. "Arabidopsis Female Gametophyte Gene Expression Map Reveals Similarities between Plant and Animal Gametes." *Current Biology* 20(6): 506–12.

Supplement Chapter 5 :

amiRNA	amiRNA target sequence 5'>3'
amiRNA against CUL4	ATGC**T**CATGATTCGTAGTATA
amiRNA against *CUL3A*	AAGGAC**C**TACACTTATTGTT**C**
amiRNA against *CUL3B*	AAGGAC**C**TACACTT**A**TTGTT**C**
amiRNA against *CUL1*	G**G**GCCCT**GC**TGAAAAACGTA**T**
amiRNA against *CUL2*	G**A**GC**A**CTATTGAAAAACGTAA

Supplement table 1: amiRNA target sequences and mismatches. Underlined and in bold are the mismatches of the amiRNA within the target sequence highlighted

		Phenotype without induction					Phenotype upon induction with 1 uM Dex for X days/hours				
Replicate	T2 line	wt	small	total	% *cul4* mutant phenotype		wt	anthocyanin	small white	total	% *cul4* mutant phenotype
1	JS166#2	74	1	75	1.33		14	3	35	52	73.08
1	JS166#11	75	3	78	3.85		9	8	34	51	82.35
1	JS166#12	66	0	66	0.00		11	1	28	40	72.50
1	JS166#5	52	3	55	5.45		41	3	0	44	6.82
2	JS166#2	41	2	43	4.65		10	44	0	54	81.48
2	JS166#11	49	0	49	0.00		8	37	0	45	82.22
2	JS166#12	48	2	50	4.00		10	42	0	52	80.77
2	JS166#5	49	1	50	2.00		45	1	0	46	2.17

Supplement table 2: Hyperphotomorphogenic phenotype in T2 of *cul4* knockdown lines. The lines JS166#2, #11, #12 showed a *cul4* mutant phenotype after induction in the range expected in T2s for single insertions if the phenotype is visible in heterozygote conditions (~ 75%).

RNASeq														
Gene Name	Gene	Embryo Gob	Embryo2_4	Meio_M	CC1	EmbrTor	EndoTor	Root	Flower	PollenM	Inorescence	EggCell	Synergids	Bud
CUL2	AT1G02980	26.27	13.03	520.57	65.01	22.69	405.57	7.13	7.07	4.84	21.17	3.69	2.71	2.33
CUL3A	AT1G26830	6.59	11.16	76.79	28.1	42.12	43.86	50.17	29.15	17.69	47.92	13.85	19.69	48.98
CUL3B	AT1G69670	5.12	4.63	7.27	0.3	14.87	12.66	25.51	6.86	2.51	14.48	8.91	6.41	25.83
CUL1	AT4G02570	132.58	110.82	555.67	327.87	672.8	752.75	895.37	544.25	796.94	632.05	88.2	128.17	686.53
CUL4	AT5G46210	91.19	51.21	184.61	208.22	531.65	641.46	607.73	318.52	36.74	347.12	703.09	76.65	451.46

Microarray																					
Gene Name	Gene	OvuleWt	Egg	Cen	Syn	MMC	seedling_pina	pollen_unicellular_honys_uc	pollen_bicellular_honys_bc	pollen_tricellular_honys_tc	pollen_mature_borges	globularEmbryo	preglobularEmbryo	heartEmbryo	inflorescence_inflorescenceAfterBolting_Col_0	flowers_floralStage10_Col_0	flowers_floralStage1011_Col_0	flowers_floralStage13_Col_0	carpels_floralStage12_Col_0	flowers_floralStage16_Col_0	carpels_floralStage15_Col_0
CUL2	AT1G02980	3.15	4.76	5.22	5.18	3.91	2.97	6.88	5.79	4.82	5.44	6.59	6.78	4.55	3.3	3.89	3.59	3.1	3.15	3.15	3.17
CUL3A	AT1G26830	8.01	8.2	7.3	7.5	7.79	7.7	6.84	7.13	7.84	8.72	8.46	8.34	8.77	7.94	8.3	7.91	7.62	7.65	7.8	7.69
CUL3B	AT1G69670	6.56	4.93	5.87	4.56	5.65	6.09	5.97	6.08	6.1	5.6	8.12	7.96	8.03	5.92	5.87	5.56	5.3	5.67	5.38	5.67
CUL1	AT4G02570	9.94	8.41	7.82	7.58	9.12	9.17	9.88	9.84	9.66	11.07	9.19	9.35	8.91	9.96	9.74	9.51	9.5	9.86	9.89	9.84
CUL4	AT5G46210	9.94	9.98	9.73	9.58	10.05	9.64	9.84	9.9	8.97	9.04	9.78	10.03	9.55	9.93	9.84	9.68	9.59	9.96	9.45	9.66

Supplement Table 3.: Normalized expression values of *CULLINs* from RNA-Seq and Microarray data. The table shows normalized expression values of *CULLINs* of RNA-Seq data from Wuest and colleagues (Wuest et al. 2010) and (B) Microarray data from Schmidt, Borges, Pina and Honys (Borges et al. 2008; Honys and Twell 2004; Pina and Pinto 2005; Schmidt et al. 2011). The script used for analyzing the RNA-Seq and Microarray data can be found at "https:// github.com/VimalRawat1010/Rscripts/blob/master/LabData/.RData".

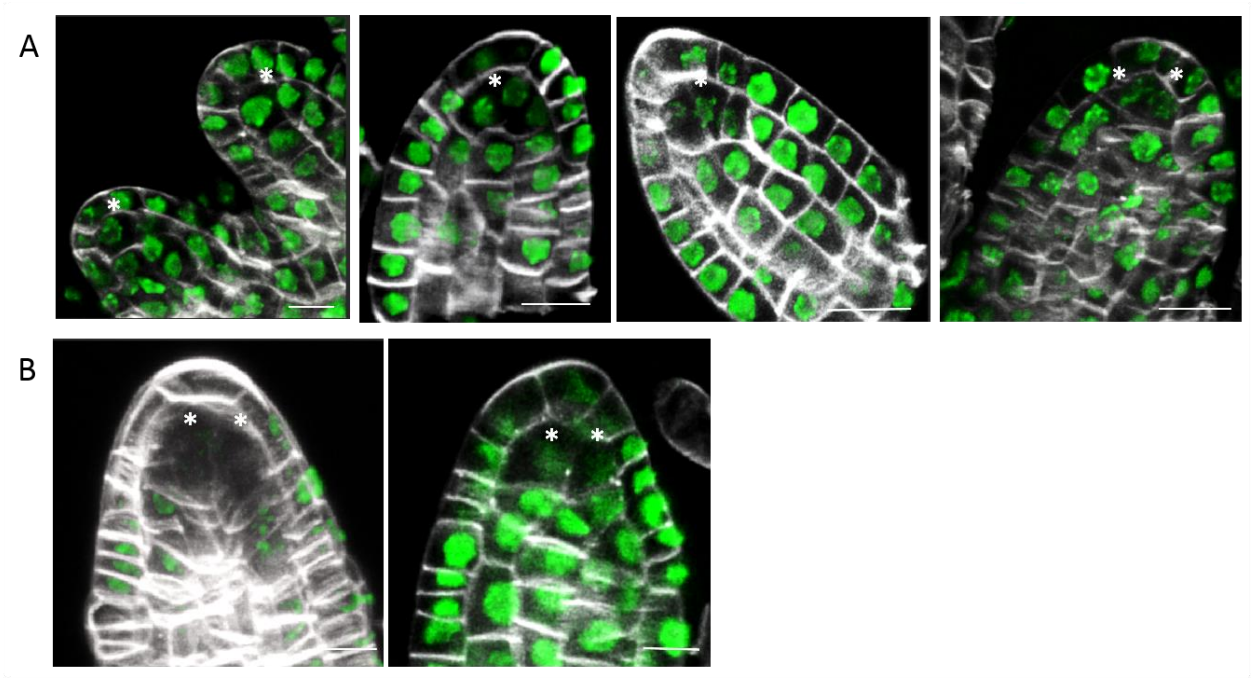

Supplement Figure 1: Induced amiRNA against *CUL4* causes ectopic MMC development. (A) Persistence of GFP signal in induced BG lines harboring inducible-amiRNA targeting *CUL4*; 4 dpi, 10 µM Dex. (B) Aberrant MMC development in plants harboring in inducible-amiRNA targeting *CUL4*; 4 dpi, 10 µM Dex. Scale bar = 10µm.

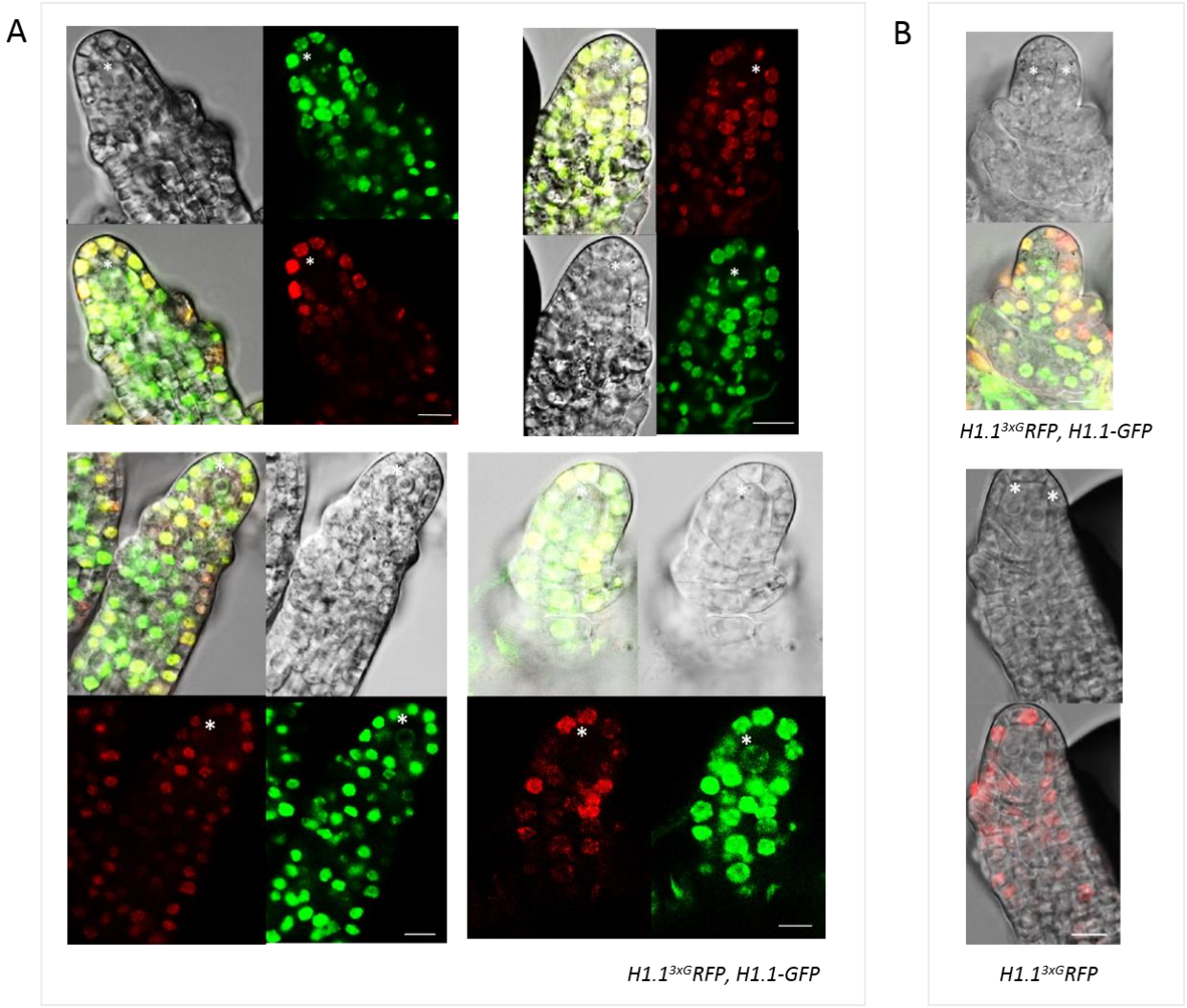

Supplement Figure 2: Altered reloading and aberrant MMC development in induced *H1.1^{3xG}RFP* plants. (A) *H1.1-GFP* expression but no *H1.1^{3xG}RFP* expression 68 hpi 10 µM Dex induction in developing MMC. (B) Double MMC like cells (~ 10%) developed during female sporogenesis 3.5 dpi with 10 µM Dex. Green = *pH1.1.::H1.1-GFP*; red = *pRPS5a>>H1.1^{3xG}RFP*. Scale bar = 10 µM.

A

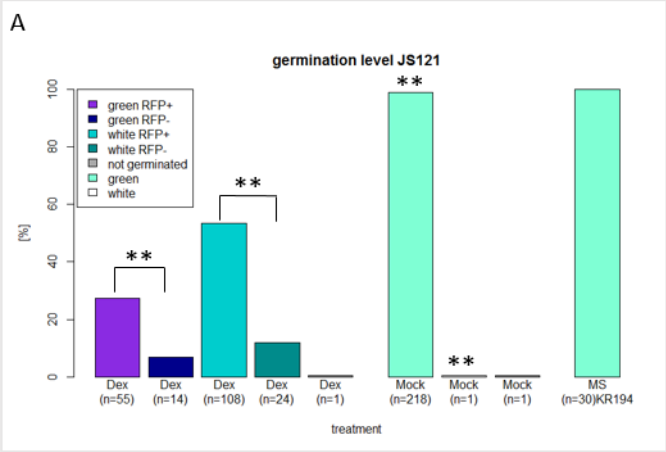
germination level JS121
green RFP+
green RFP-
white RFP+
white RFP-
not germinated
green
white
[%]
0
20
40
60
80
100
**
**
**
**
Dex (n=55)
Dex (n=14)
Dex (n=108)
Dex (n=24)
Dex (n=1)
Mock (n=218)
Mock (n=1)
Mock (n=1)
MS (n=30)KR194
treatment

B

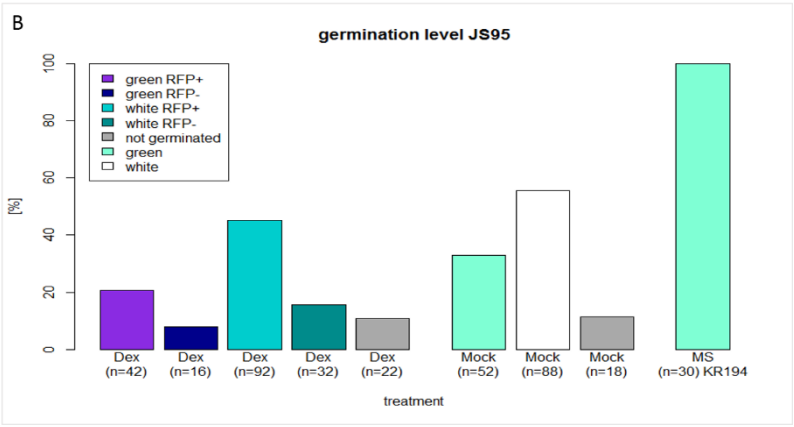
germination level JS95
green RFP+
green RFP-
white RFP+
white RFP-
not germinated
green
white
[%]
0
20
40
60
80
100
Dex (n=42)
Dex (n=16)
Dex (n=92)
Dex (n=32)
Dex (n=22)
Mock (n=52)
Mock (n=88)
Mock (n=18)
MS (n=30) KR194
treatment

C

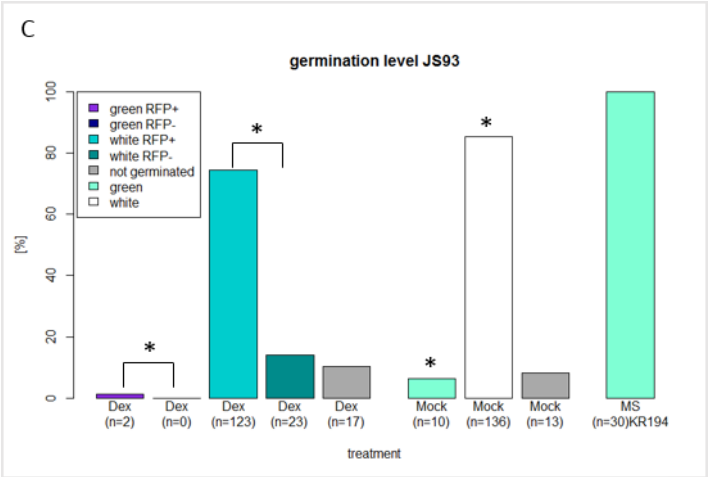
germination level JS93
green RFP+
green RFP-
white RFP+
white RFP-
not germinated
green
white
[%]
0
20
40
60
80
100
*
*
*
*
Dex (n=2)
Dex (n=0)
Dex (n=123)
Dex (n=23)
Dex (n=17)
Mock (n=10)
Mock (n=136)
Mock (n=13)
MS (n=30)KR194
treatment

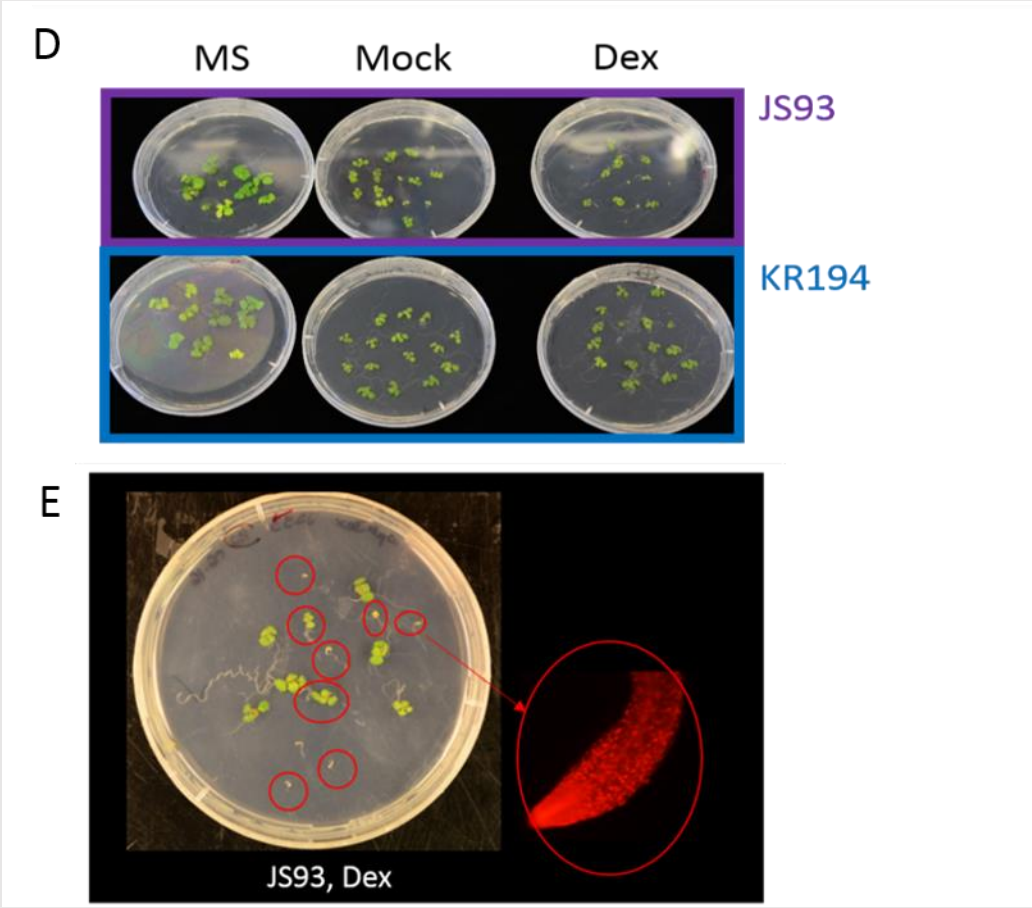

Supplement Figure 3: Phenotype of seedlings expressing *H1.1^{3xG}-RFP* mutant variant. (A to C) Blind tested for germination level in segregating T2s on 10 µM Dex, Mock and MS plates. KR194 control line (homozygote, *pH1.1::H1.1-RFP*), JS93, JS95, JS121 (*H1.1^{3xG}RFP*, independent insertion lines). N analyzed: Dex: JS121 = 202; JS95 = 204; JS93 = 165. N-total Mock: JS121 = 220; JS95 = 158; JS93 = 159. Chi-square test is significant if we compare JS121 green seedlings (including RFP+/ -), white seedlings (including RFP+/-) Dex vs. green, white on Mock. $P < 0.00001$. Chi-square test is also under the same conditions significant for JS93: $p = 0.047$; **= $p < 0.01$. * = $p < 0.05$. (D) Example image of JS93 and KR194 MS, Mock and Dex plates 10 days after transfer to light. (E) Example image of germination test on 10 µM Dex plate. Red circles mark seedlings, which express *H1.1^{3xG}RFP* tested in the root. Growth conditions as mentioned in Material and Methods part under Plant material and growth conditions. Images were taken 10 days after plates were transferred to light. KR194*: pH1.1::H1.1-RFP* (control); JS93, JS95, JS121:*H1.1^{3xG}-RFP*.

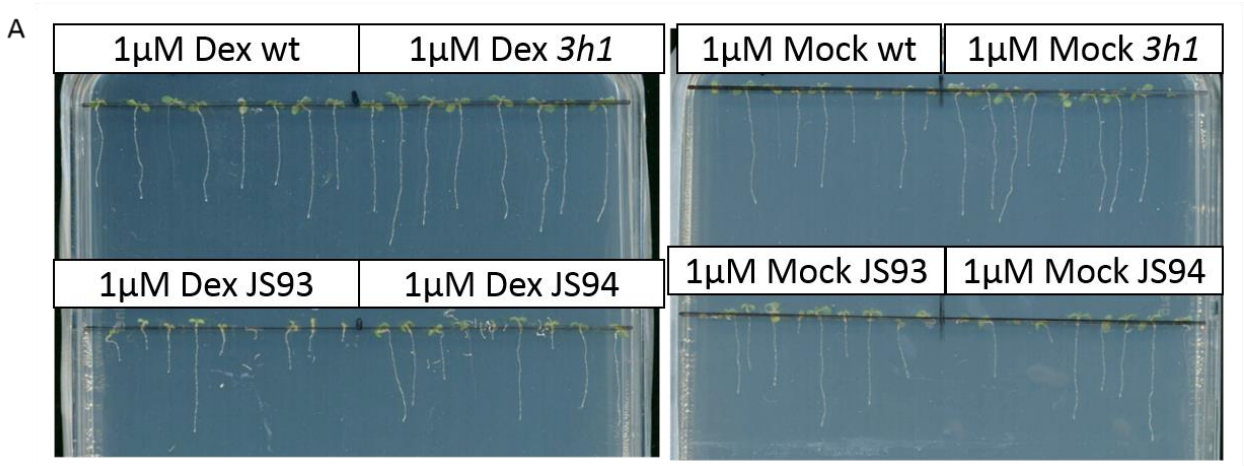

Supplement Figure 4: Lateral root of *H1.1^{3xG}RFP* mutant. We did not detect a difference between WT, *3h1* and *H1.1^{3xG}RFP* seedlings (segregating, T2s) in root length and number of lateral roots grown for 7 days under continuous light on 1 µM Dex and Mock conditions. Dex plate: JS93 (*H1.1^{3xG}RFP*) (n) = 9; JS94 (*H1.1^{3xG}RFP*) (n) = 9; WT (n) = 8; *3h1* (n) = 8. Mock plate: JS93 (*H1.1^{3xG}RFP*) (n) = 8; JS94 (*H1.1^{3xG}RFP*) (n) = 7; WT (n) = 8; *3h1* (n) = 8.

References

Borges, F. et al. 2008. “Comparative Transcriptomics of Arabidopsis Sperm Cells.” Plant Physiology 148(2): 1168–81.

Honys, David, and David Twell. 2004. “Transcriptome Analysis of Haploid Male Gametophyte Development in Arabidopsis.” Gene Biology 5(11): R85.1-R85.13.

Pina, Cristina, and Francisco Pinto. 2005. “Gene Family Analysis of the Arabidopsis Pollen Transcriptome Reveals Biological Implications for Cell Growth , Division Control , and.” Plant Physiology 138(June): 744–56.

Schmidt, Anja, Wuest, Samuel, Vijverberg, Kitty, Baroux. Celia, Kleen, Daniela, and Ueli Grossniklaus. 2011. “Transcriptome Analysis of the Arabidopsis Megaspore Mother Cell Uncovers the Importance of RNA Helicases for Plant Germline Development.” PLoS biology 9(9).

Wuest, Samuel E. et al. 2010. “Arabidopsis Female Gametophyte Gene Expression Map Reveals Similarities between Plant and Animal Gametes.” Current Biology 20(6): 506–12.

X. Chapter 6

Does citrullination play a role in H1 dynamics during sporogenesis?

Jasmin Schubert[a], Kinga Rutowicz[a], Daniel Prata[a], Zusanna Kaczmarska[b] and Célia Baroux[a1]

[a] Institute of Plant and Microbial Biology and Zürich-Basel Plant Science Center, University of Zürich, Zollikerstrasse 107, 8008 Zürich, Switzerland.

[b] EMBL, 71 Avenue des Martyrs, 38000 Grenoble, France.

[1] Author for correspondence (cbaroux@botinst.uzh.ch)

The author(s) responsible for distribution of materials integral to the findings presented in this article in accordance with the policy described in the Instructions for Authors (www.plantcell.org) is: Baroux. C. (cbaroux@botinst.uzh.ch).

Abbreviation	
3h1	*h1.1-1/h1.1-1;h1.2-2/h1.2-2; h1.3-2/h1.3-2*
amiRNA[AIH]	*pRPS5a::LhGR2-GUS::pOP6::amiRNA[AIH]; h1.1-1/h1.1-1;h1.2-2/h1.2-2; h1.3-2/h1.3-2 pH1.1::H1.1-GFP/pH1.1::H1.1-GFP; pH1.2::H1.2-ECFP/pH1.2::H1.2-ECFP*
BG	*h1.1-1/h1.1-1;h1.2-2/h1.2-2; h1.3-2/h1.3-2 pH1.1::H1.1-GFP/pH1.1::H1.1-GFP; pH1.2::H1.2-ECFP/pH1.2::H1.2-ECFP*
DAG	Days after germination
Dex	Dexamethasone
DNA	Deoxyribonucleic acid
dpi	days post induction
dpt	days post treatment
EtOH	Ethanol
FM	Functional Megaspore
GO	Gene Ontology
H1.1^{R57A}RFP	*pRPS5a::LhGR2-GUS::pOP6::H1.1^{R57A}RFP*
H1.1^{R57K}RFP	*pRPS5a::LhGR2-GUS::pOP6::H1.1^{R57K}RFP*
H1.1^{R79A}RFP	*pRPS5a::LhGR2-GUS::pOP6::H1.1^{R79A}RFP*
H1.1^{R79K}RFP	*pRPS5a::LhGR2-GUS::pOP6::H1.1^{R79K}RFP*
H1.1^{wt}RFP	*pRPS5a::LhGR2-GUS::pOP6::H1.1-RFP*
H1.2^{R79A}RFP	*pRPS5a::LhGR2-GUS::pOP6::H1.2^{R79A}RFP*
H1.2^{R79K}RFP	*pRPS5a::LhGR2-GUS::pOP6::H1.2^{R79K}RFP*
H1.2^{wt}RFP	*pRPS5a::LhGR2-GUS::pOP6::H1.2RFP*
hpi	hours post induction
hrs	hours
MMC	Megaspore Mother Cell
o/N	over Night
PCR	Polymerase Chain Reaction
PMC	Pollen Mother Cell
PTM	Post translational modification

RFP	Red fluorescent protein
RNA	Ribonucleic Acid
SEM	Standard Error of the Mean
SMC	Spore Mother Cell
TDFA	TDFA Trifluoroacetate salt
WT	Wild-type

Abstract

H1 linker histones have been described to be targets of several post-translational modifications (PTM) like phosphorylation, acetylation and methylation in plants and animals (Kotliński et al. 2016; Villar-Garea and Imhof 2008). It has been previously shown that linker histones show a dynamic presence during cell-fate changes in plants and animals (Hajkova et al. 2008; She et al. 2013). Recently the mouse embryonic stem cell (ESC) linker histone variant was identified to be a target of PEPTIDYL ARGININE DEIMINASE TYPE IV (PADI4) induced citrullination (Christophorou et al. 2014). This PTM caused H1s displacement from the DNA, chromatin decondensation and expression of pluripotency markers. To determine if a similar mechanism is involved in the dynamic H1 eviction during sporogenesis in *Arabidopsis thaliana*, we mutated amino acids, which are putative targets of citrullination and methylation. We found that the mutation of arginine 57 was sufficient to alter H1.1s stability, in Arabidopsis ovule primordia, which seemed to induce aberrant MMC development and lead to reduced fertility. Furthermore, comparative structural modeling indicated that the catalytic domain of the Arabidopsis protein AGMATINE IMINOHYDROLYASE (AIH) and of PADI4, share a strong structural homology particularly at key, conserved catalytic amino-acids. Furthermore, preliminary results of induced-knockdowns suggest a role of *AIH* in linker histone stability during sporogenesis in *A.thaliana*. Collectively, these observations open the possibility of an *AIH*-based H1 modification similar to the situation in mouse ESCs; this model remains, however, to be demonstrated.

Introduction

The transition from a somatic-to-reproductive cell during the development of the MMC and PMC is a typical example of cell-fate change in plants. She and colleagues (She et al. 2013) found that the hallmark of this cell-fate change is a transient loss of linker histones followed by a drastic rearrangement of the chromatin (She et al. 2013). Similar patterns of transient linker histone loss, prior to cell-fate changes and chromatin rearrangement have been observed in mouse Primordial Germ Cells (PGCs) (Hajkova et al. 2008). Since the eviction of linker histones prior to cell-fate changes seem to be conserved in different organisms it speaks for an important role of this transient eviction. Recently proteomic analysis of mouse embryonic stem (ES) cells, identified linker histones to be targets of PEPTIDYL ARGININE DEIMINASE TYPE IV (PADI4) (Christophorou et al. 2014). The study found that PADI4-induced citrullination in mouse ES cells on H1 lysine 54 caused H1s displacement from the DNA, chromatin decondensation and expression of pluripotency markers in those cells (Christophorou et al. 2014). These changes were reversible upon inhibition of PADI4 activity by adding the PADI4 inhibitors TDFA and Cl-amidine (Christophorou et al. 2014; Fuhrmann and Thompson 2016). Citrullination also called arginine

deimination is a hydrolytic process, which converts an arginine or a mono-methylated arginine (e.g.as a protein residue) into the amino acid citrulline (Fuhrmann and Thompson 2016), which is not encoded by the genome, but is a PTM. This conversion alters the charge of the proteins at a neutral pH, from positive to more neutral. This conversion is carried out by a small family of tissue-specific, calcium-dependent enzymes called PEPTIDYLARGININE DEIMINASES (PADs or PADIs) in human and mouse cells (Kouzarides 2007). PADIs are usually involved in cellular processes like inflammation, apoptosis and hormone-signaling (Cuthbert et al. 2004; Fuhrmann and Thompson 2016; Witalison, Thompson, and Hofseth 2015). Interestingly, other studies found roles of PADIs during development in mice. For example, Zhang and colleagues showed PADI-dependent histone H3 and H4 citrullination during preimplantation development in mouse cells. The knockout of *PADI1* led to arrest of the embryo at the 4-cell stage (Zhang et al. 2016).

Whether a similar mechanism for linker histone displacement mediated by PADIs citrullination exists in plants is not known. Arginine deamination has been implicated in senescence processes (polyamine metabolism) (Sobieszczuk-Nowicka 2017) but not as a regulatory protein PTM event so far. The aim of this work was to i) elucidate whether arginine residues play a role in H1s stability during the somatic-to-reproductive cell-fate transition, ii) whether these arginine residues could be modified by an Arabidopsis PADI4 homolog and iii) whether this putative H1 PTM has an impact on SMC differentiation.

Results

Induced ovules expressing the RFP-tagged variant *H1.1^{R57K}* show altered H1 stability during MMC development compared to ovules expressing the RFP-tagged variants *H1.1^{R57A}* or *H1.1^{wt}*

To determine which amino acids are potential homologs of the modified residues in the animal counterparts, we aligned the protein sequence of Arabidopsis H1.1, H1.2 and H1.3 to mouse H1.2 (Supplement Figure 9). We identified the arginine (R) residues 79 in H1.1 and H1.2 as homologous amino acids to the arginine residue 54 in mouse H1.2, which is in mouse a target of the PTM citrullination. Further, did we selected the R57 in Arabidopsis H1.1 as a possible target of PTMs, since it is similar to R79 described to be a target of methylation in Arabidopsis (Kotliński et al. 2016). In addition, is R57 the closest arginine residue upstream of R79 and this region of the protein is described as PTM hotspot in Arabidopsis (Kotliński et al. 2016). The R57 lies in the N-terminal tail and just 4 amino acids upstream of the globular domain, whereas the other target arginine at position 79 lies in the globular domain (Figure 1 A).

To determine if those H1.1 and H1.2 arginine residues are important for linker histone eviction during sporogenesis, we designed Dex-inducible H1.1 mutant variants, which are tagged with RFP (Shaner et al. 2008). We cloned the following variants: *H1.1^{R57K}RFP*, *H1.1^{R57A}RFP*, *H1.1^{wt}RFP*, *H1.1^{R79K}RFP*, *H1.1^{R79A}RFP*, *H1.2^{R79K}RFP*, *H1.2^{R79A}RFP* and *H1.2^{wt}RFP*. Some of the constructs are just partly cloned and their analysis needs future work. The cloning status of the different variants can be found in the material and methods section. Here we will focus on the variants: *H1.1^{R57K}RFP*, *H1.1^{R57A}RFP* and *H1.1^{wt}RFP*.

It was shown, in mouse H1.2 that a replacement of the arginine 54 to lysine was sufficient to prevent linker histone eviction in mouse embryonic stem cell lines (Christophorou et al. 2014). To follow this approach we also mutated our candidate target arginine residues R57 to either lysine (K), to retain the original charge and to prevent putative citrullination, or to alanine (A) to mimic the charge of putative citrullination (Figure 1 A). In addition, the change from arginine to either lysine or alanine prevents methylation by arginine methyltransferases, or better to say lysine can be methylated but is a target of methyltransferases different than arginine.

We found that the mutation R57K prevents H1.1 eviction at MMC developmental stages 1-II to 2-II, in two independent insertion lines up to 35% (n = 51) and 45% (n = 20) ovules 5 days after induction (Figure 1 B, C and Table 1). By contrast, we tested three independent insertion lines expressing an RFP-tagged, wild-type H1.1 variant (*H1.1^{wt}RFP*) and we scored 16 – 33% ovules (n= 20 - 25) where RFP signals were residual in the MMC (Figure 1 B and C, Table 1 and Supplement Figure 1). Furthermore, the mimic variant H1.1^{R57A} tagged with an RFP seem to be subjected to normal eviction (0 to 23% ovules with residual signals in ovules of stages 1-II and 2-II), (Figure 1 B and C, Table 1). A fisher exact test scored the difference of H1.1 eviction between *H1.1^{R57K}RFP* and *H1.1^{R57A}RFP* as highly significant, $p < 0.01$ (for the line JS188#5, n = 23) or significant, $p < 0.05$ (for the line JS188#17 n = 27 and JS188#25 n = 30) (Figure 1 B, C, Table 1 and Supplement Table 1). In addition, the fisher exact test scored the difference of H1.1 eviction between *H1.1^{R57K}RFP* (line JS147#1) and *H1.1^{wt}RFP* as significant, $p < 0.05$ (for the line JS175, JS98 and JS196) (Figure 1 B and C, Table 1 and Supplement Table 1).

These results suggest that the mutation of the arginine 57 to a lysine is sufficient to alter H1.1 stability during MMC development, which we did not see by the mutation of arginine to alanine. This might be explained by the fact that the mutation of arginine to lysine either changes the charge of the protein or because lysine is no putative target of citrullination or by preventing arginine methylation.

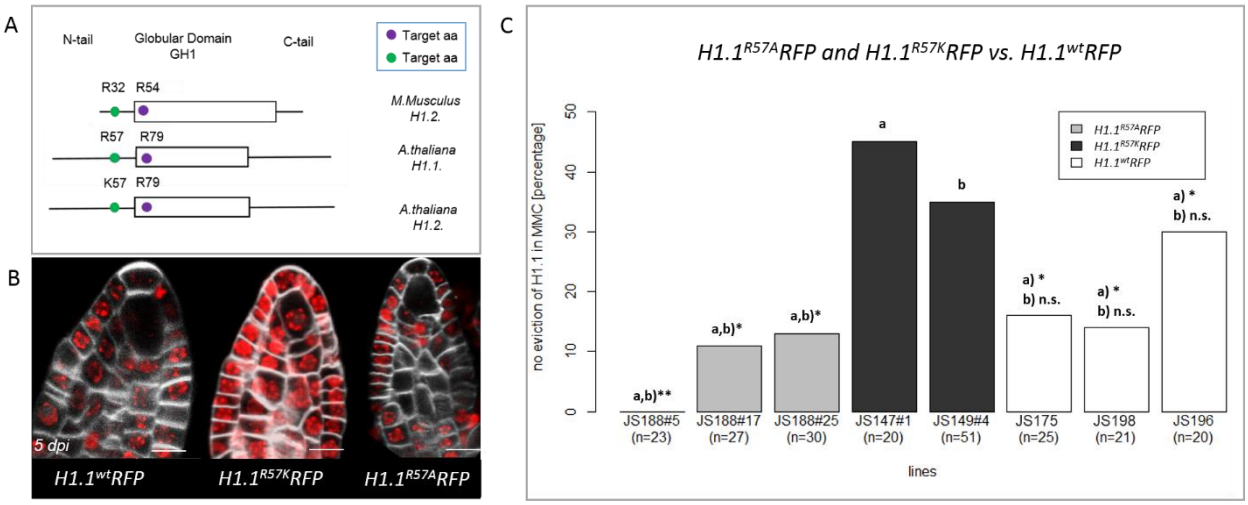

Figure 1: An arginine residue in the N-tail is required for H1 dynamics during MMC development. (A) Schematic representation of conserved arginine residues in mouse H1.2 (R54) and Arabidopsis H1.1 and H1.2 variants in the globular domain (R79) and additional candidate

arginine residue in H1.1 in the N-tail (R57), which corresponds to mouse H1.2 R32. These residues are potential citrullination targets based on protein sequence alignment (see Supplement Figure 9 and 10) and (Christophorou et al. 2014). (B) Signals of RFP-tagged *H1.1*^{wt}, *H1.1*^{R57K} and *H1.1*^{R57A} variants in ovule primordia stage 2-I after treatment with 10 µM Dex 5 dpi. Note the presence of strong signals in the MMC expressing *H1.1*^{R57K} but not *H1.1*^{wt} or *H1.1*^{R57A}. Scale bar = 10 µm. (More images also in Supplement Figure 1, 4 and 5) (C) Scoring of ovule primordia with RFP signals in the MMC in two or three independent insertion lines for each construct as indicated. ** $p < 0.01$; * $p < 0.05$; n.s. = not significant (Fisher exact test).

Table 1: Observations of presence and absence of RFP signals in induced ovules expressing different *H1.1* variants

line	genotype	% residual signal	(n) residual signal	% absent signal	(n) absent signal	(n) analyzed
JS188#5	H1.1^{R57A}RFP	0	0	100	23	23
JS188#17	H1.1^{R57A}RFP	11	3	89	24	27
JS188#25	H1.1^{R57A}RFP	13	4	87	26	30
JS147#1	H1.1^{R57K}RFP	45	9	55	11	20
JS149#4	H1.1^{R57K}RFP	35	18	65	33	51
JS175	H1.1^{wt}RFP	16	4	84	21	25
JS198	H1.1^{wt}RFP	14	3	86	18	21
JS196	H1.1^{wt}RFP	30	6	70	14	20

"(n) analyzed" corresponds to all ovules analyzed in the indicated line.

Expressing the *H1.1*^{R57K}*RFP* mutant variant induces aberrant MMC development

In mouse ESCs, H1 eviction upon citrullination is necessary to induce epigenetic reprogramming and the expression of pluripotency genes (Christophorou et al. 2014). H1 is also evicted in plant MMCs prior to a drastic chromatin reprogramming suggested to contributing the post-meiotic (pluripotent) developmental competence (She et al. 2013). We thus asked if the alteration of H1 eviction, as produced by the *H1.1R*^{57K}*RFP* variant, would also impair MMC development. For this, we fixed and cleared *H1.1*^{R57K}*RFP* expressing ovules 5 days after Dex-induction and analyzed ovule and MMC morphology (n = 107) and used Mock-treated plants of *H1.1*^{R57K}*RFP* as a control (n = 102). The results in Figure 2 illustrate different morphological changes which we found during the MMC development after induction. To better distinguish them from each other we placed them into five different categories based on morphological observation: Class 1: two MMC-like cells, class 2: two big nucleoli in one cell, class 3: no clear MMC development based on position and size, class 4: no elongated MMC based on position and size, class 5: extra periclinal division in the putative MMC. We found in the induced *H1.1*^{R57K}*RFP* variant that 2.5% of ovules had an extra periclinal division zone in the MMC (class 5, Figure 2 A & F). 2.5% had two big nucleoli in one cell (class 2; Figure 2 D). Further, we found ~ 20% had two MMC-like cells (class 1; Figure 2 C), in 5% we could not identify a clear MMC (class 3) and in 10% no elongated MMC (class 4, Figure 2 E) and roughly 60% of the developed MMCs looked like wild-type. The variety and apparent low penetrance of the mutant phenotype might be explained by a varying degree of Dex-induction efficiency (See chapter 2 of this thesis). But the frequency of aberrant MMCs is significantly

different between Dex-induced and Mock-treated plants (Figure 2 G). In the Mock-treated *H1*^{R57K}*RFP* variant 91% of the ovules analyzed looked normal (n = 92). Interestingly in the Mock-treated plants, we found also ~ 5% of class 1 MMCs, which compares well to the occurrence of ovule primordia with undistinguishable MMCs at that stage in wild-type. Later on, there is still only one that further develops in the wild-type situation. We also found one case in the induced *H1.1*^{R57K}*RFP* mutant which showed an extra division in the companion cell of the MMC (Figure 2 B), but we did not include this observation into our statistical analysis since we saw it is this mutant variant just once.

The results suggest that the mutation of *H1.1*^{R57K}*RFP* leads to altered H1 stability and this, in turn, induces aberrant development of the MMC.

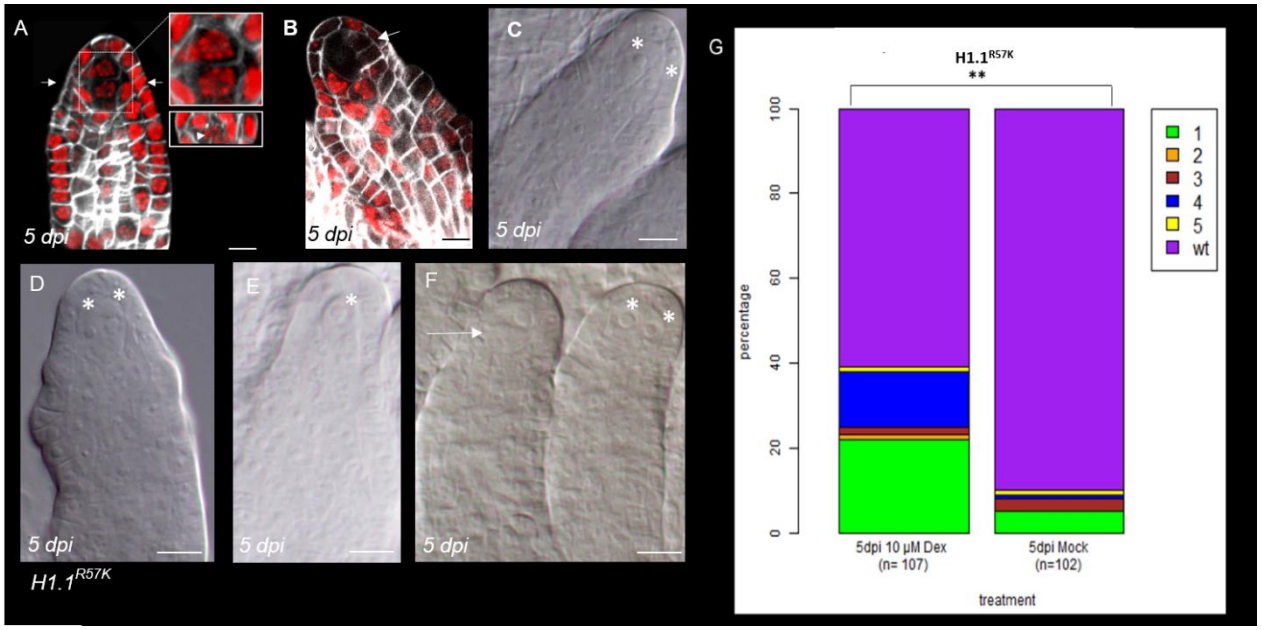

Figure 2: Aberrant MMC development 5 dpi with 10 µM Dexamethasone in *H1.1*^{R57K}*RFP* mutant. (A and B) Confocal microscope image of plant lines containing *H1.1R*^{57K}*RFP* 5 dpi with 10 µM Dexamethasone. (A) Periclinal division in MMC, both cells expressing *H1.1*^{R57K}*RFP*. (B) Extra division zone in companion cells of MMC. (C to F) Clearings of fixed material at different developing stages 5 dpi with 10 µM Dex. (C) Observation of two enlarged MMC-like cells. (D) Two enlarged cells in one MMC. (E) Underdeveloped MMC (to small). (F) Periclinal division in MMC and two enlarged cells in one MMC. Scale bars = 10 µm. (G) Quantification in percentage of aberrant MMC development after 5 dpi with 10 µM Dex in H1.1^{R57K} line JS149#4 (T1) (Dex-treatment n = 107; Mock-treatment n = 102). Aberrant MMC development classes : (1) Two MMC like cells (2) two big nucleoli in one cell (3) no MMC (4) no elongated MMC (5) periclinal division in MMC. Fisher exact test, comparison between „WT“ MMCs and aberrant MMCs. ** = $p < 0.01$.

H1.1^{R57K}*RFP*- expressing plants did not show ectopic expression of the MMC-specific *KNU* marker but might develop multiple embryo sacs.

To determine if the persistence of H1 in the *H1.1*^{R57K}*RFP* mutant variant has an influence on MMC and embryo sac development we crossed plants expressing the mutant variant to plants which

contained i) a reporter construct driven by the *KNUCKLES* (*KNU*) promoter, which marks MMCs prior to meiosis (*pKNU::nlsYFP*) (Tucker et al. 2012) and ii) a reporter construct driven by *ANTI-KEVORKIAN* (*AKV*), (*AKV::H2B-YFP*) (Pillot et al. 2010), which is a cell-identity reporter previously shown to mark nuclei during megagametogenesis prior to cellularization (Pillot et al. 2010; Schmidt et al. 2011). We hypothesized that if the aberrant expression of *H1.1^{R57K}RFP* has an influence on MMC or FM development, we would detect different YFP signals in those plants compared to Mock-treated ovules not expressing the H1.1 mutant variant. Surprisingly we found in all tested ovules expressing the *H1.1^{R57K}RFP* variant, just one cell with YFP signal after 5 dpi with 10 µM Dex. A similar result we detected in the Dex-treated control plants of the *pKNU::nlsYFP* line (Figure 3 A and 3 B) (n = 34). Also in plants showing an aberrant expression in the MMC of *H1.1^{R57K}RFP*, we always detected just one YFP signal (Figure 3 C). These results suggest that the expression of the mutant variant *H1.1^{R57K}RFP* in ovule primordia and MMCs does not alter the activity of the *KNU* promoter in those cells. Our preliminary results of the induced F1 plants of *AKV::H2B-YFP*; *H1.1^{R57K}RFP* plant line indicate that they might develop multiple embryo sacs, although to a low percentage (n = 2), compared to Dex-treated control plants expressing the *AKV::H2B-YFP* construct 7 to 8 dpi (Figure 3 D to F). But at the moment the sample size analyzed is too small to draw a final conclusion about the development of multiple embryo sacs, and additional samples need to be induced and analyzed.

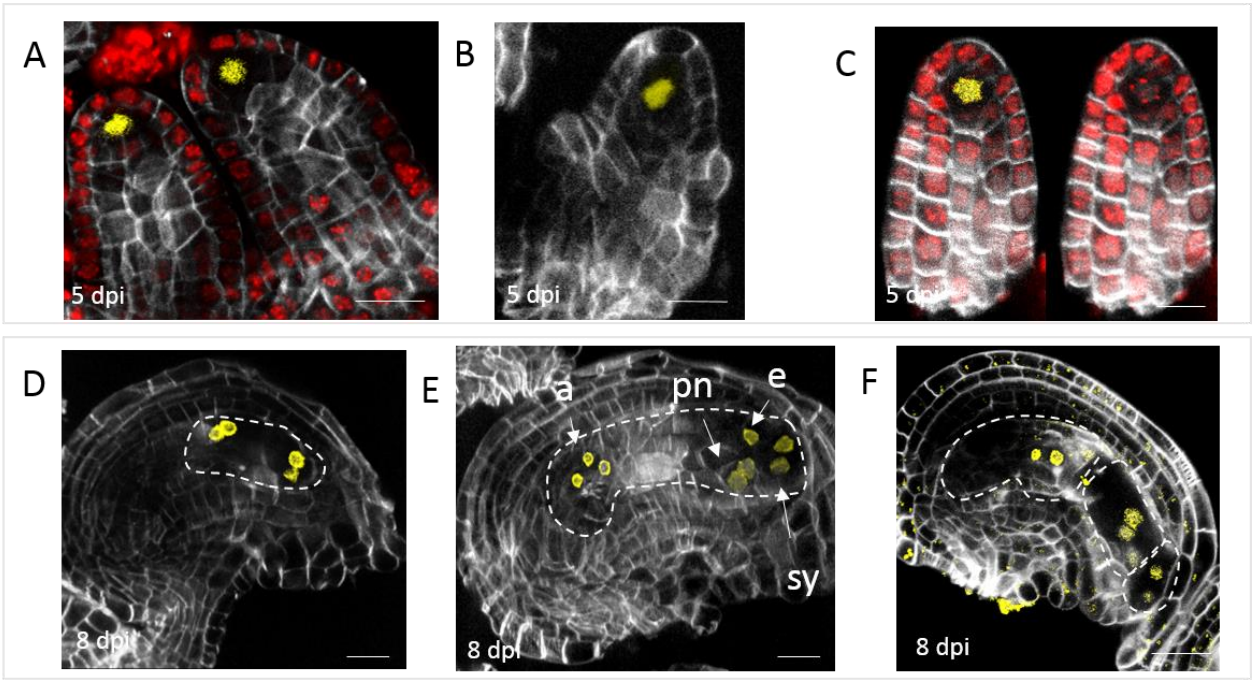

Figure 3: *H1.1^{R57K}* variant shows wild-type like *KNUCKLES* expression but might develop multiple embryo sacs. (A) One YFP signal in the MMC, which do not express *H1.1^{R57K}RFP* 5 dpi with 10 µM Dex. (B) Control shows one YFP signal 5 dpi with 10 µM Dex (*pKNU::nlsYFP)*. (C) One YFP signal in the MMC, which express *H1.1^{R57K}RFP,* 5 dpi with 10 µM Dex. (C) n = 34 two KNU signals: 0%. (A to C) Scale bar = 7 µm. (D to F) Shows YFP signals in F1 plants of *AKV::H2B-YFP*; *H1.1^{R57K}RFP*; (D) Female gametophyte at stage FG (four nuclear stage). (E) Female gametophyte at stage FG5 (8 nuclear embryo sac), (D and E) 8 days post-Mock-treatment. The white dashed line indicates the embryo sac. Scale bar = 20 µm. Yellow = *AKV::H2B-YFP*; grey =

Renaissance counterstain. a = antipodal cells, pn = polar nuclei (central cell), e = egg cell, sy = synergids. (F) Female gametophyte at stage FG5 (8 nuclear embryo sac), 7 days post 10 µM Dex-treatment. The white dashed line indicates three embryo sacs. Scale bar = 20 µm.

Plants expressing *H1.1^{R57K}RFP* variant show reduced fertility

Since we found that the *H1.1^{R57K}RFP* mutant variant has an aberrant H1.1 stability during the MMC development, we wondered whether this has an effect on the plants' fertility. To test this we watered two independent insertion lines containing the *H1.1^{R57K}RFP* variant with either 10 µM Dex or Mock for 4 weeks. The plants which were watered with Dex showed a varying degree of sterility (Figure 4 A), which we did not see in the Mock-treated plants. We found mostly infertile ovules but also in a few cases aborted seeds in the Dex-treated plants (Figure 4 A). The varying degree of sterility might be explained by the genetic status of the plant since they were segregating for the *H1.1^{R57K}RFP*. This hypothesis fits with the observation that the severity of the sterility correlated with the strength of the RFP signal. We found in both independent insertions lines treated with Dex a highly significant reduction in fertility compared to the Mock-treatment (Figure 4 A to C). Whereby in line JS173 the fertility was reduced by 40% (n (seeds) = 312) and in line JS171 by ~31% (n (seeds) = 474) (Figure 4 C, Supplement Table 3 and Supplement Figure 2).

The results indicate that the mutation of arginine 57 to lysine in the H1.1 lead to a reduction in the fertility of the plants.

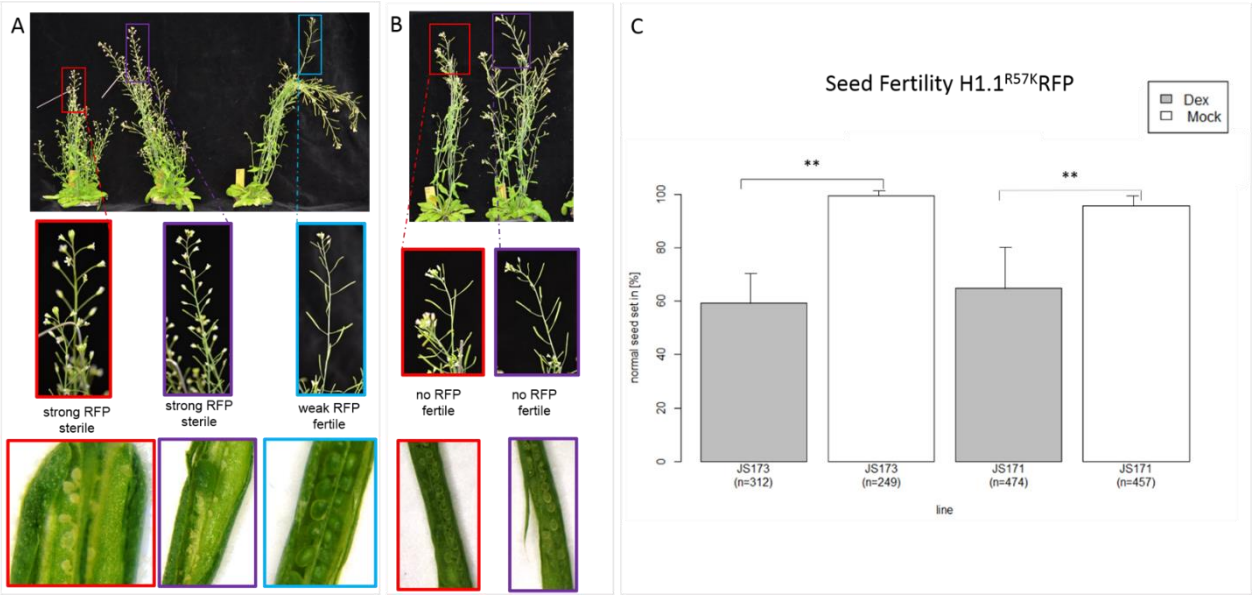

Figure 4: Plants expressing the *H1.1^{R57K}RFP* mutant variant have reduced fertility. T2 positive selected plants of *H1.1^{R57K}RFP* were watered for ~ 4 weeks with either (A) 10 µM Dex or (B) Mock starting before bolting, shortly after transferring the seedlings to soil. The plants watered with Dex (A) showed a varying degree of sterility, which was not found in Mock- (B) treated plants. The plants were checked for presence or absence or RFP signal. (A and B) Both show plant line JS171, for images of JS173 see Supplement Figure 2 and Supplement Table 3. (C) Error bars = SEM between plant individuals. In the line JS173 we found a reduction of healthy seed set of

40.2% and 30.9% in line JS171 under Dex-treatment compared to Mock. N in the plot corresponds to total seeds counted. We counted three siliques per plant of three plants per treatment. The difference in fertility between Dex- and Mock-treatment for each line was highly significant. For JS173 the fisher exact statistic is $p < 0.00001$ and for JS171 the fisher exact statistic is $p < 0.00001$; ** = $p < 0.01$.

Stability of H1.1^{R57K}RFP variant and absence of H1.1^{R57K}RFP variant in Pollen Mother Cells (PMC).

Since we found an aberrant presence of H1.1^{R57K}RFP during the MMC development and a reduction in fertility in induced plants carrying this construct, we wanted to know, if we also can detect an aberrant presence of this variant during PMC development. Our preliminary results showed no aberrant presence of H1.1^{R57K}RFP during PMC development compared to the literature (She et al. 2013) (Figure 5 A) and to the H1.1^{R57A}RFP variant (Figure 5 B and Supplement Figure 3). But the interpretation of the results is limited, due to low sample size (n (anthers) = 8), therefore the test should be repeated with a higher amount of samples. Further, we wanted to know, if the aberrant presence of H1.1^{R57K}RFP could be explained by a different stability compared to H1.1^{wt}RFP. To answer this question we did Fluorescent Recovery after Photobleaching (FRAP) analysis. We found no difference in immediate fluorescent recovery between the two constructs in the first minute (Figure 5 C). But the two constructs might have a difference in the long-term recovery phase (after 1 min). To answer this question, we suggest that further FRAP experiments should be done to explore this phase.

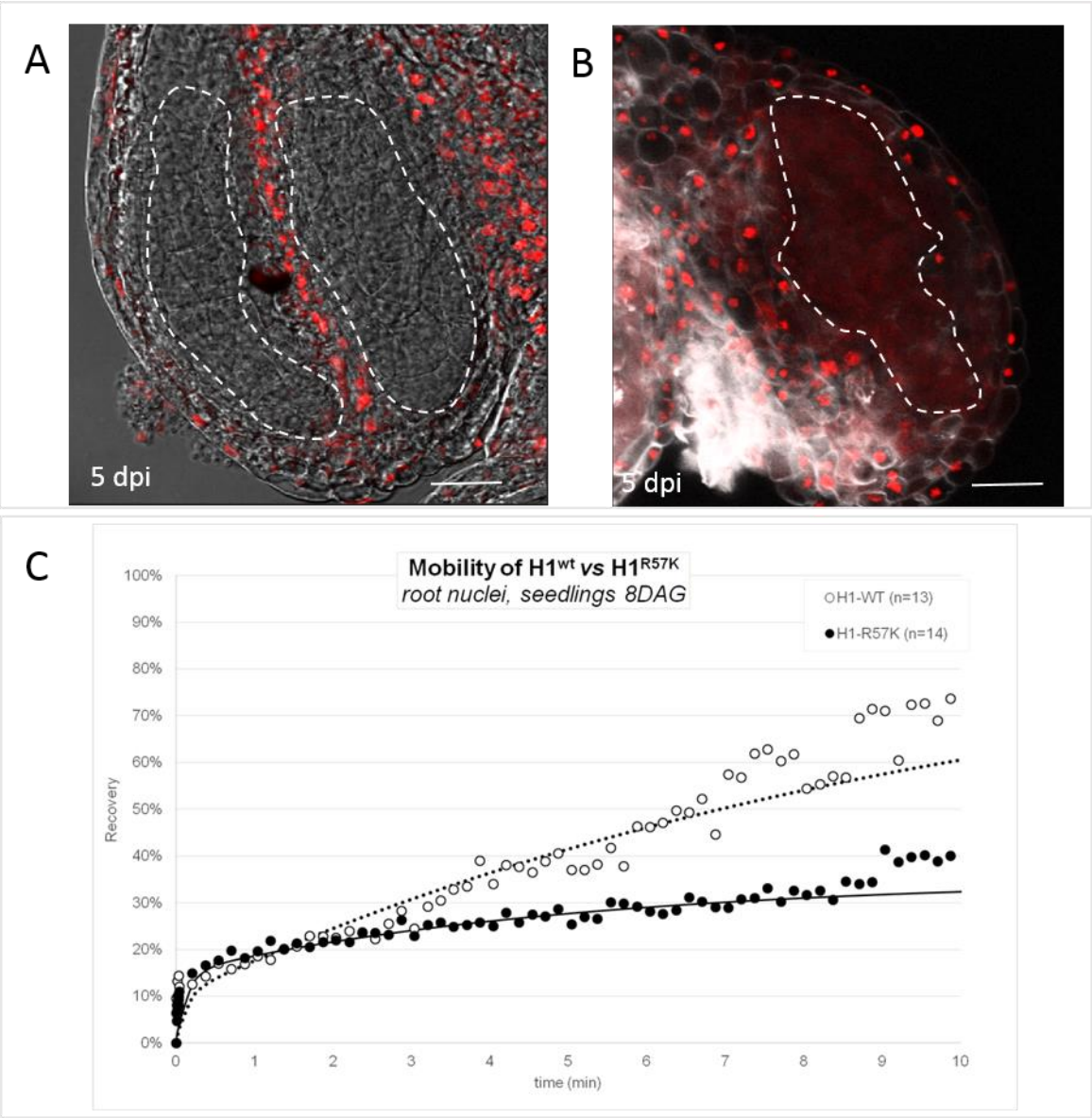

Figure 5: Stability of H1.1^{R57K}RFP variant and absence of H1.1^{R57K}RFP variant in PMC. (A) No presence of RFP signal in PMCs (dashed line) of *H1.1^{R57K}RFP* lines 5 dpi with 10 µM Dex. (B) No presence of RFP signal in PMC (dashed line) of *H1.1^{R57A}RFP* lines 5 dpi with 10 µM Dex. Scale bar = 20 µm. (C) FRAP curves show similar speed in the immediate recovery phase (no significant difference on fits in fast kinetics, 1 min) but might have a difference in the long-term recovery phase (after 1 min).

Reanalysis of published expression data of *AIH* (*AGMATINE IMINOHYDROLYASE*)

Since the mutation in H1.1 at position R57K is a putative target of citrullination we wanted to know if an enzyme is expressed during *Arabidopsis thaliana* sporogenesis which might facilitate this enzymatic reaction. By amino acid homology, we did not find a candidate in *A. thaliana*, similar to mouse PADI4, which facilitates the citrullination reaction in mouse ESCs (Christophorou et al. 2014). Therefore, we choose as a candidate the AGMATINE IMINOHYDROLASE (AIH)

(*AT5G08170*), based on its GO molecular functions described in TAIR (https://www.arabidopsis.org), which are “protein-arginine deiminase activity and agmatine deiminase activity”. In plants, AIH is described to be involved in the polyamine biosynthesis pathway and deiminase agmatine to carbamoyl putrescine (Janowitz, Kneifel, and Piotrowski 2003). It is further described that T-DNA lines of this gene are embryo defective. Whether the protein AIH can convert an arginine or mono-methylated arginine in a protein to a citrulline has not been investigated in this context.

Here we used published RNA-Seq and Microarray data to plot the relative expression of *AIH* compared to *CUL3A* (see also chapter 5) in different reproductive and embryonic tissues (Figure 7 and Supplement Table 2). The plot shows the relative expression level of *AIH* and *CUL3A* based on (A) RNA-Seq data from Wuest and colleagues (Wuest et al. 2010) and (B) Microarray data from Schmidt, Borges, Pina and Honys (Borges et al. 2008; Honys and Twell 2004; Pina and Pinto 2005; Schmidt et al. 2011). The script used for analyzing the RNA-Seq and Microarray data can be found at “https://github.com/VimalRawat1010/Rscripts/blob/master/LabData/.RData”. The reanalysis of the RNA-Seq data showed that *AIH* has its highest expression in torpedo stage embryo compared to other tissues analyzed in this plot. The level of expression in the central cell, the egg cell and also the pollen meiocytes is similar to each other. If we look at the expression data based on the Microarray data we see that *AIH* has its highest expression based on this data-set in the bi- and tricellular pollen. Further, it also shows a relatively high expression in the ovule and the MMC compared to its expression in the egg cell or the heart stage embryo. The reanalysis of the RNA-Seq and the Microarray therefore suggests that *AIH* is expressed in the ovule and has so the preconditions to play role in linker histone eviction and reloading during MMC development in *A.thaliana* maybe by facilitating citrullination.

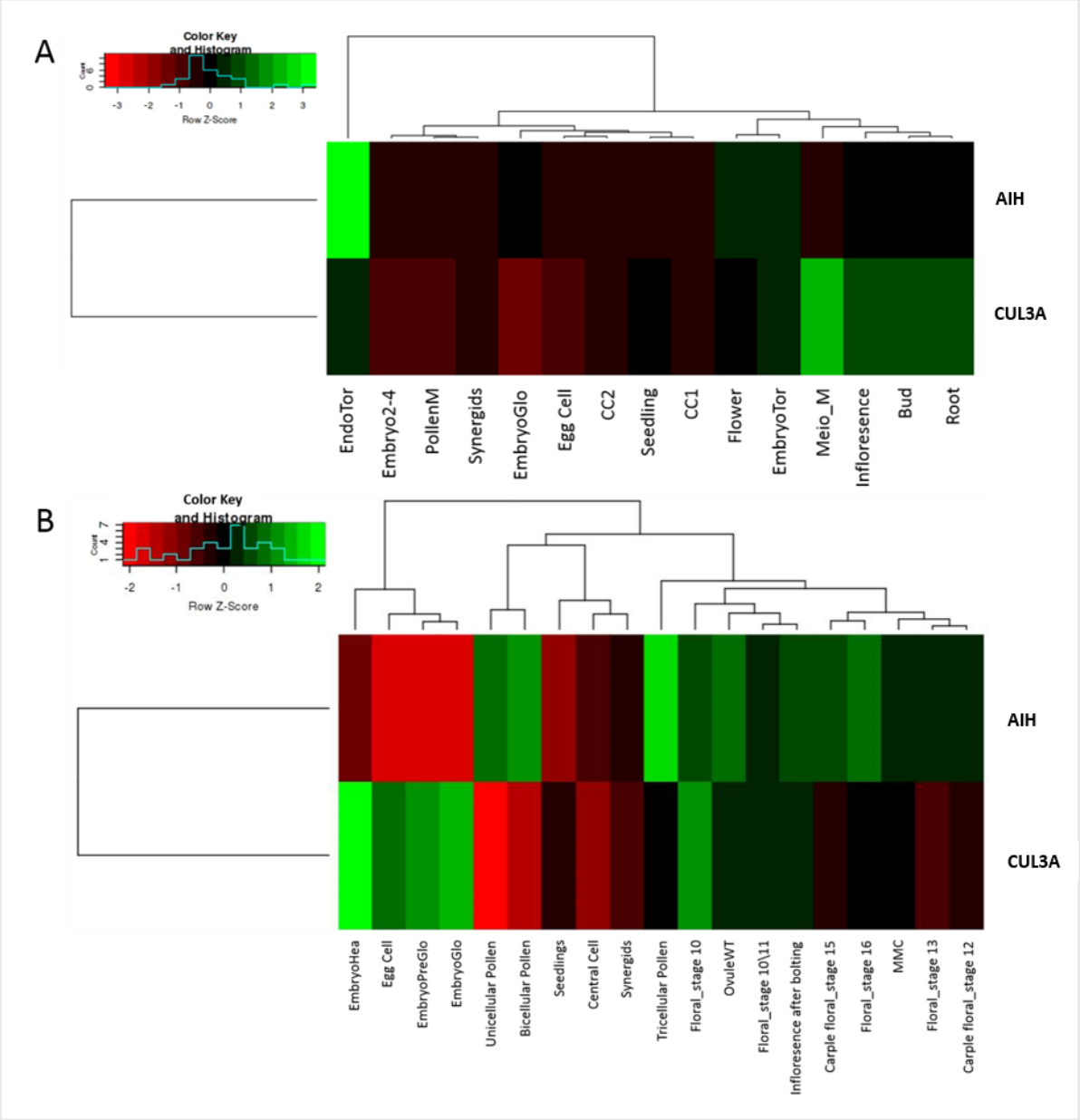

Figure 6: Heatmap, relative expression of *AT5G08170* (*AIH*) compared to *AT1G26830* (*Cul3A*) in different tissue. Presented in (A) RNA-Seq experiments from Wuest and colleagues (Wuest et al. 2010) and (B) on Affymetrix ATH1 GeneCHIP experiments from different publications (Borges et al. 2008; Honys and Twell 2004; Pina and Pinto 2005; Schmidt et al. 2011). Both heat maps are designed with the R-script published in GitHub (https://github.com/VimalRawat1010/Rscripts/blob/master/LabData/.RData). The tool considers shape and gene expression values to create the dendrograms and colors. The table with normalized expression values can be found in the Supplement Table 2. Abbreviation: (A) PollenM (pollen mature), CC1 (central cell), CC2 (central cell), Embryo2-4 (embryo cell stage 2-4), EmbryoGlo (embryo globular stage), EndoTor (endosperm torpedo stage), Meio_M (meiocytes male), EmbryoTor (embryo torpedo stage). (B) Syn (synergids), MMC (megaspore mother cell), Egg (egg cell), Cen (central cell), EmbryoGlo (embryo globular stage), EmbryoHea (embryo heart stage) and EmbryoPreGlo (embryo pre-globular stage).

Modeling overall 3D structure and catalytic pocket of PADI4 and AIH

To determine the similarity between mouse PADI4 and Arabidopsis AIH we superpositioned both 3D structures using the 3D modeling software Coot (Crystallographic Object-Oriented Toolkit) and visualized them with PyMOL (Figure 5 D). We found that the structure of AIH folds very similarly to the C-terminal tail of PADI4, which includes the catalytic domain. A zoom into the catalytic pocket with an arginine binding to it highlights the similarity between the two structures. All four catalytic amino acids (D94, H224, D226, C366) are positioned in almost the same 3D location. The difference between the catalytic amino acids of PADI4 and AIH are 0,75 Å; 1,07 Å;0,80 Å; and 0,88 Å.

This similarity in the catalytic domain makes it very probable that both proteins can bind the same molecules and thus might have the same or a similar function in their respective organisms.

***AIH* downregulation lines show after induction persistency of H1.1 in developing MMCs**

To explore the role of *AIH* on linker histone eviction during MMC development we designed an inducible amiRNA against *AIH*, which has its target sequence in the 3'UTR of the gene (Figure 4 A). Several independent knockdown lines of *AIH* showed a significant increase of up to 31% in GFP signals during ovule development in *pH1.1::H1.1-GFP* plant lines compared to the background reporter (BG) line, when both were induced with 10 µM Dex 5 dpi (Figure 4 B and C; Supplement Figure 7 and 8). Two lines showed aberrant GFP signals at stages 1-II and 2-II up to ~ 30% (n = 88) and 20% (n = 34) of all ovules tested. The BG line treated with Dex showed aberrant GFP signals in those stages of 4.5%. In summary, the difference in H1.1 presence at the stages 1-II and 2-II between the Dex-treated BG line and the *AIH* downregulation lines are 15% to 25% depending on the line. The results indicate a putative influence of AIH on the stability of H1.1 during plant sporogenesis.

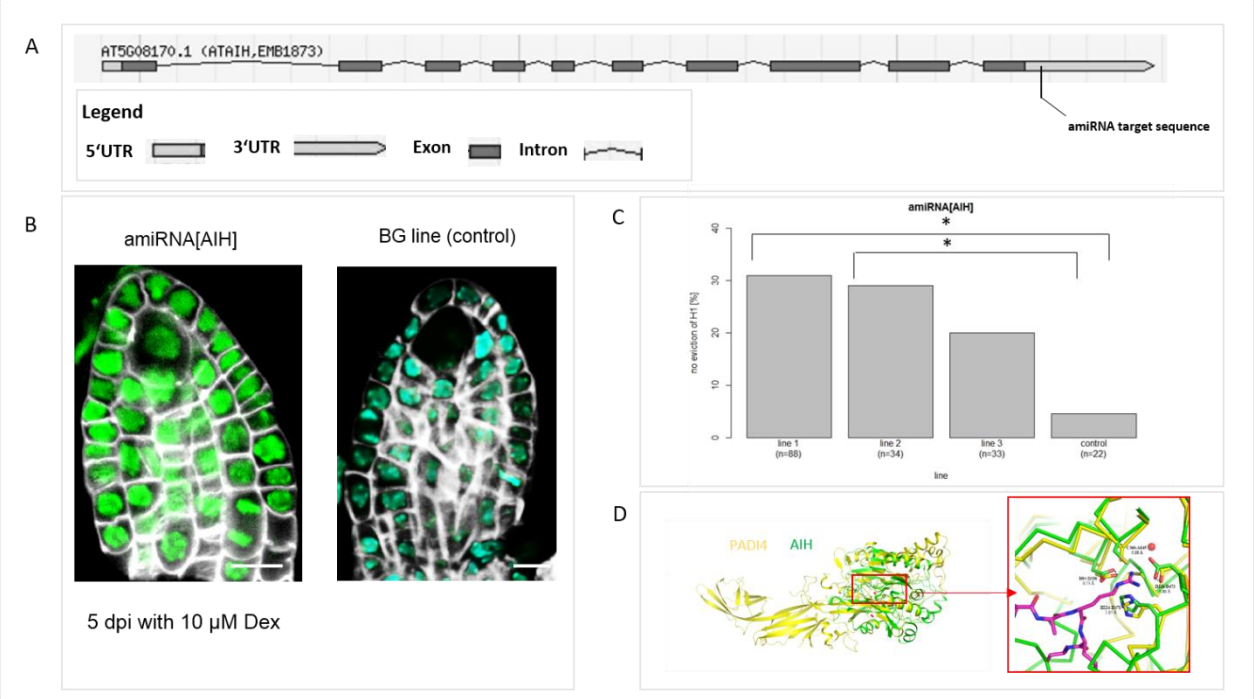

Figure 7: Linker histone signals in MMC in *AIH* downregulation lines and AIH 3D prediction model compared to PADI4. (A) Gene model of *AT5G08170.1* (*AIH*) with the amiRNA target site highlighted. The target sequence is in the 3'UTR. The target sequence and mismatches for the amiRNA can be found in the Supplement table 4. (B) GFP signals of H1.1 tagged wild-type variant in the induced *AIH* downregulation line and induced BG line, 5 dpi with 10 µM Dex. (C) Three independent insertion lines of *AIH* downregulation lines have been tested: residual signals of GFP (H1.1) and 31% (n = 88), 29% (n = 34), 20% (n = 35). One BG line was tested: residual signals of GFP (H1.1) 4.5% (n = 22). * = $p < 0.05$ (Fisher exact test) compared to induced BG control (BG line, p*H1.1::H1.1-GFP*). (D) Gene modeling in coot of PADI4 (yellow) of mouse (2DEW), compared to AIH (green) of *A.thaliana* (1VKP). Zoom in into the catalytic domain of both proteins. Purple is an arginine binding in the catalytic pocket.

Dex-inducible *AIH* downregulation lines show aberrant MMC development

To test whether the aberrant stability of H1.1 in induced *AIH* downregulation lines has an influence on MMC development similarly as above for the H1.1^{R57K}RFP variant we fixed and cleared *AIH* downregulation ovules 5 days after Dex-induction and analyzed ovule and MMC morphology. We compared ovules of two induced *AIH* downregulation lines, (n = 21 and n = 30) to Mock-treated ovules (n = 19 and n = 14) and to Dex-treated BG line ovules (n = 35). We observed several types of morphological changes during MMC development after induction (Figure 8), which we classified in five categories: Class 1: two MMC-like cells, class 2: two big nucleoli in one cell, class 3: no clear MMC development based on position and size, class 4: no elongated MMC based on position and size, class 5: extra periclinal division in putative MMC. We found in the line (JS143) an *AIH* downregulation line induced with Dex that ~ 46% of ovules exhibit an aberrant development compared to 10% under Mock-treatment. In line JS144, also an induced *AIH* downregulation line, we found that after Dex-treatment ~ 33% of ovules analyzed developed an aberrant MMC morphology compared to ~ 21% under Mock-treatment. Interestingly also our BG line (JS64)

exhibit under Dex-treatment a high amount of aberrant morphology of the MMC (~ 22%). This might be caused by the mechanical and chemical stress, plants experienced with the Dex-induction process. The difference between the aberrant development of MMCs in line JS143 under Dex- and Mock-treatment is significant (p = 0.012). Significant is also the difference of aberrant MMC morphology of this line after Dex-treatment compared to the BG line treated with Dex (p = 0.0347). The results suggest that *AIH* plays a role in normal MMC development.

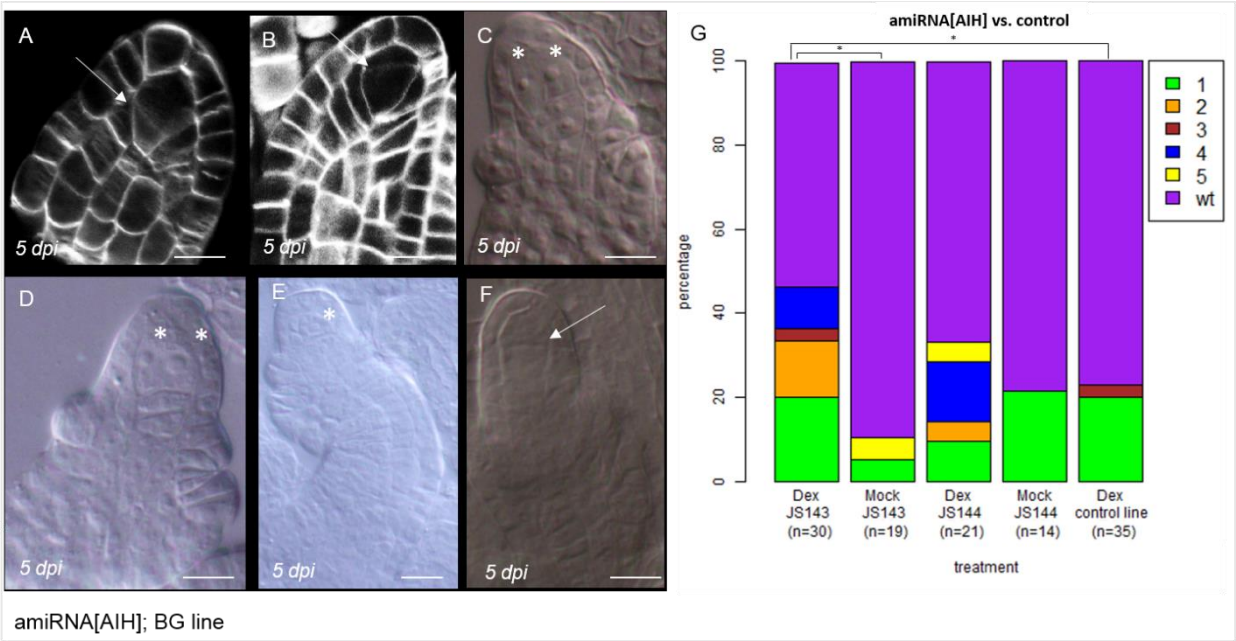

Figure 8: Aberrant MMC development in induced *AIH* downregulation lines. (A and B) Confocal image of aberrant division zone in MMC (arrow) of *AIH* downregulation lines 5 dpi with 10 µM Dex. Scale bars = 10 µm, grey = Renaissance counter stain. (C to G) Clearings of fixed material at different developing stages 5 dpi with 10 µM Dex. (C) two MMC-like cells (D) two enlarged cells in one MMC (E) underdeveloped MMC (F) periclinal division in MMC. Scale bars = 10 µm. (G) MMC phenotypic categorize in percentage in Dex- and Mock-treated *AIH* downregulation lines and a Dex-treated BG line. Measurement was 5 dpi. Categories: (1) Two MMC like cells (2) two big nucleoli in one cell (3) no MMC (4) no elongated MMC (5) periclinal division in putative MMC. Comparison Dex- and Mock-treatment of line JS143# p = 0.012 and JS144#4 p = 0.7189. Comparison of *AIH* downregulation lines after Dex-treatment to Dex-treated control line: p = 0.0347 (JS143#4 to control); p = 0.3483 (JS144#4 to control). * p< 0.05; n.s. (not significant) p > 0.1 (Statistic fisher test).

Induced *AIH* downregulation lines show no aberrant H1.1 stability in PMCs and also no significant change in the number of lateral roots after Dex-induction

Since we found in induced *AIH* downregulation lines altered H1.1 presence in the MMC, we wanted to know, if there would also be an aberrant H1.1 stability in the PMCs (Supplement figure 6). Therefore we analyzed the presence of H1.1 in PMCs 5 dpi with 10 µM Dex. Our results showed no altered presence of H1.1 in *AIH* downregulation lines after induction compared to the literature (She et al. 2013) (Supplement Figure 6). But the experiment might be repeated, due to

a small sample size (n (anthers) = 5). We also wanted to know, if the altered stability of H1.1 in the ovules and MMCs in induced *AIH* downregulation lines have an influence on other cell-fate transitions, like the ones that lead to the formation of lateral roots (see also chapter 1). Therefore we compared the number of lateral roots in induced *AIH* downregulation lines to induced BG lines (Supplement figure 11). We found no significant difference between the Dex-induced *AIH* downregulation lines compared to the Mock-treated *AIH* downregulation lines. Therefore the results indicate that *AIH* plays no role in the correct development of lateral roots.

Dex-induced *AIH* downregulation lines show at a low level altered *KNUCKELS* expression

Since we found in induced *AIH* downregulation lines an aberrant H1.1 stability during sporogenesis and altered MMC morphology, we wanted to know if also the MMC identity is altered in those lines. Therefore we crossed the inducible *AIH* downregulation lines with a *KNUCKLES* (*KNU*) reporter construct (*pKNU::nlsYFP*). *KNU* has been described to mark MMCs prior to meiosis (Tucker et al. 2012). Our results showed that in the induced *AIH* downregulation lines we found out of 80 ovules two which exhibit two YFP signals instead of one (Figure 9 A to C), which we did not found in the 70 ovules analyzed in the induced control, *pKNU::nlsYFP* alone (Figure 9 D). In summary, 2.5% of analyzed ovules in the induced *AIH* downregulation lines showed two YFP signals compared to 0% in the induced control line, (*pKNU::nlsYFP*) (Figure 9 E), but this difference is not significant (p = 0.4988).

Our results indicate that *AIH* might be involved in a process which controls or maintains that just one cell in the ovule primordia becomes an MMC. But more samples and other MMC identity markers need to be screened and analyzed to ensure a significant influence of *AIH* in this process.

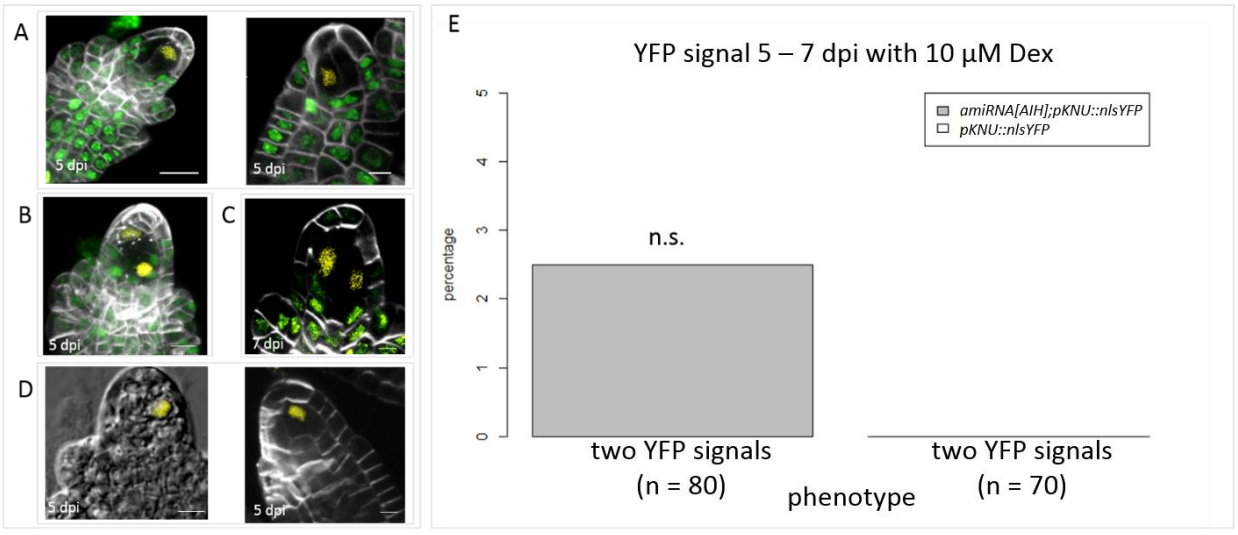

Figure 9: Induced *AIH* downregulation lines exhibit to a low percentage two cells with KNUCKELS expression. (A) MMC shows YFP signal but no GFP signal after 5 dpi with 10 µM Dex in *amiRNA[AIH];pKNU::nlsYFP;BG* lines. (B and C) Two cells show YFP signals (2.5% of n = 80), but no or just weak GFP signals after 5 dpi (B) and 7 dpi (C) with10 µM Dex (*amiRNA[AIH];pKNU::nlsYFP;BG)* .(D) We just detected one YFP signal after 7dpi with10 µM Dex

in the control, *pKNU::nlsYFP*. (A to D) yellow = YFP, grey = Renaissance counter stain; Scale bar = 10 µm. (E) The difference between two YFP signals in Dex-treated control lines (*pKNU::nlsYFP*) and Dex-treated *AIH* downregulation lines (*amiRNA[AIH];pKNU::nlsYFP;BG*) is not significant. (*p* = 0.4988) fisher exact test.

Influence of *PADI* inhibitor TDFA and Cl-amidine on H1s stability during sporogenesis

So far our results of induced ovules expressing *H1.1^{R57K}RFP* and *H1.1^{R57A}RFP* variants and the results of the induced ovules of *AIH* downregulation lines suggest as one option a model where H1.1 is citrullinated by AIH which results in H1.1s eviction. If this model holds true, we expect that inhibitors of *PADI4*, which converts the citrullination in mouse, could also prevent Arabidopsis *AIHs* function. Thus we would expect results, which mimics the ones of *AIH* downregulation and the ones of *H1.1^{R57K}RFP* expression. To test this hypothesis we choose the *PADI4* inhibitors TDFA and Cl-amidine (Christophorou et al. 2014) since those chemicals inhibit PADI4s function by blocking its catalytic domain (Fuhrmann and Thompson 2016), which has a very similar 3D structure to the catalytic domain of Arabidopsis AIH (Figure 7 D).

To test our hypothesis we treated plants of our BG line with TDFA and Cl-amidine and monitored for altered H1s signals 5 days post-treatment (dpt). We found 5 dpt with 1 µM TDFA that ~ 40% of ovules analyzed (line JS65 (n = 20)) developed an aberrant MMC. Our definition of aberrant MMC was here based on persistent H1.1 and H1.2 signals and morphological criteria (as mentioned above) (Figure 10 A and B). We found a similar result after 1 µM treatment with Cl-amidine (Figure 10 C). Here ~ 65% of analyzed ovules (n = 20) developed morphological aberrant MMCs with a weak presence of H1.1. The treatment of the same line with Mock (0.09% DMSO) in comparison showed in ~75% (n = 22) a morphological wild-type like development of MMCs and also an H1.1 stability as described in the literature (She et al. 2013) (Figure 10 D). The number of aberrant MMCs between the Cl-amidine- and Mock-treated ovules was significantly different by *p* = 0.0046, whereas the number of aberrant MMCs between the TDFA- and Mock-treatment was not significantly different (*p* = 0.32) (Figure 10 E). It needs to be mentioned that in a large part of MMCs analyzed we were not able to identify a proper MMC, based on location and size in the ovule. Out of 40% of ovules treated with TDFA and classified as containing an aberrant MMC, we could not identify in 25% a clear MMC (red line in Figure 10 E). Under Cl-amidine-treatment we could not locate in half of the samples, which we classified as “aberrant MMCs”, a clear MMC (red line Figure 10 E).

Our preliminary results partly matched our expectations that the treatment with *PADI4* inhibitors will mimic *AIH* and H1.1^{R57K}RFP phenotypes. Interestingly just the treatment with Cl-amidine but not with TDFA fulfilled our expectations. Since we missing a positive control for the effectiveness of the chemicals, we cannot exclude that TDFA was not 100% effective anymore. But what we can also not exclude is, if Cl-amidine and TDFA alone have already an influence on the development of the MMC, without altering H1.1s stability. To distinguish this effects we miss a proper control. So the experiment done here can just be used as a putative indication for a role of *AIH* and citrullination on H1.1s stability during plant sporogenesis.

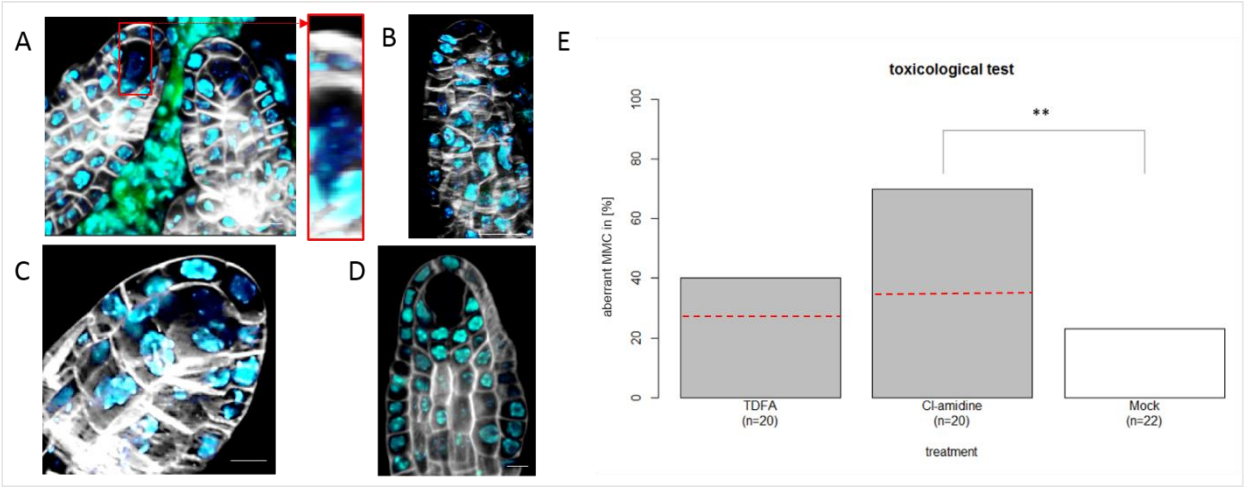

Figure 10: Test of citrullination inhibitor TDFA and Cl-amidine on H1s stability in MMCs. (A and B) 1 µM TDFA 5 dpt; in JS65 (BG line). Scale bar = 10 µm. (A) Residual presence of GFP and ECFP (H1.1 and H1.2) (B) We could not detect an MMC. (C) We detect weak H1.2 signals in JS65 (BG line), after 5 dpt with 1 µM Cl-amidine. Scale bar = 5 µm. (D) Clear MMC development and absence of GFP or ECFP signals in BG lines 5 dpt with 1 µM Mock (0.09% DMSO). (A to D) Scale bars = 10 µm; blue = *pH1.2::H1.2-ECFP*; green = *pH1.1::H1.1-GFP*; grey = Renaissance counterstain. (E) The number of aberrant MMCs is significantly different between Cl-amidine- and Mock-treatment (p = 0.0046), ** = p < 0.1. The number of aberrant MMCs between TDFA- and Mock-treatment is not significantly different (p = 0.32, Fisher exact test). The red dashed lines mark that roughly half of the MMCs described as aberrant could not be identified by us as clear MMCs, rest includes normal developed MMC but aberrant linker histone presence.

Discussion

Our goal was to determine if citrullination is involved in the transient linker histone eviction during the somatic-to-reproductive transition in *Arabidopsis thaliana*. Our results suggest that the mutation of arginine 57, which we identified as a putative citrullination target is sufficient to alter H1s stability during MMC development. We found that the plants harboring the mutation of arginine 57 to lysine, thus inhibiting a putative citrullination, showed aberrant MMC development and reduced fertility. We showed that the mutation of arginine 57 to alanine, which mimics the charge of citrullination, did not cause any alterations of H1s stability. In contrast to the citrullination target site in mouse H1.2 lies the arginine 57 in *Arabidopsis thaliana* shortly before the globular domain of H1.1 (Christophorou et al. 2014; Wisniewski et al. 2007). This is an interesting point, since arginine 57 lies close to the predicted contact sites of H1s with the DNA (Bednar et al. 2017) and a change of an arginine to citrulline changes the proteins charge under a neutral pH from positive to neutral and might result in changes in protein structure and function like molecular interaction with the DNA.

What also needs to be mentioned is that arginine 57 and arginine 79 are not only putative targets of citrullination but also targets of methylation in Arabidopsis H1.1 and H1.2 (Kotliński et al. 2016). It has been described that PADI4, which is the only PADI found so far, which can enter the nucleus (Witalison, Thompson, and Hofseth 2015), can also citrullinate mono-methylated arginine but not dimethylated ones (Cuthbert et al. 2004). Therefore PADI4 has a reversing action of PROTEIN ARGININE METHYLTRANSFERASES (PRMT) since it can remove monomethyl groups from

arginine residues through a demethyliminase activity. Similarly, deimination by PADI4 prevents arginine methylation (Cuthbert et al. 2004). Thus, PADI4 can block or reverse some of the actions of PRMTs. But in our case, it might also be possible that the phenotypes, which we observed in the *H1.1*^{R57K}*RFP* mutant plant lines, are not directly caused by an inhibition of citrullination but can also be simply caused by a lack of arginine methylation by PRMTs. The lysine in the mutated version (H1.1^{R57K}RFP) can also be methylated but not by PRMTs. Mass spectrometric analysis of PTMs in H1.1 and H1.2 by Kotlinski and colleagues (Kotliński et al. 2016) identified the region around R57as a "hot-spot" of PTMs. They found in a two amino acid window, upstream and downstream of R57, PTMs like: crotonylation, methylation and some unknown modifications (Kotliński et al. 2016). Therefore this region might be important for either the binding properties of H1.1 and H1.2 to the DNA and/or for other epigenetic- writers, -readers and –erasers.

Interestingly we did not found any changes in linker histone stability in PMCs in either the induced *H1.1*^{R57K}*RFP* variant nor in the induced *AIH* downregulation lines. This observation might be explained by either i) that the samples size was too small to detect the changes or by ii) that in PMCs another mechanism or at least another Arabidopsis *PADI* homolog is involved in linker histone eviction in those tissues. This is very likely since also the *PADIs* of mouse and human are very tissue-specific expressed and are also very substrate specific (Witalison, Thompson, and Hofseth 2015). For example, Christophorou and colleagues found citrullination and *PADI4* expression in pluripotent ES cells and in induced pluripotent stem cells but not in multipotent neural stem cells (Christophorou et al. 2014).

Further did we wanted to know, which protein might have the same or a similar function as PADI4 in mouse ES cells, to convert arginine in linker histones into citrulline. We identified AIH as a potential candidate to have this enzymatic function, based on our 3D modeling, which suggest that the catalytic domain of PADI4 and AIH are very similar. Our results showed, that after Dex-treatment of *AIH* downregulation lines, the plants exhibit aberrant H1.1 stability and aberrant MMC morphology. Interestingly we also found, albeit not significant, a few cases which showed after induction a second cell within the ovule primordia exhibiting a YFP signal driven by the *KNU* promoter. In this few case, two cells exhibit an “MMC identity” prior to meiosis. Nevertheless, the finding was not significant and therefore a bigger sample size should be looked at, to confirm the results (percentages). Interestingly reminds the phenotype of two YFP signals driven by the *KNU* reporter, of the results found by i) Zhao and colleagues (Zhao et al. 2017) in the *krp4krp6krp7* mutant and ii) the results from our lab in the *sdg2* mutant (Baroux and She, unpublished). In the first study they found that the cyclin-dependent kinase (CDK) inhibitors of the KIP-RELATED PROTEIN (KRP) class are involved in a signaling cascade which finally leads to a fine balance between *RETINOBLASTOMA HOMOLOG RBR1* and *WUSCHEL* (*WUS*), which are involved in regulating ovule primordia formation including development of the integuments and also partly controlling its entry into meiosis (Zhao et al. 2017). In the second case *SET DOMAIN GROUP 2* (*SDG2*) has been described to mediate H3K4me3, which is crucial for chromatin condensation and mitotic division during male gametogenesis in Arabidopsis (Pinon et al. 2017). In both cases leads the misexpression of the genes to the development of several MMC-like cells, similar to what we see in our induced *AIH* downregulation and *H1.1*^{R57K}*RFP* lines. This suggests that also in our case the misexpression of *AIH* or the expression of an *H1.1* mutant variant, might interfere with chromatin compaction, epigenetic reprogramming and finally with correct meiosis, by disrupting H1s eviction. If H1s are not evicted they may prohibit transcription of certain genes,

which would either give the MMC the competence to undergo meiosis and thereby change its fate or in turn, would specify or suppress the formation of more MMCs in the surrounding sporophytic tissue. Our preliminary results suggest that *AIH* might be involved in the correct formation of the MMC. But what still needs to be tested is, if the phenotypes in the induced *AIH* downregulation lines are caused by a downregulation of *AIH* or by off-targets or/and insertion site effects. To answer those questions qPCR experiments and an amiRNA resistant *AIH* variant needs to be cloned.

In summary, our results suggest a role of R57 in the stability of H1.1 during female sporogenesis. Our hypothesis is that linker histone eviction prior to meiosis (She et al. 2013) is facilitated by either citrullination at R57 or by methylation of that site. If this process is facilitated by *AIH* needs to be further investigated. But our 3D modeling and our other preliminary results suggest that *AIH* is a good candidate to have a similar function as *PADI4* in mouse. We further hypothesize that the change in charge at R57 either by citrullination or methylation might lead to an electrostatic repulsion or release of the linker histone to or from the DNA and leads to its eviction. A lack of linker histone eviction as seen in our *H1.1*^{R57K}*RFP* mutant leads to the development of aberrant MMCs and finally to reduced fertility, most probably by prohibiting chromatin decondensation and thus interfering with correct transcription and thereby influencing the cells developmental processes. But the detailed mechanism of this process still needs to be revealed.

Material and Methods

Plant material and growth conditions

Arabidopsis seeds were sterilized in 3% Bleach with 0.01% Triton X-100, washed in 70% EtOH, and sown out on 1/2 Murashige and Skoog (MS) salts (CAROLINE), 1% Sucrose, 1% (w/v) agar pH 5,6.

Seeds were sterilized and stored for 2 to 4 days at 4°C before transferring them to incubators (Percival) with long day conditions of 16 hours light [120 µE m-2 s-1] at 21°C and 8 hours dark at 16°C. The young plants were then transferred to soil and grown in a growth chamber with long day conditions (16h light/ 8h dark) at 22°C light and 18°C dark.

For FRAP experiments plants were grown on plates under long day conditions in an incubator (Percival) for 7 days.

The creation of the BG line is described in chapter 3 of this thesis.

The RFP constructs and the amiRNA against *AT5G08170* were synthesized by Genescript and GeneART (Invitrogen) and cloned via Gateway into the pRPS5a::LhGR2-GUS::pOP6 vector (Ian Moore, Oxford). The constructs were transformed via *Agrobacterium tumefaciens* (GV3101) to Col-0 plants. Positive T1s were identified based on BASTA selection, GUS reporter assay and detection of RFP signals after 10 µM Dex-treatment as described in chapter 3 of this thesis.

The Dex-inducible amiRNA targeting *AIH* was designed by using the wmd3 database (Schwab, Ossowski, and Warthmann 2010) and transformed via *Agrobacterium tumefaciens* (GV3101) to

BG lines. Positive T1s were identified based on BASTA selection and GUS reporter assay after 10 µM Dex treatment as described in chapter 3 of this thesis.

The *nls3xmVenus* (Joop Vermeer, University of Zurich) construct was cloned with the Gateway LR reaction into the pRPS5a::LhGR2-GUS::pOP6 vector (Ian Moore, Oxford). The construct was transformed via *Agrobacterium tumefaciens* (GV3101) to Col-0 plants. Positive T1s were identified based on BASTA selection, GUS reporter assay and detection of Venus signal after 10 µM Dex treatment as described in chapter 3 of this thesis.

Homozygote *pKNU::nls-YFP* plants (Tucker et al. 2012) and homozygote *AKV::H2B-YFP* (Pillot et al 2010) were crossed to T2s of *AIH* downregulation lines and /or plants of *H1.1^{R57K}RFP*. Positive plants were selected on BASTA or Hygromycin medium, GUS reporter assays and visual screen for YFP signals at the microscope as described in chapter 3.

The *pAIH::nls-mClover* construct was synthesized by GeneArt (Invitrogen) and cloned via AscI and EcoRI into vector pCambia0390 carrying the *nopaline synthase promoter:bialaphos* resistance gene. The vector was transformed via *Agrobacterium tumefaciens* (GV3101) to Col-0 and to Dex-inducible *AIH* downregulation plants (T2s).So far we identified five plants surviving BASTA selection, but none of them showed a Clover signal.

We designed the following constructs: *AIH(CDS);AIH^{mut}* which contains the CDS of *AIH* and the following mutations: D94A, H224A, D226A; *nlsRFP-T-(Gly)$_5$Ala-AIH*; *RFP-T--(Gly)$_5$Ala –AIH*; *H1.1^{R79K}RFP*; *H1.1^{R79A}RFP*; *H1.2-RFP*; *H1.2^{R79K}RFP* and *H1.2^{R79A}RFP*. The constructs were synthesize by Genescript with flanking attL sites to directly transform them into our Dex-inducible system (Ian Moore, Oxford). Further were the constructs *H1.2-RFP*, *H1.2^{R79K}RFP* and *H1.2^{R79A}RFP* directly cloned via Gateway cloning into pJS20 (*pRPS5a::LhGR2-GUS::pOP6*) by Invitrogen. All gene synthesize products were tested by restriction digest for correctness and used to produce glycerol stocks in DH5alpha. *H1.2-RFP*, *H1.2^{R79K}RFP* and *H1.2^{R79A}RFP* were verified via sequencing. The other constructs were partly re-sequenced.

Identification of putative targets sites of citrullination

We aligned the sequence of H1s between *A. thaliana* and mouse to identify putative amino acid targets of citrullination (Wisniewski et al. 2007).

Dexamethasone induction and imaging

We analyzed 3 independent lines of Dex-inducible *H1.1^{wt}*, 2 independent lines of Dex-inducible *H1.1^{R57K}RFP*, 3 independent lines of Dex-inducible *H1.1^{R57A}RFP* and 3 independent lines of Dex-inducible amiRNA against *AIH*.

Single inflorescences induced with 10 µM Dex solution (0.01% EtOH) or Mock (0.01% EtOH) were dissected after 4 to 5 days post induction (dpi). Single carpels or whole anthers were dissected in fresh Renaissance staining solution (final concentrations: 4% paraformaldehyde;1:2000 Renaissance;10% glycerol; 0,05% DMSO in 1x PBS and imaged. Recipe modified from (Musielak et al. 2015).

Serial images of fluorescent signals in whole-mount ovule primordia or PMCs were recorded by confocal laser-scanning microscopy with a Leica SP5-R (Leica Microsystems) using a 63× GLY lens (glycerol immersion, NA 1.4). Fluorescence signals of Renaissance, GFP and ECFP were acquired sequentially. Statistical test: fisher exact test.

Fixation Clearing, DMR

Single inflorescences induced with 10 µM Dex solution (0.01% EtOH) or Mock (0.01% EtOH) were fixed 4 to 5 dpi in (Acetic Acid:EtOH 3:1and stored o/N at 4°C). Afterward they were transferred in 70% EtOH and finally mounted in clearing solution (chloral hydrate: water: glycerol 8:2:1 by weight) and imaged at DMR (Leica) microscope with 20x or 40x dry objective (NA 0.75 and 0.5). Statistical test chi-square-test.

***β*-Glucuronidase (GUS) reporter assay**

Single inflorescences induced with 10 µM Dex solution (0.01% EtOH) or Mock (0.01% EtOH) were dissected after 2 days post induction (dpi). Single carpels were slightly cut open and submerged in x-Glu solution (Triton X-100 10%, EDTA 10 mM, Ferrocyanide 2 mM, Ferricyanide 2 mM, Na2HP04 100 mM, NaH2P04 100 mM, x-Glu 4 mM.), vacuum infiltrated for 5 min followed by a 2 hour incubation at 37°C, washed with phosphate buffer and mounted in 80% glycerol. Imaged at the DMR (Leica) microscope with 20x or 40x dry objective.

Modeling of protein structure

Superimposition of 1VKP for at5g08170 and 2DEW for Padi4 in coot and visualized in PyMOL.

Fertility Measurements

T2 plants were watered ~ 4 weeks with either 10 µM Dex or Mock starting before bolting, shortly after transferring the seedlings to soil. The 6^{th}, 7^{th} and 8^{th} silique were analyzed per plant. Three plants per line and treatment were analyzed. Line JS184, JS183, JS170: *amiRNA[AIH]*. Line JS175: $H1.1^{wt}RFPt$. Line: JS171, JS173: $H1.1^{R57K}RFP$. Plants were selected on BASTA plates for positive transformants. Plants treated with Dex were analyzed at the microscope for positive induction signals as described in chapter 3.

FRAP

Measurements were done on root tips of two weeks old seedlings grown as described above. One sample was prepared at a time: the root was excised and delicately mounted (ie without squashing) in 0.5x MS between slide and coverslip (precleaned with EtOH), sealed with transparent nail polish and let 10min equilibrate upside down on the microscope platform before measurements. The imaging chamber was set at a constant temperature of 20°C (higher/fluctuating temperatures induce nuclei juggling). Bleaching and imaging were done using an APO PL 40x oil immersion objective, NA 1.3, over a single plane. Bleaching was performed in

euchromatin within ROI of 1 µm diameter using 3-5 pulses until near total bleach was obtained (488nm 80% laser, 100% transmission) and post-bleach images were recorded 10 times with 1 sec interval then 10 times with 60 sec interval with a 7% transmission. For analyzing fluorescence recovery, images were first corrected for nuclear drifts occurring during acquisition, using a rigid registration approach in Fiji (Schindelin et al. 2012). When a single image captured several nuclei, registration did not always perform well for all, hence single nuclei were cropped for registration and analysis. Fluorescence measurements were done on the bleach ROI, a control ROI near and outside the nucleus, and over the whole nucleus. Calculation of fluorescence recovery was done as described by Rosa and colleagues (Rosa et al. 2014) whereby the initial intensity was normalized at 1 for each image before average calculation. Curve fitting was done in Matlab using the set of normalized data using a two-component fit.

Toxicological test with TDFA and Cl-amidine

Single inflorescences were treated with 1 µM TDFA (DMSO)or 1 µM Cl-amidine (DMSO) or just Mock (0.09% DMSO) were dissected after 5 days post induction (dpi). Single carpels were dissected in fresh Renaissance staining solution (final concentrations: 4% paraformaldehyde;1:2000 Renaissance;10% glycerol; 0,05% DMSO in 1x PBS and imaged. The Recipe is modified from (Musielak et al. 2015).

Reanalysis of published expression data

For the reanalysis of published RNA-Seq and Microarray expression data, we used a tool, for which the R-script can be found at https://github.com/VimalRawat1010/Rscripts/blob/master/LabData/.RData. The analysis includes data from(Borges et al. 2008; Honys and Twell 2004; Pina and Pinto 2005; Schmidt et al. 2011; Wuest et al. 2010). The tool considers for the dendrograms and the coloring the shape and gene expression values.

Acknowledgment

We thank Ian Moore (Oxford, UK) and Joop Vermeer (UZH, Zürich) for providing plasmids; Hugh Dickson (Oxford, UK), Marta Mendez (University of Milano, Italy) and Daphné Autran (Université de Montpellier, France) for technical support; Valeria Gagliardini for droplet PCR.

Author contributions

The experiments were designed by J.S., K.R. and C.B., and carried out by J.S., K.R., D.P. and C.B.. K.Z. contributed new computational analysis. J.S. wrote the manuscript.

Competing interest statement

The authors declare no competing financial interests.

References

Bednar, Jan et al. 2017. “Structure and Dynamics of a 197 Bp Nucleosome in Complex with Linker Histone H1.” *Molecular Cell* 66(3): 384–397.e8.

Borges, F. et al. 2008. “Comparative Transcriptomics of Arabidopsis Sperm Cells.” *Plant Physiology* 148(2): 1168–81.

Christophorou, Maria A. et al. 2014. “Citrullination Regulates Pluripotency and Histone H1 Binding to Chromatin.” *Nature* 507(7490): 104–8.

Cuthbert, Graeme L. et al. 2004. “Histone Deimination Antagonizes Arginine Methylation.” *Cell* 118(5): 545–53.

Fuhrmann, Jakob, and Paul R. Thompson. 2016. “Protein Arginine Methylation and Citrullination in Epigenetic Regulation.” *ACS Chemical Biology* 11(3): 654–68.

Hajkova, Petra et al. 2008. “Chromatin Dynamics during Epigenetic Reprogramming in the Mouse Germ Line.” *Nature* 452(7189): 877–81.

Honys, David, and David Twell. 2004. “Transcriptome Analysis of Haploid Male Gametophyte Development in Arabidopsis.” *Gene Biology* 5(11): R85.1-R85.13.

Janowitz, Tim, Helmut Kneifel, and Markus Piotrowski. 2003. “Identification and Characterization of Plant Agmatine Iminohydrolase, the Last Missing Link in Polyamine Biosynthesis of Plants.” *FEBS Letters* 544(1–3): 258–61.

Kotliński, Maciej et al. 2016. “Histone H1 Variants in Arabidopsis Are Subject to Numerous Post-Translational Modifications, Both Conserved and Previously Unknown in Histones, Suggesting Complex Functions of H1 in Plants.” *PLoS ONE* 11(1): 1–19.

Kouzarides, Tony. 2007. “Chromatin Modifications and Their Function.” *Cell* 128(4): 693–705.

Musielak, Thomas J. et al. 2015. “A Simple and Versatile Cell Wall Staining Protocol to Study Plant Reproduction.” *Plant Reproduction* 28(3–4): 161–69.

Pillot, M. et al. 2010. “Embryo and Endosperm Inherit Distinct Chromatin and Transcriptional States from the Female Gametes in Arabidopsis.” *The Plant Cell* 22(2): 307–20.

Pina, Cristina, and Francisco Pinto. 2005. “Gene Family Analysis of the Arabidopsis Pollen Transcriptome Reveals Biological Implications for Cell Growth , Division Control , and Gene Expression Regulation” *Plant Physiology* 138(June): 744–56.

Pinon, Violaine, Xiaozhen Yao, Aiwu Dong, and Wen-Hui Shen. 2017. “SDG2-Mediated H3K4me3 Is Crucial for Chromatin Condensation and Mitotic Division during Male Gametogenesis in Arabidopsis.” *Plant Physiology* 174(2): 1205–15.

Rosa, Stefanie et al. 2014. “Cell Differentiation and Development in *Arabidopsis* Are Associated with Changes in Histone Dynamics at the Single-Cell Level.” *The Plant Cell Online* 26(12): 4821–33.

Schindelin, Johannes et al. 2012. “Fiji: An Open Source Platform for Biological Image Analysis.” *Nature Methods* 9(7): 676–82.

Schmidt, Anja, Wuest, Samuel, Vijverberg, Kitty, Baroux. Celia, Kleen, Daniela, and Ueli Grossniklaus. 2011. “Transcriptome Analysis of the Arabidopsis Megaspore Mother Cell Uncovers the Importance of RNA Helicases for Plant Germline Development.” *PLoS biology* 9(9).

Schwab, Rebecca, Stephan Ossowski, and Norman Warthmann. 2010. “Plant MicroRNAs” eds. Blake C. Meyers and Pamela J. Green. 592: 71–88.

Shaner, Nathan et al. 2008. “Improvng the Photostability of Bright Monomeric Orange and Red Fluorescent Proteins.” *Nature Methods* 5(6): 545–51.

She, Wenjing et al. 2013. “Chromatin Reprogramming during the Somatic-to-Reproductive Cell Fate Transition in Plants.” *Development (Cambridge, England)* 140(19): 4008–19.

Sobieszczuk-Nowicka, E. 2017. “Polyamine Catabolism Adds Fuel to Leaf Senescence.” *Amino Acids* 49(1): 49–56.

Tucker, Matthew R. et al. 2012. “Somatic Small RNA Pathways Promote the Mitotic Events of Megagametogenesis during Female Reproductive Development in Arabidopsis.” *Development (Cambridge, England)* 139(8): 1399–1404.

Villar-Garea, Ana, and Axel Imhof. 2008. “Fine Mapping of Posttranslational Modifications of the Linker Histone H1 from Drosophila Melanogaster.” *PLoS ONE* 3(2).

Wisniewski, Jacek R., Alexandre Zougman, Sonja Krüger, and Matthias Mann. 2007. “Mass Spectrometric Mapping of Linker Histone H1 Variants Reveals Multiple Acetylations, Methylations, and Phosphorylation as Well as Differences between Cell Culture and Tissue.” *Molecular & cellular proteomics : MCP* 6(1): 72–87.

Witalison, Erin E., Paul R. Thompson, and Lorne J. Hofseth. 2015. “Protein Arginine Deiminases and Associated Citrullination: Physiological Functions and Diseases Associated with Dysregulation.” *Curr Drug Targets* 16(7): 700–710.

Wuest, Samuel E. et al. 2010. “Arabidopsis Female Gametophyte Gene Expression Map Reveals Similarities between Plant and Animal Gametes.” *Current Biology* 20(6): 506–12.

Zhang, Xiaoqian et al. 2016. “Peptidylarginine Deiminase 1-Catalyzed Histone Citrullination Is Essential for Early Embryo Development.” *Scientific Reports* 6(1): 38727.

Zhao, Xin’Ai et al. 2017. “RETINOBLASTOMA RELATED1 Mediates Germline Entry in Arabidopsis.” *Science* 356(6336).

Supplement Chapter 6:

Fisher exact test	**genotype**	***p-value***
JS188#5 vs. JS147#1	*H1.1^{R57A}RFP vs. H1.1^{R57K}RFP*	0.000
JS188#5 vs. JS149#4	*H1.1^{R57A}RFP vs. H1.1^{R57K}RFP*	0.001
JS188#17 vs. JS147#1	*H1.1^{R57A}RFP vs. H1.1^{R57K}RFP*	0.016
JS188#17 vs. JS149#4	*H1.1^{R57A}RFP vs. H1.1^{R57K}RFP*	0.031
JS188#25 vs. JS147#1	*H1.1^{R57A}RFP vs. H1.1^{R57K}RFP*	0.021
JS188#25 vs. JS149#4	*H1.1^{R57A}RFP vs. H1.1^{R57K}RFP*	0.040
JS175 vs. JS147#1	*H1.1^{wt}RFP vs. H1.1^{R57}KRFP*	0.049
JS175 vs. JS149#4	*H1.1^{wt}RFP vs. H1.1^{R57K}RFP*	0.109
JS198 vs. JS147#1	*H1.1^{wt}RFP vs. H1.1^{R57K}RFP*	0.043
JS198 vs. JS149#4	*H1.1^{wt}RFP vs. H1.1^{R57K}RFP*	0.092
JS196 vs. JS147#1	*H1.1^{wt}RFP vs. H1.1^{R57K}RFP*	0.049
JS196 vs. JS149#4	*H1.1^{wt}RFP vs. H1.1^{R57K}RFP*	0.784

Supplement table 1: Fisher exact test scoring the difference between RFP signal presence and absence in induced ovules expressing different *H1.1* variants

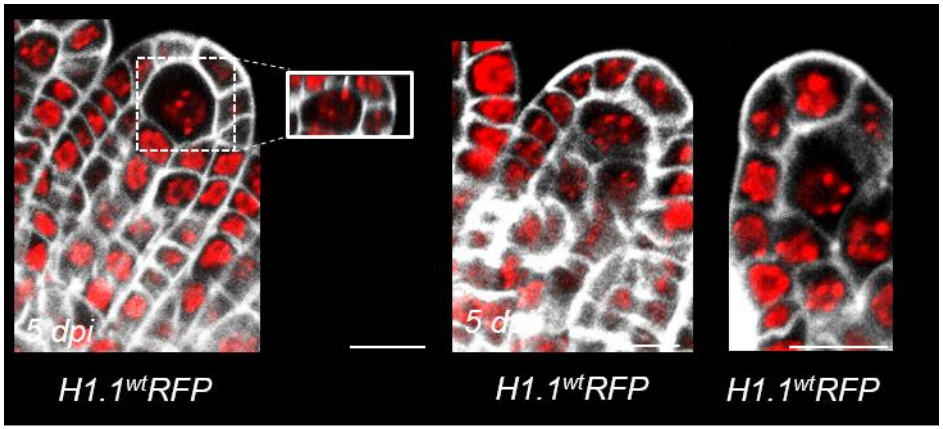

Supplement Figure 1: Example for residual signal in H1.1^{wt}RFP 5 dpi 10 µM Dex. Example for residual RFP signal in ovules 5 dpi with 10 µM Dex expressing *H1.1^{wt}RFP* (line S175#9). Grey = Renaissance counter stain, red = RFP, scale bar = 10 µm

RNASeq																
Gene Name	**Gene**	**EmbryoGob**	**Embryo2_4**	**Meio_M**	**CC1**	**CC2**	**EmbrTor**	**EndoTor**	**Seedling**	**Root**	**Flower**	**PollenM**	**Inorescence**	**EggCell**	**Synergids**	**Bud**
AIH	*AT5G08170*	59.65	5.82	47.31	48.37	29.68	123.73	479.49	45.83	93.39	120.89	6.29	66.16	27.81	9.48	87.76
CUL3B	*AT1G69670*	5.12	4.63	7.27	0.3	2.84	14.87	12.66	10.12	25.51	6.86	2.51	14.48	8.91	6.41	25.83

Microarray																				
Gene Name	**Gene**	**Ovule Wt**	**Egg**	**Cen**	**Syn**	**MMC**	**seedling_pina**	**pollen_unicellular_honys_uc**	**pollen_bicellular_honys_bc**	**pollen_tricellular_honys_tc**	**pollen_mature_borges**	**globularEmbryo**	**pre_globularEmbryo**	**heartEmbryo**	**inflorescence_infloresceneAfterBolting_Col_0**	**flowers_floralStage10_Col_0**	**flowers_floralStage1011_Col_0**	**flowers_floralStage13_Col_0**	**carpels_floralStage12_Col_0**	**flowers_floralStage16_Col_0**	**carpels_floralStage15_Col_0**
AIH	*AT5G08170*	6.56	4.93	5.87	4.56	5.65	6.09	5.97	6.08	6.1	5.6	8.12	7.96	8.03	5.92	5.87	5.56	5.3	5.67	5.38	5.67
CUL3B	*AT1G69670*	8.37	7.09	7.57	7.75	8.09	7.51	8.43	8.57	8.9	8.23	7.06	7.05	7.45	8.2	8.3	8.12	8.15	8.19	8.37	8.28

Supplement Table 2: Normalized expression value of *AIH* and *CUL3B* from RNASeq and Microarray data. The table shows normalized expression values of *AIH* and *CUL3B* of RNASeq data from Wuest and colleagues (Wuest et al. 2010) and (B) Microarray data from Schmidt, Borges, Pina and Honys (Borges et al. 2008; Honys and Twell 2004; Pina and Pinto 2005; Schmidt et al. 2011). The script used for analyzing the RNAseq and Microarray data can be found at "https://github.com/VimalRawat1010/Rscripts/blob/master/LabData/.RData".

JS184#1 Mock	A	B	C	n-total per plant	in %	average % per line
Healthy	34	37	38	109	88.6	86.2
Aborted	4	1	4	9	7.3	
Infertil	1	2	2	5	4.1	
total-n per silique	**39**	**40**	**44**	**123**	**100**	
JS184#2 Mock	A	B	C			
Healthy	24	27	38	89	75.4	
Aborted	7	10	0	17	14.4	
Infertil	6	6	0	12	10.2	
total-n per silique	**37**	**43**	**38**	**118**	**100**	
JS184#3 Mock	A	B	C			
Healthy	50	40	33	123	94.6	
Aborted	0	1	1	2	1.5	
Infertil	0	2	3	5	3.8	
total-n per silique	**50**	**43**	**37**	**130**	**100**	

JS184#1 Dex	A	B	C	n-total per plant	in %	average % per line
Healthy	49	39	43	131	93.6	92.1
Aborted	0	0	0	0	0.0	
Infertil	3	4	2	9	6.4	
total-n per silique	**52**	**43**	**45**	**140**	**100.0**	
JS184#2 Dex	A	B	C			
Healthy	46	49	47	142	97.9	
Aborted	0	0	0	0	0.0	
Infertil	2	1	0	3	2.1	
total-n per silique	**48**	**50**	**47**	**145**	**100.0**	
JS184#3 Dex	A	B	C			
Healthy	41	35	41	117	84.8	
Aborted	8	5	1	14	10.1	
Infertil	2	2	3	7	5.1	
total-n per silique	**51**	**42**	**45**	**138**	**100.0**	

LS183#1 Mock	A	B	C	n-total per plant	in %	average % per line
Healthy	34	41	37	112	75.7	74.7
Aborted	13	12	11	36	24.3	
Infertil	0	0	0	0	0.0	
total-n per silique	**47**	**53**	**48**	**148**	**100.0**	
JS183#2 Mock	A	B	C			
Healthy	27	3	32	62	68.9	
Aborted	8	1	9	18	20.0	
Infertil	5	4	1	10	11.1	
total-n per silique	**40**	**8**	**42**	**90**	**100.0**	
JS183#3 Mock	A	B	C			
Healthy	32	37	35	104	79.4	
Aborted	8	2	5	15	11.5	
Infertil	1	3	8	12	9.2	
total-n per silique	**41**	**42**	**48**	**131**	**100.0**	

JS183#1 Dex	A	B	C	n-total per plant	in %	average % per line
Healthy	46	36	39	121	82.3	77.4
Aborted	3	2	1	6	4.1	
Infertil	8	4	8	20	13.6	
total-n per silique	**57**	**42**	**48**	**147**	**100.0**	
JS183#2 Dex	A	B	C			
Healthy	30	29	36	95	77.2	
Aborted	8	4	0	12	9.8	
Infertil	4	6	6	16	13.0	
total-n per silique	**42**	**39**	**42**	**123**	**100.0**	
JS183#3 Dex	A	B	C			
Healthy	32	31	28	91	72.8	
Aborted	6	0	14	20	16.0	
Infertil	8	6	0	14	11.2	
total-n per silique	**46**	**37**	**42**	**125**	**100.0**	

JS170#1 Mock	A	B	C	n-total per plant	in %	average % per line
Healthy	46	43	48	137	97.9	99.3
Aborted	1	2	0	3	2.1	
Infertil	0	0	0	0	0.0	
total-n per silique	**47**	**45**	**48**	**140**	**100.0**	
JS170#2 Mock	A	B	C			
Healthy	43	41	45	129	100.0	
Aborted	0	0	0	0	0.0	
Infertil	0	0	0	0	0.0	
total-n per silique	**43**	**41**	**45**	**129**	**100.0**	
JS170#3	A	B	C			
Healthy	52	49	53	154	100.0	
Aborted	0	0	0	0	0.0	
Infertil	0	0	0	0	0.0	
total-n per silique	**52**	**49**	**53**	**154**	**100.0**	

JS170#1 Dex	A	B	C	n-total per plant	in %	average % per line
Healthy	40	42	47	129	98.5	96.4
Aborted	0	0	0	0	0.0	
Infertil	0	1	1	2	1.5	
total-n per silique	**40**	**43**	**48**	**131**	**100.0**	
JS170#2 Dex	A	B	C			
Healthy	44	43	40	127	96.9	
Aborted	0	0	1	1	0.8	
Infertil	2	0	1	3	2.3	
total-n per silique	**46**	**43**	**42**	**131**	**100.0**	
JS170#3 Dex	A	B	C			
Healthy	46	48	42	136	93.8	
Aborted	1	0	0	1	0.7	
Infertil	2	2	4	8	5.5	
total-n per silique	**49**	**50**	**46**	**145**	**100.0**	

JS175#1 Mock	A	B	C	n-total per plant	in %	average % per line
Healthy	48	40	45	133	108.1	121.0
Aborted	0	0	0	0	0.0	
Infertil	1	1	0	2	1.6	
total-n per silique	**49**	**41**	**45**	**135**	**109.8**	
JS175#2 Mock	A	B	C			
Healthy	45	60	56	161	136.4	
Aborted	0	3	0	3	2.5	
Infertil	2	0	0	2	1.7	
total-n per silique	**47**	**63**	**56**	**166**	**140.7**	
JS175#3 Mock	A	B	C			
Healthy	51	60	43	154	118.5	
Aborted	3	0	2	5	3.8	
Infertil	1	0	0	1	0.8	
total-n per silique	**55**	**60**	**45**	**160**	**123.1**	

Js175#2 Dex	A	B	C	n-total per plant	in %	average % per line
Healthy	25	34	29	88	62.9	56.9
Aborted	0	0	0	0	0.0	
Infertil	6	12	6	24	17.1	
total-n per silique	**31**	**46**	**35**	**112**	**80.0**	
JS175#1 Dex	A	B	C			
Healthy	19	25	22	66	45.5	
Aborted	0	0	0	0	0.0	
Infertil	21	13	13	47	32.4	
total-n per silique	**40**	**38**	**35**	**113**	**77.9**	
JS175#3 Dex	A	B	C			
Healthy	23	37	26	86	62.3	
Aborted	0	0	0	0	0.0	
Infertil	15	6	14	35	25.4	
total-n per silique	**38**	**43**	**40**	**121**	**87.7**	

JS173#1 Mock	A	B	C	n-total per plant	in %	average % per line
Healthy	22	21	37	80	65.0	66.8
Aborted	0	0	0	0	0.0	
Infertil	0	0	0	0	0.0	
total-n per silique	**22**	**21**	**37**	**80**	**65.0**	
JS173#2 Mock	A	B	C			
Healthy	25	29	25	79	66.9	
Aborted	0	0	0	0	0.0	
Infertil	0	0	0	0	0.0	
total-n per silique	**25**	**29**	**25**	**79**	**66.9**	
JS173#3 Mock	A	B	C			
Healthy	25	35	29	89	68.5	
Aborted	0	0	0	0	0.0	
Infertil	0	1	0	1	0.8	
total-n per silique	**25**	**36**	**29**	**90**	**69.2**	

JS173#2 Dex	A	B	C	n-total per plant	in %	average % per line
Healthy	47	41	49	137	97.9	58.6
Aborted	0	0	0	0	0.0	
Infertil	0	1	0	1	0.7	
total-n per silique	**47**	**42**	**49**	**138**	**98.6**	
JS173#1 Dex	A	B	C			
Healthy	38	nichts	nichts	38	27.1	
Aborted	0	nichts	nichts	0	0.0	
Infertil	8	nichts	nichts	8	5.7	
total-n per silique	**46**	**0**	**0**	**46**	**32.9**	
JS173#3 Dex	A	B	C			
Healthy	21	25	25	71	50.7	
Aborted	0	0	0	0	0.0	
Infertil	18	16	23	57	40.7	
total-n per silique	**39**	**41**	**48**	**128**	**91.4**	

JS171#4 Mock	A	B	C	n-total per plant	in %	average % per line
Healthy	45	54	47	146	95.4	95.9
Aborted	2	4	0	6	3.9	
Infertil	0	0	1	1	0.7	
total-n per silique	**47**	**58**	**48**	**153**	100.0	
JS171#6 Mock	A	B	C			
Healthy	58	47	55	160	95.2	
Aborted	1	6	1	8	4.8	
Infertil	0	0	0	0	0.0	
total-n per silique	**59**	**53**	**56**	**168**	100.0	
JS171#5 Mock	A	B	C			
Healthy	41	44	47	132	97.1	
Aborted	0	1	0	1	0.7	
Infertil	2	1	0	3	2.2	
total-n per silique	**43**	**46**	**47**	**136**	100.0	

JS171#2 Dex	A	B	C	n-total per plant	in %	average % per line
Healthy	12	0	20	32	23.7	65.0
Aborted	0	0	0	0	0.0	
Infertil	28	35	40	103	76.3	
total-n per silique	**40**	**35**	**60**	**135**	100.0	
JS171#3 Dex	A	B	C	0		
Healthy	62	13	57	132	77.2	
Aborted	0	0	0	0	0.0	
Infertil	0	35	4	39	22.8	
total-n per silique	**62**	**48**	**61**	**171**	100.0	
JS171#1 Dex	A	B	C	0		
Healthy	60	43	55	158	94.0	
Aborted	0	6	0	6	3.6	
Infertil	3	1	0	4	2.4	
total-n per silique	**63**	**50**	**55**	**168**	100.0	

Supplement Table 3: Seed Set measurement after 4 weeks of 10 µM Dex- or Mock-watering. T2 plants were watered ~4 weeks with either 10 µM Dex or Mock (0.01% EtOH) starting before bolting, shortly after transferring the seedlings to the soil. The 6th, 7th and 8th silique were analyzed per plant. Three plants per line and treatment were analyzed. Line JS184, JS183, JS170: *amiRNA[AIH]*. Line JS175: *H1.1^{wt}RFP*. Line: JS171, JS173: *H1.1^{R57K}RFP*. Plants were selected on BASTA plates for positive transformants. Plants treated with Dex were analyzed at the microscope for positive induction signals (as described in chapter 3). No difference in the seed set was found in the *amiRNA[AIH]* line (+/-3%;+6%) treated with Dex compared with Mock treatment. In the *H1.1^{wt}RFP* line a reduction of 27.9% normal seed set was found under Dex-treatment compared to Mock-treatment. In the *H1.1^{R57K}RFP* line a reduction of 40.2% in line JS173 and 30.9% in line JS171 was found under Dex-treatment compared to Mock.

Supplement Figure 2: Seed Set measurement in induced *AIH* downregulation lines after 4 weeks of 10 µM Dex- or Mock-watering. (A) JS173 (*H1.1^{R57K}RFP*) watered with 10 µM Dex for three weeks, exhibit phenotypes ranging from strongly affected plants to nearly not detectable phenotypes. In all induced plants we detected RFP signals (not shown in the image). (B) JS173 (*H1.1^{R57K}RFP*) watered with Mock (0.01% EtOH) for 3 weeks, exhibit no sterility phenotypes and also no RFP signals.

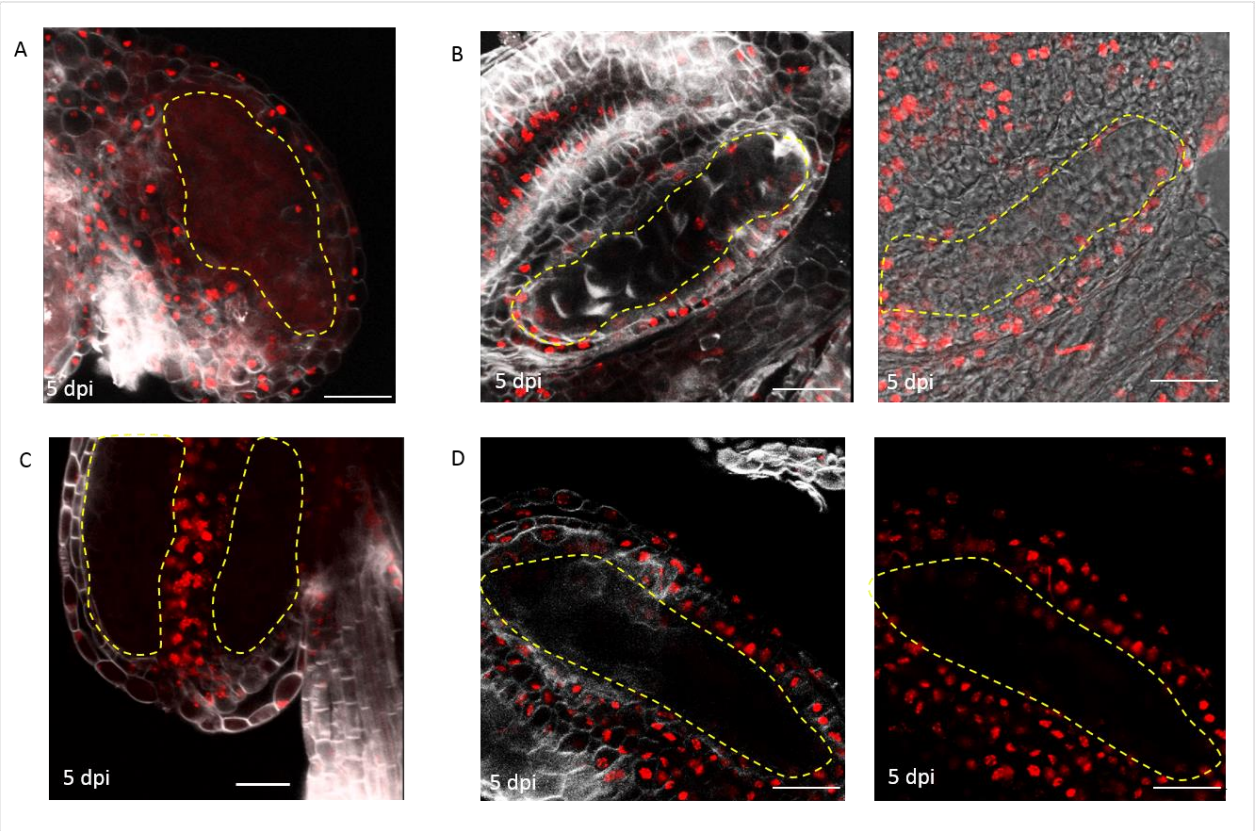

Supplement Figure 3: H1.1^{R57A}RFP and H1.1^{R57K}RFP are normally evicted in PMC (A) 5 dpi with 10 µM Dex we found no signals of RFP in PMC (Pollen Mother Cell) in *H1.1^{R57A}RFP* lines. (B to D) 5 dpi with 10 µM Dex we found no presence of RFP in PMC in *H1.1^{R57K}RFP*. Yellow dashed line indicates PMCs. Scale bar = 20 µm.

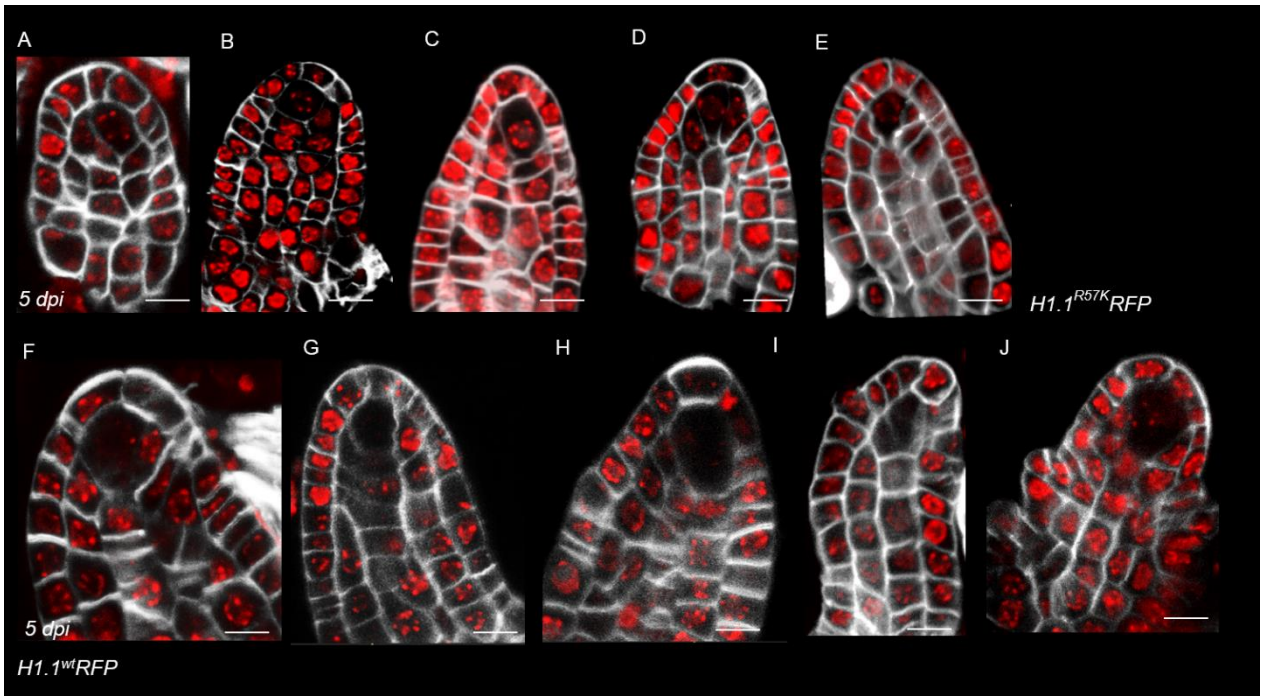

Supplement Figure 4: Eviction and reloading of Dex-inducible linker histone H1.1 variants in Megaspore Mother cell (MMC) development. (A) to (E) Confocal imaging of *H1.1^{R57K}RFP*. No eviction of H1.1 during MMC development. RFP fluorescence is shown in red and the Renaissance cell wall staining in white. 5 dpi with 10 µM Dex. (F to J) shows eviction of RFP signal in *H1.1^{wt}RFP* at stage 1-II and the absence of the signal persists until the stage 2-II / 2-III where *H1.1^{wt}RFP* is reloaded (J). Scale Bar = 10 µm. Developmental stages: 1-I (A), 1-II (B,F), 2-I (C,G), 2-II (D,H), 2-III (E,I), 2-III (J).

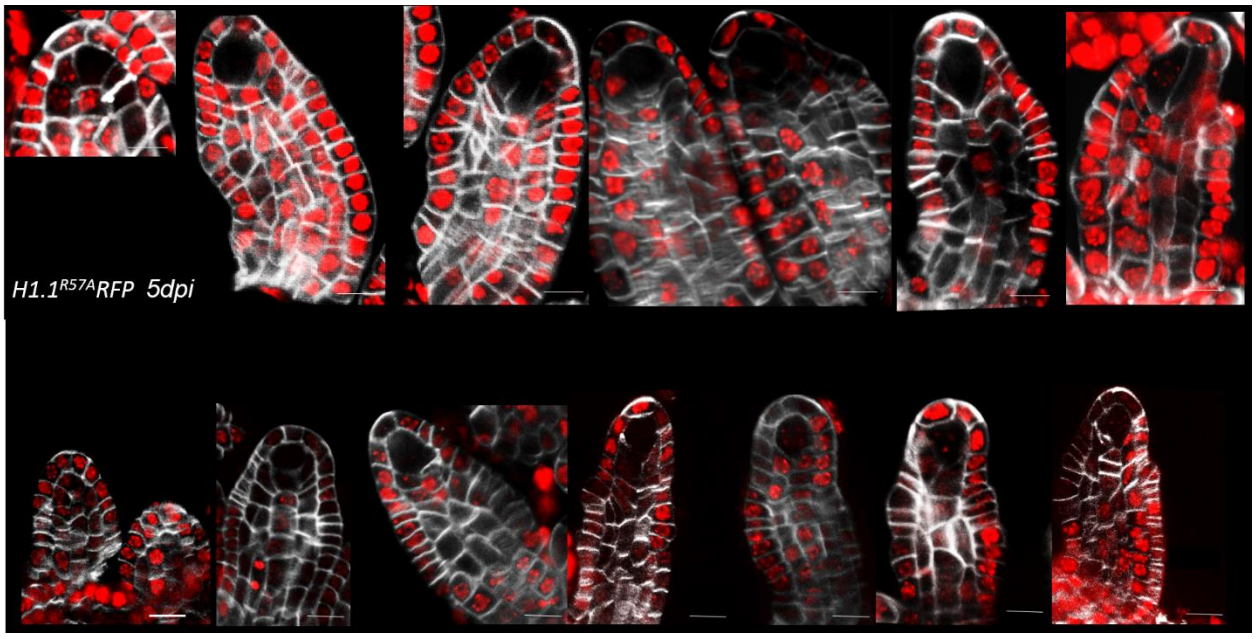

Supplement Figure 5: Expression of *H1.1^{R57A}RFP*. (A to M) 5 dpi 10 µM Dex. Eviction and reloading of H1.1 show patterns similar to the wild-type variant and as previously published (She et al. 2013). Scale bar = 10 µm. Grey = Renaissance counterstain.

amiRNA	**amiRNA target sequence 5'>3'**
amiRNA *AIH*	ACG**A**GAGCCGTTCATTAATTG

Supplement table 4: amiRNA target sequence and mismatch. Underlined and in bold is the mismatch of the amiRNA within the target sequence highlighted.

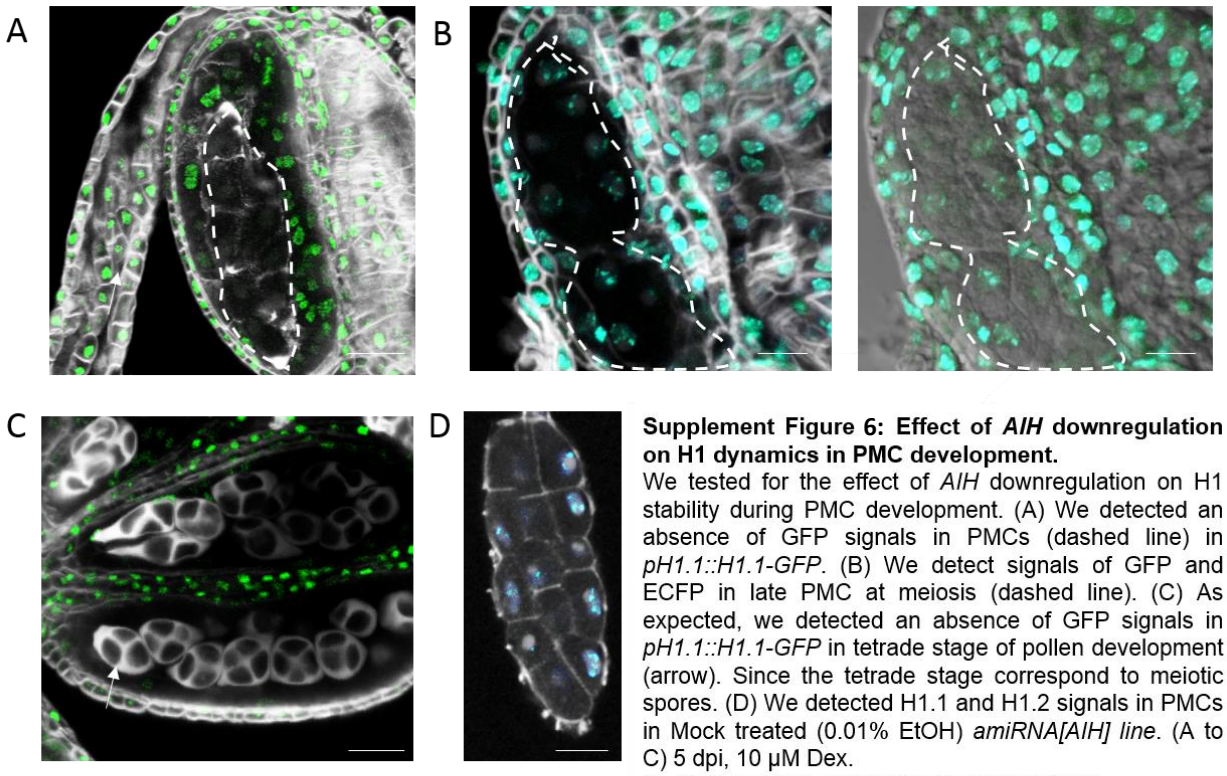

Supplement Figure 6: Effect of *AIH* downregulation on H1 dynamics in PMC development.
We tested for the effect of *AIH* downregulation on H1 stability during PMC development. (A) We detected an absence of GFP signals in PMCs (dashed line) in *pH1.1::H1.1-GFP*. (B) We detect signals of GFP and ECFP in late PMC at meiosis (dashed line). (C) As expected, we detected an absence of GFP signals in *pH1.1::H1.1-GFP* in tetrade stage of pollen development (arrow). Since the tetrade stage correspond to meiotic spores. (D) We detected H1.1 and H1.2 signals in PMCs in Mock treated (0.01% EtOH) *amiRNA[AIH] line*. (A to C) 5 dpi, 10 µM Dex.
(A, C) *pH1.1::H1.1-GFP* (*3h1*); *amiRNA[AIH]*.
(B) *pH1.1::H1.1-GFP*; blue = *pH1.2::H1.2-ECFP (3h1) amiRNA[AIH]*.
(A to D) Scale bar = 10 µm, grey = Renaissance counter stain, green = *pH1.1::H1.1-GFP*; blue = *pH1.2::H1.2-ECFP*.

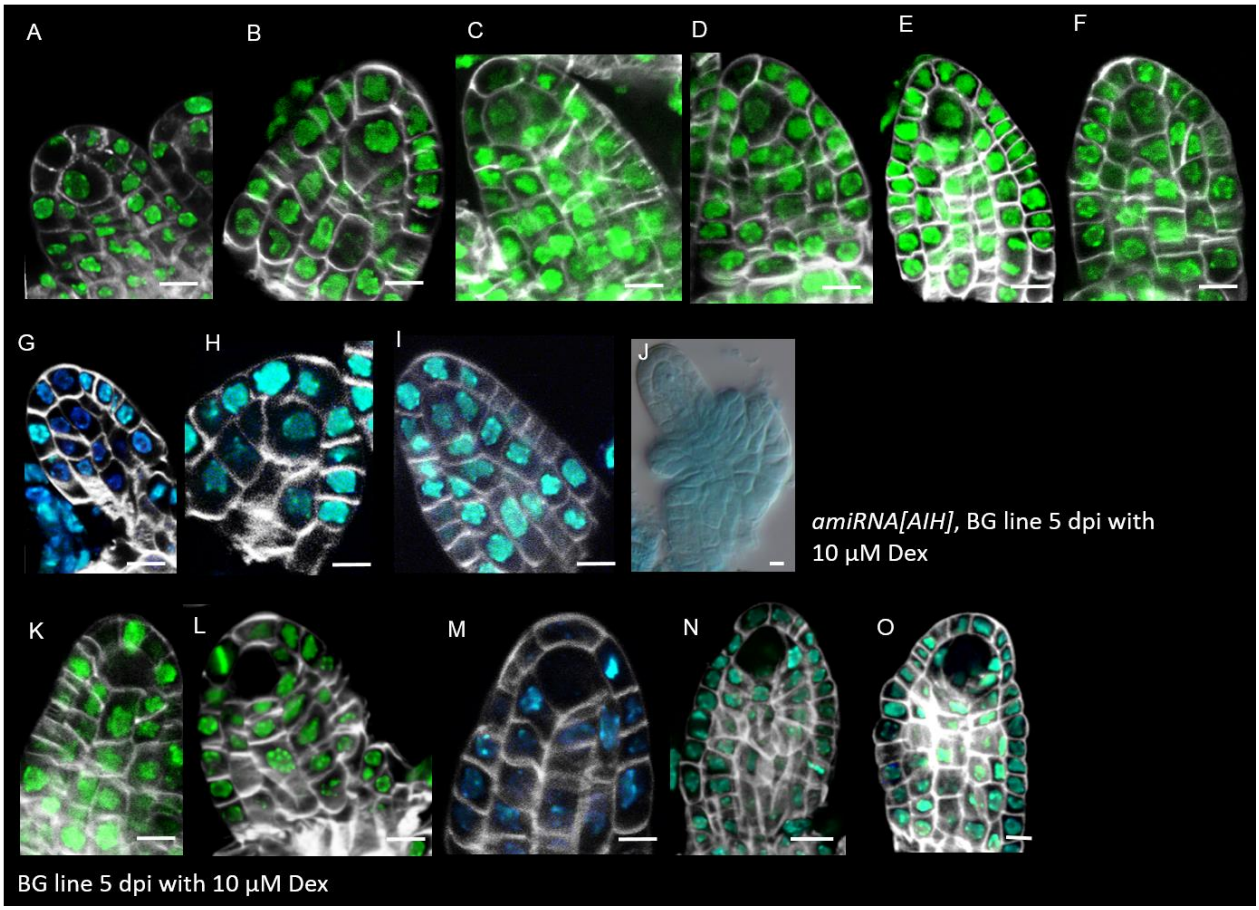

Supplement Figure 7: Effect of *AIH* downregulation on H1.1 and H1.2 dynamics. (A to O) green = *pH1.1.::H1.1-GFP*; blue = *pH1.2::H1.2-ECFP*; grey = Renaissance counterstain; 5 dpi with 10 µM Dex. Scale bar = 10 µm. In (A to I) No eviction of H1.1; in *amiRNA[AIH]*; (J) Histochemical staining of GUS in/of *amiRNA[AIH]*; (K to O) control background reporter line shows eviction of H1.1 and H1.2.

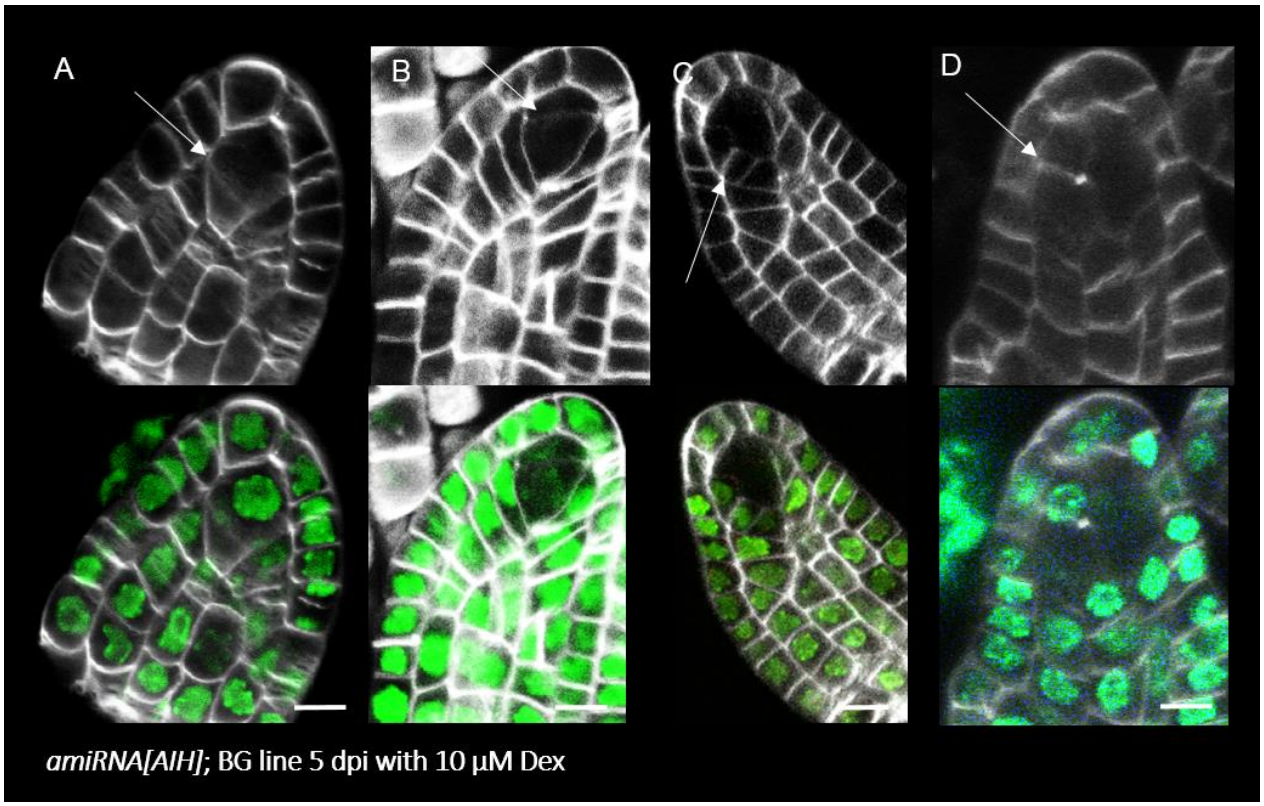

Supplement Figure 8: **Ectopic MMC development in *AIH* knockdown lines.** (A - D) Confocal imaging of *amiRNA[AIH]*; BG line. 5 dpi with 10 µM Dex. Grey = Renaissance counterstain, green = *pH1.1::H1.1-GFP*; blue = *pH1.2::H1.2-ECFP*. Scale Bar = 10 µm. The arrow points to (A and B) an additional division in the MMC and in (C and D) to an additional division in the companion cell.

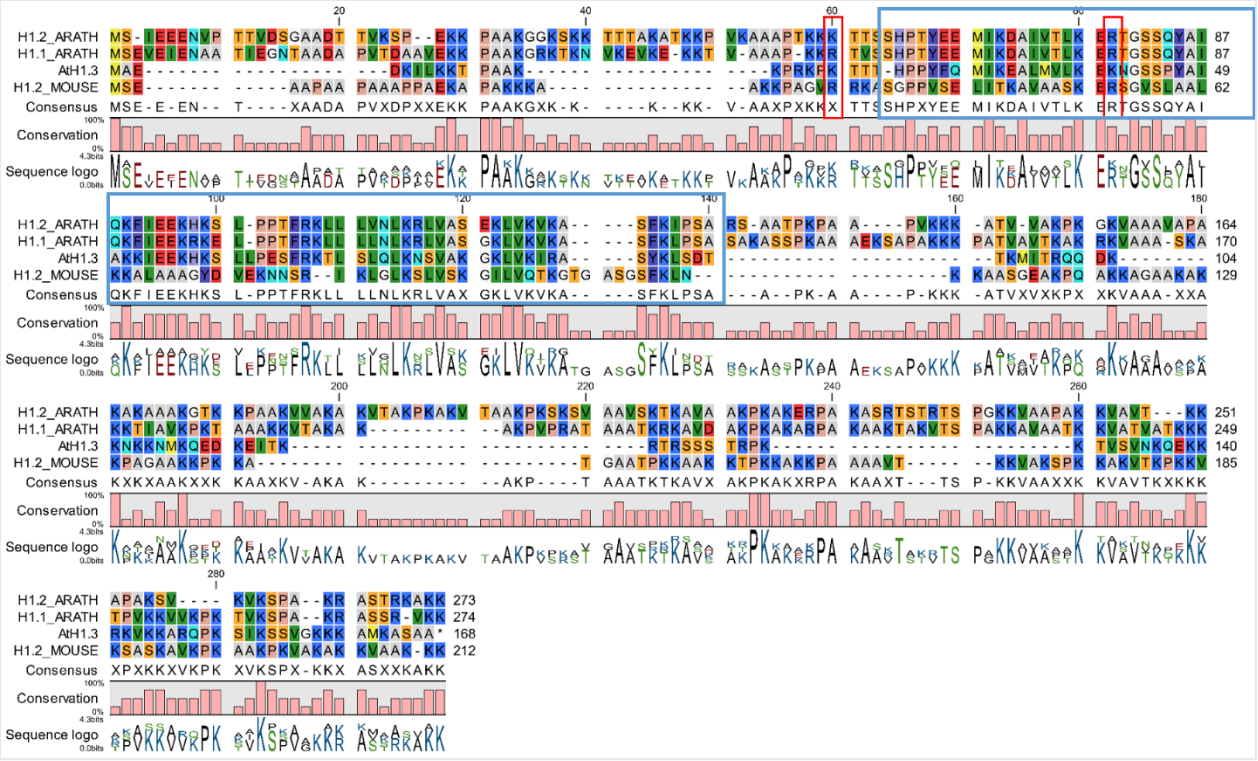

Supplement Figure 9: Protein sequence alignment of H1.1, H1.2, H1.3 of *A.thaliana* to H1.2 of *M.musculus.* Highlighted in red are the possible targets of citrullination/methylation of K32 and R54 in *M.musculus* and R57 and R79 in *A.thaliana*. Highlighted in blue is the globular domain of the H1s based on *A.thaliana* H1.1 and H1.2.

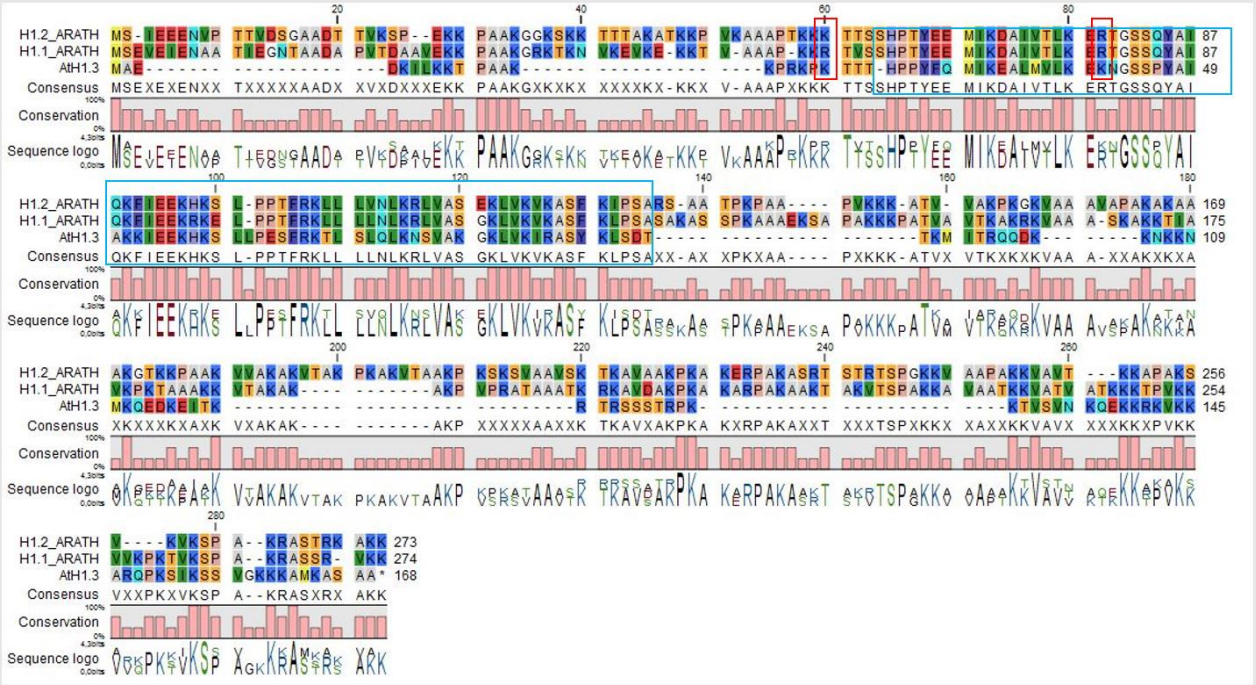

Supplement Figure 10: Protein sequence alignment of all three linker histones of *A.thaliana* (H1.1; H1.2; H1.3). Highlighted in red are the two possible citrullination/methylation targets. Highlighted in blue is the globular domain of the H1s.

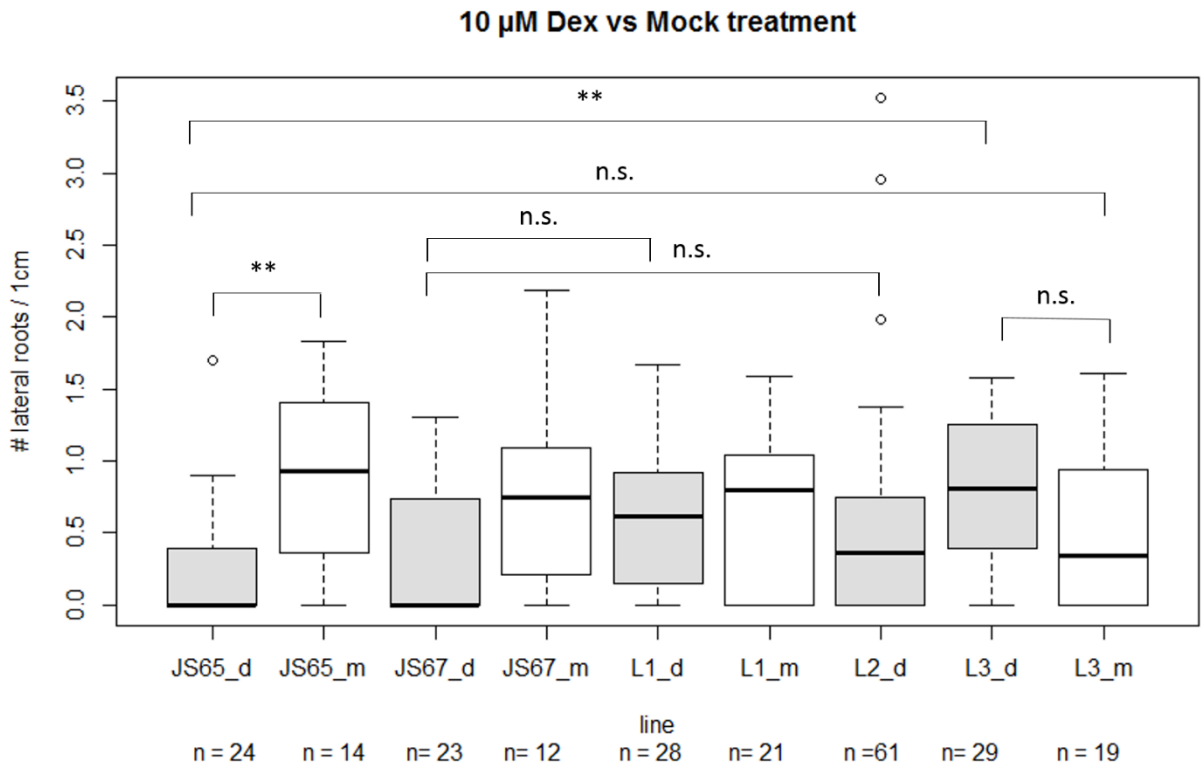

Supplement Figure 11: Number of lateral roots in inducible *AIH* knockdowns lines. (A) Number of lateral roots per 1 cm on 10 µM Dex and Mock (0.01% EtOH) plates. Background lines (JS65 and JS67, *pH1.1::H1.1-GFP*, *pH1.2::H1.2-ECFP*, *3h1*: BG line) compared to three independent insertion lines (T2s) of *amiRNA[AIH]* (L1: JS144#3; L2: JS144#4, L3: JS143#4). d = Dex; m = Mock; n= number of seedlings per line; n.s. = not significant; ** = $p > 0.01$ (two tailed t-test, with equal variance). Line L3 on induction of *amiRNA[AIH]* shows a significantly higher amount of lateral roots/root length to its parental line JS65 under Dex treatment. But we found no significant difference between the Dex-induced and not induced (Mock) treated L3 line on the number of lateral roots. In addition, we already found a significant difference of the number of lateral roots in the parental line JS65 (BG line), which suggest that the chemical Dex itself already has an influence in this line on the number of lateral roots. P-values: JS67 Dex vs. L2 Dex (p = 0.0656); JS65 Mock vs. L3 Mock (p = 0.2568); JS67 Dex vs. L2 Dex (p = 0.1258); JS65 Dex vs L3 Dex (p = 0.0003); JS65 Dex vs. JS65 Mock (p = 0.004); L3 Mock vs. L3 Dex (p = 0.1652). The rest we did not test for significance, since it is clear from the graphics that there is no significant difference.

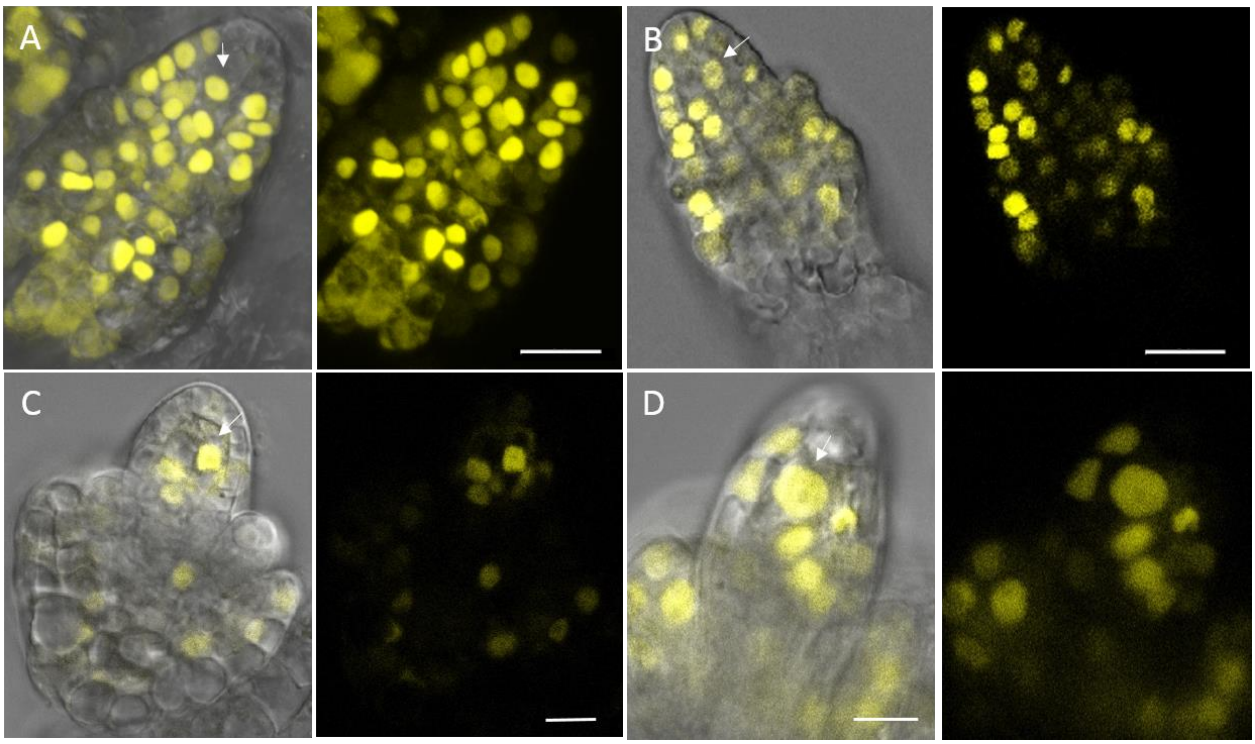

Supplement Figure 12: Induction control *pRPS5a>>nls3xmVenus* shows expression in the Megaspore Mother Cell and Functional Megaspore. 24 hpi with 10 µM Dex. Development stages (A) 1-II (B) 2-II (C and D) Functional Megaspore. (A and B) The arrow points to the Megaspore Mother Cell or (C and D) the Functional Megaspore. Scale Bar = 10 µm

References:

Borges, F. et al. 2008. "Comparative Transcriptomics of Arabidopsis Sperm Cells." *Plant Physiology* 148(2): 1168–81.

Honys, David, and David Twell. 2004. "Transcriptome Analysis of Haploid Male Gametophyte Development in Arabidopsis." *Gene Biology* 5(11): R85.1-R85.13.

Pina, Cristina, and Francisco Pinto. 2005. "Gene Family Analysis of the Arabidopsis Pollen Transcriptome Reveals Biological Implications for Cell Growth , Division Control , and." *Plant Physiology* 138(June): 744–56.

Schmidt, Anja, Wuest, Samuel, Vijverberg, Kitty, Baroux. Célia, Kleen, Daniela, and Ueli Grossniklaus. 2011. "Transcriptome Analysis of the Arabidopsis Megaspore Mother Cell Uncovers the Importance of RNA Helicases for Plant Germline Development." *PLoS biology* 9(9).

She, Wenjing et al. 2013. "Chromatin Reprogramming during the Somatic-to-Reproductive Cell Fate Transition in Plants." *Development (Cambridge, England)* 140(19): 4008–19.

Wuest, Samuel E. et al. 2010. "Arabidopsis Female Gametophyte Gene Expression Map Reveals Similarities between Plant and Animal Gametes." *Current Biology* 20(6): 506–12.

XI. Résumé

Plant sexual reproduction includes several cell fate transitions. Accumulating evidence showed that fate transitions are underlined by chromatin reprogramming (Autran et al. 2011; Baroux et al. 2007; Baroux, Raissig, and Grossniklaus 2011; Houben et al. 2011; Ingouff et al. 2010; Pillot et al. 2010). This reprogramming affects chromatin structure, changes in histone modifications and DNA methylation (Baroux et al. 2007; Ingouff et al. 2007, 2017; Jullien et al. 2012). One of the cell fate transition during plant sexual reproduction is the somatic-to-reproductive cell fate change during sporogenesis. Recently, She and colleagues showed that during this fate transition in male and female tissues of *Arabidopsis thaliana* a large-scale chromatin rearrangement is happening (She et al. 2013). During the development of the female Megaspore Mother Cell (MMC) chromatin rearrangement establishes an epigenetic and transcriptional state in the MMC that is distinct from that in the surrounding somatic tissue. These chromatin changes likely contribute to the acquisition of reproductive fate, rather than being only a precondition for meiosis. This was suggested with the observation that additional sub-epidermal enlarged cells reminiscent of aposporic initial cells of natural apomicts that are present in *ago9*, *sdg2* and *rdr6* mutants have similar histone modifications and histone variant dynamics (She et al. 2013, review in Schmidt et al. 2015). A similar process has been found to happen during the development of the germline lineage in mammals (Hajkova et al. 2008). Primordial germ cells (PGCs), which are the functional equivalent of plant Spore Mother Cells (SMCs), also undergo an extensive epigenetic reprogramming, which removes epigenetic barriers to achieve a ground-state of the epigenome necessary to establish pluripotency (Hackett, Zylicz, and Surani 2012; Hajkova et al. 2002, 2008). Recently, Hajkova and colleagues (Hill et al. 2018) could further provide evidence that the erasure of epigenetic information has a central function to ensure timely and efficient activation of certain genes to enabling progression towards gametogenesis. The hallmark in both, animals PGCs- and plants SMCs differentiation is the eviction of linker histones (Hajkova et al. 2008; She et al. 2013).

The results of several studies put H1s in plants, as suspects to function in epigenetic regulation like in DNA methylation (Brzeski and Jerzmanowski 2003; Rea et al. 2012; Rutowicz et al. 2015; Wierzbicki and Jerzmanowski 2005; Zemach et al. 2013). Epigenetic marks a quite important during developmental and differentiation processes, since their distribution influences transcription (Meister, Mango, and Gasser 2011). Therefore linker histones might also be involved in development and cell differentiation by influence not only DNA methylation but also by modulating chromatins accessibility for transcriptional reprogramming (Pan and Fan 2016; Terme et al. 2011; Zhang et al. 2012). These findings suggest that H1s are potential key regulators in cell fate transition. In support of this hypothesis, Ricci and colleagues showed in mouse ESCs that nucleosomes assembled in heterogeneous groups of varying size, termed “clutches”, which correlates with the heterogeneous distribution of H1s along the chromatin fiber (Ricci et al. 2015). Whereby, ground-state pluripotent stem cells had on average fewer nucleosomes clutches and H1s, whereas less potent cells had on average more and large nucleosome clutches containing enriched numbers of linker histones. These findings indicate that linker histones are involved in the process of pluripotency acquisition.

Taken together, there is evidence that in plants linker histones play roles in chromatin organization and in DNA methylation and demethylation processes during plant development and reproduction but also in stress responds (Brzeski and Jerzmanowski 2003; Rea et al. 2012; Rutowicz et al.

2015; She et al. 2013; Wierzbicki and Jerzmanowski 2005; Zemach et al. 2013). Further does their dynamic presence correlate with, cell–fate transitions and cells potency changes in plants and animals. This evidences and correlations led to the following questions of my thesis:

What is the role of H1 eviction in meiotic precursor cells? Is this event necessary for transcriptional reprogramming or is it already a consequence of cell fate change? Does H1 has an impact on the immediate developmental transition or has it a long-term (epigenetic) impact on gametogenesis and/or embryogenesis?

Thus, for my PhD, I aimed to explore the mechanism of transient linker histone eviction during MMC development and its role during sporogenesis in *A.thaliana*.

Full knockdown of H1 variants in Arabidopsis is detrimental to plant development and fertility (Wierzbicki and Jerzmanowski 2005). Here, to study linker histones dynamic during MMC development we required a molecular genetic approach to induce genetic mutations altering H1 deposition in a conditional manner to avoid constitutive defects impairing on plant fertility and development. This required to establish a method to efficiently and reproducibly induce the engineered mutations in the developing MMC in the ovule which is deeply embedded in the floral tissue. To overcome this technical limitation, I adapted and developed an application protocol enabling me to control gene expression in developing ovules, *in planta*, using a dexamethasone (Dex)- based gene transactivation system (Craft et al. 2005). This system allows inducing transgenes in an efficient and precise spatial and temporal manner without compromising plant fertility and temporal development (Chapter 2). To monitor linker histone dynamics during MMC development I created plant lines, also called background reporter lines (BG), which contained linker histone variants tagged with fluorescent markers to monitor for altered linker histone presence during plant sporogenesis in engineered mutants (Chapter 3). We considered several approaches to perturb H1 deposition: (i) down-regulation of factors regulating H1 stability: histone chaperones and proteasome-related components, (ii) expressing H1 mutant variants with altered amino acid residues potentially impairing their post-translational modifications.

I initiated research to test the role of different histone chaperones on linker histone eviction during plant sporogenesis (Chapter 4) since some of them (NAPs and HIRA) have already been described to be involved in H1 eviction during the formation of the mouse germline (Hajkova et al. 2008). This process also describes a cell fate transition, similar to the on at plant sporogenesis. Further is already known that HIRA is responsible for the deposition of the histone H3.3/H3.1 in plants. This process plays an important role in reprogramming events associated with differentiation (Nie et al. 2014). In Chapter 5 I report on an approach testing the role of the proteasome-degradation pathway on linker histone eviction during MMC differentiation. I got interested in this question since She and colleagues (She et al. 2013) showed that H1 eviction at the somatic-to-reproductive-transition phase is susceptible to proteasome inhibition suggesting a putative role for H1 ubiquitination. In detail, I looked at (i) the role of Cullin-based E3 ligases since those facilitate ubiquitination in plants (Biedermann and Hellmann 2011) and (ii) the contribution of candidate amino acids, potential sites for ubiquitination. The results indicate that at least three amino acids in the globular domain of H1, which are putative targets of ubiquitination, and a functional CULLIN4 are important for H1 stability and MMC formation during the somatic-to-reproductive cell fate change. In Chapter 6 I report on an analysis addressing the possible role of a new post-translational modification (PTM), arginine citrullination, in linker histone eviction during

sporogenesis in *Arabidopsis thaliana*. Christophorou and colleagues showed in mouse embryonic stem cells that linker histones are targets of PEPTIDYL ARGININE DEIMINASE TYPE IV (PADI4), which induce the post-translational modification citrulline (Christophorou et al. 2014). This PTM causes H1 displacement from the DNA, chromatin decondensation and expression of pluripotency markers. I found that the mutation of arginine 57 was sufficient to alter H1s stability and induce aberrant MMC development. After we watered plants with Dex for several weeks we detected reduced fertility in plants expressing the *H1.1*^{R57K}*RFP* mutant variant. Our hypothesis is that the altered H1.1 presence in the developing MMC, causes the reduced fertility. But at the moment we do not know if the altered H1.1 presence has an immediate impact on the developmental transition or if it rather has a long-term, epigenetic impact on either gametogenesis and/or embryogenesis. Further experiments should clarify the exact stage of perturbation in the fertility. I also explored the possible role of *A.thaliana* AGMATINE IMINOHYDROLYASE (AIH). Indeed AIH has a strong structural similarity to PADI4 with a preserved 3D structure of the catalytic domain suggesting that they might have similar enzymatic activity, although this still needs to be biochemically tested. The preliminary results of induced-knockdowns of *AIH* suggest a role in linker histone stability during sporogenesis in *A.thaliana* (Chapter 6) thus motivating for further investigations.

In summary, my work contributed to creating novel tools and knowledge that pave the way for future investigation. The inducible genetic tools and application techniques to conditionally induce transgenes of interest in ovules *in planta* promise to be useful for further studies on the role of linker histones in Arabidopsis, beyond reproductive development. In addition, my results provide good preliminary evidence for a role of specific amino-acids, likely targets of PTMs, and of key enzymes (such as the Ubiquitination-ligase CULLIN4 and the putative arginine modifier AIH) to uncover the mechanisms of linker histone dynamics in cell fate changes in plants. Furthermore, my PhD work also contributed a better understanding of H1 function in developmental programs other than reproduction such as flowering and lateral root formation.

Future work based on these studies should uncover the detailed mechanism of linker histone eviction and its influence on chromatin rearrangement at sporogenesis. This will help to understand how chromatin rearrangement influences transcriptional patterns and cell function. Therefore, the characterization of the interplay between chromatin dynamics and transcriptional networks in differentiating SMCs will be crucial to understanding the functional significance of chromatin reprogramming events for reproductive cell fate acquisition.

References

Autran, Daphné et al. 2011. “Maternal Epigenetic Pathways Control Parental Contributions to Arabidopsis Early Embryogenesis.” *Cell* 145(5): 707–19.

Baroux, C. et al. 2007. “The Triploid Endosperm Genome of Arabidopsis Adopts a Peculiar, Parental-Dosage-Dependent Chromatin Organization.” *the Plant Cell* 19(6): 1782–94.

Baroux, Célia, Michael T. Raissig, and Ueli Grossniklaus. 2011. “Epigenetic Regulation and Reprogramming during Gamete Formation in Plants.” *Current Opinion in Genetics and Development* 21(2): 124–33.

Biedermann, Sascha, and Hanjo Hellmann. 2011. “WD40 and CUL4-Based E3 Ligases: Lubricating All Aspects of Life.” *Trends in Plant Science* 16(1): 38–46.

Brzeski, Jan, and Andrzej Jerzmanowski. 2003. “Deficient in DNA Methylation 1 (DDM1) Defines a Novel Family of Chromatin-Remodeling Factors.” *Journal of Biological Chemistry* 278(2): 823–28.

Christophorou, Maria A. et al. 2014. “Citrullination Regulates Pluripotency and Histone H1 Binding to Chromatin.” *Nature* 507(7490): 104–8.

Craft, Judith et al. 2005. “New pOp/LhG4 Vectors for Stringent Glucocorticoid-Dependent Transgene Expression in Arabidopsis.” *The Plant Journal : for cell and molecular biology* 41(6): 899–918.

Hackett, Jamie A., Jan J. Zylicz, and M. Azim Surani. 2012. “Parallel Mechanisms of Epigenetic Reprogramming in the Germline.” *Trends in Genetics* 28(4): 164–74.

Hajkova, Petra et al. 2002. “Epigenetic Reprogramming in Mouse Primordial Germ Cells.” *Mechanisms of Development* 117(1–2): 15–23.

Hajkova et al. 2008. “Chromatin Dynamics during Epigenetic Reprogramming in the Mouse Germ Line.” *Nature* 452(7189): 877–81.

Hill, Peter W. S. et al. 2018. “Epigenetic Reprogramming Enables the Transition from Primordial Germ Cell to Gonocyte.” *Nature*.

Houben, Andreas, Katrin Kumke, Kiyotaka Nagaki, and Gerd Hause. 2011. “CENH3 Distribution and Differential Chromatin Modifications during Pollen Development in Rye (Secale Cereale L.).” *Chromosome Research* 19(4): 471–80.

Ingouff et al. 2007. “Distinct Dynamics of HISTONE3 Variants between the Two Fertilization Products in Plants.” *Current Biology* 17(12): 1032–37.

Ingouff et al. 2010. “Zygotic Resetting of the HISTONE 3 Variant Repertoire Participates in Epigenetic Reprogramming in Arabidopsis.” *Current Biology* 20(23): 2137–43.

Ingouff et al. 2017. “Live-Cell Analysis of DNA Methylation during Sexual Reproduction in Arabidopsis Reveals Context and Sex-Specific Dynamics Controlled by Noncanonical RdDM.” *Genes and Development* (31): 72–83.

Jullien, Pauline E. et al. 2012. “DNA Methylation Dynamics during Sexual Reproduction in Arabidopsis Thaliana.” *Current Biology* 22(19): 1825–30.

Meister, Peter, Susan E. Mango, and Susan M. Gasser. 2011. “Locking the Genome: Nuclear Organization and Cell Fate.” *Current Opinion in Genetics and Development* 21(2): 167–74.

Nie, Xin et al. 2014. “The HIRA Complex That Deposits the Histone H3.3 Is Conserved in Arabidopsis and Facilitates Transcriptional Dynamics.” *Biology open* 3: 794–802.

Pan, Chenyi, and Yuhong Fan. 2016. “Role of H1 Linker Histones in Mammalian Development and Stem Cell Differentiation.” *Biochimica et Biophysica Acta - Gene Regulatory Mechanisms* 1859(3): 496–509.

Pillot, M. et al. 2010. “Embryo and Endosperm Inherit Distinct Chromatin and Transcriptional States from the Female Gametes in Arabidopsis.” *The Plant Cell* 22(2): 307–20.

Rea, M. et al. 2012. “Histone H1 Affects Gene Imprinting and DNA Methylation in Arabidopsis.” *The Plant Journal : for cell and molecular biology* 71(5): 776–86.

Ricci, Maria A. et al. 2015. “Chromatin Fibers Are Formed by Heterogeneous Groups of Nucleosomes In Vivo.” *Cell* 160(6): 1145–58.

Rutowicz, Kinga et al. 2015. “A Specialized Histone H1 Variant Is Required for Adaptive Responses to Complex Abiotic Stress and Related DNA Methylation in Arabidopsis.” *Plant Physiology* 169(November): 2080–2101.

She, Wenjing et al. 2013. “Chromatin Reprogramming during the Somatic-to-Reproductive Cell Fate Transition in Plants.” *Development (Cambridge, England)* 140(19): 4008–19.

Terme, Jean Michel et al. 2011. “Histone H1 Variants Are Differentially Expressed and Incorporated into Chromatin during Differentiation and Reprogramming to Pluripotency.” *Journal of Biological Chemistry* 286(41): 35347–57.

Wierzbicki, Andrzej T, and Andrzej Jerzmanowski. 2005. “Suppression of Histone H1 Genes in Arabidopsis Results in Heritable Developmental Defects and Stochastic Changes in DNA Methylation.” *Genetics* 169(2): 997–1008.

Zemach, Assaf et al. 2013. “The Arabidopsis Nucleosome Remodeler DDM1 Allows DNA Methyltransferases to Access H1-Containing Heterochromatin.” *Cell* 153(1): 193–205.

Zhang, Yunzhe et al. 2012. “Histone h1 Depletion Impairs Embryonic Stem Cell Differentiation.” *PLoS genetics* 8(5): e1002691.

XII. Acknowledgment

I thank Prof. Ueli Grossniklaus for the opportunity to do my PhD in his lab. I am grateful for his work on creating a stimulating atmosphere both at the scientific and social level.

Furthermore, I thank PD. Dr. Célia Baroux for the chance to do my PhD on her project and for reviewing this thesis and paper manuscripts. Moreover, I want to thank her for her tireless support, her professional and expert guidance and for all the discussion about the project.

Moreover, I thank Prof. Andrzej Jerzmanowski, Prof. Christoph Ringli and Dr. Fredy Barneche to be part of my PhD Committee. They gave me great input and suggestions during and at the end of my PhD time.

In addition, I thank Prof. Ian Moore and Prof. Joop Vermeer for providing plasmids and lab material, Prof. Hugh Dickson and Dr. Marta Mendez for discussions and information about the dexamethasone inducible system and Dr. Zusanna Kaczmarska for the 3D modeling of AIH.

I would like to express my sincere gratitude Dr. Kinga Rutowicz for sharing her expertise of linker histones and for her help in experiments and insightful discussions during all stages of this work. Furthermore, I would like to thank her for carefully reading the manuscript and finding the small mistakes.

Further, I thank Dr. Nina Chumak, Margarida Sofia Nobre and Anja Herrmann for critical reading parts of my thesis and their helpful comments.

Special thanks go to Daniel Prata who help me a lot during the last month of my PhD with wet lab work.

I am grateful to Dr. Afif Hedhly for helping with DMR settings and clearings, Dr. Ethel Mendocilla Sato for discussion on confocal microscopy and sharing plant material, Dr. Wenjing She, Anja Hermann and Margarida Sofia Nobre for discussion on my project, Dr. Valeria Gagliardini for ddPCR and Dr. Vimal Rawat for providing an online tool to analyze gene expression data.

My warm appreciations go to the TA Team: Peter Kopf, Dr. Christof Eichenberger, Arturo Bolaños, Daniela Guthörl, Anja Frey and Dr. Frédérique Pasquer for helping with the daily business in the lab.

Special thanks go to previous and current members of the Cheri Club: Dr. Roger Schmid, Guillaume Fauser-Misslin, Dr. Nuno Piers, Dr. Moritz Rövekamp and Michele A. Wyler.

My thanks must be extended to all previous and current members of P2/10-11 lab: Margarida Sofia Nobre, Anja Herrmann, Lucas Waser, Tiago Meier, Dr. Szymon Tylewicz, Dr. Wendy Gu and Dr. Stefan Grob.

Overall, I would like to thank the entire people of the P2 floor for the positive working atmosphere, their support and help with my project. Last but not least, I would like to thank my family and friends, especially Robert Fritze, Ralf Schubert and Anita Schubert, who always encouraged and supported me during my whole PhD student time.